

Copyright

by

Padmakar Ayyalasomayajula

2003

**The Dissertation Committee for Padmakar S. Ayyalasomayajula  
certifies that this is the approved version of the following  
dissertation:**

**Prediction of Bulk and Interfacial Thermodynamic Properties of  
Polar Mixtures by Statistical Associating Fluid Theory**

**Committee:**

---

Mukul M. Sharma, Supervisor

---

Roger T. Bonnecaze

---

Keith P. Johnston

---

Gary A. Pope

---

Isaac C. Sanchez

**Prediction of Bulk and Interfacial Thermodynamic Properties of  
Polar Mixtures by Statistical Associating Fluid Theory**

**by**

**Padmakar S. Ayyalasomayajula, B.S, M.S.**

**Dissertation**

Presented to the Faculty of the Graduate School of

The University of Texas at Austin

in Partial Fulfillment

of the Requirements

for the Degree of

**Doctor of Philosophy**

**The University of Texas at Austin**

**May, 2003**

## **Acknowledgements**

I am extremely grateful to Dr. Mukul M. Sharma for his constant guidance, motivation and supervision throughout the course of this work.

My special thanks to Dr Gary A. Pope, Dr. Isaac C. Sanchez, Dr. Keith P. Johnston and Dr. Roger T. Bonnecaze for managing time out of their busy schedules to be on this dissertation committee.

I greatly appreciate the e-mail correspondences with Dr. Walter Chapman at Rice University, Dr. S.J.Suresh at Unilever India Limited, and Dr. Hertanto Adidharma and Dr. Maciej Radosj at the Louisiana State University.

My special thanks to Nilesh, Shailesh, Aditya, Phani, Behl, Rana, Shukla, Bimal, Rakesh and Ravi for their friendship and support that produced many good memories during my stay in Austin.

# **Prediction of Bulk and Interfacial Thermodynamic Properties of Polar Mixtures by Statistical Associating Fluid Theory**

Publication No. \_\_\_\_\_

Padmakar S. Ayyalasomayajula, Ph. D  
The University of Texas at Austin, 2003

Supervisor: Mukul M. Sharma

A Statistical Associating Fluid Theory (SAFT) for multi-component mixtures has been implemented in conjunction with a phase-stability and flash algorithm. The model has been extensively tested for various non-associating and associating mixtures and comparisons are made with the Peng-Robinson equation of state. Both Peng-Robinson and SAFT are equally suitable for simple non-associating mixtures but SAFT clearly is more accurate when polar mixtures are modeled. The phase behavior of methanol-water-hydrocarbon mixtures is studied with the SAFT equation and the Peng-Robinson equation and comparisons are made with experimental liquid dropout data. The SAFT equation of state is shown to give better predictions for methanol-hydrocarbon and methanol-water-hydrocarbon mixtures over a range of pressures and compositions. The effect of

methanol concentration and temperature on dew-point to bubble-point transition of a gas-condensate mixture is studied with the SAFT equation of state.

The SAFT equation of state is coupled with the Gradient Theory to calculate the interfacial tension of pure components as well as multi-component mixtures. Pure component interaction parameters ( $c_{ii}$ ) for the calculation of interfacial tension with the SAFT equation have been introduced. A mixing interaction coefficient for interfaces ( $m_{ij}$ ) has been defined to satisfactorily predict the interfacial tension of certain mixtures such as water-methanol and water-ethanol systems. The effect of temperature and pressure is studied for a methane-water mixture and it is shown that no further adjustable parameters need to be introduced to accurately predict the interfacial tension over a range of temperatures and pressures.

Finally, the SAFT equation of state has also been integrated in to the reservoir simulator (UTCOMP) so as to be able to do flow simulations of complex polar mixtures. The flow simulations with SAFT have also been compared with experimental core flood studies and it is shown that both the PR and the SAFT equation give reasonable agreement with experimental data. However, it is shown that the SAFT based model predictions are slightly better during the methanol injection stage of the experiment. However, significantly larger computational time discourages the use of SAFT for such flow simulations.

## Table of Contents

Table of Contents .....	vii
List of Tables .....	xi
List of Figures .....	xii
<b>CHAPTER 1 INTRODUCTION</b>	<b>1</b>
1.1 Research Objectives .....	1
1.2 Overview .....	2
<b>CHAPTER 2 LITERATURE SURVEY</b>	<b>4</b>
2.1 Classical Equations of State .....	4
2.2 SAFT Equation of State .....	5
2.3 Microthermodynamics .....	6
2.4 Liquid Theories Based on Hard Sphere Model .....	8
2.5 Perturbation Theory for Dispersion Forces .....	9
2.6 Models for Association Effects .....	10
2.6.1 Early Models .....	10
2.6.2 Statistical Mechanical Models .....	11
2.6.3 Wertheim's Association Model .....	12
2.7 Chains of Hard Spheres .....	14
Nomenclature .....	15
References .....	16
<b>CHAPTER 3 SAFT EQUATION OF STATE FOR MULTICOMPONENT MIXTURES</b>	<b>20</b>
3.1 Mixtures of Hard Spheres .....	21
3.2 Mixture of Chains .....	24
3.3 Mixture of Associating Spheres .....	26
3.4 Dispersion Term .....	29

3.5 Multiphase Equilibrium Algorithm .....	33
3.5.1 Phase Stability Analysis .....	34
3.5.2 Method of Stationary Point Locations .....	35
3.5.3 Flash Calculation .....	43
3.5.4 Accelerated Successive Substitution Method .....	44
3.6 Pseudo Component Parameter Evaluation .....	52
3.6.1 Incorporation of Pseudo components in SAFT .....	54
Nomenclature .....	56
References .....	59
<b>CHAPTER 4 BULK THERMODYNAMIC PROPERTIES OF MIXTURES</b>	<b>69</b>
4.1 Pure Components .....	69
4.2 Binary and Ternary Mixtures .....	70
4.3 Pseudocomponents .....	75
4.4 Conclusions .....	76
References .....	78
<b>CHAPTER 5 BULK THERMODYNAMIC PROPERTIES OF GAS CONDENSATE MIXTURES</b>	<b>98</b>
5.1 Introduction .....	98
5.2 Pure Gas Condensate Mixtures .....	99
5.3 Gas Condensate-Methanol Mixtures .....	101
5.4 Effect of Methanol Concentration on Gas condensate-Methanol Mixtures .....	103
5.5 Water-Methanol Mixtures .....	104
5.6 Gas Condensate-Water-Methanol Systems .....	106
5.7 Hydrocarbon-Methanol-Water Mixtures .....	110
5.8 Conclusions .....	112
References .....	113
<b>CHAPTER 6 SAFT BASED INTERFACIAL TENSION MODEL</b>	<b>154</b>
6.1 Background .....	154



6.2 Solubility parameters and surface tension.....	155
6.3 Density functional theory .....	159
6.3.1 Correlation Functions.....	159
6.3.2 Thermodynamic Functions.....	162
6.4 SAFT based IFT Model with Gradient Theory .....	165
Nomenclature .....	174
References .....	176
<b>CHAPTER 7 INTERFACIAL PROPERTIES OF PURE COMPONENTS AND MIXTURES</b>	<b>179</b>
7.1 Pure Components .....	179
7.2 Binary Mixtures.....	180
7.3 Conclusions .....	184
References .....	186
<b>CHAPTER 8 SAFT BASED PHASE BEHAVIOR MODEL IN A RESERVOIR FLOW SIMULATOR</b>	<b>215</b>
8.1 Introduction .....	215
8.2 Basic Equations .....	216
8.3 Pressure Equation.....	218
8.4 Chemical potential and compressibility derivatives with saft equation	222
8.4.1. Hard Sphere Terms.....	222
8.4.2. Mixture of Chains Term.....	225
8.4.3 Mixture of Associating Spheres Term .....	228
8.4.3 Dispersion Term .....	231
8.5 Simulation of Core Flood Experiments.....	235
8.6 Conclusions .....	238
Nomenclature .....	239
References .....	241
<b>CHAPTER 9 SUMMARY AND CONCLUSIONS</b>	<b>248</b>
9.1 Recommendations and Future Work.....	252

<b>APPENDIX A</b>	<b>255</b>
<b>APPENDIX B</b>	<b>257</b>
<b>BIBLIOGRAPHY</b>	<b>260</b>
Vita .....	268

## List of Tables

Table 3.1: Correlation of segment number $m$ for hydrocarbons .....	61
Table 3.2: Correlation of closed packed molar volume $mv^\infty$ for hydrocarbons .....	61
Table 3.3: Correlation of segment energy $u_0/k$ for n-alkanes and polynuclear aromatics .....	62
Table 3.4: Correlation of segment energy $u_0/k$ for other hydrocarbons .....	62
Table 4.1: Segment parameters for nonassociating fluids (Huang et al., 1991) .....	80
Table 4.2: Segment and site-site parameters for associating fluids (Huang et al., 1991).....	80
Table 4.3: Composition of Mixture 1 of North Sea gas condensate, (Pedersen, 1989).....	81
Table 4.4: Composition of Mixture 2 of North Sea black oil (Pedersen, 1989) .....	82
Table 5.1: Overall composition of gas-condensate for various mixtures used in this study .....	115
Table 5.2: Binary interaction coefficients, $k_{ij}$ , between hydrocarbons used in the SAFT Equation of state .....	115
Table 5.3: Binary interaction coefficients, $k_{ij}$ , between methanol and water with other components with the PR and the SAFT equations-of-state .....	116
Table 5.4: Experimental mixture compositions in GPA RR 117 report (Ng. et al., 1988).....	116
Table 7.1: Interfacial tension parameter for gradient theory with SAFT equation of state .....	187
Table 8.1: Coreflood experiment summary for Texas Cream limestone and Berea sandstone.....	242

## List of Figures

Figure 2.1: Only two molecules can form a bond at a single associating site .....	19
Figure 2.2: No site on one molecule bond simultaneously to two sites on another molecule .....	19
Figure 2.3: Double bonding between molecule is not allowed .....	19
Figure 3.1: Graphical interpretation of phase stability analysis by Michelson's Method.....	63
Figure 3.2: Algorithm for phase equilibrium calculation.....	64
Figure 3.3: Segment number $m$ as a linear function of molar mass for n-alkanes and long chain polymers (Huang et al.,1991) .....	66
Figure 3.4: Segment number $m$ for n-alkanes and polynuclear aromatics. The branched curves represent n-alkyl derivatives of polynuclear aromatics (Huang et al.,1991) .....	67
Figure 3.5: Close-packed molar volumes $m v^\infty$ for n-alkanes and polynuclear aromatics as functions of molar mass. (Huang et al.,1991).....	67
Figure 3.6: Segment energies $u^0/k$ for n-alkanes and polynuclear aromatics as functions of molar mass. The branched curves represent n-alkyl derivatives of poly-aromatics (Huang et al.,1991).....	68
Figure 4.1: Vapor pressure curves of n-alkanes .....	83
Figure 4.2: Liquid density curves of n-alkanes .....	83
Figure 4.3: Vapor pressure curves for polar compounds .....	84
Figure 4.4: Liquid densities of polar compounds.....	84
Figure 4.5: Vapor liquid equilibrium for butane-hexane mixture at 293.15 K.....	85
Figure 4.6: Vapor liquid equilibrium for methane-hexabutane at 462 K.....	85
Figure 4.7: Vapor liquid equilibrium curve for methane-hexadecane mixture at 462 K and 623 K.....	86
Figure 4.8: Vapor liquid equilibrium curve for ethane-ethanol mixture at 313.4 K.....	86
Figure 4.9: Vapor liquid equilibrium curve for ethane-ethanol mixture at 333.4 K.....	87

Figure 4.10: Vapor liquid equilibrium curve for methane-ethanol mixture at 313.4 K.....	87
Figure 4.11: Vapor liquid equilibrium curve for methane-ethanol mixture at 333.4 K.....	88
Figure 4.12: Vapor liquid equilibrium curve for CO <sub>2</sub> -methanol mixture at 313.4 K.....	88
Figure 4.13: Vapor liquid equilibrium curve for CO <sub>2</sub> -ethanol mixture at 313.4 K.....	89
Figure 4.14: Vapor liquid equilibrium curve for CO <sub>2</sub> -ethanol mixture at 333.4 K.....	89
Figure 4.15: Vapor liquid equilibrium curve for CO <sub>2</sub> -propanol mixture at 313.4 K.....	90
Figure 4.16: Vapor liquid equilibrium curve for CO <sub>2</sub> -propanol mixture at 333.4 K.....	90
Figure 4.17: Vapor liquid equilibrium curve for ethane-propanol mixture at 313.4 K.....	91
Figure 4.18: Vapor liquid equilibrium curve for ethane-propanol mixture at 333.4 K.....	91
Figure 4.19: Vapor liquid equilibrium curve for methanol-hexane mixture at 1 atm.....	92
Figure 4.20: Vapor liquid equilibrium curve for propanol-heptane at 1 atm.....	92
Figure 4.21: Vapor liquid equilibrium for ethanol-water mixture at 298.14 K.....	93
Figure 4.22: VLE curves for methane-ethane-propane system at -75 C, 100 psia.....	93
Figure 4.23: VLE curves for methane-ethane-propane system at -75 C, 200 psia.....	94
Figure 4.24: VLE curves for methane-ethane-propane system at -75 C, 400 psia.....	94
Figure 4.25: VLE curves for methane-ethane-propane system at -75 C, 600 psia.....	95
Figure 4.26: VLE curves for methane-ethane-propane system at -75 C, 800 psia.....	95
Figure 4.27: Gas phase compressibility factor for Mixture 1(North sea gas condensate) in a constant mass expansion study at 155 C.....	96

Figure 4.28: Gas phase compressibility factor of Mixture 2 (North Sea black oil) in a differential liberation study at 92.8 C .....	96
Figure 4.29: Liquid phase densities of Mixture 2 (North Sea black oil) in a differential liberation study at 92.8 C .....	97
Figure 5. 1: Liquid volume fraction curves for a gas condensate fluid (Mixture 1 in Table 5.1) at 145 F with the PR equation .....	117
Figure 5.2: Gas-condensate molar density variation at 145 F with PR EOS .....	117
Figure 5.3: Liquid phase compositions for the gas-condensate fluid at 145 F with the PR equation .....	118
Figure 5.4: Vapor phase compositions for the gas-condensate fluid at 145 F with PR equation .....	118
Figure 5.5: Liquid volume fraction curves for a gas condensate fluid (mixture 1 in Table 5.1 at 145 F using the SAFT equation with and without binary interaction coefficients .....	119
Figure 5.6: Molar density curves for gas condensate fluids at 145 F using the SAFT equation without binary interaction coefficients .....	119
Figure 5.7: Liquid phase compositions for gas-condensate fluid at 145 F using the SAFT equation without binary interaction coefficients .....	120
Figure 5.8: Gas phase compositions for gas-condensate fluid at 145 F using the SAFT equation without binary interaction coefficients .....	120
Figure 5.9: Molar density curves for gas condensate fluids at 145 F using the SAFT equation with binary interaction coefficients .....	121
Figure 5.10: Liquid phase compositions for gas-condensate fluid at 145 F using the SAFT equation with binary interaction coefficients .....	121
Figure 5.11: Gas phase compositions for gas-condensate fluid at 145 F using the SAFT equation with binary interaction coefficients .....	122
Figure 5.12: Liquid volume fraction curves for a 10 mol % methanol and 90 mol % gas condensate mixture (Mixture 2 in Table 5.1) at 145 F using the PR equation of state .....	122
Figure 5.13: Gas condensate molar density variation for a 10 mol % methanol and 90 mol % gas condensate mixture at 145 F using the PR equation of state .....	123

Figure 5.14: Liquid phase compositions for a 10 mol % methanol and 90 mol % gas condensate mixture at 145 F using the PR equation of state .....	123
Figure 5.15: Vapor phase compositions for a 10 mol % methanol and 90 mol % gas condensate mixture at 145 F using the PR equation of state .....	124
Figure 5.16: Liquid volume fraction curves for a 10 mol % methanol and 90 mol % gas condensate mixture (Mixture 2 in Table 5.1) at 145 F using the SAFT equation .....	124
Figure 5.17: Molar density curves for 10 mol % methanol and 90 mol % gas condensate fluids at 145 F using the SAFT equation without methanol binary interaction coefficients.....	125
Figure 5.18: Liquid phase compositions for 10 mol % methanol and 90 mol % gas condensate fluid at 145 F using SAFT without methanol binary interaction coefficients.....	125
Figure 5.19: Vapor phase compositions for 10 mol % methanol and 90 mol % gas-condensate fluid at 145 F using SAFT without methanol binary interaction coefficients.....	126
Figure 5.20: Molar density curves for 10 mole % methanol and 90 mole % gas condensate fluids at 145 F using SAFT with methanol binary interaction coefficients.....	126
Figure 5.21: Liquid phase compositions for 10 mol % methanol and 90 mol % gas-condensate fluid at 145 F using SAFT with methanol binary interaction coefficients.....	127
Figure 5.22: Gas phase compositions for 10 mol % methanol and 90 mol % gas-condensate fluid at 145 F using SAFT with methanol binary interaction coefficients.....	127
Figure 5.23: Liquid volume fraction curves for a 50 mol % methanol and 50 mol % gas condensate mixture (Mixture 3 in Table 5.1) at 145 F using the PR equation .....	128
Figure 5.24: Molar density curves for 50 mol % methanol and 50 mol % gas condensate fluids at 145 F using the PR equation .....	128
Figure 5.25: Liquid phase compositions for 50 mol % methanol and 50 mol % gas-condensate fluid at 145 F using the PR equation.....	129
Figure 5.26: Gas phase compositions for 50 mol % methanol and 50 mol % gas-condensate fluid at 145 F using the PR equation.....	129

Figure 5.27: Liquid volume fraction curves for a 50 mol % methanol and 50 mol % gas condensate mixture (Mixture 3 in Table 5.1) at 145 F using the SAFT equation .....	130
Figure 5.28: Molar density curves for 50 mol % methanol and 50 mol % gas condensate fluids at 145 F using the SAFT equation .....	130
Figure 5.29: Liquid phase compositions for 50 mol % methanol and 50 mol % gas-condensate fluid at 145 F using SAFT with binary interaction coefficients .....	131
Figure 5.30: Gas phase compositions for 50 mol % methanol and 50 mol % gas-condensate fluid at 145 F using SAFT with binary interaction coefficients .....	131
Figure 5.31: Liquid volume fraction curves for gas condensate mixtures at 145 F with change in methanol concentration .....	132
Figure 5.32: Liquid volume fraction curves for gas condensate mixtures at 250 F with change in methanol concentration .....	132
Figure 5.33: Liquid volume fraction curves for gas condensate mixtures at 350 F with change in methanol concentration .....	133
Figure 5.34: Vapor liquid equilibrium of methanol-water at 39.9 C with the PR and SAFT equation.....	133
Figure 5.35: Density of methanol-water(2) mixtures at 140 F with the PR equation (Sentenac, 1998).....	134
Figure 5.36: Volume fraction diagram for Mixture 4 in Table 5.1 with the PR equation at 145 F.....	134
Figure 5.37: Molar density curves for for Mixture 4 in Table 5.1 with the PR equation at 145 F.....	135
Figure 5.38: Mole fraction of various components in liquid phase for Mixture 4 in Table 5.1 with PR equation.....	135
Figure 5.39: Mole fraction of various components in vapor phase for Mixture 4 in Table 5.1 with PR equation.....	136
Figure 5.40: Mole fraction of various components in aqueous phase for Mixture 4 in Table 5.1 with PR equation.....	136
Figure 5.41: Volume fraction diagram for Mixture 5 in Table 5.1 at 145 °F with PR equation.....	137
Figure 5.42: Molar density curves for Mixture 5 in Table 5.1with the PR equation at 145 F.....	137



Figure 5.43: Mole fraction of various components in liquid phase for Mixture 5 in Table 5.1 with PR equation.....	138
Figure 5.44: Mole fraction of various components in vapor phase for Mixture 5 in Table 5.1 with PR equation.....	138
Figure 5.45: Mole fraction of various components in aqueous phase for Mixture 5 in Table 5.1 with PR equation.....	139
Figure 5.46: Volume fraction diagram for Mixture 4 in Table 5.1 at 145 °F with SAFT Equation .....	139
Figure 5.47 Molar density curves for Mixture 4 in Table 5.1 with the SAFT equation at 145 F .....	140
Figure 5.48: Mole fraction of various components in liquid phase for Mixture 4 in Table 5.1 with SAFT equation.....	140
Figure 5.49: Mole fraction of various components in vapor phase for Mixture 4 in Table 5.1 with SAFT equation.....	141
Figure 5.50: Mole fraction of various components in aqueous phase for Mixture 4 in Table 5.1 with SAFT equation.....	141
Figure 5.51: Volume fraction diagram for Mixture 5 in Table 5.1 at 145 °F with SAFT equation .....	142
Figure 5.52: Molar density curves for Mixture 5 in Table 5.1 with the SAFT equation at 145 F .....	142
Figure 5.53: Mole fraction of various components in liquid phase for Mixture 5 in Table 5.1 with SAFT equation.....	143
Figure 5.54: Mole fraction of various components in vapor phase for Mixture 5 in Table 5.1 with SAFT equation.....	143
Figure 5.55: Mole fraction of various components in aqueous phase for Mixture 5 in Table 5.1 with SAFT equation.....	144
Figure 5.56: Vapor hydrocarbon phase mole fractions at 122 F hydrocarbon-water-methanol (Mixture 1) in Table 5.5 .....	144
Figure 5.57: Liquid hydrocarbon phase mole fractions at 122 F hydrocarbon-water-methanol (Mixture 1) in Table 5.5 .....	145
Figure 5.58: Aqueous phase mole fractions at 122 F hydrocarbon-water-methanol (Mixture 1) in Table 5.5 .....	145
Figure 5.59: Vapor phase mole fractions at 122 F hydrocarbon-water-methanol (Mixture 2) in Table 5.5 .....	146

Figure 5.60: Liquid hydrocarbon phase mole fractions at 122 F for hydrocarbon-water-methanol (Mixture 2) in Table 5.5 .....	146
Figure 5.61: Aqueous phase mole fractions at 122 F for hydrocarbon-water-methanol (Mixture 2) in Table 5.5 .....	147
Figure 5.62: Vapor phase mole fractions at 68 F hydrocarbons-water-methanol (Mixture 3) in Table 5.5 .....	147
Figure 5.63: Liquid hydrocarbon phase mole fractions at 68 F for hydrocarbon-water-methanol (Mixture 3) in Table 5.5 .....	148
Figure 5.64: Aqueous phase mole fractions at 68 F for hydrocarbon-water-methanol (Mixture 3) in Table 5.5 .....	148
Figure 5.65: Vapor phase mole fractions at 68 F for hydrocarbon-water-methanol (Mixture 4) in Table 5.5 .....	149
Figure 5.66: Liquid hydrocarbon phase mole fractions at 68 F for hydrocarbon-water-methanol (Mixture 4) in Table 5.5 .....	149
Figure 5.67: Aqueous phase mole fractions at 68 F for hydrocarbon-water-methanol (Mixture 4) in Table 5.5 .....	150
Figure 5.68: Vapor phase mole fractions at 14 F for hydrocarbon-water-methanol (Mixture 5) in Table 5.5 .....	150
Figure 5.69: Liquid hydrocarbon phase mole fractions at 14 F for hydrocarbon-water-methanol (Mixture 5) in Table 5.5 .....	151
Figure 5.70: Aqueous phase mole fractions at 14 F for hydrocarbon-water-methanol (Mixture 5) in Table 5.5 .....	151
Figure 5.71: Vapor phase mole fractions at 14 F for hydrocarbon-water-methanol (Mixture 6) in Table 5.5 .....	152
Figure 5.72: Liquid hydrocarbon phase mole fractions at 14 F for hydrocarbon-water-methanol (Mixture 6) in Table 5.5 .....	152
Figure 5.73: Aqueous phase mole fractions at 14 F for hydrocarbon-water-methanol (Mixture 6) in Table 5.5 .....	153
Figure 6.1: Comparison of solubility factor calculations from van Oss parameters with the Hansen solubility parameter for the LW component .....	178
Figure 6.2: Comparison of solubility factor calculations from van Oss parameters with the Hansen solubility parameter for the Acid-Base component .....	178
Figure 7.1: Prediction of interfacial tension with SAFT equation for CO <sub>2</sub> .....	188

Figure 7.2: Prediction of interfacial tension with SAFT equation for N <sub>2</sub> .....	188
Figure 7.3: Prediction of interfacial tension with SAFT equation for heptane .....	189
Figure 7.4: Prediction of interfacial tension with SAFT equation for decane.....	189
Figure 7.5: Prediction of interfacial tension with SAFT equation for methanol.....	190
Figure 7.6: Prediction of interfacial tension with SAFT equation for ethanol.....	190
Figure 7.7: Prediction of interfacial tension with SAFT equation for butanol.....	191
Figure 7.8: Prediction of interfacial tension with SAFT equation for water.....	191
Figure 7.9: Interfacial profile of CO <sub>2</sub> -Decane mixture at 344 K and 6.94 MPa .....	192
Figure 7.10: Interfacial profile of CO <sub>2</sub> -Decane mixture at 344 K and .94 MPa .....	192
Figure 7.11: Interfacial profile of CO <sub>2</sub> -Decane mixture at 344 K and 11.7 MPa .....	193
Figure 7.12: Interfacial profile of CO <sub>2</sub> -Decane mixture at 344 K and 12.2 MPa .....	193
Figure 7.13: Interfacial Tension of CO <sub>2</sub> – Decane mixture with equilibrium CO <sub>2</sub> composition.....	194
Figure 7.14: Interfacial profile for 10.4 % ethanol - 90.3 % heptane mixture at 0.101 Mpa, 298.1 K .....	194
Figure 7.15: Interfacial profile for 21.6 % ethanol – 78.1 % heptane mixture at 0.101 Mpa, 298.1 K .....	195
Figure 7.16: Interfacial profile for 55.5 % ethanol – 44.3 % heptane mixture at 0.101 Mpa, 298.1 K .....	195
Figure 7.17: Interfacial profile for 66.7 % ethanol – 33 % heptane mixture at 0.101 Mpa, 298.1 K.....	196
Figure 7.18: Interfacial profile for 78 % ethanol – 21.8 % heptane mixture at 0.101 Mpa, 298.1 K.....	196
Figure 7.19: Interfacial profile for 87.7 % ethanol – 7.47 % heptane mixture at 0.101 Mpa, 298.1 K .....	197

Figure 7.20: Interfacial profile for 88.9 % ethanol – 7.7 % heptane mixture at 0.101 Mpa, 298.1 K.....	197
Figure 7.21: Interfacial profile for 89.8 % ethanol – 7.8 % heptane mixture at 0.101 Mpa, 298.1 K.....	198
Figure 7.22: Interfacial profile for 91.5 % ethanol – 8.5 % heptane mixture at 0.101 Mpa, 298.1 K.....	198
Figure 7.23: Interfacial tension of ethanol-heptane mixture at 0.101 MPa and 298.15 K.....	199
Figure 7.24: Interfacial profile for 99.47 % methanol – 0.5 % water mixture at 0.101 Mpa, 263.15 K.....	199
Figure 7.25: Interfacial profile for 87.9 % methanol – 12 % water mixture at 0.101 Mpa, 263.15 K.....	200
Figure 7.26: Interfacial profile for 53.29 % methanol – 46.7 % water mixture at 0.101 Mpa, 263.15 K.....	200
Figure 7.27: Interfacial profile for 10.245 % methanol – 89.75 % water mixture at 0.101 Mpa, 263.15 K.....	201
Figure 7.28: Interfacial profile for 4 % methanol – 96 % water mixture at 0.101 Mpa, 263.15 K.....	201
Figure 7.29: Interfacial profile for 1 % methanol – 99 % water mixture at 0.101 Mpa, 263.15 K.....	202
Figure 7.30: Interfacial tension of methanol-water mixture at 0.101 MPa and 263.15 K.....	202
Figure 7.31: Interfacial profile for 99.5 % ethanol – 0.5 % water mixture at 0.101 Mpa, 288.1 K.....	203
Figure 7.32: Interfacial profile for 88.8 % ethanol –11.2 % water mixture at 0.101 Mpa, 288.1 K.....	203
Figure 7.33: Interfacial profile for 33.8 % ethanol – 66.2 % water mixture at 0.101 Mpa, 288.1 K.....	204
Figure 7.34: Interfacial profile for 4 % ethanol – 96 % water mixture at 0.101 Mpa, 288.1 K.....	204
Figure 7.35: Interfacial profile for 0.5 % ethanol – 99.5 % water mixture at 0.101 Mpa, 288.1 K.....	205
Figure 7.36: Interfacial tension of ethanol-water mixture at 0.101 MPa and 288.1 K.....	205
Figure 7.37: Interfacial profile for methane-water mixture at 25 C and 63.38 psia .....	206

Figure 7.38: Interfacial profile for methane-water mixture at 25 C and 145.03 psia .....	206
Figure 7.39: Interfacial profile for methane-water mixture at 25 C and 1450.3 psia .....	207
Figure 7.40: Interfacial profile for methane-water mixture at 25 C and 6677.8 psia .....	207
Figure 7.41: Interfacial tension of Methane-Water mixture at 25 C .....	208
Figure 7.42: Interfacial profile for methane-water mixture at 106 C and 10 MPa .....	208
Figure 7.43: Interfacial profile for methane-water mixture at 106 C and 30 MPa .....	209
Figure 7.44: Interfacial profile for methane-water mixture at 106 C and 60 MPa .....	209
Figure 7.45: Interfacial tension of methane-water mixture at 106 C .....	210
Figure 7.46: Interfacial profile for methane-water mixture at 176.7 C and 10 MPa .....	210
Figure 7.47: Interfacial profile for methane-water mixture at 176.7 C and 40 Mpa .....	211
Figure 7.48: Interfacial profile for methane-water mixture at 176.7 C and 50 MPa .....	211
Figure 7.49: Interfacial tension of methane-water mixture at 176.7 C .....	212
Figure 7.50: Interfacial profile for water-CO <sub>2</sub> mixture at 25 C and 1 atm.....	212
Figure 7.51: Interfacial profile for water-CO <sub>2</sub> mixture at 25 C and 50 atm.....	213
Figure 7.52: Interfacial profile for water-CO <sub>2</sub> mixture at 25 C and 60 atm.....	213
Figure 7.53: Interfacial tension of water-CO <sub>2</sub> mixture at 25 C .....	214
Figure 8.1: Experiment 15 – Pressure drop across core during single phase gas mixture injection ( T = 145 F, P = 3000 psi and Q = 48 cc/hr) .....	243
Figure 8.2: Experiment 15 – Pressure drop across core during two phase mixture injection ( T = 145 F, P = 1200 psi and Q = 18 cc/hr).....	243
Figure 8.3: Experiment 15 – Pressure drop across core during single phase equilibrium gas mixture injection ( T = 145 F, P = 1200 psi and Q = 99 cc/hr).....	244
Figure 8.4: Experiment 15 – Pressure drop across core during methanol treatment ( T = 145 F, P = 3000 psi and Q = 99 cc/hr).....	244

Figure 8.5: Experiment 12 – Pressure drop across core during single phase gas mixture injection ( T = 145 F, P = 3000 psi and Q = 600 cc/hr) .....	245
Figure 8.6: Experiment 12 – Pressure drop across core during two phase mixture injection ( T = 145 F, P = 1200 psi and Q = 600 cc/hr) .....	245
Figure 8.7: Experiment 12 – Pressure drop across core during single phase equilibrium gas mixture injection ( T = 145 F, P = 1200 psi and Q = 600 cc/hr).....	246
Figure 8.8: Experiment 12 – Pressure drop across core during methanol injection ( T = 145 F, P = 1200 psi and Q = 300 cc/hr) .....	246
Figure 8.9: Experiment 12 – Pressure drop across core during second two phase gas mixture injection ( T = 145 F, P = 1200 psi and Q = 600 cc/hr) .....	247
Figure 8.10: Experiment 12 – Pressure drop across core during second equilibrium gas mixture injection ( T = 145 F, P = 1200 psi and Q = 600 cc/hr).....	247

# CHAPTER 1

## INTRODUCTION

### 1.1 RESEARCH OBJECTIVES

Polar, associating molecules play a very important role in diverse physical systems such as molecular biology, polymer blends, oil recovery and microelectronics. Only recently has it been possible to include association effects in molecular models for predicting bulk thermodynamic properties. Chapman et al., (1988) have proposed a statistical mechanics based equation of state, Statistical Associating Fluid Theory (SAFT) which accounts for associating molecules. Their approach is to use a reference fluid that incorporates, both the chain length (molecular size and shape) and molecular association, in place of the much simpler hard sphere reference fluid. The prediction of the interfacial behavior of these systems is also dependent on our understanding of intermolecular association effect of these systems. There has been relatively little work done to develop models for predicting the interfacial behavior of two-phase multicomponent systems containing associating molecules.

In this study we extend some of these recent developments in the theory of hydrogen bonding into thermodynamic models, to predict the bulk and interfacial thermodynamic properties of multi-component mixtures. As part of this work, we have implemented a Statistical Associating Fluid theory (SAFT) model for multi-

component mixtures. The model in conjunction with a phase-stability and flash algorithm has been used to study the phase behavior and bulk thermodynamic properties of mixtures of associating molecules commonly encountered in petroleum reservoir fluids. We have done extensive testing of the phase behavior of non-associating and associating binary mixtures using the SAFT model and compared its predictions with a popular engineering equation of state. We have also extended this model to predict interfacial properties, such as surface tension, interfacial tension and interfacial compositions of pure and multi-component mixtures of alcohols. We have implemented the SAFT equation of state in a flow-based reservoir simulator to study the effect of compositional models on the flow of hydrocarbon-alcohol-water mixtures.

## **1.2 OVERVIEW**

In Chapter 2 a review of the equation of states for complex associating mixtures is presented. Chapter 3 discusses the theory behind the statistical mechanical ideas and lays out the formulation for the Statistical Associating Fluid Theory (SAFT). The mathematical expressions for various bulk thermodynamic terms and also the multiphase equilibrium flash algorithm as implemented in UTCOMP a numerical reservoir simulator into which the SAFT model has been currently merged are also discussed in this chapter. Chapter 4 provides phase behavior results for several binary and multi-component mixtures. In Chapter 5 the phase behavior of gas condensate-methanol-water mixtures is studied. In



Chapter 6 the concepts of associating fluids are extended to develop models for interfacial tension. In Chapter 7 results and discussion for the interfacial tension model applied to pure components and mixtures are provided. In Chapter 8 the equations required for using SAFT equation in a flow simulation are presented. A few example flow simulations with the SAFT equation of state for hydrocarbon mixtures are also presented in this chapter.

## CHAPTER 2

### LITERATURE SURVEY

#### 2.1 CLASSICAL EQUATIONS OF STATE

Equations of state that have been proposed in the literature generally have limitations with regard to the range of temperatures and pressures in which they are applicable and the fluids that they can be used to model. Some equations are better for PVT relations, others for phase equilibria, and still others for enthalpy or entropy deviations. Cubic equations of state that are explicit in pressure and third degree in volume are among the most successful of the simpler forms. van der Waals [1], Redlich-Kwong [2] and Peng-Robinson equations of state [3,4] are some of the successful equations in this class. The advantages of these equations are that they are easy to implement in computer programs for repeated evaluations of properties. The van der Waals and Redlich-Kwong equations are not applicable to liquid phases and the Peng-Robinson equation does not do well for low temperatures and for polar compounds. The Benedict-Webb-Rubin [5,6] EOS is one of the equations that successfully predicts behavior under cryogenic conditions. The Lee-Kesler [7] equation has been shown to predict enthalpy deviations very well.

For liquids, activity coefficient models have been shown to be quite successful. The group contribution method has been developed for calculation of activity coefficients. In this method the activity coefficient is considered to be the sum of the contributions of each individual group and the interaction between two groups as determined by matching the experimental phase equilibrium data. These methods have been shown to do well for polar compounds as well, but only for low pressure systems [7]. The UNIFAC model is the most popular group contribution method [8-9].

## **2.2 SAFT EQUATION OF STATE**

The other main class of equations is those based on intermolecular potentials. These are based on the viewpoint that the bulk properties of substances are a result of properties of individual molecules and interactions between them. Molecularly based equations allow for separating and quantifying the effects of molecular structure and interactions on bulk properties and phase behavior. Examples of such effects are the molecular size and shape(e.g., chain length), association(e.g., hydrogen bonding) energy, and mean field (e.g., dispersion and induction) energy. In the next section we provide some basic concepts of obtaining the macroscopic thermodynamic properties from the information on molecular forces which falls under the domain of microthermodynamics.

## 2.3 MICROTHERMODYNAMICS

Microthermodynamics is the interpretation of macroscopic thermodynamic properties in terms of the molecular potential functions [10]. The basic idea is that if we know the spatial distributions of molecules as well as the interaction energy among them, we could sum the energies between the molecules over the intermolecular distances, as given by the distribution, to obtain the total energy. We construct the canonical ensemble for the calculation of the energy. As we shall see, for all practical purposes only the pair, and, sometimes the triplet correlation functions are needed for a full determination of the thermodynamic properties. Higher order correlations are rarely required.

As an example, the internal energy arises due to the interaction forces among the molecules within the system. The differential relation in the canonical ensemble as

$$U = \langle E \rangle = - \left. \frac{\partial \ln Z_N}{\partial \beta} \right|_{V, N} \quad (2.1)$$

For pair-wise additive potentials the partition function is given as,

$$Z_N = \frac{1}{N! \Lambda^{3N}} \int dr_1 \dots dr_N \exp[-\beta \sum_{i < j}^N u(r_{ij})] \quad (2.2)$$

Carrying out the differentiation with respect to  $\beta$ , we get

$$-\left. \frac{\partial \ln Z_N}{\partial \beta} \right|_{V,N} = \frac{-1}{Z_N} \left( \frac{1}{N! \Lambda^{3N}} \int d\mathbf{r}^N \left[ - \sum_i \sum_j^N u(r_{ij}) \right] \exp(-\beta V_N) - \frac{3NZ_N}{\Lambda} \frac{\partial \Lambda}{\partial \beta} \right) \quad (2.3)$$

For identical particles,  $u(r_{ij}) = u(r_{km})$  for all  $i, j, k$ , and  $m$  as long as  $r_{ij} = r_{km}$ . There are  $N(N-1)/2$  distinct pairs in the summation. Thus we have

$$U = \frac{1}{Q_N} \frac{N(N-1)}{2} \int d\mathbf{r}_1 d\mathbf{r}_2 \dots d\mathbf{r}_N u(r_{12}) e^{-\beta V_N} + \frac{3N}{\Lambda} \frac{\partial \Lambda}{\partial \beta} \quad (2.4)$$

Since  $\Lambda$  the de Broglie wavelength is given as

$$\Lambda = h\beta^{1/2} (2\pi m)^{-1/2} \quad (2.5)$$

$$\frac{\partial \Lambda}{\partial \beta} = \frac{\Lambda}{2\beta} \quad (2.6)$$

Also noting that

$$\rho^{(2)}(r_1, r_2) = \frac{1}{Q_N} \frac{N(N-1)}{2} \int d\mathbf{r}_3 d\mathbf{r}_4 \dots d\mathbf{r}_N e^{-\beta V_N} \quad (2.7)$$

We have

$$U = \frac{3}{2} NkT + \frac{1}{2} \int_V d\mathbf{r}_1 \int_V d\mathbf{r}_2 u(r_{12}) \rho^{(2)}(r_1, r_2) \quad (2.8)$$

For an isotropic and homogeneous fluid

$$\rho^{(2)}(r_1, r_2) = \rho^2 g^{(2)}(r_1, r_2) = \rho^2 g^{(2)}(r_{12}) \quad (2.9)$$

and

$$\int dr_1 dr_2 = \int dr_1 dr_{12} = V \int dr_{12} \quad (2.10)$$

So the equation for internal energy is

$$\frac{U}{NkT} = \frac{3}{2} + \frac{\rho}{2kT} \int_0^{\infty} dr_{12} 4\pi r_{12}^2 u(r_{12}) g^{(2)}(r_{12}) \quad (2.11)$$

The upper limit can be taken to be infinity when the intermolecular forces are short ranged in comparison to the macroscopic dimensions. The above equation shows that the macroscopic energy can be obtained in terms of the molecular pair potential ( $u(r_{12})$ ) and the radial distribution function ( $g(r_{12})$ ), which are both microscopic two-body functions. A similar procedure can be used to obtain other macroscopic thermodynamic properties.

## 2.4 LIQUID THEORIES BASED ON HARD SPHERE MODEL

The relation between inter-molecular interactions and bulk properties of the system has been established in the previous section. In statistical mechanics the structure of a liquid is expressed in terms of a molecular radial distribution function. These distribution functions give the time averaged spatial configuration of the molecules in the liquid. The radial distribution function is obtained from the

knowledge of the intermolecular pair potential using, for example, the integral equation theories. The simplest pair potential model is to assume that the fluid is made up of hard spheres. By studying the exact molecular dynamics results for hard-sphere fluids Carnahan and Starling [11] were able to propose an accurate equation for the radial distribution function. Knowing the radial distribution function other thermodynamic properties can be evaluated. The basic idea is that once the spatial distribution of molecules as well as the interaction energies among them is known, the total energy is obtained as the summation of the energies between the molecules.

## **2.5 PERTURBATION THEORY FOR DISPERSION FORCES**

In the previous section a simple model of hard-spheres was mentioned. In reality the interaction potentials are more complicated. For example, most real gases are polar or multi-polar: carbon dioxide is quadrupolar, and hydrogen chloride is both dipolar and quadrupolar. In addition, polyatomic molecules are nonspherical: the breadth-to-length ratio of bromine is 0.547, and that of carbon disulfide is about 0.9. All these factors influence the physical properties of the substance. A simple spherically symmetric potential function cannot adequately describe these effects. However, simpler models could serve as reference potentials, and the additional effects, such as quadrupolar forces, could be treated as perturbations on the reference systems. In principle, when the reference system chosen is close to the final system, one would also expect the properties produced

by adding the perturbations to be close to the final system. This is the basis of the perturbation approach. The general theory of perturbation methods was first clearly described by Zwanzig[12]. The dispersion term used in this study is a power series initially fitted by Alder et al. [13]. This equation also provided the basis for the Perturbed Hard Chain Theory of Beret and Prausnitz [14] and by Chen and Kreglewski [15] in their equation of state, and was extended to mixtures by Simnick et al. [16].

## **2.6 MODELS FOR ASSOCIATION EFFECTS**

### **2.6.1 Early Models**

As mentioned in the previous section, perturbation theories give accurate results when the reference system chosen is close to the real pair potential. In the case of molecules with specific directional associating sites such as alkanols, water and acids the simple hard sphere reference fluid proposed earlier is inadequate. There have been many attempts in the past to model association effects in fluid phase equilibria. The best known concepts in association bonding is the chemical theory of Dolezalek [17], which postulates the existence of distinct molecular species in solution, which are a result of chemical reactions assumed to be in a state of chemical equilibrium. This concept has been adopted in many approaches that usually utilize the chemical equilibrium constants involving the chemical entropy and enthalpy terms (in effect binary parameters) to allow for temperature dependence. These concepts are reviewed in Prausnitz et al. [18].



An alternative approach is that of lattice theories based on modeling the fluid structure as having essentially a solid-like lattice structure. Guggenheim [19] used the quasi-chemical approximation to treat non-random mixtures. Barker and Fock [20] used this theory for model mixtures. Several lattice models have been proposed to determine the properties of mixtures of strongly interacting molecules. There are several equations of state based on lattice theories that are popular in chemical engineering. The activity coefficient models applicable to nonrandom associating solution, for example, the models of Wilson [21], Abrams and Prausnitz [22], and Renon and Prausnitz [23], are based on these ideas.

### **2.6.2 Statistical Mechanical Models**

A more promising route leading to an understanding of associating fluids involves theories based on statistical mechanics. One approach has been to introduce molecular association into commonly used integral equation theories. Cummins and Stell [24], solved the integral equation in the Percus-Yevick approximation for the chemical association  $A+B=AB$  by using a spherically symmetric bonding potential. The model can be solved analytically in the limit of an infinitesimally wide and infinitely deep potential well; no effect of bonding orientation is included in the theory. Later Cummins and Blum [25] examined the directional character of the interaction in a study of the model for water. The system was solved in the PY approximation for the limit of surface adhesion.

### 2.6.3 Wertheim's Association Model

Andersen was one of the first to introduce the geometry of the interaction at an early stage of the theory [26, 27]. He proposed a cluster (virial) expansion in terms of the total singlet number density ( $\rho$ ) similar to the conventional approaches in simple fluids for obtaining the grand canonical ensemble partition function. The virial coefficients in the density expansion are dependent on the intermolecular forces. The virial coefficients in the expansion are also referred to as graphs in the literature because of the use of pictorial graphs to represent the complex integration over volumes involved in these coefficients. The key concept in Andersen's model is that since the interaction is short-ranged and highly directional, the repulsive cores will restrict the system to single bonds at each attractive site. As a result many of the graphs in the expansion will be negligible. Although the incorporation of graph cancellation is cumbersome, Andersen's ideas have influenced later theories on associating fluids. Hoyer and Olaussen [28] extended Andersen's approach by using a cluster expansion in terms of the monomer density rather than in terms of the overall density. They find that such an approach leads to much faster convergence.

The next most important advancement in the modeling of associating fluids is by Wertheim [29-32]. Wertheim did the resummed cluster expansion in terms of two densities, the total number density and the monomer density. This

results in the applicability of the theory over a wide range of densities. Similar to Andersen, Wertheim was also able to simplify the complex graphical expansions by assuming that the repulsive core of each molecule restricts the orientation-dependent attractive forces to only single bonds at each attractive site. Some of the steric incompatibilities that result in graph cancellations are shown schematically in Figure 2.1 to Figure 2.3. The first type involves three molecules: when the sites A and B on molecules 1 and 2 respectively get sufficiently close to form a bond, then the repulsive cores of molecules 1, 2 and 3 prevent molecule 3 from coming close enough to bond to either site A or B (Figure 2.1). Another type of steric incompatibility prevents a site A on molecule 1 from bonding to two or more sites on molecules 2 (Figure 2.2). One can also restrict the bonding between molecules to single bonding (Figure 2.3).

Based on the graph cancellations discussed above, Wertheim was able to develop a key relationship between the residual Helmholtz energy due to association and the monomer density. This monomer density is related to a function  $\Delta$  characterizing the association strength. Initially Wertheim had developed this theory for systems with a single attractive site but later extended it to systems with multiple bonding sites. Wertheim's theory has been extended to mixtures of spheres [33].

## 2.7 CHAINS OF HARD SPHERES

The origin of the Helmholtz's free energy contribution due to formation of chains can be visualized as  $m$  hard spheres at contact formed by imposing strong, covalent-like bonds on the hard spheres. In contrast to Wertheim's model where each hard-sphere can have multiple associating sites, for chain-formation each hard sphere needs to have two covalent bond forming sites on each of the hard-spheres in the interior of the chain and one covalent-bonding site on the end segments of the chain. With this simplification Wertheim's theory can be applied to chain formation taking into account the strength of the covalent bond. Chapman et al., [34] have derived a simplified expression for chain formation on the basis of the above formalism.

## Nomenclature

$U$	internal energy (Joules)
$Z_N$	canonical partition function
$\beta$	inverse temperature $1/kT$ (1/Joules)
$k$	Boltzmann Constant (J/K)
$T$	temperature (K)
$\Lambda$	de Broglie wavelength (m)
$N$	number of particles
$u(r_{12})$	intermolecular potential function (Joules)
$V$	volume of the ensemble ( $m^3$ )
$M$	molecular weight
$r_i$	radial distance (m)
$\rho$	singlet density ( $/m^3$ )
$\rho^{(2)}(r_1, r_2)$	two body correlation function ( $/m^6$ )
$g^{(2)}(r_{12})$	radial distribution function

## References

- 1) van der Waals, J.H, *Continuity of the Gaseous and Liquid State of Matter*, (1873).
- 2) Redlich, O., and Kwong, J.N.S., “On the Thermodynamics of Solutions. V. An Equation of State. Fugacities of Gaseous Solutions”, *Chem. Review.*, **44**, 233 (1949).
- 3) Peng, D.Y., and Robinson, D.B.;; “A New Two Constant Equation of State”, *Ind. Eng. Chem. Fundamen.*, **15**, 59 (1976).
- 4) Peng, D.Y., and Robinson, D.B.;; “The Characterization of Heptanes and Heavier Fractions for the GPA Peng-Robinson Programs”, *Ind. Eng. Chem. Fundamen.*, **15**, 59 (1976).
- 5) Benedict, M., Webb, G.B., and Rubin, L.C., “An Empirical Equation for Thermodynamic Properties of Light Hydrocarbons and their Mixtures. I. Methane, Ethane, Propane and n-Butane”, “An Empirical Equation for Thermodynamic Properties of Light Hydrocarbons and their Mixtures. I. Mixtures of Methane, Ethane, Propane and n-Butane”,*J. Chem. Physics.*, **8**, 334 (1940); **10**, 747 (1942).
- 6) Benedict, M., Webb, G.B., and Rubin, L.C., “An Empirical Equation for Thermodynamic Properties of Light Hydrocarbons and their Mixtures. Constants for twelve Hydrocarbons”, *Chem. Eng. Progress*, **47(8)**, 419 (1951); “Thermodynamic Properties of Light Hydrocarbons – Fugacities and Liquid-Vapor Equilibria”, **47(9)**, 449 (1951).
- 7) Lee, B.I., and Kesler M.G., “A Generalized Thermodynamic Correlation based on three-parameter Corresponding States”, *AIChE Journal*, **21**, 510 (1975).
- 8) Chao, K.C., and Seader, J.D., “A General Correlation of Vapor-Liquid Equilibria in Hydrocarbon Mixtures”, *AIChE Journal*, **7**, 598 (1961).
- 9) Fredenslund, A.M ., Gmehling J., Michlsen, M.L., Ramussen P., and Prausnitz., “Computerized Design of Multicomponent Distillation Columns using the UNIFAC Group Contribution Method for calculation of Activity Coefficients”, *Ind. Eng. Chem. Process Des. Dev.*, **16**, 450 (1977).

- 10) Lee, L.L., *Molecular Thermodynamics of Non Ideal Fluids*, Butterworth Publishers, 1988.
- 11) Carnahan, N. F., and Starling, K. E.,: “Equation of State for Nonattracting Rigid Spheres”, *J. Chem. Phys.*, **51**, 635 (1969).
- 12) Zwanzig R. W., “High temperature Equation of State by a Perturbation Method. I. Nonpolar Gases”, *J. Chem. Phys.*, **22**, 1420 (1954).
- 13) Alder, B.J., Young, D.A., and Mark, M.A., “Studies in Molecular Dynamics. X. Corrections to the Augmented van der Waals theory for the Square Well Fluid”, *J. Chem. Phys.*, **56**, 3013 (1972).
- 14) Beret, S., and Prausnitz, J.M., “Perturbed Hard-Chain Theory: An Equation of State for Fluids containing Small or Large Molecules”, *AIChE J.* **21**, 1123 (1975).
- 15) Chen, S.S., and Kreglewski, A.,: “Application of the Augmented van der Waals Theory of Fluids. I. Pure Fluids”, *Ber. Bunsen-Ges. Phys. Chem.*, **81**, 1048 (1977).
- 16) Simnick, J.J., Lin, H.M., and Chao, K.C., *Adv. Chem. Ser.*, **182**, 209 (1979).
- 17) Dolezalek, F. Z., : “Theorie der Binaren Gemische und Konzentrierten Loungen”, *Z. Phys. Chem.*, **64**, 727(1908).
- 18) Prausnitz, J.M., Lichtenthaler, R.N., De Azevedo, E.G., *Molecular Thermodynamics of Fluid Phase Equilibria*, Prentice-Hall:Englewood Cliffs, NJ, 1986.
- 19) Guggenheim, E.A., *Applications of Statistical Mechanics*, Oxford University Press, Oxford, U.K., 1955.
- 20) Barker, J.A., and Fock, W., *Discuss. Faraday Soc.*, **15**, 188 (1953).
- 21) Wilson, G.M.,: “Vapor-Liquid Equilibrium. XI. A New Expression for the Excess Free Energy of Mixing”, *J. Am. Chem. Soc.*, **86**, 127 (1964).
- 22) Abrams, D., and Prausnitz, J.M.,: “Statistical Thermodynamics of Liquid Mixtures: A New Expression for the Excess Gibbs Energy of Partly or Completely Miscible Systems”, *AIChE J.*, **21**, 116 (1975).

- 23) Renon, H., and Prausnitz, J.M.: "Local Compositions in Thermodynamic Excess Functions for Liquid Mixtures", *AIChE J.*, **14**, 135 (1968).
- 24) Cummins, P.T., and Stell, G. S.: "Statistical Mechanical Models of Chemical Reactions: Analytic Solution of Models of  $A+B = AB$  in the Percus-Yevick Approximation", *Molec. Phys.*, **51**, 253 (1984).
- 25) Cummins, P.T., and Blum, L.: "Analytical Solution of the Molecular Ornstein-Zernike Equation for Nonspherical Molecules. Spheres with Anisotropic Surface Adhesion", *J. Chem. Phys.*, **84**, 1833 (1986).
- 26) Andersen, H.C.: "Cluster Expansions for Hydrogen Bonded Fluids. I. Molecular Association in Dilute Gases", *J. Chem. Phys.*, **59**, 4714 (1973).
- 27) Andersen, H.C.: "Cluster Expansions for Hydrogen Bonded Fluids. II. Dense Liquids", *J. Chem. Phys.*, **61**, 4985 (1974).
- 28) Hoye, J.S., and Olaussen, K., *Physica A.*, **104**, 435 (1980).
- 29) Wertheim, M.S.: "Fluids with Highly Directional Attractive Forces. I. Statistical Thermodynamics", *Journal of Statistical Physics*, **35**,1,19 (1984).
- 30) Wertheim, M.S.: "Fluids with Highly Directional Attractive Forces. II. Thermodynamic Perturbation Theory and Integral Equations", *Journal of Statistical Physics*, **35**,1,35 (1984).
- 31) Wertheim, M.S.: "Fluids with Highly Directional Attractive Forces. III. Multiple Attraction Sites", *Journal of Statistical Physics*, **42**, **3**, 459(1986).
- 32) Wertheim, M.S.: "Fluids with Highly Directional Attractive Forces. III. Equilibrium Polymerization", *Journal of Statistical Physics*, **42**,**3**, 477(1986).
- 33) Jackson G., Chapman, W.G., and Gubbins K.E.: "Phase equilibria of associating fluids: Spherical molecules with multiple bonding sites", *Molecular Physics*, **65**, **1**,1 (1988).
- 34) Chapman, W.G., Jackson G., and Gubbins K.E., : "Phase equilibria of associating fluids: Chain molecules with multiple bonding sites", *Molecular Physics*, **65**, **5**,1057 (1988).



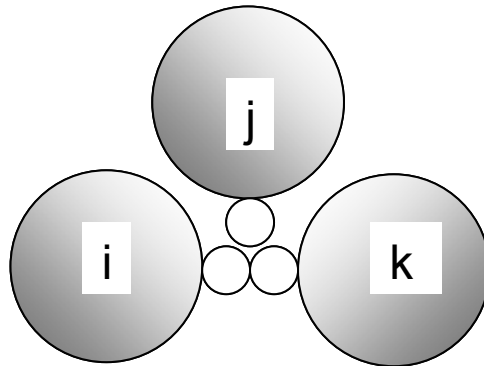


**Figure 2.1: Only two molecules can form a bond at a single associating site**

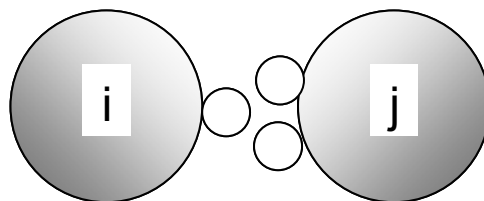


**Figure 2.2: No site on one molecule bond simultaneously to two sites on another molecule**

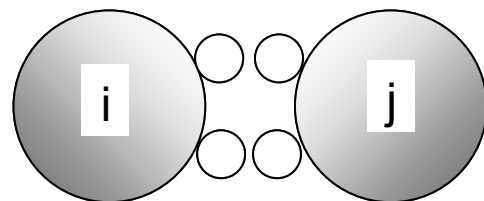


**Figure 2.3: Double bonding between molecule is not allowed**

## CHAPTER 3

### SAFT EQUATION OF STATE FOR MULTICOMPONENT MIXTURES

Ideally, a single equation of state should incorporate all the effects described in Chapter 2. Chapman et al., [1,2] proposed such an equation of state. The essence of their approach, referred to as the Statistical Associating Fluid Theory (SAFT) is to use a reference fluid that incorporates both chain formation and association bonding, in place of the much simpler hard sphere reference fluid used in most existing engineering equations of state.

The theoretical results underlying the equation of state are given in this section which is expressed in terms of the residual Helmholtz energy  $a^{\text{res}}$  per mole, defined as  $a^{\text{res}}(T,V,N)=a^{\text{total}}(T,V,N) - a^{\text{ideal}}(T,V,N)$ , at the same temperature and density. All other thermodynamic quantities can be derived following a standard procedure as described, for example, by Topliss [3].

The residual Helmholtz energy is a sum of reference and dispersion parts:

$$a^{\text{res}} = a^{\text{ref}} + a^{\text{disp}} \quad (3.1a)$$

$$a^{\text{ref}}(T,V,N) = a^{\text{hs}}(T,V,N) + a^{\text{chain}}(T,V,N) + a^{\text{assoc}}(T,V,N) \quad (3.1b)$$

### 3.1 MIXTURES OF HARD SPHERES

The hard sphere term used is based on a theoretical result obtained by Mansoori et al. [4]. The Helmholtz energy is given by,

$$\frac{a^{hs}}{RT} = \frac{6}{\pi\rho} \left[ \frac{(\zeta_2)^3 + 3\zeta_1\zeta_2\zeta_3 - 3\zeta_1\zeta_2(\zeta_3)^2}{\zeta_3(1-\zeta_3)^2} - \left\{ \zeta_0 - \frac{(\zeta_2)^3}{(\zeta_3)^2} \right\} \ln(1-\zeta_3) \right] \quad (3.2)$$

$\zeta_k$  ( $k = 0$  to  $3$ ) are functions of the molar density  $\rho$ . Since the reference fluid considered here contains hard spheres, which can be bonded to form chains, we use the  $\zeta$  functions proposed by Chapman et al. [2], which are applicable to bonded spheres:

$$\zeta_k = (\pi / 6) \rho \sum x_i m_i (d_i)^k \quad (3.3)$$

where  $x$  is the mole fraction,  $m_i$  is the number of segments(hard-spheres) per molecule, and  $d_i$  is the effective, temperature-dependent segment diameter.

The temperature dependence of the segment diameter  $d_i$  in the above equation is given based on the Barker-Henderson approach [5]. The equation used for  $d_i$  is given below based on the work of Chen and Kreglewski [6], who obtained  $d_i$  by solving the Barker-Henderson integral equation

$$d_i = \int_{\sigma}^{\infty} [1 - \exp(-u(r)/kT)] dr \quad (3.4)$$

using a square-well potential. The final expression for  $d$  is

$$d_i = \sigma \left[ 1 - C \exp \left[ \frac{-3u^0}{kT} \right] \right] \quad (3.5)$$

$u^0 / k$  (in Kelvin) in the above equation is the well depth, a temperature-independent LJ energy parameter, characteristic of nonspecific segment-segment interactions which will be referred to as the segment energy. Following Chen and Kreglewski, the integration constant  $C$  is set to 0.12.

We note that for pure components, Equation 3.2 reduces to

$$\frac{a^{hs}}{RT} = m \frac{a_0^{hs}}{RT} \quad (3.6)$$

where the hard-sphere term for pure segments  $a_0$ , is that proposed by Carnahan and Starling [7]:

$$\frac{a_0^{hs}}{RT} = \frac{4\zeta_3 - 3\zeta_3^2}{(1 - \zeta_3)^2} \quad (3.7)$$

where  $\zeta_3$  is a segment packing fraction (reduced density):

$$\zeta_k = (\pi / 6) \rho m d^3 \quad (\text{pure components}) \quad (3.8)$$

Mansoori et al. [4], have also derived the pair correlation function for a mixture of hard spheres (which can be approximated for hard segments), which shall be invoked later:

$$g_{ij}(d_i, d_j)^{\text{seg}} = g_{ij}(d_i, d_j)^{\text{hs}} = \frac{1}{1-\zeta_3} + \frac{3d_i d_j}{d_i + d_j} \frac{\zeta_2}{(1-\zeta_3)^2} + 2 \left[ \frac{d_i d_j}{d_i + d_j} \right]^2 \frac{\zeta_2^2}{(1-\zeta_3)^3} \quad (3.9)$$

$$g_{ii}(d_i)^{\text{seg}} = g_{ii}(d_i)^{\text{hs}} = \frac{1}{1-\zeta_3} + \frac{3d_i}{2} \frac{\zeta_2}{(1-\zeta_3)^2} + 2 \left[ \frac{d_i}{2} \right]^2 \frac{\zeta_2^2}{(1-\zeta_3)^3} \quad (3.10)$$

The hard-segment distribution function in the above equations depends on the effective sphere diameter  $d_i$  and on  $\zeta_k$  (Equation 3.3).

The corresponding expression for the chemical potential due to the hard-sphere term for mixtures is given by [8].

$$\begin{aligned} \frac{\mu_i^{\text{hs}}}{kT} = & -\ln(1-\zeta_3) + \frac{\Pi P_{\text{CS}}^{\text{hs}} d_i^3}{6kT} + \frac{3\zeta_2 d_i}{1-\zeta_3} + \frac{3\zeta_1 d_i^2}{1-\zeta_3} + \frac{9\zeta_2^2 d_i^2}{2(1-\zeta_3)^2} \\ & + 3 \left( \frac{\zeta_2 d_i}{\zeta_3} \right)^2 \left[ \ln(1-\zeta_3) + \frac{\zeta_3}{1-\zeta_3} + \frac{\zeta_3^2}{2(1-\zeta_3)^2} \right] - \left( \frac{\zeta_2 d_i}{\zeta_3} \right)^3 \left[ 2\ln(1-\zeta_3) + \frac{\zeta_3(2-\zeta_3)}{1-\zeta_3} \right] \end{aligned} \quad (3.11)$$

where  $P_{\text{CS}}^{\text{hs}}$  is the contribution to the pressure from the hard-sphere terms. For mixtures, the Carnahan-Starling radial distribution function gives the hard-sphere contribution to pressure as [8],

$$P_{\text{CS}}^{\text{hs}} = \frac{6kT}{\Pi} \left[ \frac{\zeta_0}{1-\zeta_3} + \frac{3\zeta_1 \zeta_2}{(1-\zeta_3)^2} + \frac{3\zeta_2^3}{(1-\zeta_3)^3} - \frac{\zeta_3 \zeta_2^3}{(1-\zeta_3)^3} \right] \quad (3.12)$$

Note that the above expression for pressure includes the ideal-gas part as well. Hence the compressibility contribution from only hard-spheres ( $z^{\text{hs}}$ ) is,

$$z^{\text{hs}} = m (z_0^{\text{hs}} - 1) \quad (3.13)$$

and  $z_0^{\text{hs}}$  is given as,

$$z_0^{\text{hs}} = \frac{P_{\text{CS}}^{\text{hs}}}{m\rho kT} \quad (3.14)$$

For pure components, the corresponding expressions for the hard sphere part are,

$$\mu^{\text{hs}} = m(RT) \left[ \frac{4\zeta_3 - 3\zeta_3^2}{(1 - \zeta_3)^2} + \frac{4\zeta_3 - 2\zeta_3^2}{(1 - \zeta_3)^3} \right] \quad (3.15)$$

and

$$z^{\text{hs}} = m \frac{4\zeta_3 - 2\zeta_3^2}{(1 - \zeta_3)^3} \quad (3.16)$$

### 3.2 MIXTURE OF CHAINS

The pair correlation function given by Equation 3.9 is used to determine the Helmholtz energy contribution due to chain formation:

$$\frac{a^{\text{chain}}}{RT} = \sum x_i (1 - m_i) \ln(g_{ii}(d_i)^{\text{hs}}) \quad (3.17)$$

where  $g_{ii}$  is evaluated for the interaction of two spheres  $i$  in a mixture of spheres, evaluated at the hard-sphere contact. Equation 3.17 has been derived on the basis of the associating fluid theory, where the association bonds are replaced by covalent, chain-forming bonds, as given by Chapman et al. [1,2].

The corresponding expression for chemical potential is given by,

$$\frac{\mu_i^{\text{chain}}}{RT} = (1 - m_i) \ln(g_{ii}(d_i)^{\text{hs}}) + \sum_j x_j \rho (1 - m_j) \left[ \frac{\partial \ln g_{jj}(d_j)^{\text{hs}}}{\partial \rho_i} \right]_{T, \rho_{j \neq i}} \quad (3.18)$$

where the partial derivative of the pair correlation function is given by

$$\begin{aligned} & \left[ \frac{\partial \ln g_{jj}(d_j)^{\text{hs}}}{\partial \rho_i} \right]_{T, \rho_{j \neq i}} \\ &= \frac{\Pi}{6} \frac{m_i}{g_{jj}(d_j)^{\text{hs}}} \left[ \frac{d_i^3}{(1 - \zeta_3)^2} + \frac{3 d_j d_i^2}{2 (1 - \zeta_3)^2} + \frac{3 d_j d_i^3 \zeta_2}{(1 - \zeta_3)^3} + \frac{d_j^2 d_i^2 \zeta_2}{(1 - \zeta_3)^3} + \frac{3 d_j^2 d_i^3 \zeta_2^2}{2 (1 - \zeta_3)^4} \right] \end{aligned} \quad (3.19)$$

Similarly the contribution to the compressibility factor is given as

$$Z^{\text{chain}} = \sum_i x_i (1 - m_i) \rho \left[ \frac{\partial \ln g_{ii}(d_i)^{\text{hs}}}{\partial \rho} \right]_{T, x_j} \quad (3.20)$$

where

$$\rho \left[ \frac{\partial \ln g_{ij}(\mathbf{d}_j)^{hs}}{\partial \rho} \right]_{T,x_j} \quad (3.21)$$

$$= \frac{1}{g_{ii}(\mathbf{d}_j)^{hs}} \left[ \frac{\zeta_3}{(1-\zeta_3)^2} + \frac{3}{2} \frac{d_i \zeta_2}{(1-\zeta_3)^2} + \frac{3d_i \zeta_2 \zeta_3}{(1-\zeta_3)^3} + \frac{d_i^2 \zeta_2^2}{(1-\zeta_3)^3} + \frac{3}{2} \frac{d_i^2 \zeta_2^2 \zeta_3}{(1-\zeta_3)^4} \right]$$

### 3.3 MIXTURE OF ASSOCIATING SPHERES

The Helmholtz energy due to association, for pure components is given by Huang and Radosz [9], and is given for mixtures by Chapman et al., [2] and Huang and Radosz [9].

$$\frac{a^{assoc}}{RT} = \sum_i x_i \left[ \sum_{A_i} \left[ \ln Y^{A_i} - \frac{Y^{A_i}}{2} \right] + \frac{1}{2} M_i \right] \quad (3.22)$$

where  $Y^{A_i}$ , the mole fraction of molecules  $i$  not bonded at site  $A$ , in mixture with other components, is given by,

$$Y^{A_i} = \left[ 1 + \sum_i \sum_{B_j} \rho_j Y^{B_j} \Delta^{A_i B_j} \right]^{-1} \quad (3.23)$$

where  $\sum_{B_j}$  is the summation over all sites on molecule  $j$ :  $A_j, B_j, C_j$  etc., and  $\sum_i$  means summation over all components.



It is seen that  $Y_i^A$  depends on the molar density  $\rho_j$ :

$$\rho_j = x_j \rho_{\text{mix}} \quad (3.24)$$

and on the association strength  $\Delta_{ij}^{A,B}$ :

$$\Delta_{ij}^{A,B_j} = g_{ij}(d_j, d_j)^{\text{seg}} \left[ \exp(\varepsilon^{A,B_j} / k T) - 1 \right] (\sigma_{ij})^3 \kappa^{A,B_j} \quad (3.25)$$

where  $\sigma_{ij} = (\sigma_{ii} + \sigma_{jj}) / 2$ . The segment radial distribution function in the above equation is approximated from Equation. 3.9. The association bonding for mixtures in certain is given by:

$$\varepsilon^{A,B_j} = \sqrt{\varepsilon^{A_i} \varepsilon^{B_j}} \quad (3.25a)$$

$$\kappa^{A,B_j} = (1 - a_{ij}) \sqrt{\kappa^{A_i} \kappa^{B_j}} \quad (3.25b)$$

The term  $a_{ij}$  is known as the associating interaction coefficient and is similar to the binary interaction coefficient used for non-polar mixtures.

The association contribution to the chemical potential  $\mu_i^{\text{assoc}}$

$$\frac{\mu_i^{\text{assoc}}}{RT} = \sum_{A_i} \left[ \ln Y^{A_i} - \frac{Y^{A_i}}{2} \right] + \frac{1}{2} M_i + \sum_j \rho_j \left[ \sum_{A_j} \left( \frac{\partial Y^{A_j}}{\partial \rho_i} \right)_{T, \rho_{j \neq i}} \left[ \frac{1}{Y^{A_j}} - \frac{1}{2} \right] \right]$$

(3.26)

$$\begin{aligned} & \left[ \frac{\partial Y^{A_j}}{\partial \rho_i} \right]_{T, \rho_{l \neq i}} \\ &= -(Y^{A_j})^2 \left[ \sum_{B_i} Y^{B_i} \Delta^{A_j B_i} + \sum_k \sum_{B_k} \rho_k \left[ \Delta^{A_j B_k} \left( \frac{\partial Y^{B_k}}{\partial \rho_i} \right)_{T, \rho_{l \neq i}} + Y^{B_k} \left( \frac{\partial \Delta^{A_j B_k}}{\partial \rho_i} \right)_{T, \rho_{l \neq i}} \right] \right] \end{aligned} \quad (3.27)$$

and

$$\left[ \frac{\partial \Delta^{A_j B_k}}{\partial \rho_i} \right]_{T, \rho_{l \neq i}} = \left( \frac{d_j + d_k}{2} \right)^3 \left[ \frac{\partial g_{jk}(d_j, d_k)}{\partial \rho_i} \right]_{T, \rho_{l \neq i}} [\exp(\varepsilon^{A_j B_k} / kT) - 1] \kappa^{A_j B_k} \quad (3.28)$$

$$\begin{aligned} \left[ \frac{\partial g_{jk}(d_j, d_k)^{hs}}{\partial \rho_i} \right]_{T, \rho_{l \neq i}} &= \frac{\pi}{6} m_i \left[ \frac{d_i^3}{(1-\zeta_3)^2} + 3 \left( \frac{d_j d_k}{d_j + d_k} \right) \left[ \frac{d_i^2}{(1-\zeta_3)^2} + \frac{2d_i^3 \zeta_2}{(1-\zeta_3)^3} \right] \right. \\ &\quad \left. + 2 \left( \frac{d_j d_k}{d_j + d_k} \right)^2 \left[ \frac{2d_i^2 \zeta_2}{(1-\zeta_3)^3} + \frac{3d_i^3 \zeta_2^2}{(1-\zeta_3)^4} \right] \right] \end{aligned} \quad (3.29)$$

The corresponding expression for the compressibility factor due to association is

$$Z^{\text{assoc}} = \sum_i x_i \frac{\mu_i^{\text{assoc}}}{RT} - \frac{a^{\text{assoc}}}{RT} \quad (3.30)$$

### 3.4 DISPERSION TERM

A general expression for the dispersion term is

$$\frac{a^{\text{disp}}}{RT} = m \frac{a_0^{\text{disp}}}{RT} \quad (3.31)$$

where  $m$  is the segment number and  $a_0^{\text{disp}}$  is the dispersion Helmholtz energy, per mole of segments. The  $a_0^{\text{disp}}$  term is a function of the segment energy  $u / kT$  [9].

$$\frac{a_0^{\text{disp}}}{RT} = \sum_j \sum_k D_{jk} \left[ \frac{u}{kT} \right]^j \left[ \frac{\zeta_3}{\tau} \right]^k \quad (3.32)$$

where  $D_{jk}$  are universal constants. In this work  $D_{jk}$  that have been refitted to accurate PVT, internal energy and second virial coefficient data for argon, by Chen and Kreglewski [6] have been used.  $\tau=0.74048$  is the segment volume fraction in a close-packed arrangement. Hence, there are two parameters in the dispersion term,  $u/kT$  and  $m$  that have to be generalized for mixtures.

The mixing rule of the conformal solution [10], van der Waals one-fluid theory (vdW1) is used. It defines the molecular energy and size (volume) of a hypothetical pure fluid having the same residual properties as the mixture of interest. The vdW1 averaging equations are:

$$\frac{u}{kT} = \frac{\sum_i \sum_j x_i x_j m_i m_j \left[ \frac{u_{ij}}{kT} \right] (v^0)_{ij}}{\sum_i \sum_j x_i x_j m_i m_j (v^0)_{ij}} \quad (3.33)$$

$$(v^0)_{ij} = \left[ \frac{1}{2} [(v^0)_i^{1/3} + (v^0)_j^{1/3}] \right]^3 \quad (3.34)$$

$$u_{ij} = (1 - k_{ij})(u_{ii} u_{jj})^{1/2} \quad (3.35)$$

where  $k_{ij}$  is an empirical binary parameter, fitted to experimental data.

The temperature dependence of  $u$  as given by Chen and Kreglewski, [6]

$$u = u^0 \left[ 1 + \frac{e}{kT} \right] \quad (3.36)$$

and

$$v_i^0 = \frac{\Pi}{6\tau} d_i^3 \quad (3.37)$$

where  $e/k$  is a constant that was related to Pitzer's acentric factor and the critical temperature [6, 11] for various molecules. Since the energy parameter in this model is for segments rather than for molecules,  $e/k$  is set equal to 10 for all molecules. The only exceptions are a few small molecules where the  $e/k$  values close to those derived by Kreglewski have been used ( $e/k = 0$  for argon; 1 for

methane, ammonia, and water; 3 for nitrogen; 4.2 for CO; 18 for chlorine; 38 for CS<sub>2</sub>; 40 for CO<sub>2</sub>; and 88 for SO<sub>2</sub> ).

Since the segment volume parameters  $V^\infty$  and  $v^0$  are defined on a per-segment basis and hence do not vary much from molecule to molecule, especially for large molecules, we will use the segment number  $m$  as a measure of the molecular size. Therefore, our mixing rule for  $m$  (the average segment number for mixtures) is,

$$m = \sum_i \sum_j x_i x_j m_{ij} \quad (3.38)$$

where

$$m_{ij} = \frac{1}{2} (m_i + m_j) \quad (3.39)$$

The corresponding equation for the chemical potential is

$$\begin{aligned} \mu_i^{\text{disp}} = & m_i \sum_j \sum_k D_{jk} \left[ \frac{u}{kT} \right]^j \left[ \frac{\zeta_3}{\tau} \right]^k + m \sum_j \sum_k j D_{jk} \left[ \frac{u}{kT} \right]^{j-1} \frac{\partial}{\partial n_i} \left( \frac{u}{kT} \right) \left[ \frac{\zeta_3}{\tau} \right]^k \\ & + m \sum_j \sum_k k D_{jk} \left[ \frac{u}{kT} \right]^j \left[ \frac{\zeta_3}{\tau} \right]^{k-1} \frac{1}{\tau} \frac{\Pi}{6} m_i \rho d_i^3 \end{aligned} \quad (3.40)$$

The corresponding compressibility factor is

$$z^{\text{disp}} = m \sum_j \sum_k k D_{jk} \left[ \frac{u}{kT} \right]^j \left[ \frac{\zeta_3}{\tau} \right]^k \quad (3.41)$$

The equation of state can be presented as the compressibility factor terms  $Z$ . taking into account all the different contributions can then be written as

$$Z=1 + Z^{hs} + Z^{chain} + Z^{assoc} + Z^{disp} \quad (3.42)$$

and the pressure of the system is given as

$$P = Z \rho K T \quad (3.43)$$

The chemical potential of the system can be calculated as

$$\mu_i = \mu_i^{ideal} + \mu_i^{hs} + \mu_i^{chain} + \mu_i^{assoc} + \mu_i^{disp} \quad (3.44)$$

The chemical potential contribution due to the ideal part  $\mu_i^{ideal}$  is given by Reed and Gubbins [8].

$$\mu_i^{ideal} = RT \ln(\rho x_i) \quad (3.45)$$

The above expressions have been used to correlate vapor-liquid equilibria for many real fluid mixtures.

### 3.5 MULTIPHASE EQUILIBRIUM ALGORITHM

Much of the difficulty in multiphase equilibrium calculations lies in determining how many equilibrium phases should be considered. The algorithm described here for the phase equilibrium calculation is a sequential process. Initially, the overall composition of the mixture is tested for stability. If the mixture is found unstable, a phase is added, now making a two-phase mixture, and a calculation is initiated to find the compositions of the two, assumed, equilibrium phases. Had the stability analysis indicated that the mixture of overall composition was stable, no further calculations would be done, i.e., we would conclude that a single-phase equilibrium mixture exists.

After the compositions of the two phases have been calculated, the stability of one of these phases is tested. If the stability analysis indicates that the phase is stable, it is concluded that the proper equilibrium state requires only two phases. If, however, the indication is that the phase is unstable, a third phase is added and a calculation is begun to find the equilibrium compositions of this, now, three-phase mixture. A phase is added one at a time and only as necessary.

In summary then, the algorithm implemented here uses a sequential procedure outlined by the following steps:

Step 1: Test the overall composition,  $z$ , for phase stability.

Step 2: If unstable, add a second phase and compute the compositions assuming two-phase equilibrium.

Step 3: Test the stability of the composition of one of the phases calculated in Step (2).

Step 4: If the phase composition is unstable, add a third phase and compute phase compositions assuming three-phase equilibrium.

If phase stability calculations show a phase composition to be stable, either in Step(1) or Step(3) no further calculations are required. The following sections explain Step 1 (phase stability analysis) and the Step 2 the (flash algorithm) in detail.

### 3.5.1 Phase Stability Analysis

A stability analysis calculation for a mixture with overall hydrocarbon composition  $z$  is a search for a trial phase, taken from the overall mixture that, when combined with the remainder of the mixture, gives a value of Gibbs free energy that is lower than a single phase mixture of overall hydrocarbon composition,  $z$ . Mathematically, this condition is written as

$$\Delta G = \sum_{i=1}^{n_c} n_i [ \mu_i(\vec{y}) - \mu_i(\vec{z}) ] \quad (3.46)$$

Where  $\mu_i$  is the chemical potential of component  $i$  and  $\vec{y}$  is the mole fraction corresponding to the mole numbers  $\vec{n}$ . Substituting fugacity coefficients in terms of  $\mu_i$  results in a more usable expression of the change in free energy



$$\Delta G = \sum_{i=1}^{n_c} n_i [ \ln y_i + \ln \phi_i(\vec{y}) - \ln z_i + \ln \phi_i(\vec{z}) ] \quad (3.47)$$

where  $\vec{y}$  and  $\vec{z}$  are the mole fraction compositions corresponding to the mole numbers  $\bar{n}$  and the test compositions.

If for any set of mole fractions the value of  $\Delta G$  at constant temperature and pressure is greater than zero, then the phase will be stable. If a set of mole fractions can be found such that  $\Delta G < 0$ , the phase will be unstable. The following is an algorithm for minimization of the free energy.

### 3.5.2 Method of Stationary Point Locations

Michelsen [12] reasoned that not all values of the phase space are important. In particular, only those sets of  $\bar{n}$  at the stationary points of  $\Delta G$  need to be examined for stability to be established.

The variables  $n_i$  in Equation (3.47) could be replaced by the product  $\epsilon y_i$ , where  $\epsilon$  is the sum of all  $n_i$ . Making this substitution and dividing by  $\epsilon$ , the function  $\Delta G$  may be modified to,

$$\Delta G = \sum_{i=1}^{n_c} y_i [ \ln y_i + \ln \phi_i(\vec{y}) - h_i ] \quad (3.48)$$

where,

$$h_i = \ln z_i + \ln \varphi_i(z) \text{ for } i = 1, \dots, n_c \quad (3.49)$$

The stationary points of  $\Delta G(\vec{y})$  occur where the derivatives with respect to the  $n_c - 1$  independent variables  $y_i$  are zero. Differentiating,

$$\left( \frac{\partial \Delta G}{\partial y_i} \right)_{y_s, (s \neq 1, \dots, n_c)} = \ln y_i + \ln \varphi_i(\vec{y}) - h_i - k = 0 \quad \text{for } i = 1, 2, \dots, (n_c - 1) \quad (3.50)$$

where, taking  $y_{n_c}$  as the dependent mole fraction

$$k = \ln y_{n_c} + \ln \varphi_{n_c}(z) - h_{n_c} \quad \text{for } i = 1, \dots, n_c \quad (3.51)$$

Note that  $k$  is a constant for all the derivative conditions. Substitution of  $k$  into Equation (3.48) illustrates that at a stationary point,

$$\Delta G = \sum_{i=1}^{n_c} y_i k = k \quad (3.52)$$

and for stability,  $\Delta G > 0$  implies  $k > 0$

Figure (3.1) shows a graphic interpretation of the theory using a Gibbs free energy of mixing curve. In this example, the stability of a mixture of 20 mole percent carbon dioxide and 80 mole percent ethane is examined. At the overall

composition, a tangent to the Gibbs free energy of mixing curve can be drawn. A phase of this composition will be stable provided the tangent lies below the curve at all other points. Mathematically, the distance between the Gibbs free energy of mixing curve at a composition  $\bar{y}$  and the tangent is given by the value of the function  $\Delta G(\bar{y})$ , Equation (3.48).

Also shown in Figure (3.1) is a stationary point. This is a point which is either a local maximum or minimum, or a saddle point, of the function  $\Delta G(\bar{y})$ . A tangent to the Gibbs free energy of mixing curve at the stationary point will be parallel to the tangent drawn at the overall composition. The distance between the two tangents is given by Equation (3.52).

Hence, if this distance is greater than or equal to zero, the phase will be stable. In Figure (3.1), the distance is negative for the mixture of 20-mole percent carbon dioxide, and therefore, the phase is unstable. The strategy of the method of Michelsen, then, is to locate the stationary points and infer phase stability at those points.

From the derivative conditions, there are  $n_c$  equations of the form

$$\ln y_i - k + \ln \varphi_i(\bar{y}) - h_i = 0 \quad \text{for } i = 1, 2, \dots, n_c \quad (3.53)$$

A set of variables  $\bar{Y}$  can be defined such that

$$\ln Y_i = \ln y_i - k \quad \text{for } i = 1, 2, \dots, n_c \quad (3.54)$$

Equation (3.54) becomes

$$\ln Y_i + \ln \phi_i(\bar{y}) - h_i = 0 \quad \text{for } i = 1, 2, \dots, n_c \quad (3.55)$$

after substitution of  $\ln Y_i$ ,

$$1 = \sum_{i=1}^{n_c} y_i = \sum_{i=1}^{n_c} Y_i e^k \quad (3.56)$$

Then with Equation (3.54)

$$y_i = \frac{y_i}{\sum_{r=1}^{n_c} y_r} = \frac{Y_i}{\sum_{r=1}^{n_c} Y_r} \quad (3.57)$$

which establishes the relationship between the mole fractions  $\bar{y}$  and the variables  $\bar{Y}$ . Note from Equation (3.56) that for  $K \geq 0$  which indicates a stable phase, the sum of the variables  $Y_i$  must be less than or equal to one. This then is the condition that indicates stability.

To locate the stationary points, a set of nonlinear equations is solved for the variables  $Y$

$$\ln Y_i + \ln \phi_i(\vec{y}) - h_i = 0 \text{ for } i = 1, \dots, n_c \quad (3.58)$$

where the mole fraction  $\bar{y}$  is related to these variables by

$$y_i = \frac{Y_i}{\sum_{s=1}^{n_c} Y_s} \text{ for } i = 1, \dots, n_c \quad (3.59)$$

Once a solution to the above equation is found, stability of the phase is inferred by the sum of the variables  $\vec{Y}$ . If the sum is less than or equal to one, the phase is stable, otherwise it is unstable.

The numerical solution technique used to solve the above equation is successive substitution method for which the updating equation is given by

$$Y_i^{K+1} = \exp [ h_i - \ln \phi_i(\vec{y}) ] \text{ for } i = 1, \dots, n_c \quad (3.60)$$

For the successive substitution method the residual  $r_i$  can be defined as

$$r_i = \ln Y_i + \ln \phi_i(\vec{y}) - h_i \text{ for } i = 1, \dots, n_c \quad (3.61)$$

The calculation steps can be summarized as follows

- 1) Compute variable  $h_i$  from Equation (3.49).
- 2) Estimate values for variable  $Y_i$ .
- 3) Compute  $\varphi_i(y)$  where  $y_i$  is given by Equation (3.59).
- 4) Calculate the value of the variables  $r$  by Equation (3.61).
- 5) Check the convergence of the successive substitution iteration by satisfying the condition.

$$\text{Max } |r_i| \leq \varepsilon_{\text{con}} \quad \text{for } i = 1, \dots, n_C.$$

- 6) Update variable  $Y_i$  using Equation (3.60) and go to step (3) to continue successive substitution iteration.
- 7) Calculate the value of the residuals, equation (3.61) and check for the convergence criterion.
- 8) If it is not converged, go to step (3).

After convergence is achieved, the solution needs to be checked for stability of the equilibrium phases. The non-triviality of the solution is checked by comparison with the feed composition. A phase composition is considered non-trivial if the following condition is satisfied

$$\left[ \sum_{i=1}^{n_C} (y_i - z_i)^2 \right]^{1/2} \geq \frac{\varepsilon_{\text{triv}}}{n_C} \quad (3.62)$$

If a solution does not satisfy this condition or if convergence is not achieved in a certain maximum number of iterations, the entire procedure is begun again with a new estimate for  $Y$ . A phase is assumed to be stable if all initial estimates lead to the trivial solution.

If Equation (3.62) above is satisfied by a converged composition  $y$ , a second condition is checked to determine stability. A phase is considered to be unstable if

$$\sum_{i=1}^{n_c} Y_i - 1 \geq \varepsilon_{\text{stab}} \quad (3.63)$$

Otherwise it is assumed to be stable. If the non-triviality condition is met but the above stability condition is not met then the procedure is repeated with a different initial estimate of  $Y$ . In addition to checking for convergence to a nontrivial solution, Equation (3.63) is tested whenever a  $Y$  is found such that the condition  $\Delta G < 0$  is satisfied. If Equation (3.63) is also satisfied then the phase is unstable.

For testing an overall composition for single-phase stability, two initial estimates may be used. The first estimate for  $Y$  is computed from

$$Y_i = z_i K_i \quad \text{for } i = 1, \dots, n_c \quad (3.64)$$

and the second estimate is

$$Y_i = z_i / K_i \quad (3.65)$$

where K-values are computed using the correlation [13]

$$K_i = \frac{P_{Ci}}{P} \exp[5.37(1 + \omega_i)(1 - \frac{T_{Ci}}{T})] \quad \text{for } i = 1, \dots, n_C \quad (3.66)$$

When testing the stability of a two-phase mixture, the computational procedure is the same as that for a single-phase mixture except that now one of the two-phase composition is used in Equation (3.46) instead of the overall composition.

Four different sets of initial estimates are used

$$Y_i = (1/2)(x_{i2} + x_{i3}) \quad \text{for } i = 1, \dots, n_C \quad (3.67)$$

$$Y_1 = 0.999 \text{ and } Y_i = 0.001/(n_C - 1) \quad \text{for } i = 2, \dots, n_C \quad (3.68)$$

$$Y_{n_C} = 0.999 \text{ and } Y_i = 0.001 / (n_C - 1) \text{ for } i = 1, \dots, n_C - 1 \quad (3.69)$$

and



$$Y_i = \exp h_i \quad \text{for } i = 1, \dots, n_C \quad (3.70)$$

Two trivial solutions, which are the composition of the two phases, may result. A test analogous to Equation (3.62) should be also done but this time for both phase compositions.

### 3.5.3 Flash Calculation

Once a mixture has been shown to split into more than one phase by the stability analysis calculation, the amounts and composition of each phase must be found. Two different algorithms are implemented in UTCOMP compositional reservoir simulator for flash calculations[14]. One is a flash formulation using K-values with an accelerated successive substitution method (ACSS) [15]. The second method determines phase compositions by minimization of the Gibbs free energy using an implementation of the reduced gradient approach described by Trangenstein [16]. Perschke [17] presents the complete formulation for both the methods. We present the ACSS algorithm here as it has been the method used for flash calculations with the SAFT equation of state.

### 3.5.4 Accelerated Successive Substitution Method

A flash calculation is made to find the composition and amounts of each phase of an  $n_p$  phase system. In terms of mole fractions, as is done in conventional vapor/liquid calculations, the unknowns are the phase mole fractions,  $x_{ij}$ , and the amounts of each phase given as the ratio of moles in a phase to the total number of moles in the mixture. This ratio, for phase  $j$ , is denoted  $L_j$ . Thus, there are  $n_p + n_p n_c$  unknowns:  $L_j$  and  $x_{ij}$ .

Not all these variables, are independent. The mole fractions are constrained by

$$\sum_{i=1}^{n_c} x_{ij} = 1 \quad \text{for } j = 1, 2, \dots, n_p - 1 \quad (3.71)$$

and the phase distribution is constrained by

$$\sum_{j=1}^{n_p} L_j = 1 \quad (3.72)$$

The number of independent variables can be reduced even more by using the component molar balance constraints

$$z_i = \sum_{j=1}^{n_p} x_{ij} L_j \quad \text{for } i = 1, 2, \dots, n_c \quad (3.73)$$

which reduces the number of independent variables by  $n_c$ . Note that there are only  $n_p - 1$  independent expressions of the form of Equation (3.71) because given Equation (3.72) and Equation (3.73), the  $n_p$  th expression may be derived. With Equation (3.71), Equation (3.72) and Equation (3.73) the number of independent variables can be reduced to  $n_c (n_p - 1)$ .

As is done in vapor/liquid calculations,  $K$  – values are defined as the ratio of the component mole fraction in a reference phase to that in another phase

$$K_{ij} = \frac{x_{i1}}{x_{ij}} \quad \text{for } i = 1, 2, \dots, n_c, \quad \text{and } j = 2, 3, \dots, n_p \quad (3.74)$$

The choice of the reference phase 1 is entirely arbitrary. When the vapor phase is chosen as the reference the above equation reduced to the conventional vapor/liquid equilibrium constants.

By substituting for the fugacity in the thermodynamic conditions for equilibrium, the  $K$ -values can be related to the fugacity coefficients:

$$\ln K_{ij} = \ln \phi_{ij} - \ln \phi_{i1} \quad \text{for } i = 1, 2, \dots, n_c \quad \text{and } j = 2, 3, \dots, n_p \quad (3.75)$$

With expressions for the fugacity coefficients given by Equation (3.44), Equation (3.71) through Equation (3.75) form a set of  $2 n_p n_c + n_p - n_c$  equations in

as many unknowns:  $K_{ij}$ ,  $L_j$  and  $x_{ij}$ . In the formulation implemented here, the  $n_c$  ( $n_p - 1$ ) independent variables are chosen to be  $K_{ij}$  for  $i = 1, 2, \dots, n_c$  and  $j = 2, 3, \dots, n_p$ , and the set of  $n_c$  ( $n_p - 1$ ) equations given by Equation (3.75) are solved for these variables.

Since the phase distribution variables and phase mole fractions are now treated as dependent variables, Equation (3.71) through Equation (3.74) must be used in such a way that these dependent variables can be calculated from the  $K -$  values.

After solving Equation (3.72) for  $L_1$ , for example, this expression can be substituted in Equation (3.73). With the  $K -$  value definitions of Equation (3.74) and the relations

$$\sum_{i=1}^{n_c} x_{ij} - \sum_{i=1}^{n_c} x_{i1} = 0 \quad \text{for } j = 2, 3, \dots, n_p \quad (3.76)$$

expressions of the following form may be derived

$$g_j(L_2, L_3, \dots, L_{n_p}) = \sum_{i=1}^{n_c} \frac{z_i \left( \frac{1}{K_{ij}} - 1 \right)}{1 + \sum_{k=2}^{n_p} L_k \left( \frac{1}{K_{ij}} - 1 \right)} = 0 \quad \text{for } j = 2, 3, \dots, n_p \quad (3.77)$$

Equation (3.77) is also called the flash equation. For an  $n_p$  phase mixture,  $n_p - 1$  equation of this form can be written. With a given set of  $K$  - values, these non-linear equations can be solved for the variables  $L_j$ , for  $j = 2, 3, \dots, n_p$ . The remaining variable  $L_1$  can be computed from Equation (3.72).

Phase mole fractions for the reference phase may be computed once the flash equation has been solved from

$$x_{i1} = \frac{z_i}{1 + \sum_{k=2}^{n_p} L_k \left( \frac{1}{K_{ik}} - 1 \right)} \quad \text{for } i = 1, 2, \dots, n_c - 1 \quad (3.78)$$

The mole fractions for the remaining phases can be found from Equation (3.74) given  $K_{ij}$  and  $x_{i1}$ .

The numerical technique used for solution of Equation (3.73) is an accelerated successive substitution algorithm. In this method,  $K$ -values are updated by

$$K_{ij}^{n+1} = K_{ij}^n \exp \left( -\lambda^{n+1} \frac{f_{i1}}{f_{ij}} \right) \quad \text{for } i = 1, 2, \dots, n_c \quad \text{and } j = 2, 3, \dots, n_p \quad (3.79)$$

where  $\lambda^{n+1}$  is an acceleration factor computed by method three of Mehra, Hidemann, and Aziz[15].

The acceleration factor is computed in a recursive fashion. For  $n = 0$ ,  $\lambda^1$  is set to 1, which implies that a successive substitution step is taken. For  $n > 1$ ,  $\lambda$  is found from

$$\lambda^{n+1} = \frac{\lambda^n \sum_{j=2}^{n_p} \sum_{i=1}^{n_c} [s_{ij}^n]^2}{\sum_{j=2}^{n_p} \sum_{i=1}^{n_c} [s_{ij}^n s_{ij}^{n+1}] - \sum_{j=2}^{n_p} \sum_{i=1}^{n_c} [s_{ij}^n]^2} \quad (3.80)$$

where

$$s_{ij} = \ln f_{ij} - \ln f_{i1} \quad \text{for } i = 1, 2, \dots, n_c \quad \text{and } j = 2, 3, \dots, n_p \quad (3.81)$$

The acceleration factor is kept within the range  $1 \leq \lambda^{n+1} \leq 4$ . If  $\lambda^{n+1}$  falls outside these limits then it is set to the limiting value.

It is essential that a solution of Equation (3.77) be found for each set of  $K$  – valued computed. In this algorithm, Newton's method is used. At each iteration  $L_j$  is updated by

$$L_j^{n+1} = L_j^n + \Delta L_j^n \quad \text{for } j = 2, 3, \dots, n_p \quad (3.82)$$

Where  $\Delta L_j^n$  is calculated by the solution of

$$J^n \Delta L^n = -f^n \quad (3.83)$$

The elements of J, the Jacobian matrix, are given by

$$j_{jk} = - \sum_{i=1}^{n_c} \frac{z_i \left(\frac{1}{K_{ij}} - 1\right) \left(\frac{1}{K_{ik}} - 1\right)}{\left[1 + \sum_{h=2}^{n_p} L_h \left(\frac{1}{K_{ih}} - 1\right)\right]} \quad \text{for } j,k = 2,3, \dots, n_p \quad (3.84)$$

and f is a vector whose elements are the function values for  $g_j$  given in Equation (3.77). For a three-phase mixture, J is a symmetric 2 x 2 matrix

Iteration is assumed to have converged when either

$$\max |g_j(L_2, L_3, \dots, L_{n_p})| \leq \epsilon_{tol} \quad \text{for } j = 2,3, \dots, n_p \quad (3.85)$$

or

$$\max |\Delta L_j^n| \leq \epsilon_{tol} \quad \text{for } j = 2,3, \dots, n_p \quad (3.86)$$

where  $\epsilon_{tol}$  has a small value of, for example,  $1.0 \times 10^{-10}$

Because Newton's method is used, a good initial estimate must be available for convergence to be achieved. Special precautions are taken to locate, a small interval containing the solution for two-phase calculations. For a two-

phase mixture, there is only one equation of the form of Equation (3.84) in one unknown,  $L_2$ . The derivative of this function with respect to  $L_2$  is given by

$$\frac{d g_2}{d L_2} = - \sum_{i=1}^{n_c} \frac{z_i \left(\frac{1}{K_i} - 1\right)^2}{\left[1 + L_2 \left(\frac{1}{K_i} - 1\right)\right]^2} \quad (3.87)$$

hence the function  $g_2 (L_2 )$  is monotonically decreasing. For a solution to exist in the physically meaningful interval of  $0 \leq L_2 \leq 1$ , then  $g_2 ( 0 ) > 0$  and  $g_2 ( 1 ) < 0$ .

To locate an interval about the solution, a value for  $L_2$  is chosen and  $g_2 (L_2 )$  is computed. Depending on the sign of  $g_2 (L_2 )$ ,  $L_2$  is either increased, if  $g_2 (L_2 ) > 0$ , or decreased, if  $g_2 (L_2 ) < 0$ , until an interval has been located in which the value of  $g_2 (L_2 )$  changes sign. The initial estimate of  $L_2$  is taken as the halfway point between the interval boundaries.

In summary, one method implemented for calculation of phase amounts and compositions is to solve the  $n_c (n_p - 1)$  equations given by Equation (3.75) for the  $n_c (n_p - 1)$  variables,  $K_{ij}$ . Equation (3.77), Equation (3.79), Equation (3.71) and Equation (3.72) are used to relate the phase distribution and phase mole fractions to the K-values. An accelerated substitution algorithm is used to solve Equation (3.88). The procedure is given by the following steps:



1. Estimate K-values, either from phase stability analysis results or correlations.
2. Calculate the phase distribution,  $L_j$ , from Equation (3.77) using Newton's method
3. Calculate the reference phase composition from Equation (3.78) and the remaining phase mole fractions with Equation (3.74) and the given Kvalues
4. Using the equation of state, compute fugacity coefficients for each phase
5. Calculate the acceleration factor Equation (3.80).
6. Update K-values from Equation (3.79)
7. Check for convergence
8. Go to step (2) with new K-values if not converged.

Convergence is assumed when

$$\max |s_{ij}| \leq \epsilon_{\text{con}} \quad \text{for } i = 1, 2, \dots, n_c \quad \text{and } j = 2, 3, \dots, n_p \quad (3.88)$$

and

$$\max \left| \frac{K_{ij}^{n+1} - K_{ij}^n}{K_{ij}^n} \right| \leq \epsilon_{\text{con}} \quad \text{for } i = 1, 2, \dots, n_c \quad \text{and } j = 2, 3, \dots, n_p \quad (3.89)$$

where  $s_{ij}$  is given by Equation (3.77). The value of  $\epsilon_{\text{con}}$  is, for example,  $1.0 \times 10^{-10}$ . Note that accelerated successive substitution steps are taken only if that step reduces the Gibbs free energy. Otherwise a successive substitution step is made. UTCOMP is an isothermal, three-dimensional compositional reservoir simulator developed at the University of Texas at Austin [14]. The phase behavior

aspect of the reservoir simulator (UTCOMP) is incorporated in the subroutine FLASH. The algorithm for the working of FLASH is given in Figure (3.2).

### 3.6 PSEUDO COMPONENT PARAMETER EVALUATION

The average absolute deviation in vapor pressure ( $p^{\text{sat}}$ ) and liquid molar volume ( $v^{\text{liq}}$ ) predicted by SAFT is as good as can be usually expected for a reasonable, three-parameter equation of state. However, there is an important challenge in estimating the equation of state parameters for polydispersed, poorly defined pseudocomponents of real fluid mixtures. Huang and Radosz [9] have observed that the pure component SAFT parameters are well-behaved and suggest predictable trends with the molar mass of similar compounds. They have shown that a single linear relationship holds not only for small n-alkanes, but also for macromolecular branched chains, such as polypropylene, polyethylene, and polyisobutylene as shown in Figure 3.3. Huang and Radosz have also shown that the segment number  $m$  increases linearly with increasing molar mass within each homologous series. for various homologous series as given in Figure 3.3. The chain length  $m$  is essentially a linear function of molar mass for different homologous series of aromatic molecules, i.e., upon increasing the side chain length for alkylbenzenes, alkylnaphthalenes, etc., which is replotted in Figure 3.4. This plot suggest that the segment number of all molecules is bounded by the n-alkane chain length at the upper and by the polynuclear aromatics at the lower

end. It can be deduced that for the same molar mass the chain length decreases with increasing aromaticity.

The effective segment numbers  $m$  reported for hydrocarbons by Huang and Radosz are systematically smaller than the corresponding carbon numbers. This suggests that the physical picture of a *n*-alkane therefore is that of a chain of overlapping spherical segments where  $v^\infty$  corresponds to the volume occupied by such segments. Expectedly, the segment volume  $v^\infty$  for methane is the largest among alkanes because it corresponds to a single  $\text{CH}_4$  unit, and it gradually decreases upon increasing the chain length, reaching an asymptotic value of 12 for long chains.

Since  $v^\infty$  does not vary much with chain length and remains constant for long chains and since  $m$  is a linear function of the molar mass, the product  $m v^\infty$  (the volume occupied by a mole of molecules in a closed packed arrangement) is also a linear function as shown in Figure 3.5.

Finally, a similar correlation can be developed for the segment energy  $u^0 / k$ , which is shown in Figure 3.6. As in the case for  $m$  and  $m v^\infty$ , *n* alkanes and plain polynuclear aromatics set the boundaries for  $u^0 / k$  for all hydrocarbons. However  $u^0/k$  varies nonlinearly with the molar mass in contrast to the segment number  $m$  and the term  $m v^\infty$ .

For ease of estimation,  $m$ ,  $mv^\infty$ , and  $u^0/k$  have been regressed as simple functions of the molar mass (MM) for many homologous series. For example,

$$m = A^{(1)} + A^{(2)} \text{ MM} \quad \text{for all hydrocarbons} \quad (3.90)$$

$$m v^\infty = A^{(1)} + A^{(2)} \text{ MM} \quad \text{for all hydrocarbons} \quad (3.91)$$

$$u^0/k = A^{(1)} - A^{(2)} \exp(-A^{(3)} \text{ MM}) \quad \text{for n-alkanes and poly nuclear aromatics} \quad (3.92)$$

$$u^0/k = A^{(1)} - A^{(2)} \text{ MM} \quad \text{for all other hydrocarbons} \quad (3.93)$$

Equation (3.93) is only a linear approximation that is valid up to the MM of the corresponding n-alkane; for higher MM values, the  $u^0/k$  is the same as that of the corresponding n-alkane. The regression coefficients are reported in Table (3.1) to Table (3.4).

### 3.6.1 Incorporation of Pseudo components in SAFT

The SAFT parameter evaluation for pseudo components is done in the subroutine `saft_input_values`. An extra parameter group is introduced in the input data file which indicates the type of the pseudo component. The user inputs the type of the pseudo component (whether it is an n-alkane etc.) and the subroutine

calculates the SAFT parameters using equations (3.90-3.93) with the corresponding constants obtained from Table (3.1) to Table (3.4).

## Nomenclature

$a^{\text{res}}$	residual Helmholtz free energy per mole of molecules (J/mol)
$a^{\text{total}}$	total Helmholtz free energy per mole of molecules (J/mol)
$a^{\text{ideal}}$	ideal Helmholtz free energy per mole of molecules (J/mol)
$a^{\text{hs}}$	hard sphere Helmholtz free energy per mole of molecules (J/mol)
$a^{\text{chain}}$	chain Helmholtz free energy per mole of molecules (J/mol)
$a^{\text{assoc}}$	association Helmholtz free energy per mole of molecules (J/mol)
$\rho$	density of the mixture (mol/ Cu. A)
$\xi_i$	reduced density (dimensionless)
$R$	gas constant
$T$	temperature of the system (K)
$P$	pressure of the system (Pa)
$V$	volume of the system (Cu. A)
$x_i$	mole fraction of component i
$m_i$	chain length of component i
$g_{ii}$	radial distribution function of component i
$m$	average chain length of mixture
$d_i$	temperature dependent segment diameter (A)
$\sigma_i$	temperature independent segment diameter (A)
$u^0/k$	temperature independent energy parameter (K)
$P_{\text{hs}}^{\text{CS}}$	Carnahan-Starling Pressure contribution
$\mu^{\text{hs}}$	hard sphere chemical potential
$Z^{\text{hs}}$	hard-sphere compressibility factor
$\mu^{\text{chain}}$	chain chemical potential
$Z^{\text{chain}}$	chain compressibility factor
$Y_i^A$	mole fraction of molecules i not bonded at site A

$\Delta_{ij}^{A,B}$	association bonding strength between sites $A_i$ and $B_j$
$\varepsilon_{ij}^{A,B}$	association energy between sites $A_i$ and $B_j$
$\kappa_{ij}^{A,B}$	association entropy between sites $A_i$ and $B_j$
$a_{ij}$	association interaction coefficient between component $i$ and $j$
$\mu_i^{\text{assoc}}$	association chemical potential of component $i$
$Z^{\text{assoc}}$	association compressibility factor
$u_{ii}$	dispersion energy of component $i$
$D_{jk}$	Chen and Kreglewski constants for dispersion potential
$\tau$	closed packing density limit (0.74048)
$k_{ij}$	binary interaction coefficient between component $i$ and $j$
$\mu_i^{\text{disp}}$	dispersion chemical potential of component $i$
$Z^{\text{disp}}$	dispersion compressibility factor
$Z$	compressibility factor of the system
$z_i$	initial feed composition of component $i$ for flash and stability calculations
$\Delta G$	change in Gibbs free energy
$\phi_i$	fugacity coefficient
$y_i$	mole fraction of $i$ in a trial phase
$h_i$	constant for component $i$ in stability analysis
$Y_i$	independent variable for stability analysis
$J$	Jacobian matrix
$\varepsilon$	tolerance for iteration to converge
$L_j$	ratio of moles of phase $j$ to total moles
$K_{ij}$	equilibrium constant for component $i$ in phase $j$
$\lambda_{n+1}$	acceleration factor for the ACSS method
$f_i$	fugacity of component $i$
$s_{ij}$	logarithm of component fugacity ratio
$A(i)$	regression constants used in SAFT equation of state

MM molar mass of pseudocomponents



## References

- 1) Chapman, W.G., Gubbins, K.E., Jackson, G., and Radosz, M.: "SAFT Equation of State Solution Model for Associating Fluids", *Fluid Phase Equilibrium*. **52**, 31(1989).
- 2) Chapman, W.G., Gubbins, K.E., Jackson, G., and Radosz, M.: "New Reference Equation of State for Associating Liquids", *Ind. Eng. Chem. Res.*, **29**, 1709 (1990).
- 3) Topliss, R. J., *Techniques to facilitate the use of equations of state for complex fluid-phase equilibria*. Ph.D. Dissertation, Univ. of California, Berkley, 1985.
- 4) Mansoori, G.A., Carnahan, N.F., Starling, K.E., and Leland, T.W.: "Equilibrium Thermodynamic Properties of the Mixture of Hard Spheres", *J. Chem. Phys.* **54**, 1523 (1971).
- 5) Barker, J.A., and Henderson, D.: "Perturbation Theory and Equation of State for Fluids. II. A Successful Theory of Liquids", *J. Chem. Phys.*, **21**, 1123 (1967).
- 6) Chen, S.S., and Kreglewski, A.: "Application of the Augmented van der Waals Theory of Fluids. I. Pure Fluids", *Ber. Bunsen-Ges. Phys. Chem.*, **81**, 1048 (1977).
- 7) Carnahan, N. F., and Starling, K. E.: "Equation of State for Nonattracting Rigid Spheres", *J. Chem. Phys.*, **51**, 635 (1969).
- 8) Reed, T.J., and Gubbins, K.E., *Applied Statistical Thermodynamics*, Mc. Graw-Hill, 1973.
- 9) Huang, H.H., and Radosz, M., *Ind. Eng. Chem. Res.*: "Equation of State for Small, Large, Polydisperse, and Associating Molecules", **29**, 2284 (1990).
- 10) Huang, H.H., and Radosz, M., "Equation of State for Small, Large, Polydisperse, and Associating Molecules: Extension to Fluid Mixtures", *Ind. Eng. Chem. Res.*, **30**, 1994 (1991).

- 11) Kreglewski, A., *Equilibrium Properties of Fluids and Fluid Mixtures.*, The Texas Engineering Experiment Station (TEES) Monograph Series; Texas A&M University Press: College Station., 1984.
- 12) Michelsen, M.L.,: “The Isothermal Flash Problem. Part I. Stability”, “The Isothermal Flash Problem. Part II Phase Split Calculation”, *Fluid Phase Equilibria*, **9**, 1,(1982).
- 13) Wilson, G.M.,: “ A Modified Redlich-Kwong Equation of State – Application to General Physical Data Calculations”, 65<sup>th</sup> National AIChE Meeting, Cleveland, OH, May 4-7, 1969.
- 14) Chang, Y.B.,: “Development and Application of an Equation of State Compositional Simulator”, Ph. D Dissertation, University of Texas at Austin, 1990.
- 15) Mehra, R.K., Heidemann, R.A., and Aziz, K.,: “An Accelerated Successive Substitution Algorithm”, *Can. J. of Chem. Eng.*, **61**,590, (1983).
- 16) Trangenstein, J.A.,: “Customized Minimization Techniques for Phase Equilibrium Computations in Reservoir Simulation”, *Chem. Eng. Sci.*, **42**, 2847, (1987).
- 17) Perschke, D.R.,: “Equation of State Phase Equilibria Calculations”, M.S. Thesis, University of Texas at Austin, 1984.

	$A^{(1)}$	$A^{(2)}$	<b>MM range in fitting</b>
<b>n-alkanes</b>	0.70402	0.046647	16-619
<b>Polynuclear aromatics</b>	2.6733	0.014781	78-202
<b>n-alkylcyclopentanes</b>	0.82360	0.039044	70-140
<b>n-alkylcyclohexanes</b>	-0.010038	0.043096	84-154
<b>n-alkylbenzenes</b>	0.51928	0.041112	78-134
<b>1-n-alkylnaphthalene</b>	-2.3190	0.054566	128-184

**Table 3.1: Correlation of segment number  $m$  for hydrocarbons**

	$A^{(1)}$	$A^{(2)}$	<b>MM range in fitting</b>
<b>n-alkane</b>	0.70402	0.046647	16-619
<b>Polynuclear aromatics</b>	2.6733	0.014781	78-202
<b>n-alkylcyclopentanes</b>	0.82360	0.039044	70-140
<b>n-alkylcyclohexanes</b>	-0.010038	0.043096	84-154
<b>n-alkylbenzenes</b>	0.51928	0.041112	78-134
<b>1-n-alkylnaphthalene</b>	-2.3190	0.054566	128-184

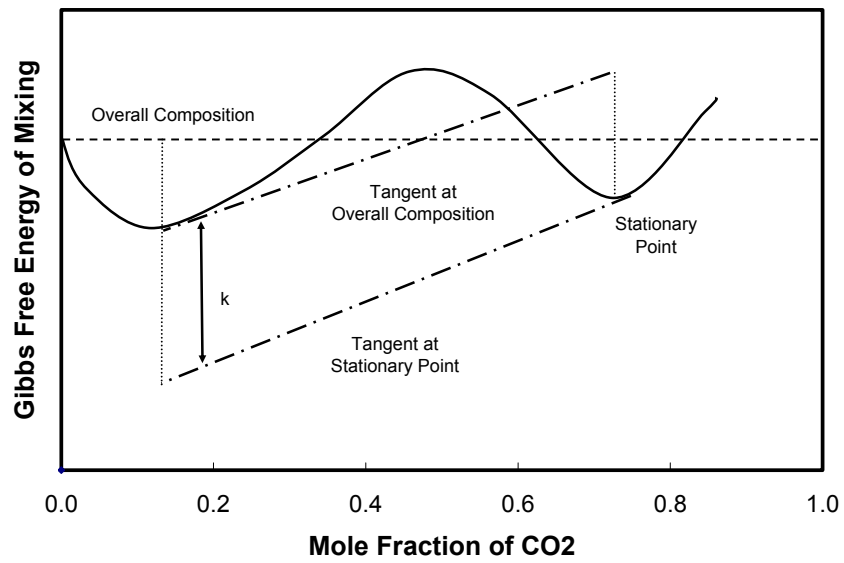
**Table 3.2: Correlation of closed packed molar volume  $mv^\infty$  for hydrocarbons**

	$A^{(1)}$	$A^{(2)}$	$A^{(3)}$	MM range in fitting
<b>n-alkane</b>	210.0	26.886	0.013341	16-619
<b>Polynuclear aromatics</b>	472.84	357.02	0.0060129	78-228

**Table 3.3: Correlation of segment energy  $u^0/k$  for n-alkanes and polynuclear aromatics**

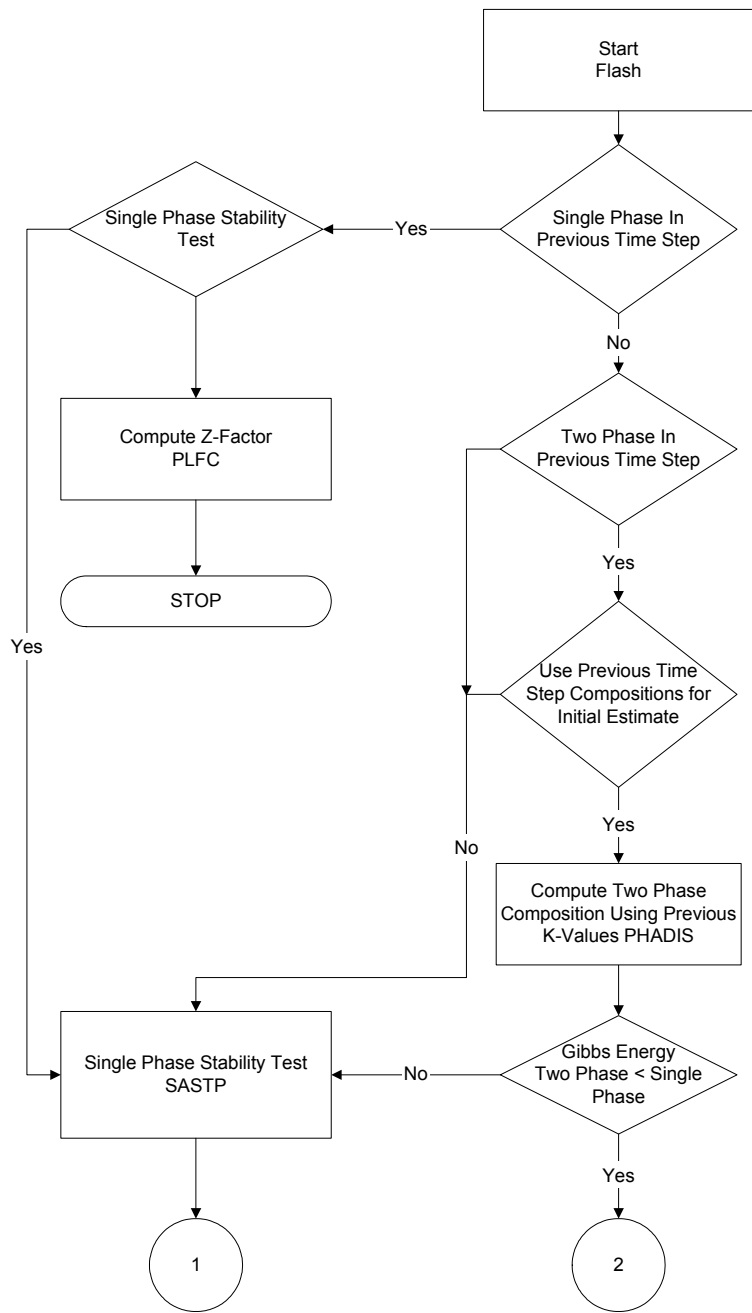
	$A^{(1)}$	$A^{(2)}$	MM range in fitting
<b>n-alkylcyclopentanes</b>	239.56	0.085618	98-140
<b>n-alkylcyclohexanes</b>	278.59	0.31311	98-154
<b>n-alkylbenzenes</b>	267.39	0.21825	78-134
<b>1-n-alkylnaphthalene</b>	425.70	0.94111	128-184

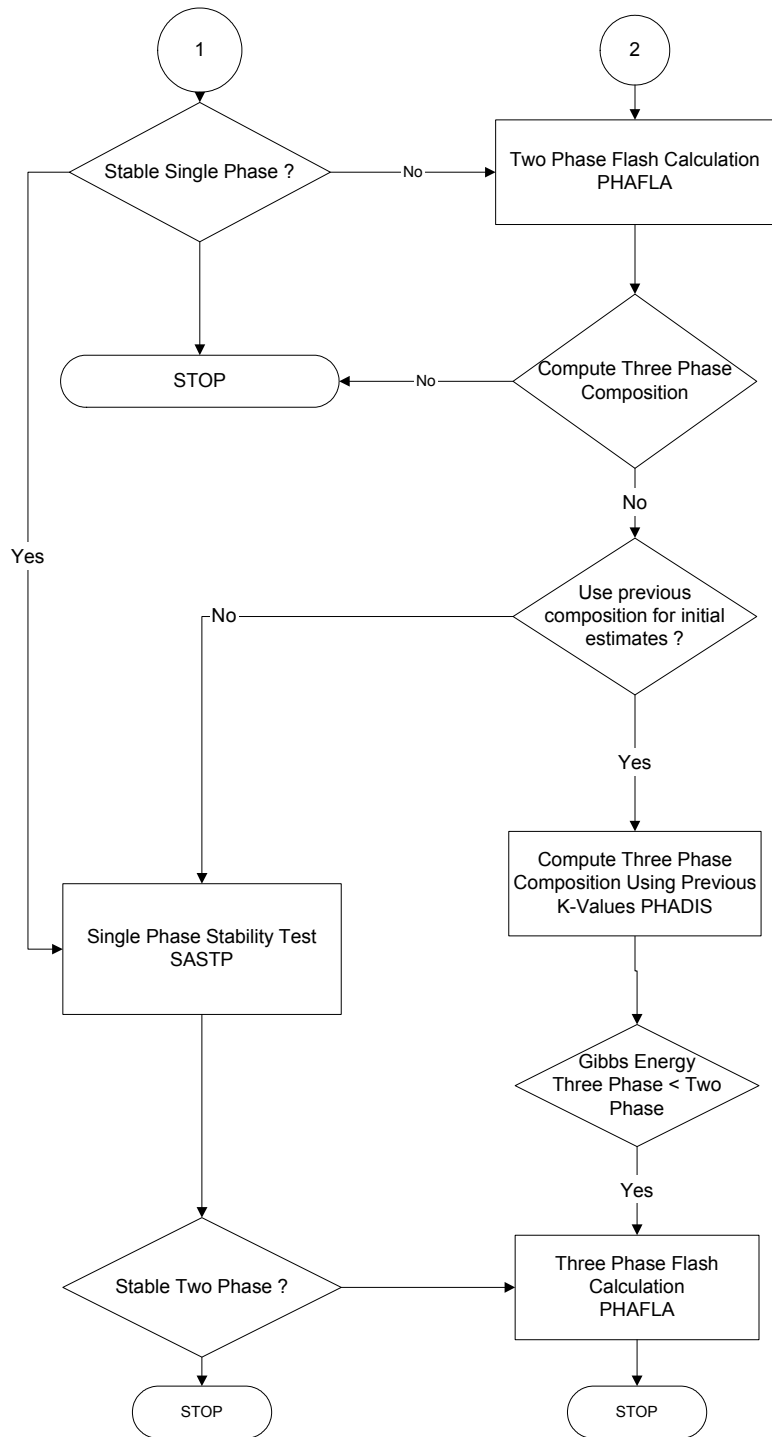
**Table 3.4: Correlation of segment energy  $u^0/k$  for other hydrocarbons**



**Figure 3.1: Graphical interpretation of phase stability analysis by Michelson's Method**

**Figure 3. 2: Algorithm for phase equilibrium calculation**





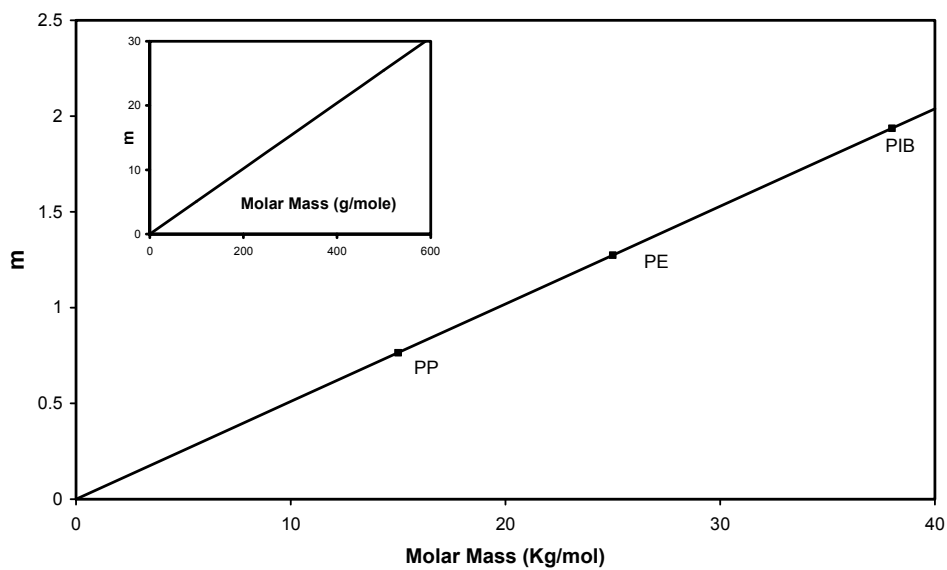


**Figure 3.3: Segment number  $m$  as a linear function of molar mass for n-alkanes and long chain polymers (Huang et al.,1991)**



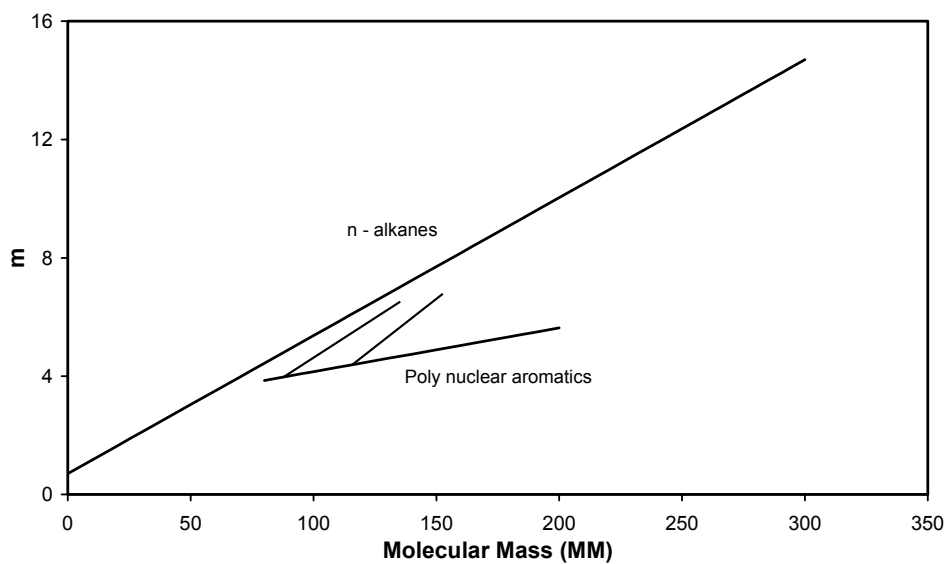


**Figure 3.4: Segment number  $m$  for n-alkanes and polynuclear aromatics. The branched curves represent n-alkyl derivatives of polynuclear aromatics (Huang et al.,1991)**

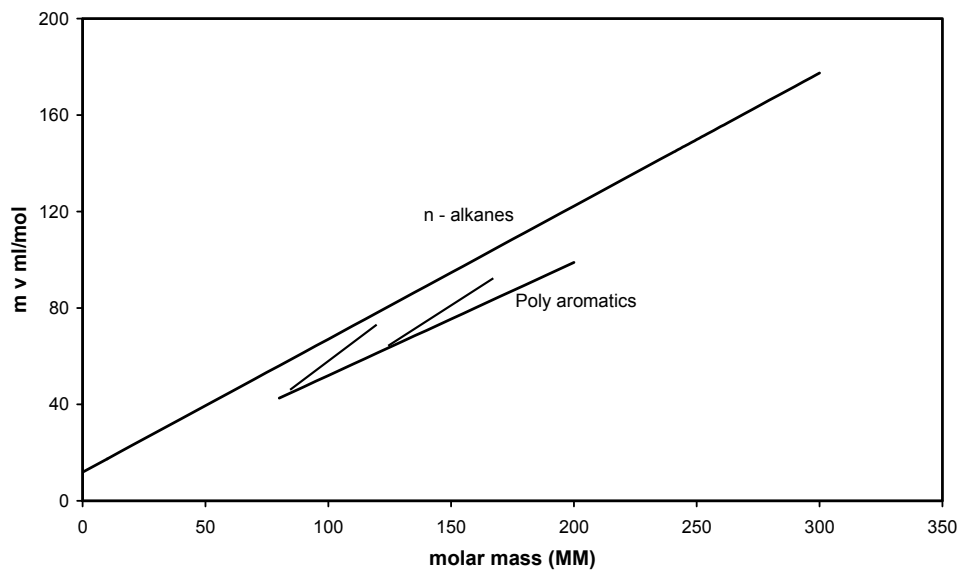


**Figure 3.5: Close-packed molar volumes  $m v^\infty$  for n-alkanes and polynuclear aromatics as functions of molar mass. (Huang et al.,1991)**

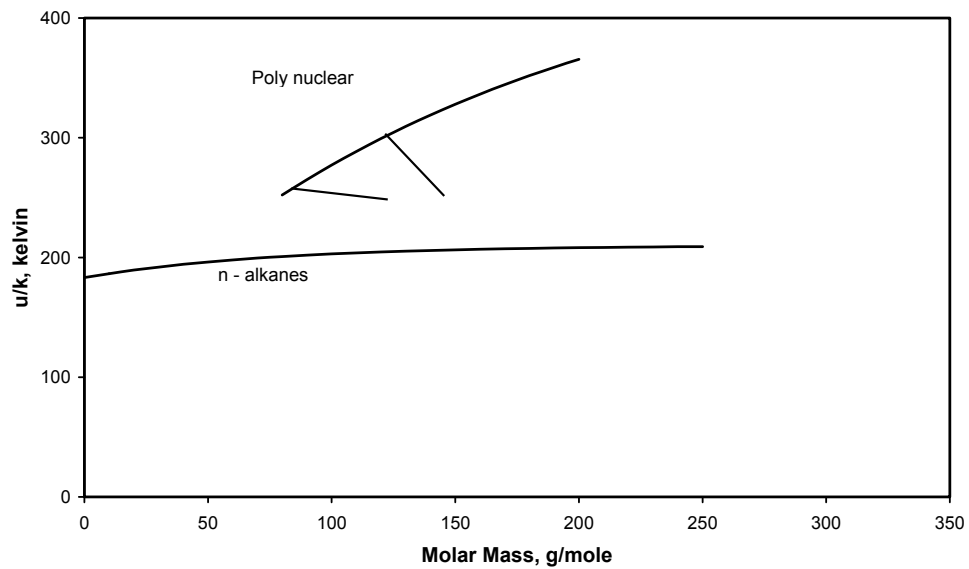


**Figure 3.6: Segment energies  $u^0/k$  for n-alkanes and polynuclear aromatics as functions of molar mass. The branched curves represent n-alkyl derivatives of poly-aromatics (Huang et al.,1991)**

## CHAPTER 4

### BULK THERMODYNAMIC PROPERTIES OF MIXTURES

In this chapter we present some results and discuss the effectiveness of SAFT for predicting the bulk thermodynamic properties of different types of fluid mixtures. We also compare the results with those obtained from the Peng-Robinson equation.

#### 4.1 PURE COMPONENTS

Figure 4.1 shows the vapor pressure curves for a few alkanes. Alkanes have been chosen initially to check the non-associating terms (hard-sphere, dispersion and chain terms) in SAFT. It is observed that the percentage average absolute deviation (% AAD) from experimental data, in the vapor pressure is 1.9 % for hexane. Similarly the % AAD for heptane and octane are 1.8 % and 1.6 % respectively which can be considered an excellent fit for engineering equations of state. In Figure 4.2 the liquid specific volume curves are presented for n-alkanes as calculated from the SAFT equation of state. The % AADs for liquid specific volumes are also very low: 3.5 % for hexane, 3.4 % for heptane and 3.4 % for octane. Table 4.1 lists the SAFT parameters used for non-polar compounds.

Figure 4.3 shows vapor pressure curves for ammonia and ethanol each of which have association bonding sites on them. Ammonia has three proton donor sites and one proton acceptor site. It is assumed that all the different hydrogen bonds formed are equivalent in terms of the energy of interaction and the volume of the bond. This approximation is aimed at reducing the total number of fitting parameters in the equation of state. Only two additional parameters are introduced in the equation of state (the energy and entropy of bonding) which along with the other non-associating parameters are given in Table 4.2. The % AAD in the vapor pressure curve of ammonia is 1.6 %. Similarly ethanol has two proton donors and two electron donors and the interactions amongst them are all considered equivalent. The % AAD in the vapor pressure of ethanol is 0.86 % which is an excellent fit. Figure 4.4 shows the liquid saturated density curves for ammonia and ethanol and the respective % AADs are 3.2 % and 0.88 %. Thus SAFT works very well even for highly polar compounds. Figures 4.1 to 4.4 confirm the usefulness of SAFT for pure components.

## **4.2 BINARY AND TERNARY MIXTURES**

In this section we present SAFT results for binary and ternary mixtures. First, we test the system for small molecular weight hydrocarbon mixtures. For binary mixtures, we have also compared the SAFT results with phase equilibrium data obtained using a conventional three-parameter equation of state such as the

Peng-Robinson equation of state. In Figure 4.5, the vapor-liquid equilibrium curve for butane-hexane at 293.15 K is presented. Both, SAFT and PR curves have been obtained without adjusting the binary interaction coefficient. We see that both SAFT and PR predict the liquid phase mole fractions fairly accurately. It should be noted that PR equation of state does remarkably well for hydrocarbon mixtures. This is because, PR equation of state parameters have been tuned particularly well for hydrocarbons.

In Figure 4.6, the vapor-liquid equilibrium for a methane-hexadecane system is presented. This mixture has been selected to study the effect of the chain-term on the phase-behavior calculation. Hexadecane is a long chain molecule with the chain length as calculated from the pure component vapor pressure and liquid density data to be 12.3. So the mixture is expected to show a significant effect of the chain term on the vapor-liquid equilibrium predictive capability of SAFT. Interestingly, we observe that although SAFT predicts the vapor phase mole fractions fairly accurately, the liquid phase methane mole fractions are over-predicted. On the other hand, the PR equation of state predicts both the vapor-phase and the liquid phase mole fractions very accurately. It is seen in Figure 4.7 that when the binary interaction coefficient ( $k_{ij}$ ) is adjusted to 0.118, then SAFT predicts both the liquid and the vapor phase mole fractions accurately. Once  $k_{ij}$  has been established the same parameter can be used to predict the VLE curve at a different temperature. This is shown by the second plot in Figure 4.7, which has been obtained at 623 K.

After this analysis of SAFT for non-associating binary mixtures, we tested SAFT for associating binary mixtures to evaluate the effect of the association term on the vapor-liquid phase equilibrium predictions. In Figure 4.8 the vapor-liquid equilibrium curve for an ethane-ethanol mixture at 313.4 K is presented. We have shown the PR equation of state predictions as well to compare the effect of the association term. Both the curves have been obtained without adjusting the binary interaction coefficient. It is seen clearly that SAFT predicts both the gas phase and the liquid phase mole fraction reasonably accurately. The PR equation of state, on the other hand, does not do a very good job of predicting the liquid phase mole fractions. This is expected as the PR equation of state has been designed for hydrocarbons and thus cannot handle polar components such as ethanol. Figure 4.9 shows the VLE curve for the same mixture at a higher temperature of 333.4 K. SAFT without any adjustment of the binary interaction parameter predicts the vapor-phase and the liquid-phase mole fractions fairly accurately. PR predicts the gas phase mole fraction, but over-predicts ethane liquid phase mole fractions. We tested another three-parameter equation of state: Redlich Kwong equation of state, for this case. We observe that the predictions are even worse. We do not consider this equation of state in further comparisons. Figure 4.10 shows the VLE curve for methane-ethanol mixture at 313.4 K. In this case we observe that although ethanol is an associating compound, the PR equation of state which does not explicitly account for association, does predict the liquid phase mole fractions very accurately. On the contrary, SAFT over-

predicts the liquid-phase methane mole fractions. When the binary interaction coefficient is adjusted to 0.05, SAFT is able to predict the liquid-phase mole fractions. This trend is again repeated at a different temperature of 333.4 K for the same system as shown in Figure 4.11.

Figure 4.12 shows the VLE curve for a CO<sub>2</sub>-methanol system. Again we observe that for associating systems, SAFT shows a better predictive capability than the PR equation of state without adjusting the binary interaction coefficient. Figure 4.13 and Figure 4.14 show the VLE curve for a CO<sub>2</sub>-ethanol system at two different temperatures. Although SAFT predictions are better than those of the PR equation of state are, the CO<sub>2</sub> liquid phase mole fractions are still over-predicted by SAFT. Figures 4.15 and 4.16 show the VLE curve for a CO<sub>2</sub>-propanol system. Here the improvement in liquid mole fraction prediction by SAFT is only marginal. This could be due to the poorer modeling of the non-associating part of the model, whose effects become significant for heavier molecules. When the binary interaction coefficient is adjusted to 0.062 we get an excellent agreement of the vapor and the liquid phase mole fractions.

Figures 4.17 and 4.18 show the VLE curve for a ethane-propanol system. SAFT without any adjustment in the binary interaction coefficient predicts the liquid phase and the gas phase mole fractions accurately. The PR equation of state over-predicts the ethane liquid phase mole fractions.

Figure 4.19 shows SAFT predictions for an azeotrope forming mixture of methanol-hexane. A binary interaction coefficient of 0.044 captures the azeotrope and the liquid and the gas phase mole fractions very accurately. The PR equation of state is not able to capture even the correct trend for such azeotrope forming mixtures even with the adjustment of binary interaction coefficients. Figure 4.20 shows the VLE curve for another azeotrope forming mixture of propanol and heptane where again SAFT with an adjustable binary interaction coefficient of 0.018 captures the azeotrope behavior. SAFT without any adjustment of the binary interaction coefficient does not do well around the azeotrope concentration, but predicts the phase behavior reasonably accurately at very low and very high concentrations of propanol.

In Figure 4.21 we present the vapor-liquid equilibrium curve for an ethanol-water mixture at 298.14 K. We observe that we have to adjust both the binary interaction coefficient ( $k_{ij}$ ) as well as the association interaction coefficient ( $a_{ij}$ ) for the SAFT equation of state in order to be able to get a good fit to the experimental data. It is also interesting to observe that there are at least two pairs of binary and association interaction coefficients which can effectively give a good fit to the experimental data. We searched the binary and association interaction coefficient phase space and have found two pairs which effectively give the same reduction in error with the experimental data. We have done similar studies on methanol-water mixtures which we shall present in the next chapter.



We now proceed to test SAFT for the phase behavior of ternary mixtures. Figure 4.22 shows the VLE diagram of a ternary mixture of methane-ethane-propane system at  $-75$  C and 100 psia. The SAFT predictions are not accurate in the liquid phase. PR equation of state, on the other hand, predicts the liquid and the gas phase mole fractions extremely accurately. Figure 4.23 shows the VLE curve of the same system at a higher pressure of 200 psia. The deviations in the SAFT predictions are even higher whereas the PR equation of state still accurately predicts the liquid and gas phase mole fractions. This suggests that the defects in the non-associating part of the SAFT formulation become even more significant when handling ternary mixtures. The same trend is maintained at 400 psia, 600 psia and 800 psia as shown in Figures 4.24 to 4.26. It is observed that the two-phase region shrinks as the pressure is increased.

### 4.3 PSEUDOCOMPONENTS

Mixture 1 shown in Table 4.3 is a North Sea gas condensate whose fluid composition is given by Pedersen[66]. Figure 4.27 shows the variation of the gas phase compressibility factor with pressure at a temperature of 155 C. It is seen that SAFT consistently under predicts the compressibility factor. The dew point as predicted by SAFT is 315 K whereas the experimental value reported in literature is 388 K. Figure 4.28 shows the variation of the gas phase compressibility factor at 92.8 C for a North Sea black oil whose composition is given in Table 4.4 as reported by Pedersen et al., [66]. The gas phase compressibility factor is over

predicted by SAFT. There are no theoretical predictions above 100 psi as the bubble point is reached at this temperature as against an experimental value of 260 psi. Figure 4.29 shows the variation of the liquid specific gravity with pressure for the same mixture. We note that the SAFT predictions are not very good for this case. The general poor agreement between SAFT predictions and experimental data could be due to the zero binary interaction coefficients used amongst all the hydrocarbons and the pseudocomponents although this is generally the norm in the industry when applying a conventional equation of state like the Peng-Robinson equation. The only adjustable parameters used in these equations are the pseudocomponent molecular weights which cannot be measured experimentally with great accuracy.

#### **4.4 CONCLUSIONS**

We have developed a SAFT based model for phase behavior of multi-component mixtures of associating molecules. As shown in the previous section we have extensively tested the SAFT model for pure-components and binary mixtures. We have extensively studied binary mixtures of non-associating and associating mixtures. We conclude that both Peng-Robinson and SAFT are equally suitable for simple non-associating mixtures but SAFT clearly is more accurate when polar mixtures are modeled. We have also done some testing on ternary systems. We have implemented the SAFT parameter evaluation for

pseudo-components generally encountered in the modeling of reservoir fluids although the predictions for the mixtures with SAFT are generally poor.

We have successfully merged SAFT into an existing compositional reservoir simulator (UTCMP) which helps us in accurate predictions of thermodynamic properties in reservoir studies. Phase compositions are obtained by flash calculations. A rigorous stability analysis test is done before all flash calculations to determine the number of phases. UTCMP has a three-phase calculation capability. The incorporation of an accurate thermodynamic model such as SAFT in a reservoir simulator such as UTCMP as an alternative to the existing Peng-Robinson equation of state is expected to greatly enhance the prediction of thermodynamic properties of complicated hydrocarbon reservoir fluid mixtures.

## References

- 1) Pedersen, K.S., Fredenslund, Aa., Thomassen, P., *Properties of Oils and Natural Gases*, Gulf Publishing, 1989.
- 2) Vargaftik, N.B., *Tables on the Thermophysical properties of Liquids and Gases*, John Wiley & Sons, New York, 1970
- 3) Hoepfner, A., Kreiblich, U.T., and Schaefer, K., "Einfluß der Molekülform auf die thermodynamischen Eigenschaften binärer Organischer Nichtelektrolytsysteme unpolarer Flüssigkeiten", *Ber. Bunsen-Ges. Phys. Chem.*, 74, 1016 (1970).
- 4) Lin, H.M., Sebastian, H.M., Chao, K.C., "Gas-Liquid Equilibrium in Hydrogen + n-Hexadecane and Methane+n-Hexadecane at Elevated Temperatures and Pressures", *J. Chem. Eng. Data*, 25, 252 (1980).
- 5) Suzuki, K., Sue, H., Itou, M., Smith, R.L, Inomata, H., Arai, K., Saito, S., "Isothermal vapor-liquid equilibrium data for binary systems at high pressures: carbon dioxide-methanol, carbon dioxide-ethanol, carbon dioxide – 1-propanol, methane-ethanol, methane-1-propanol, ethane-ethanol, and ethane-1-propanol systems", *J. Chem. Eng. Data*, 35, 63 (1990).
- 6) Ohgaki, K., Katayama, T., "Isothermal Vapor-Liquid Equilibrium Data for Binary Systems Containing Carbon dioxide at High Pressures: Methanol-Carbon Dioxide, n-Hexane-Carbon Dioxide, and Benzene-Carbon Dioxide Systems", *J. Chem. Eng. Data*, 21, 53 (1979).
- 7) Raal, J.D., Code, R. K., Best, D. A., "Examination of Ethanol-n-Heptane, Methanol-n-Hexane Systems Using New Vapor-Liquid Equilibrium Still", *J. Chem. Eng. Data*, 17, 211 (1972).
- 8) Gurkul S.M.K.A., Raju, B.N., "Isobaric Vapor-Liquid Equilibria of the 1-Propanol-n-Heptane System", *J. Chem. Eng. Data*, 11, 501 (1966).
- 9) Phutela, R.C., Kooner, Z.S. and Fenby, D.V., "Vapor Pressure study of Deuterium exchange Reactions in Water-Ethanol system: Equilibrium Constant Determination", *Aust. J. Chem.*, 32, 2353 (1979).

- 10) Wichterle, I., and Kobayashi, R., "Vapor-Liquid Equilibrium of Methane-Ethane-Propane system at Low Temperatures and High Pressures", *J. Chem. Eng. Data*, 17, 13 (1972).

	m	$v^\infty$ (mL/mol)	$u^0/k$ (K)
Methane	1.000	21.576	190.29
Ethane	1.941	14.460	191.44
Propane	2.696	13.457	193.03
Butane	3.458	12.599	195.11
Heptane	5.391	12.282	204.61
Decane	7.527	11.723	205.46
Hexadecane	11.209	12.300	210.65
Nitrogen	1.000	19.457	123.53
CO <sub>2</sub>	1.417	13.578	216.08

**Table 4.1: Segment parameters for nonassociating fluids (Huang et al., 1991)**

	M	$v^\infty$ (mL/mol)	$u^0/k$ (K)	$\epsilon/k$ (K)	$10^2 \kappa$
Methanol	1.776	12.0	216.13	2714	4.856
Ethanol	2.457	12.0	213.48	2759	2.920
Propanol	3.240	12.0	225.68	2619	1.968
Butanol	3.971	12.0	225.96	2605	1.639
Ammonia	1.503	10.0	283.18	893.1	3.270
Water	1.179	10.0	528.17	1809	1.593

**Table 4.2: Segment and site-site parameters for associating fluids (Huang et al., 1991)**

	Weight %	Mole %	Molecular Weight	Density (g/cm <sup>3</sup> ) at 15 C , 1 atm
N <sub>2</sub>	0.571	0.6		
CO <sub>2</sub>	5.031	3.34		
C <sub>1</sub>	40.667	74.16		
C <sub>2</sub>	8.126	7.90		
C <sub>3</sub>	6.254	4.15		
i-C <sub>4</sub>	1.401	0.71		
n-C <sub>4</sub>	2.855	1.44		
i-C <sub>5</sub>	1.306	0.53		
n-C <sub>5</sub>	1.637	0.66		
C <sub>6</sub>	2.355	0.81		
C <sub>7</sub>	3.749	1.20	91.2	0.746
C <sub>8</sub>	4.100	1.15	104.0	0.770
C <sub>9</sub>	2.577	0.63	119.0	0.788
C <sub>10</sub>	2.329	0.50	133.0	0.795
C <sub>11</sub>	1.466	0.29	144.0	0.790
C <sub>12</sub>	1.458	0.27	155.0	0.802
C <sub>13</sub>	1.624	0.28	168.0	0.814
C <sub>14</sub>	1.413	0.22	181.0	0.824
C <sub>15</sub>	1.165	0.17	195.0	0.833
C <sub>16</sub>	1.057	0.15	204.0	0.836
C <sub>17</sub>	1.096	0.14	224.0	0.837
C <sub>18</sub>	0.729	0.09	234.0	0.839
C <sub>19</sub>	1.137	0.13	248.0	0.844
C <sub>20+</sub>	5.896	0.47	362.0	0.877

**Table 4.3: Composition of Mixture 1 of North Sea gas condensate, (Pedersen, 1989)**

Component	Weight %	Mole %	Molecular Weight	Density (g/cm <sup>3</sup> ) at 15 C , 1 atm
N <sub>2</sub>	0.145	0.56		
CO <sub>2</sub>	1.450	3.55		
C <sub>1</sub>	6.757	45.34		
C <sub>2</sub>	1.531	5.48		
C <sub>3</sub>	1.516	3.70		
i-C <sub>4</sub>	0.378	0.70		
n-C <sub>4</sub>	0.891	1.65		
i-C <sub>5</sub>	0.489	0.73		
n-C <sub>5</sub>	0.580	0.87		
C <sub>6</sub>	1.043	1.33		
C <sub>7</sub>	2.276	2.73	89.9	0.757
C <sub>8</sub>	3.125	3.26	103.2	0.777
C <sub>9</sub>	2.342	2.14	117.7	0.796
C <sub>10</sub>	2.379	1.94	133.0	0.796
C <sub>11</sub>	2.205	1.62	147.0	0.800
C <sub>12</sub>	2.179	1.47	160.0	0.815
C <sub>13</sub>	2.693	1.69	172.0	0.833
C <sub>14</sub>	2.789	1.62	186.0	0.843
C <sub>15</sub>	2.937	1.59	200.0	0.849
C <sub>16</sub>	2.553	1.30	213.0	0.858
C <sub>17</sub>	2.388	1.11	233.0	0.851
C <sub>18</sub>	2.885	1.26	247.0	0.856
C <sub>19</sub>	2.571	1.07	258.0	0.868
C <sub>20+</sub>	51.898	13.32	421.0	0.914

**Table 4.4: Composition of Mixture 2 of North Sea black oil (Pedersen, 1989)**



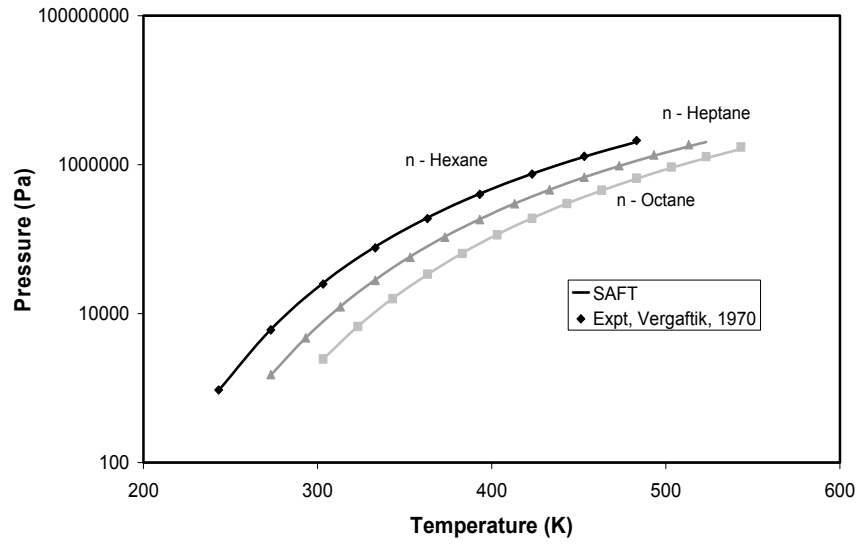


**Figure 4.1: Vapor pressure curves of n-alkanes**

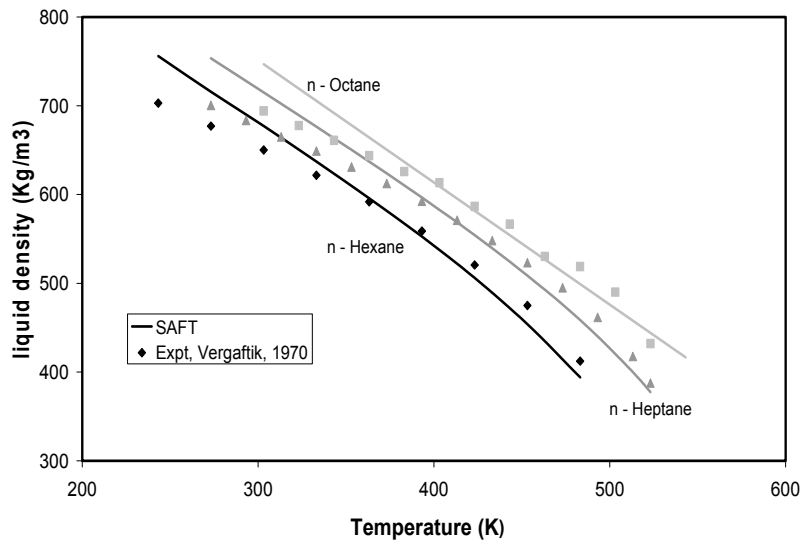


**Figure 4.2: Liquid density curves of n-alkanes**

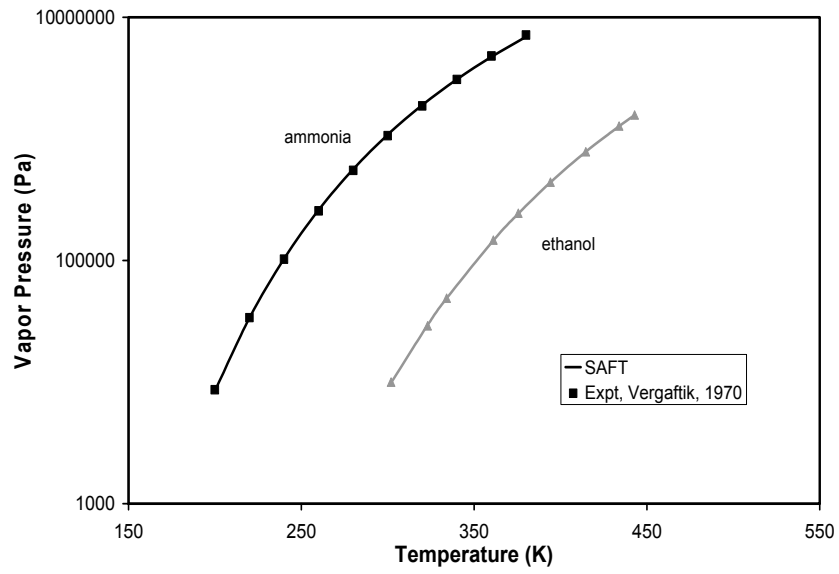


**Figure 4.3: Vapor pressure curves for polar compounds**

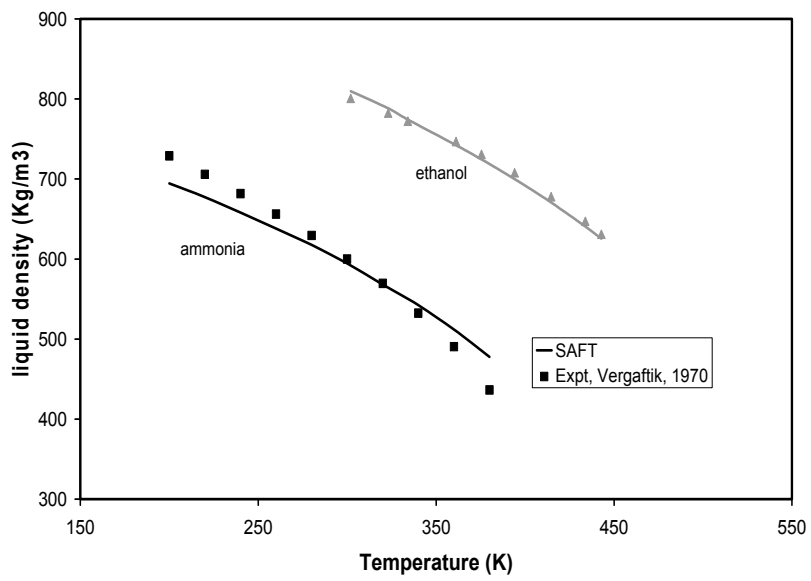


**Figure 4.4: Liquid densities of polar compounds**

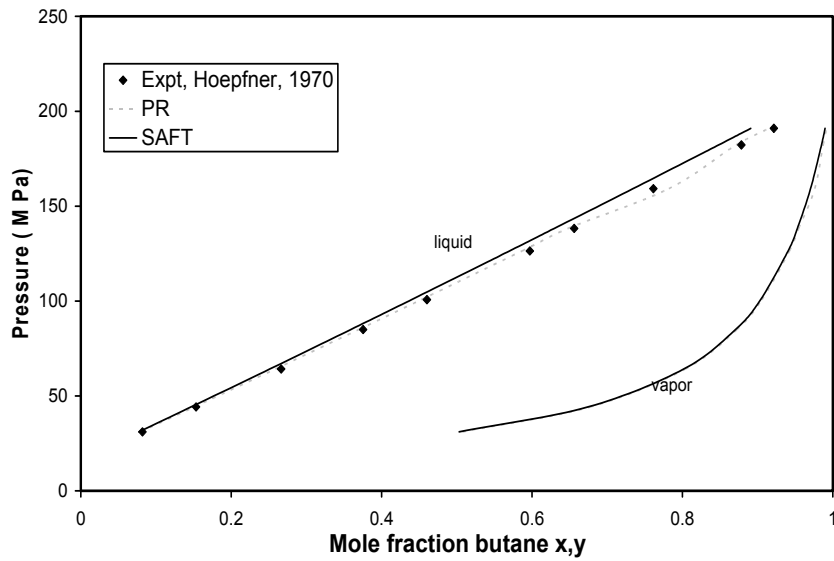


Figure 4.5: Vapor liquid equilibrium for butane-hexane mixture at 293.15 K

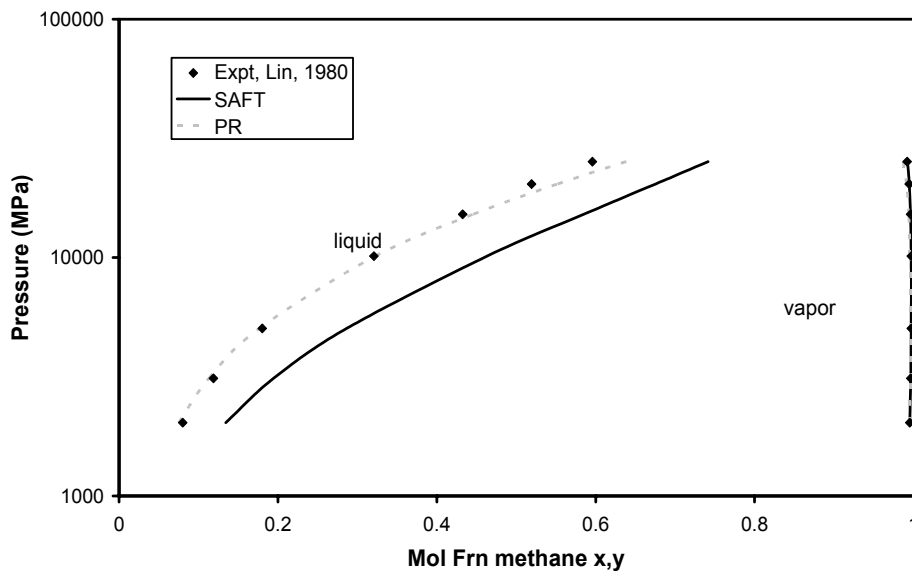
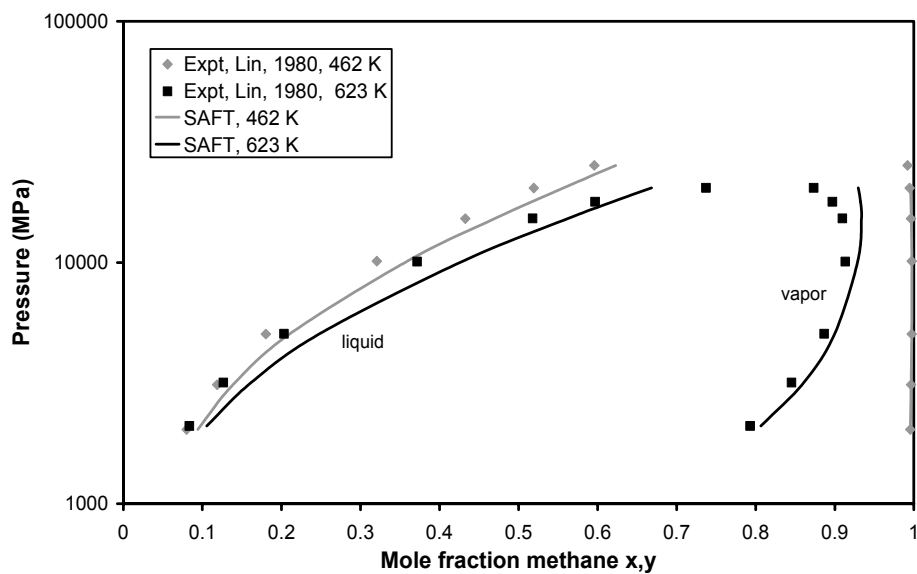
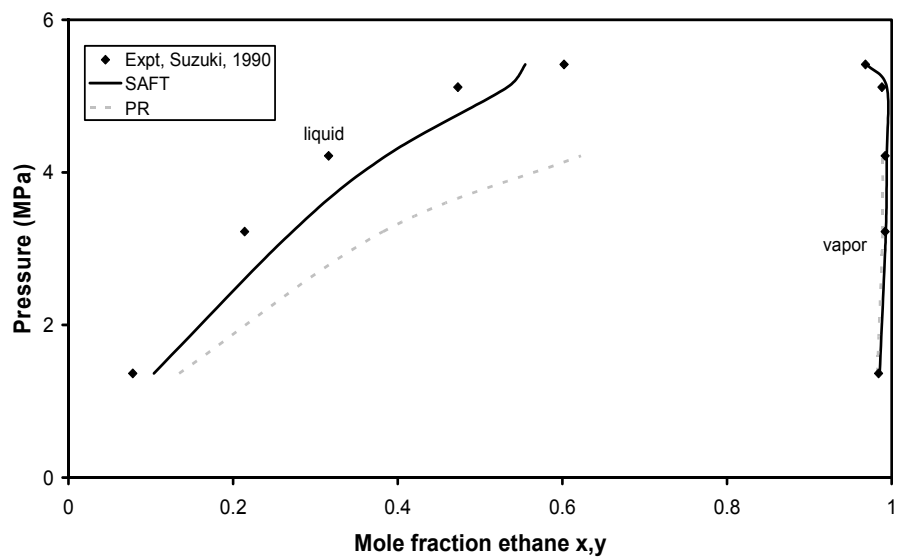


Figure 4.6: Vapor liquid equilibrium for methane-hexabutane at 462 K



**Figure 4.7: Vapor liquid equilibrium curve for methane-hexadecane mixture at 462 K and 623 K**



**Figure 4.8: Vapor liquid equilibrium curve for ethane-ethanol mixture at 313.4 K**

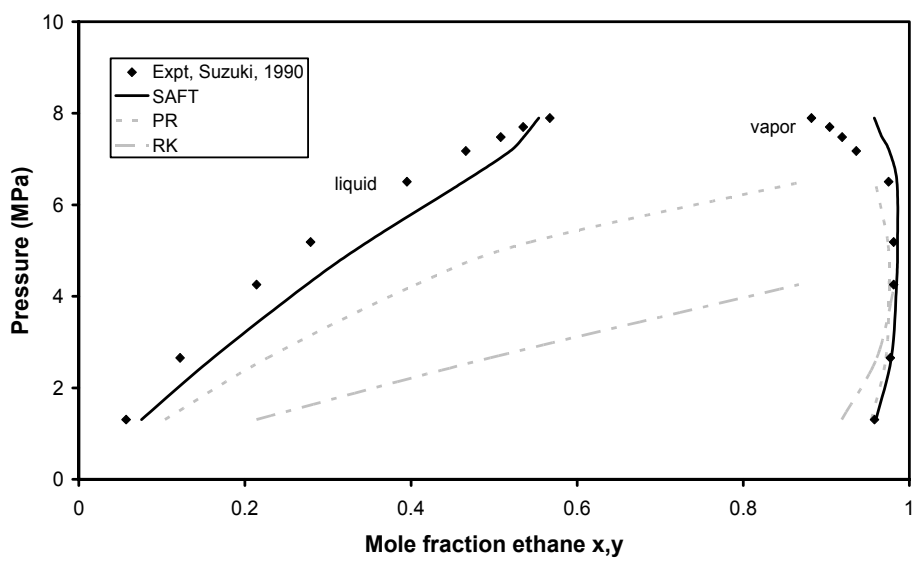


**Figure 4.9: Vapor liquid equilibrium curve for ethane-ethanol mixture at 333.4 K**

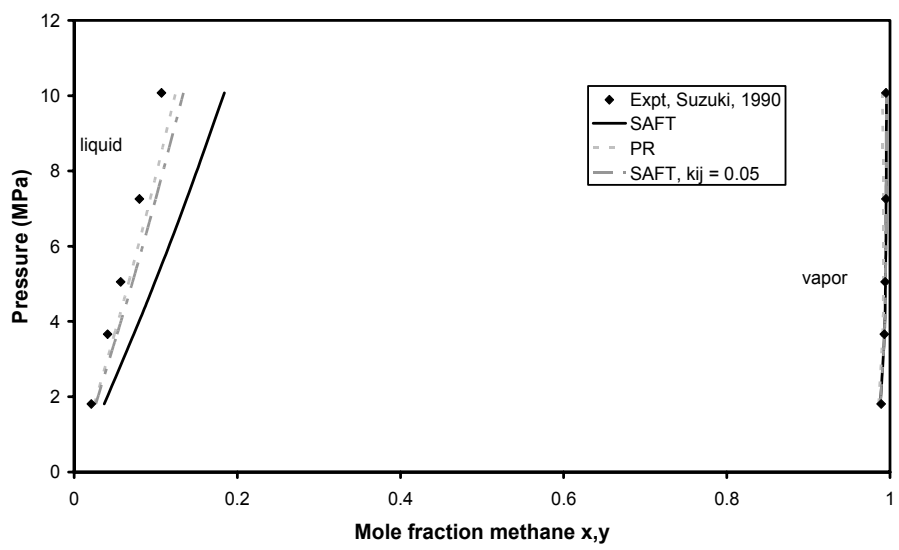


**Figure 4.10: Vapor liquid equilibrium curve for methane-ethanol mixture at 313.4 K**

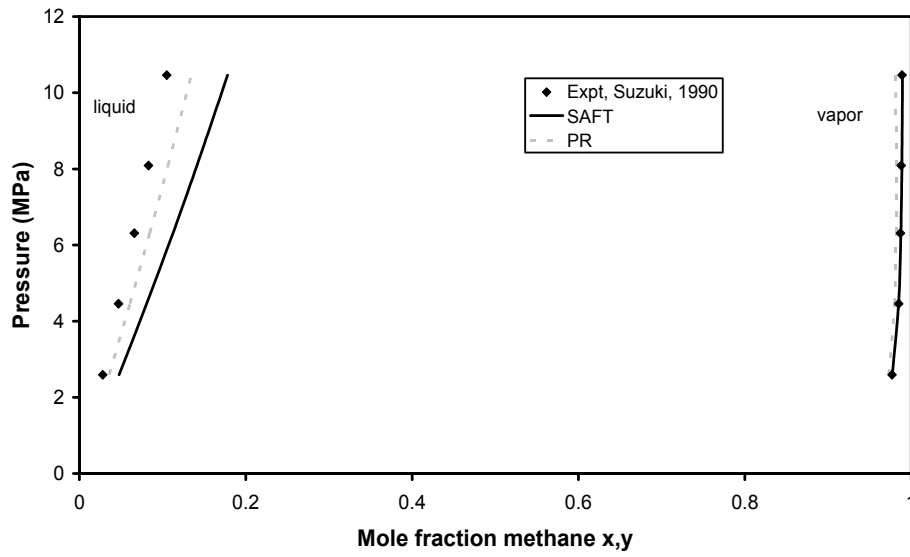


**Figure 4.11: Vapor liquid equilibrium curve for methane-ethanol mixture at 333.4 K**

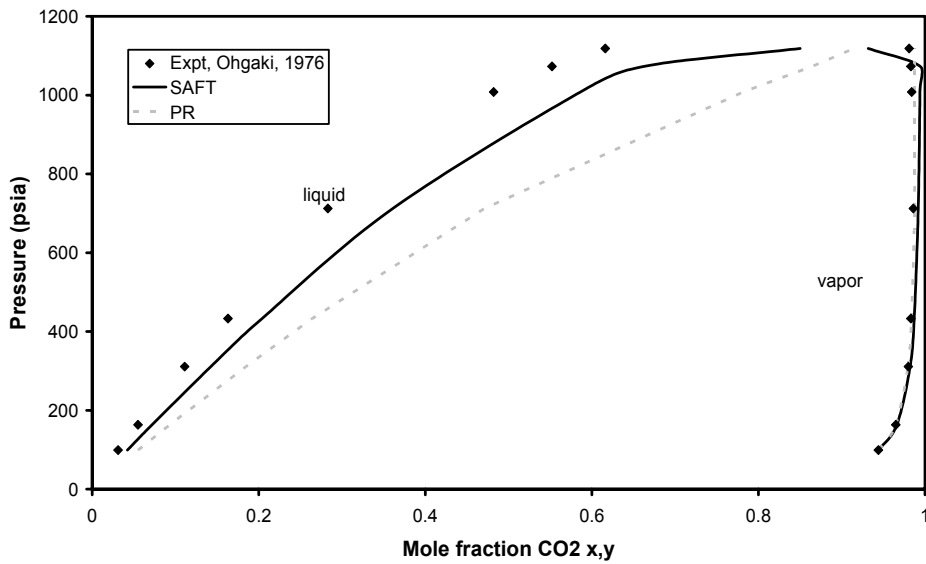


**Figure 4.12: Vapor liquid equilibrium curve for CO<sub>2</sub>-methanol mixture at 313.4 K**

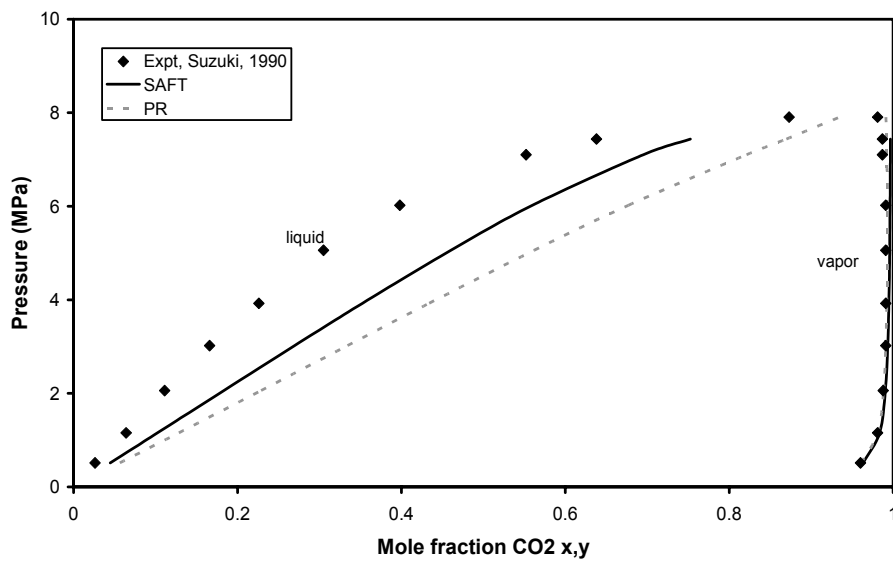


Figure 4.13: Vapor liquid equilibrium curve for CO<sub>2</sub>-ethanol mixture at 313.4 K

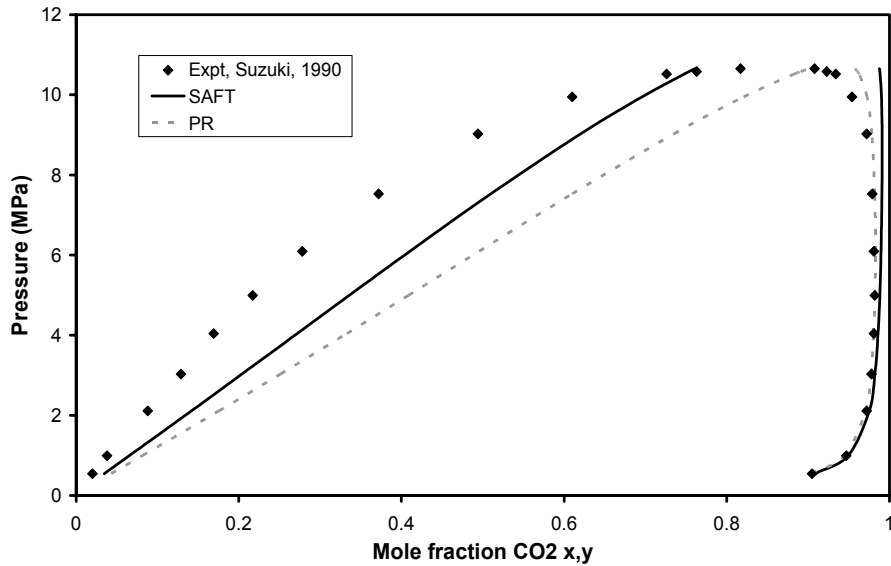


Figure 4.14: Vapor liquid equilibrium curve for CO<sub>2</sub>-ethanol mixture at 333.4 K

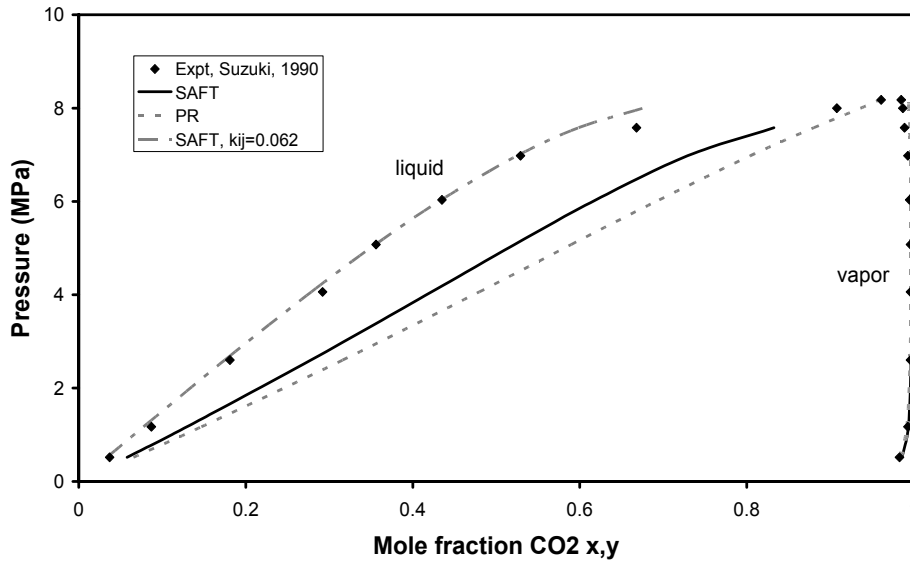


Figure 4.15: Vapor liquid equilibrium curve for CO<sub>2</sub>-propanol mixture at 313.4 K

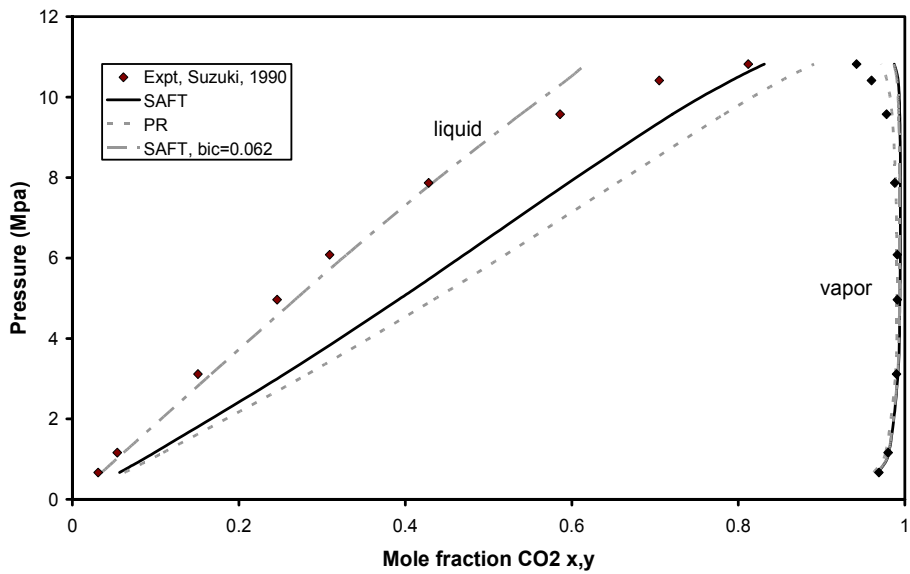


Figure 4.16: Vapor liquid equilibrium curve for CO<sub>2</sub>-propanol mixture at 333.4 K



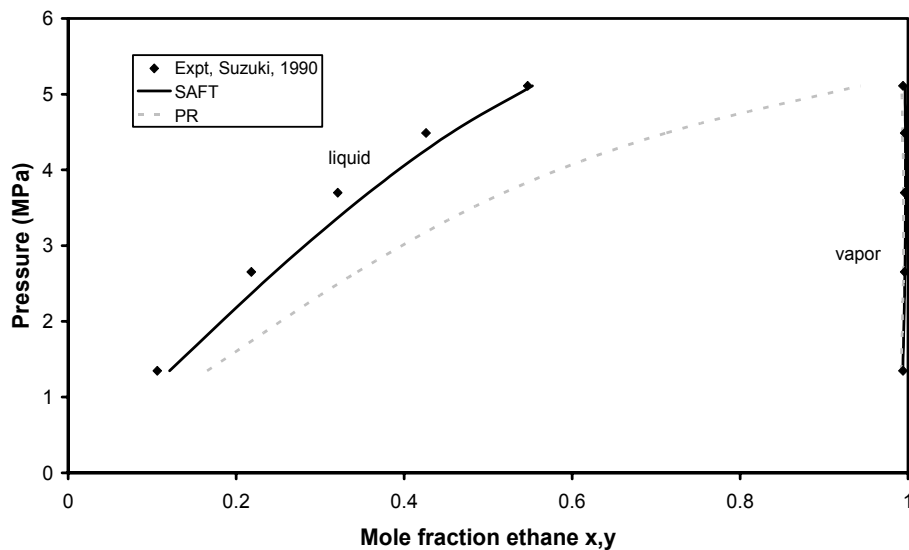


Figure 4.17: Vapor liquid equilibrium curve for ethane-propanol mixture at 313.4 K

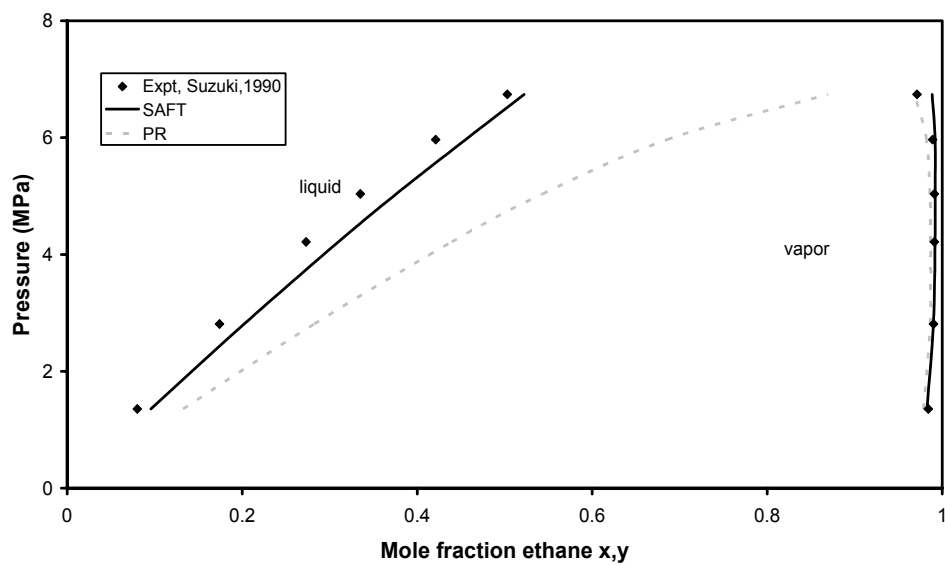
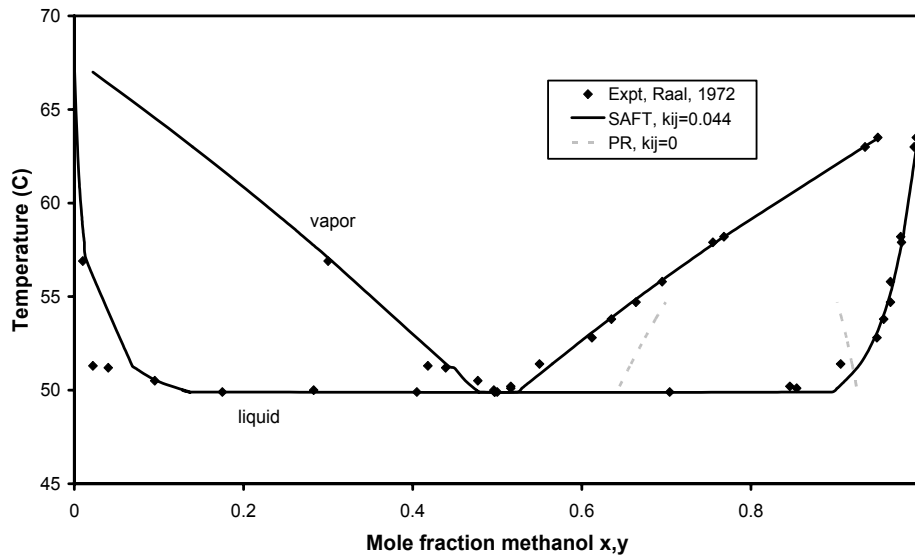
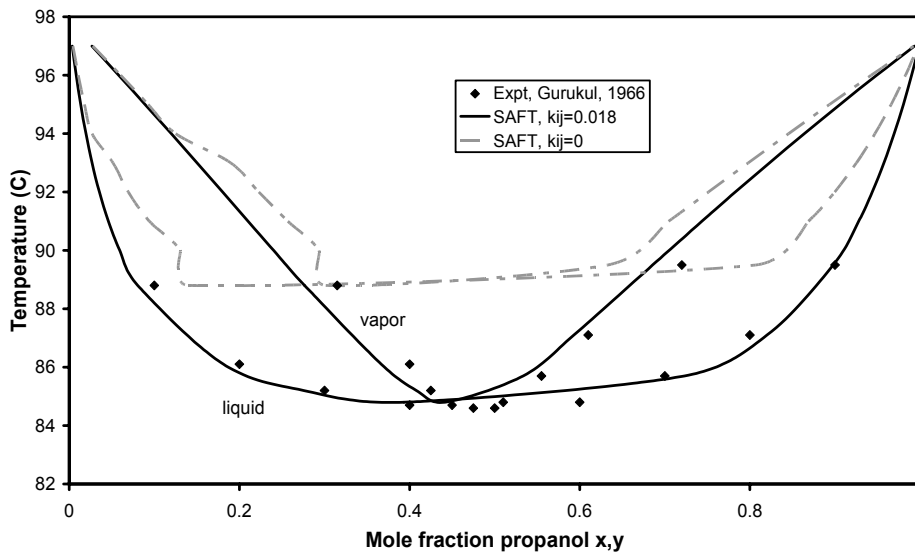


Figure 4.18: Vapor liquid equilibrium curve for ethane-propanol mixture at 333.4 K



**Figure 4.19: Vapor liquid equilibrium curve for methanol-hexane mixture at 1 atm**



**Figure 4.20: Vapor liquid equilibrium curve for propanol-heptane at 1 atm**

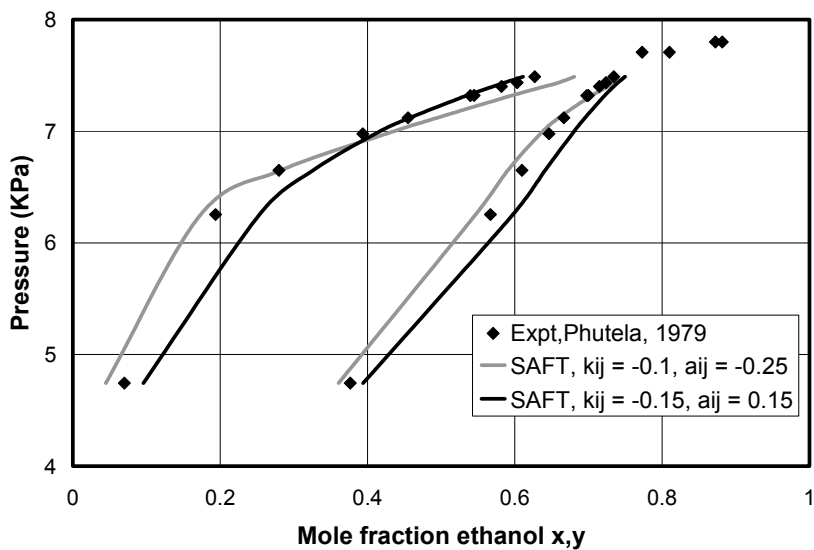


Figure 4.21: Vapor liquid equilibrium for ethanol-water mixture at 298.14 K

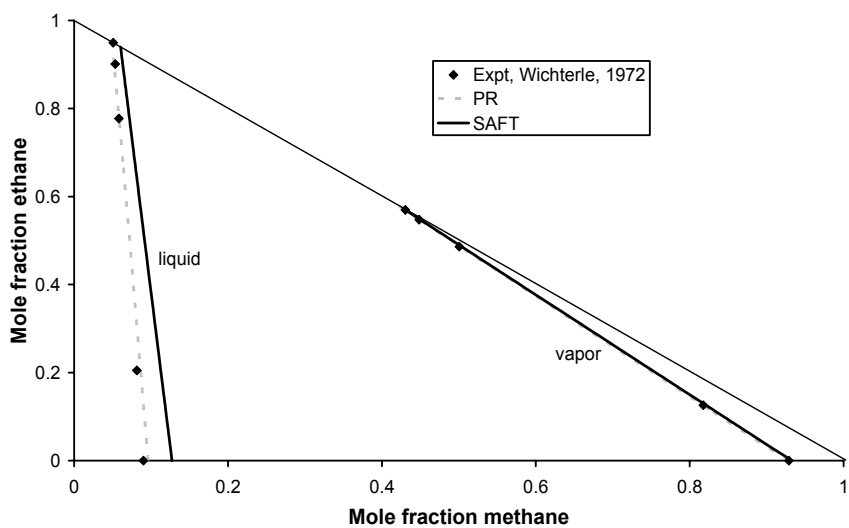
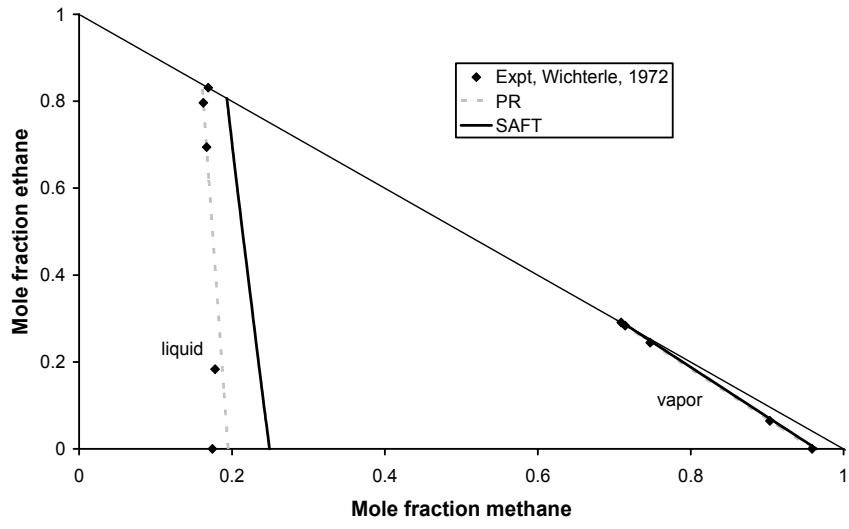
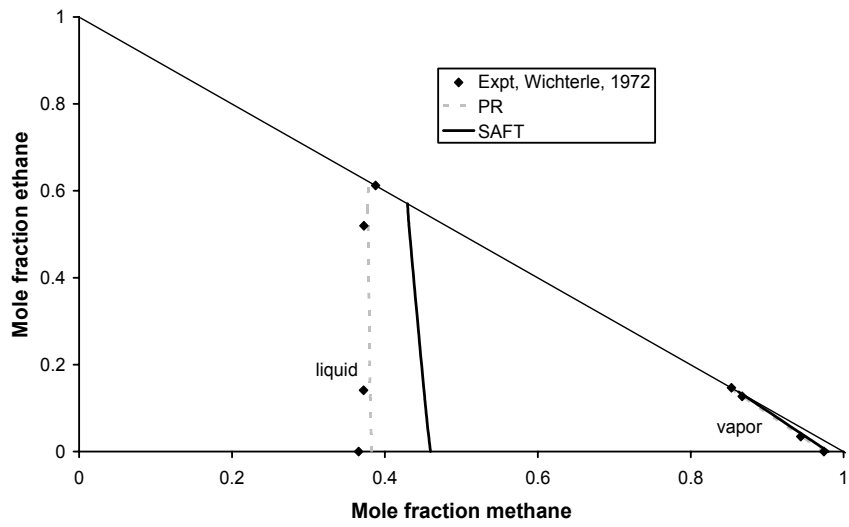


Figure 4.22: VLE curves for methane-ethane-propane system at  $-75\text{ C}$ , 100 psia



**Figure 4.23: VLE curves for methane-ethane-propane system at -75 C, 200 psia**



**Figure 4.24: VLE curves for methane-ethane-propane system at -75 C, 400 psia**

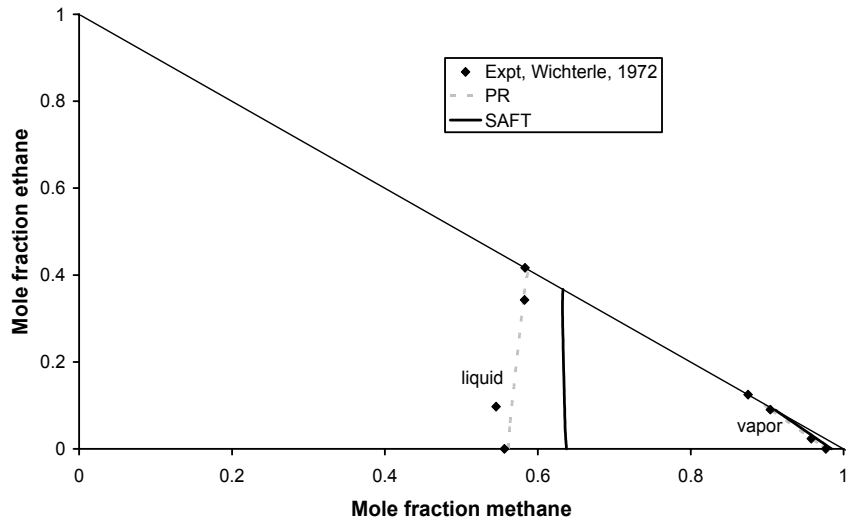


**Figure 4.25: VLE curves for methane-ethane-propane system at  $-75\text{ C}$ ,  $600\text{ psia}$**

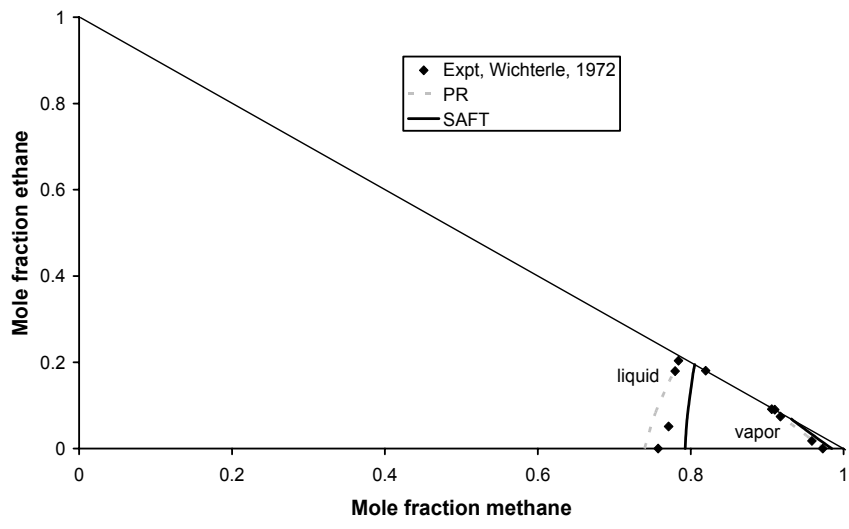


**Figure 4.26: VLE curves for methane-ethane-propane system at  $-75\text{ C}$ ,  $800\text{ psia}$**

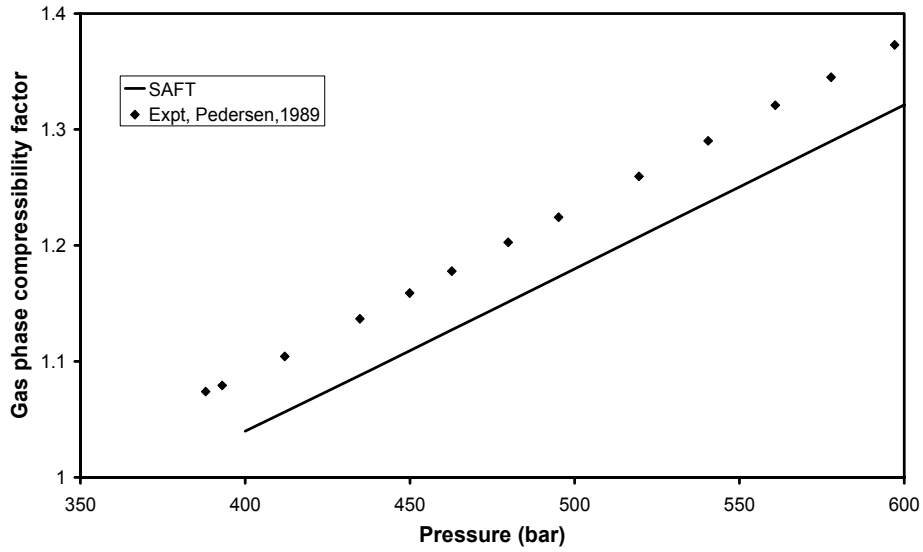


**Figure 4.27: Gas phase compressibility factor for Mixture 1(North sea gas condensate) in a constant mass expansion study at 155 C**

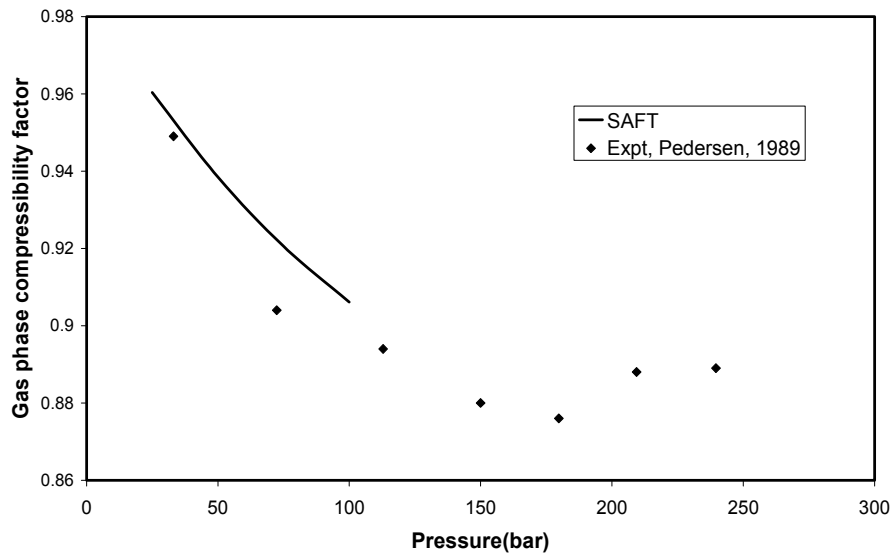


**Figure 4.28: Gas phase compressibility factor of Mixture 2 (North Sea black oil) in a differential liberation study at 92.8 C**

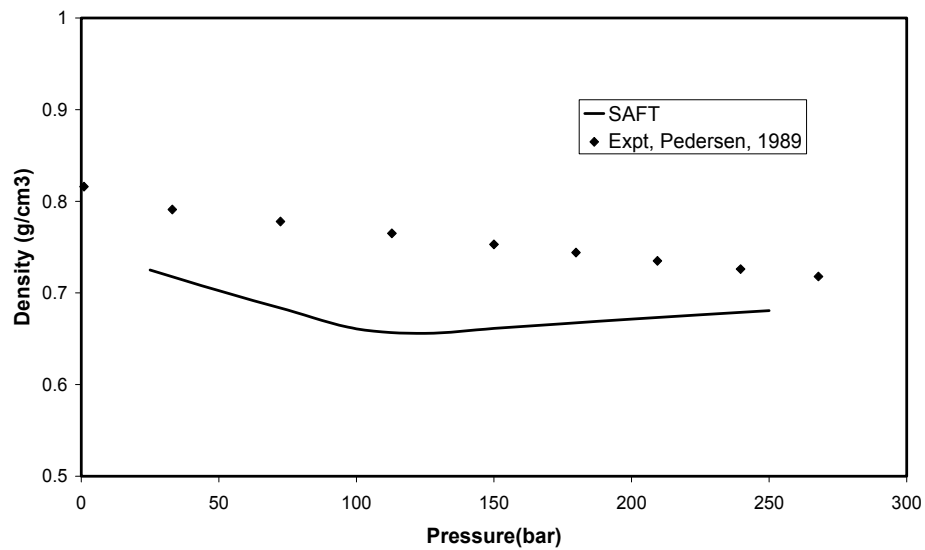


**Figure 4.29: Liquid phase densities of Mixture 2 (North Sea black oil) in a differential liberation study at 92.8 C**

## CHAPTER 5

### BULK THERMODYNAMIC PROPERTIES OF GAS CONDENSATE MIXTURES

#### 5.1 INTRODUCTION

Gas condensate reservoirs form a great percentage of gas reservoirs in the world. In such reservoirs, a liquid hydrocarbon phase drops out when the pressure falls below the dew point of the fluid. This results in a build-up of liquid in the reservoir and/or around the well-bore resulting in decrease in the relative permeability of gas and thus a sharp decrease in gas productivity. Afidick et al[1]., have reported field data from the giant Arun field in Indonesia that show a reduction in well productivity due to condensate accumulation by a factor of 2 to 4.

The phase behavior of gas condensate hydrocarbons has been extensively studied (Sarkar et al.,[2] ). There have been very few studies (Kokal [3], Robinson [4] ) however on the influence of water on the phase behavior and properties of gas-condensate fluids. Recently, experimental studies have shown (Du et al., [5], Walker [6] ) that methanol treatment can significantly lower condensate build-up near the well-bore and thus increase the gas productivity. There has been no work done to model the phase behavior of gas condensate-water-methanol systems, using conventional or any other equation of state.



In this study we model the phase behavior of gas condensates using a Peng-Robinson equation of state and also an equation of state based on statistical mechanics, i.e., the Statistical Associating Fluid Theory (SAFT). An important property of interest in gas condensate modeling is the prediction of liquid dropout. We also attempt to model the effect of polar compounds such as water and methanol to study the changes in condensate dropout .

## **5.2 PURE GAS CONDENSATE MIXTURES**

One of the major objectives of this study is to match the experimental liquid dropout data obtained at 145 F by Walker [6] for the gas-condensate mixture (Mixture 1) shown in Table 5.1. Figure 5.1 shows the total liquid volume fraction curves as predicted by the Peng-Robinson equation. There are no binary interaction coefficients used amongst hydrocarbons. We see that the prediction of the Peng-Robinson equation is extremely good for pure hydrocarbon mixtures. Figure 5.2 shows the liquid and vapor molar density variations with pressure. Figures 5.3 and 5.4 show the mole fractions of the different components in the liquid and vapor phases respectively. At high pressure the liquid phase contains a significant amount of methane but as the pressure is lowered the heavy fraction is the only component left in the liquid phase.

On the other hand, Figure 5.5 shows the SAFT predictions for the same gas condensate mixture with and without adjusting the binary interaction coefficient. We observe that the liquid volume fraction curves are not very well predicted without adjusting the binary interaction coefficients. Once the binary interaction coefficients are adjusted we get a very good fit using the SAFT equation as well. Table 5.2 shows the binary interaction coefficients used to fit the liquid volume fractions with the SAFT equation. Since the PR EOS was developed for hydrocarbons it is not surprising to see that it fits the data better for pure hydrocarbon mixtures. Figure 5.6 shows the liquid and gas molar densities of this mixture using the SAFT equation of state without adjusting the binary interaction coefficients. Figure 5.7 and 5.8 are the mole fractions of various components in liquid and gas phases as predicted by SAFT without binary interaction coefficients. Figure 5.9 shows the liquid and gas molar densities predicted by SAFT with binary interaction coefficients. Figure 5.10 and 5.11 are the mole fraction curves for various components in the liquid and gas phase predicted by SAFT after adjusting the binary interaction coefficients. We notice that there is no significant change in the component mole fractions and the densities but the total liquid volume fraction curves are significantly affected by adjusting the binary interaction coefficients.

### 5.3 GAS CONDENSATE-METHANOL MIXTURES

The prediction of these two equations of state for gas-condensate mixtures with the addition of a polar solvent (methanol) shows some interesting comparisons with data. We have adjusted the overall composition so that 10 % of the mixture is methanol and the rest is the original gas-condensate mixture. The mixture composition is shown as Mixture 2 in Table 5.1. Figure 5.12 shows the liquid volume fraction curves with the adjusted binary interaction coefficients for the PR equation of state. Table 5.3 shows the methanol-hydrocarbon binary interaction coefficients used in the PR equation to fit to the experimental data. We note that only the methanol-hydrocarbon binary interaction coefficients are adjusted to get a good fit to data. Figure 5.13 shows the liquid and gas density variation for this mixture as predicted by the PR equation. The liquid density increases due to the addition of methanol from the pure gas condensate mixture values. Figure 5.14 and 5.15 show the liquid and gas phase mole fractions of each of the components. The methanol essentially drops off into the liquid phase for the entire pressure range at this temperature.

Figure 5.16 shows the SAFT prediction of liquid volume fraction curves for a 10 mol % methanol and 90 mol % gas condensate mixture with and without adjusting the hydrocarbon-methanol binary interaction coefficients. The hydrocarbon-hydrocarbon binary interaction coefficients have not been changed from those given in Table 5.2. When we do not adjust the hydrocarbon-methanol

binary interaction coefficients the fit to experimental data is not good. Once the methanol-hydrocarbon binary interaction coefficients are adjusted, as given in Table 5.3, we get a very good fit to experimental data. Figure 5.17 and Figure 5.20 present the molar density curves without and with the binary interaction coefficients for the methanol component. We observe that the magnitude in the binary interaction coefficients required is smaller than those required in the Peng-Robinson equation. Figure 5.18 and Figure 5.21 show the liquid phase mole fraction without and with binary interaction coefficients respectively with SAFT. Figure 5.19 and Figure 5.22 show the corresponding gas phase mole fractions.

We have matched the liquid volume fraction curves for 10 mol % methanol with both the Peng-Robinson and SAFT equations so far. Now, with the tuned binary interaction parameters we predict the behavior of these two equations for a 50 mol % methanol with 50 mol % gas-condensate fluid. Figure 5.23 shows the liquid volume fraction curves as predicted by the Peng-Robinson equation with the methanol-hydrocarbon binary interaction coefficients tuned for the 10 mol % methanol case. We observe that the Peng-Robinson equation under-predicts the liquid volume fraction curves. Figure 5.24 shows the liquid and vapor molar densities. Figure 5.25 shows the mole fractions of the various components in the liquid phase, which is essentially concentrated with methanol over the entire pressure range. There are trace amounts of hydrocarbons present in the liquid phase. Figure 5.26 shows the mole fractions of the various components in the gas phase as predicted by the PR equation. Here we observe that the gas phase

is mainly concentrated with methane for the entire pressure range. Next we see the predictions for the same mixture using the SAFT equation of state. Here again we use the binary interaction coefficients tuned to match the 10 mol % methanol and 90 mol % gas-condensate mixture. Figure 5.27 shows the liquid volume fraction curves. We observe that SAFT slightly over-predicts the liquid volume fractions but captures the correct trend with pressure. Figure 5.28 shows the liquid and vapor molar densities as predicted by SAFT. The liquid molar density is essentially constant over the given pressure range. Figure 5.29 show the mole fractions of various components in the liquid phase as predicted by SAFT which shows that as the pressure decreases the methanol concentration in the liquid phase increases. This is because at lower pressure the hydrocarbons tend to be present in the vapor phase. Figure 5.30 shows the mole fractions of the various components in the vapor phase which contains mostly methane.

#### **5.4 EFFECT OF METHANOL CONCENTRATION ON GAS CONDENSATE-METHANOL MIXTURES**

In this section we present the effect of varying methanol concentration on the liquid-volume fraction curves at various temperatures. Figures 5.31 to 5.33 show the changes in the liquid volume fraction curves with varying methanol concentration in a temperature range of 145 F to 350 F. These plots have been generated using the SAFT equation of state with the binary interaction coefficients given in Table 5.2 and Table 5.3. In Figure 5.31 the mixture temperature is 145 F. We observe that at 10 and 15 mol % methanol

concentrations the mixture exhibits retrograde behavior. That is we observe a dew point for the system at which the first drop of liquid is seen. There is a transition from a dew-point system to a bubble-point system in the methanol concentration range of 20 %. At higher methanol concentrations of 30 % and above the mixture behaves as a bubble-point system. Figure 5.32 shows the liquid volume fraction curves at 250 F. The transition from a dew-point system to a bubble-point system occurs between 20 and 25 mol % methanol concentration. The dew point at 0 % methanol concentration is about 2700 psi. Figure 5.33 shows the liquid volume fraction curves at 350 F. We observe that the dew-point to bubble-point transition occurs at a still higher concentration of 35-40 mol % methanol in this case. In summary we observe that the transition from a dew-point system to a bubble-point system occurs at a higher methanol concentration as the mixture temperature is increased.

## **5.5 WATER-METHANOL MIXTURES**

Figure 5.34 shows the vapor liquid equilibrium curve for a water-methanol system at 40 C. We see that the Peng-Robinson equation of state gives a very good fit to the experimental data [8] even for a very highly associating system of water and methanol just by adjusting the binary interaction coefficient. However, we need to adjust the binary interaction coefficient to a negative value. We observe that without any adjustment in the binary interaction coefficient or by using positive values of the binary interaction coefficient we are able to match the

methanol-lean phase but the methanol-rich phase mole fraction predictions are very poor. When the binary interaction coefficient is adjusted to  $-0.1$  both the methanol-lean phase and the methanol-rich phase mole fractions are predicted very accurately. Although the mole fraction predictions are accurate at this temperature we are operating in a very low-pressure range in comparison to gas-condensate phase behavior studies, where the operating pressure range is about 1000 to 5000 psi. The data available in the literature [8] for methanol-water mixtures for this pressure range is the liquid density. Figure 5.35 shows the liquid density predictions of methanol-water mixtures at various methanol concentration at 140 F. We use the same binary interaction coefficient of  $-0.1$  in the Peng-Robinson equation. We observe that the predicted liquid densities are less than the experimental value. However, it is very important to note that if we use no binary interaction coefficient or use a positive binary interaction coefficient, the PR equation predicts two separate phases for this methanol-water mixture at these high pressures. Clearly, this is an artifact introduced by the improper selection of the binary interaction coefficients.

We also present the SAFT predictions of the binary mixture of methanol-water as shown in Figure 5.34. We observe that even in the case of SAFT the water-methanol binary interaction coefficients have to be adjusted to a negative value of  $-0.15$ , so as to be able to match the experimental data. We have been able to cover only a small concentration range with the SAFT equation of state whereas with the PR equation of state we have been able to cover the entire

concentration range. The binary interaction coefficients have been obtained by searching across the entire binary interaction-association interaction coefficient phase space and minimizing the error between the experimental and predicted values. It is surprising that despite explicitly accounting for association terms in the SAFT EOS, the behavior of associating mixtures such as water and methanol cannot be adequately predicted without adjusting the binary interaction coefficients.

## **5.6 GAS CONDENSATE-WATER-METHANOL SYSTEMS**

Based on the knowledge on the binary interaction coefficient that we gained so far, we predict the behavior of the gas condensate-water-methanol system. Figure 5.36 shows the gas phase volume fraction curves for a 30 mol % water, 17 mol % methanol and 53 mol % gas condensate mixture whose composition are as given in Mixture 4 in Table 5.1. The phase volume fractions have been measured experimentally at 145 F at various pressures. The solid lines are the Peng-Robinson predictions with the water-hydrocarbon binary interaction coefficients adjusted. The binary interaction coefficients for hydrocarbon – water mixtures have been obtained from Wang et al.,[7] and are as shown in Table 5.3. We see that the PR equation fits the phase volume fractions fairly accurately. We observe that the system exhibits a two-phase behavior above the dew-point pressure of about 2700 psi. Above this pressure the hydrocarbons form a single-phase whereas water and methanol mix completely to form the heavier liquid



phase. Below the dew point pressure the hydrocarbon gas phase drops out to form a lighter liquid phase which is consistent with its retrograde behavior.

Figure 5.37 shows the molar densities of the three phases as predicted for the above mixture with the PR equation. We observe that the aqueous phase density is constant with pressure. The liquid and the vapor phase density are similar to the values when the water is not present in mixture. Figure 5.38 shows the mole fractions of the various components in the liquid phase as predicted by the PR equation. We see that as the pressure is decreased the lighter hydrocarbon namely C1 decreases and by corollary the mole fractions of heavier hydrocarbons n-C4, n-C7 and n-C10 increases. There are very negligible amounts of water and methanol in the lighter liquid. Figure 5.39 shows mole fractions of various components in the vapor phase which essentially contains almost 90 % of methane and about 10 % of butane. The heavier hydrocarbons, methanol and water are present in trace amounts. Figure 5.40 shows the mole fractions of various components in the heavy liquid. Almost all of the water and the methanol in the original mixture drops out to form this heavy liquid phase. There are very trace amounts of hydrocarbons present in this phase. Without the water-hydrocarbon binary interaction coefficients taken into account the water concentration in the vapor phase ranges between 0.5 to 1 % whereas with the binary interaction coefficients the water concentration in the vapor phase is in a lower range of 0.2 to 0.4 % . These binary interaction coefficients will play an

important role at higher temperatures where the concentration of water in the vapor phase could become significantly higher.

Figure 5.41 shows a comparison of the PR EOS predictions of the phase volume fractions with the measured data for a 13 mol % water, 65 mol % methanol and 22 mol % gas-condensate mixture with the overall composition of Mixture 5 in Table 5.1. The PR EOS captures the phase behavior qualitatively without any adjustment of the binary interaction coefficients, but it does not agree with the data quantitatively except it does predict the pressure for the transition between two and three phases rather well. Above pressures corresponding to the original gas-condensate dew point pressure of about 2700 psia, the data show a gas phase and an aqueous phase rather than just a gas phase as observed without the water and methanol components in the mixture. Figure 5.42 shows the molar densities of the three phases as predicted for the above mixture with the PR equation. Figure 5.43 to Figure 5.45 shows the mole fractions of the various components in the liquid, vapor and the aqueous phase respectively as predicted by the PR equation. We see that the trends in the mole fraction of the phases are similar to those predicted by the PR equation for Mixture 4.

Figure 5.46 shows the phase volume fraction calculations for SAFT equation of state for 30 mol % water, 17 mol % methanol and 53 mol % gas condensate mixture whose composition are as given in Mixture 4 in Table 5.1. Similar to the Peng-Robinson case the water-hydrocarbon binary interaction

coefficients only have been adjusted and as expected the SAFT calculations agree well with the experimental data for this case. Figure 5.47 shows the molar densities of the three phases as predicted for the above mixture with the SAFT equation. We observe that the aqueous phase density is different than the corresponding calculation obtained from the PR equation of state. Figure 5.48 to Figure 5.50 shows the mole fractions of the various components in the liquid, vapor and the aqueous phase respectively as predicted by the SAFT equation. The trends in the mole fraction of the phases are similar to those predicted by the PR equation for the same mixture.

Figure 5.51 shows a comparison of the SAFT EOS predictions of the phase volume fractions with the measured data for a 13 mol % water, 65 mol % methanol and 22 mol % gas-condensate mixture with the overall composition of Mixture 5 in Table 5.1. The SAFT equation of state shows good agreement with the experimental data without any adjustment of the binary interaction coefficients from those given in Tables 5.2 and 5.3. This indicates that the SAFT equation of state provides better predictions for mixtures with methanol and water as expected from theoretical considerations. Figure 5.52 shows the molar densities of the three phases as predicted for the above mixture with the SAFT equation. Figure 5.53 to Figure 5.55 shows the mole fractions of the various components in the liquid, vapor and the aqueous phase respectively as predicted by the SAFT equation. We see that the trends in the mole fraction of the phases are similar to those predicted by the PR equation, except in the liquid hydrocarbon phase. In

this phase, the methanol concentration predicted by the SAFT equation is significantly higher than that predicted by the PR equation.

## 5.7 HYDROCARBON-METHANOL-WATER MIXTURES

We have also made comparisons with experimental composition data available in the literature for hydrocarbon-water-methanol mixtures. Table 5.4 shows the two different mixtures from a Gas Processors Association Report for which experimental Liquid-Liquid-Vapor equilibrium data were measured by Ng *et al.*, [9] in the context of gas-hydrate inhibition. Figure 5.56 to 5.58 show the phase mole fraction comparisons of both the Peng-Robinson and SAFT equation with the experimental data for Mixture 1 given in Table 5.4. The binary interaction coefficients for both the equations of state are those given in Tables 5.2 and Table 5.3 which have been obtained by matching the experimental data in the previous section. We observe that both the PR and SAFT equations predict the vapor phase mole fractions reasonably well. The methane concentration is slightly under predicted in the liquid phase with the SAFT equation whereas the nC7 mole fractions are slightly over predicted as shown in Figure 5.56. The nC7 mole fraction in the liquid hydrocarbon phase is slightly under predicted with the PR equation as can be seen in Figure 5.57. Figure 5.58 shows that in the aqueous phase the methanol and water mole fractions are predicted fairly accurately by both the PR and SAFT equation of state. The phase volume fractions are also reasonably accurately predicted with both the equations for a hydrocarbon-

methanol-water mixture at 122 °F. Figures 5.59 to 5.61 show the phase mole fraction for Mixture 2 in Table 5.4 which has about 22 % methanol in the feed. We observe similar behavior as in the previous case only that the heaviest phase contains about 55 % methanol and 45 % water which is again reasonably accurately predicted by both the equation of states. Since the binary interaction coefficients obtained so far have been tuned to experimental data at 145 F we would like to see how these binary interaction coefficients hold at different temperatures. Figures 5.62 to 5.64 show the phase mole fractions for a 11 % methanol mixture at 68 °F. We find that the SAFT equation of state predicts the phase mole fractions accurately even at this temperature. Interestingly enough, even the Peng-Robinson equation of state predicts the phase mole fractions and the phase volume fractions accurately although the binary interaction coefficients in this case have been obtained by matching a different set of experimental data at a different temperature. Similarly, Figures 5.65 to 5.67 show the phase mole fractions and the volume fractions at 68 °F and 24 mol % methanol which is given as Mixture 4 in Table 5.4. Next we look at still lower temperature of 14 F. Figures 5.68 to 5.73 show the phase mole fractions for mixtures 5 and 6 at 14 F. Here again we see the same trend with both the equations. Interestingly, at this lower temperature although the predictions of the PR equation are in line with the experimental data, the SAFT prediction tend to deviate more from the experimental data especially in the case of the liquid hydrocarbon phase methane and nC7 mole fractions. This of great interest in reservoir simulators as Peng-

Robinson equation of state is widely used for speed and here we show that they are accurate for a fairly wide range of temperatures and compositions.

## 5.8 CONCLUSIONS

We have studied the phase behavior of water-methanol-hydrocarbon mixtures with both the Peng-Robinson and SAFT equation of state. The methanol-water and methanol-hydrocarbon binary interaction coefficients play a very important role in the phase behavior modeling of these mixtures using both the equations-of-state. We have also shown the effect of methanol concentration and temperature on the dew-point to bubble-point transition of a gas-condensate mixture. The transition from a bubble point to dew-point behavior occurs at a higher methanol concentration with increasing temperature. We have been able to tune the binary interaction coefficients of both the PR and SAFT equations to fit the experimental phase behavior data at a given temperature, but as would be expected the SAFT equation gives better predictions at different system conditions. We have also shown that both the equations of state predict the phase mole fractions also really well at different system temperatures.

## References

- 1) Afidick, D., Kaczorowski N. J., and Bette., "Production Performance of a Retrograde Gas: A Case Study of the Arun Field", paper *SPE 28749* presented at the 1994 Asia Pacific Oil & Gas Conference, Melbourne, Australia, Nov. 7-10
- 2) Sarkar, R., Danesh A.S., and Todd A.C., "Phase Behavior Modeling of Gas-Condensate Fluids Using an Equation of State", paper *SPE 22714* presented at the 66<sup>th</sup> Annual Technical Conference and Exhibition of the Society of Petroleum Engineers, Dallas, Texas, October 6-9, 1991.
- 3) Kokal, S., Al-Dokhi, M., and Sayegh, S., "Phase Behavior of Gas Condensate/Water System", paper *SPE 62931* presented at the 200 SPE Annual Technical Conference and Exhibition held in Dallas, Texas, October 2000.
- 4) Ng, H.J., Robinson, D.B., "The Influence of Water and Carbon Dioxide on the Phase behavior and Properties of a Condensate Fluid", paper *SPE 15401* prepared for presentation at 61<sup>st</sup> Annual Technical Conference and Exhibition of the Society of Petroleum Engineers held in New Orleans, Louisiana, October 5-8, 1986.
- 5) Du, Liangui, Walker, J.G., Pope, G. A., Sharma, M. M., Wang, P., "Use of Solvents to Improve the Productivity of Gas Condensate Wells", Paper *SPE 62935* presented at the SPE Annual Technical Conference and Exhibition, Dallas, TX (October 1-4, 2000).
- 6) Walker, J.G., "Laboratory Evaluation of Alcohols and Surfactants to Increase Production from Gas-Condensate Reservoirs", MS Thesis, The University of Texas at Austin, December 2000.
- 7) Wang, P, Pope, G.A., Sepehrnoori, K., "Development of Equations of State for Gas condensate for Compositional Petroleum Reservoir Simulation", *In Situ*, **24** (2&3) 2000.
- 8) Sentenac, P., Bur, Y., Rauzy, E., and Berro, C., "Density of Methanol+Water between 250 K and 440 K and up to 40 Mpa and Vapor-Liquid Equilibria from 363 K to 440 K", *J. Chem. Eng. Data.*, 1998, 43, 592-600.

- 9) Ng, H.J., Robinson, D.B.: "The solubility of methanol or glycol in water-hydrocarbon systems", *Gas Proc. Assn. RR 117*, March, 1988.



Component	Mixture 1	Mixture 2	Mixture 3	Mixture 4	Mixture 5
Water	0.000	0.0000	0.000	0.307	0.128
Methanol	0.000	0.1000	0.500	0.173	0.654
Methane	0.800	0.7200	0.400	0.416	0.174
Butane	0.150	0.1350	0.075	0.078	0.033
Heptane	0.038	0.0342	0.019	0.020	0.008
Decane	0.012	0.0108	0.006	0.006	0.003

**Table 5.1: Overall composition of gas-condensate for various mixtures used in this study**

	Methane	Butane	Heptane	Decane
Methane	0			
Butane	0.025	0		
Heptane	0.13	0.05	0	
Decane	0.16	0.1	0	0

**Table 5.2: Binary interaction coefficients,  $k_{ij}$ , between hydrocarbons used in the SAFT Equation of state**

	Binary interaction coefficients With methanol		Binary interaction coefficients With water	
	PR	SAFT	PR	SAFT
Methane	0.2	0	0.50	0.2
Butane	0.4	0	0.47	0.15
Heptane	0.1	0.05	0.47	0.05
Decane	0.2	0.05	0.45	0
Methanol	0	0	-0.1	-0.15

**Table 5.3: Binary interaction coefficients,  $k_{ij}$ , between methanol and water with other components with the PR and the SAFT equations-of-state.**

Component	Mixture 1	Mixture 2	Mixture 3	Mixture 4	Mixture 5	Mixture 6
Temp (C)	122	122	68	68	14	14
Press (bar)	1026	1021	1001	1003	1003	1004
CH3OH	0.1188	0.2446	0.1186	0.2495	0.111	0.2208
H2O	0.3917	0.1864	0.3909	0.19	0.3659	0.168
CH4	0.2937	0.3412	0.2943	0.3363	0.3139	0.3667
nC7	0.1958	0.2275	0.1962	0.2242	0.2092	0.2445

**Table 5.4: Experimental mixture compositions in GPA RR 117 report (Ng. et al., 1988)**

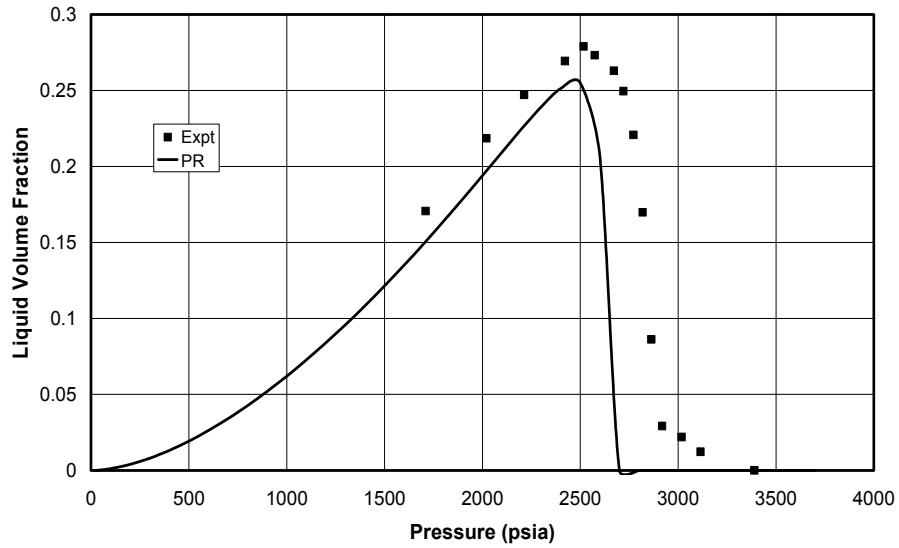


**Figure 5. 1: Liquid volume fraction curves for a gas condensate fluid (Mixture 1 in Table 5.1) at 145 F with the PR equation**

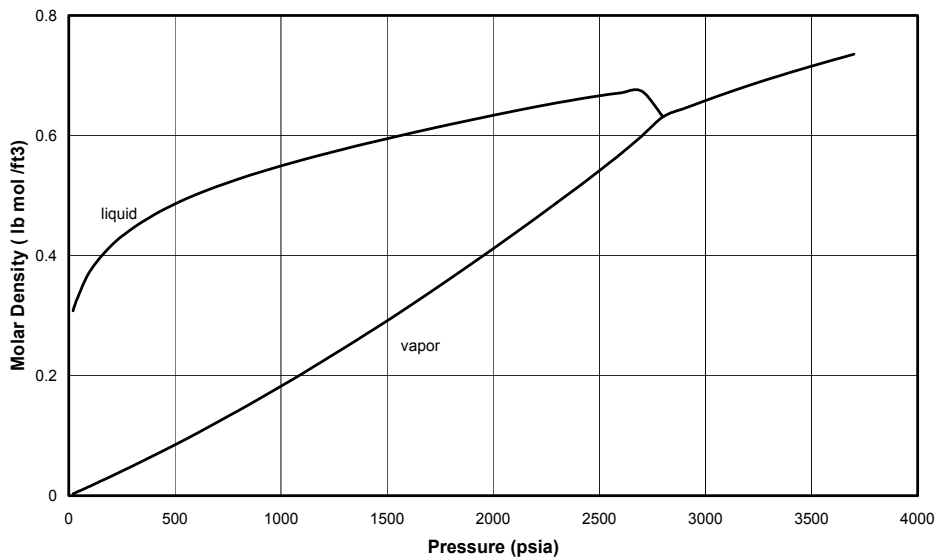


**Figure 5.2: Gas-condensate molar density variation at 145 F with PR EOS**

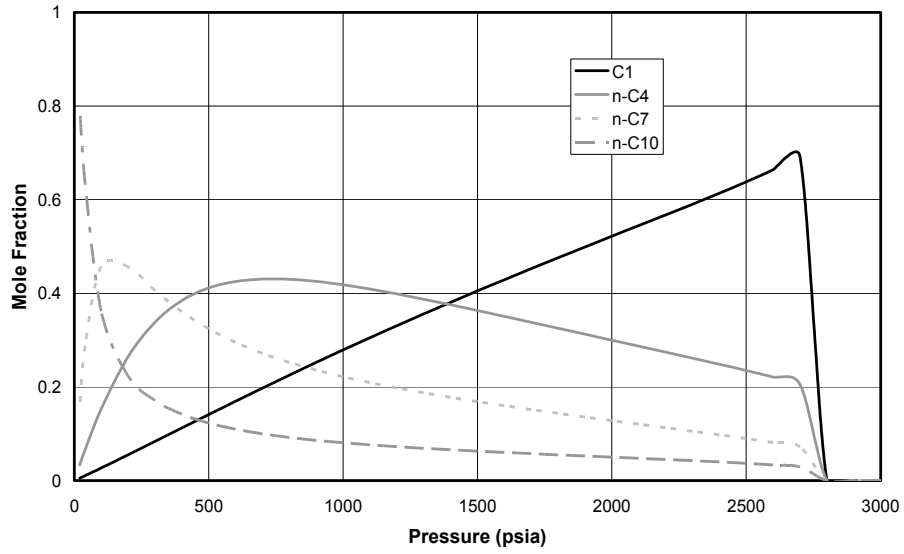


**Figure 5.3: Liquid phase compositions for the gas-condensate fluid at 145 F with the PR equation**

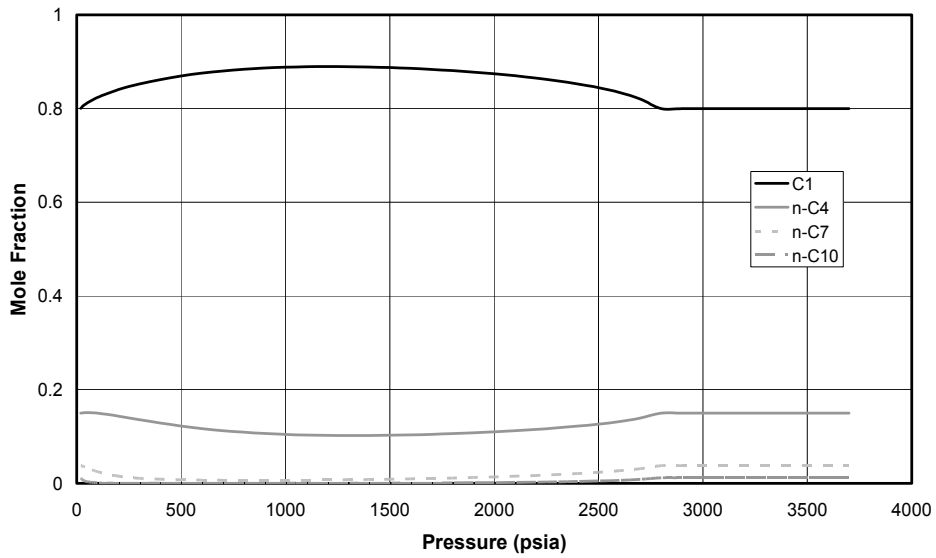


**Figure 5.4: Vapor phase compositions for the gas-condensate fluid at 145 F with PR equation**

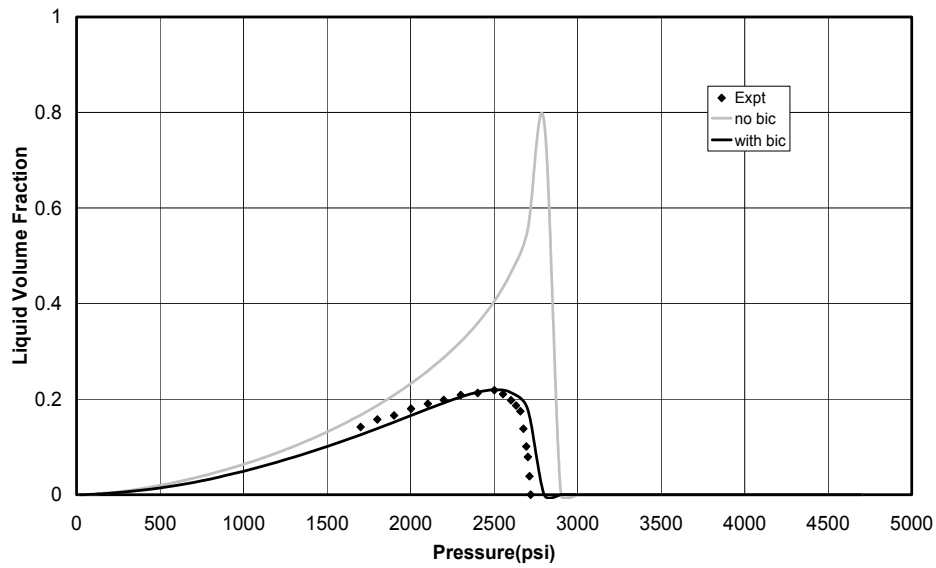


**Figure 5.5: Liquid volume fraction curves for a gas condensate fluid (mixture 1 in Table 5.1 at 145 F using the SAFT equation with and without binary interaction coefficients)**

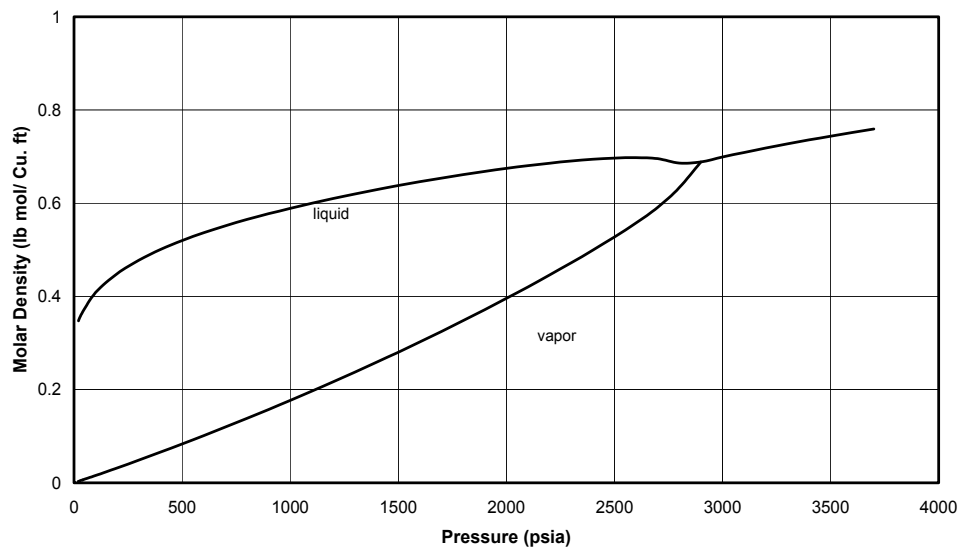


**Figure 5.6: Molar density curves for gas condensate fluids at 145 F using the SAFT equation without binary interaction coefficients**

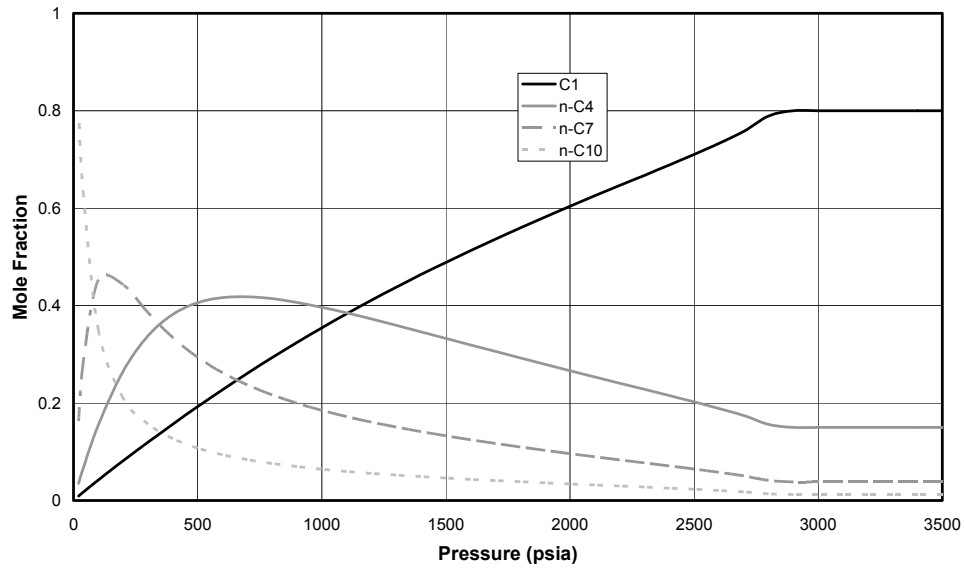


**Figure 5.7: Liquid phase compositions for gas-condensate fluid at 145 F using the SAFT equation without binary interaction coefficients**

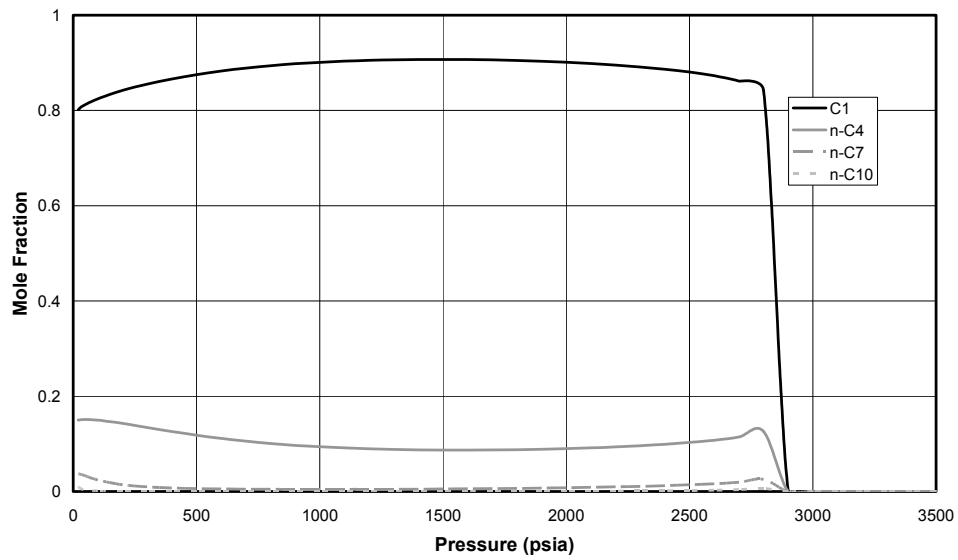


**Figure 5.8: Gas phase compositions for gas-condensate fluid at 145 F using the SAFT equation without binary interaction coefficients**

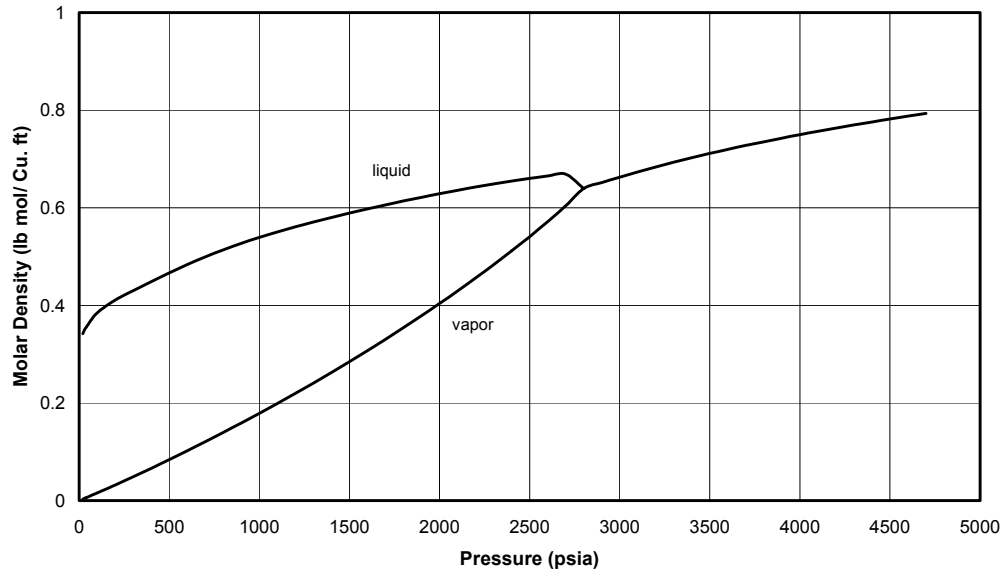


**Figure 5.9: Molar density curves for gas condensate fluids at 145 F using the SAFT equation with binary interaction coefficients**

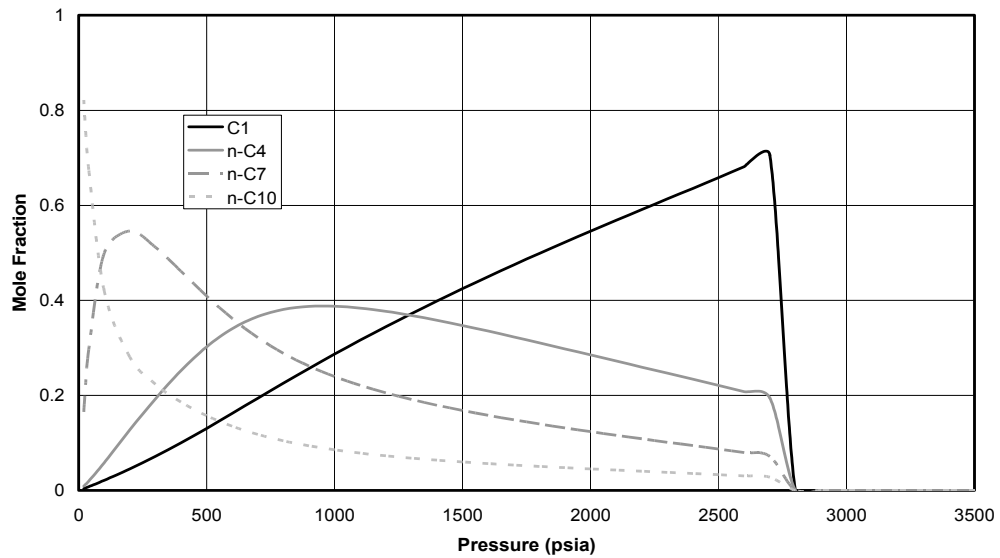


**Figure 5.10: Liquid phase compositions for gas-condensate fluid at 145 F using the SAFT equation with binary interaction coefficients**

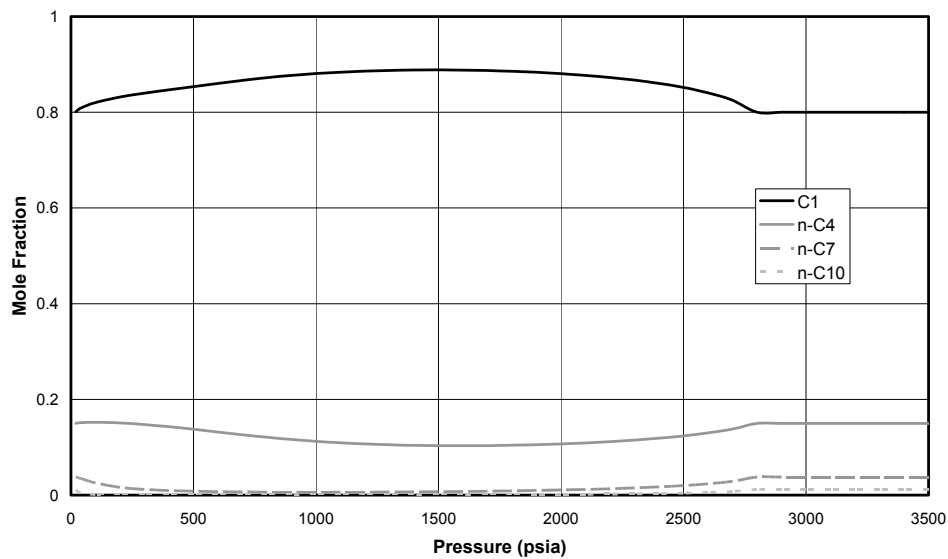


**Figure 5.11: Gas phase compositions for gas-condensate fluid at 145 F using the SAFT equation with binary interaction coefficients**

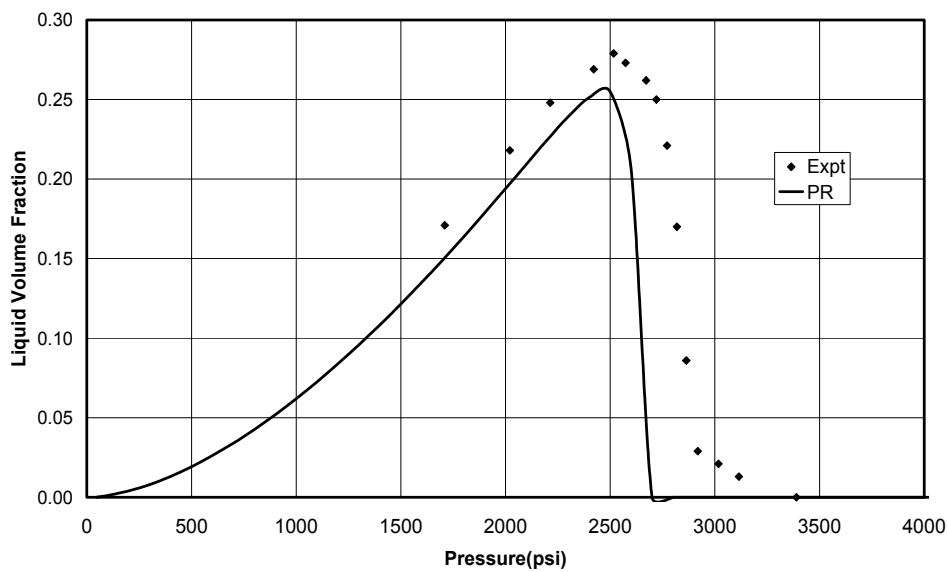


**Figure 5.12: Liquid volume fraction curves for a 10 mol % methanol and 90 mol % gas condensate mixture (Mixture 2 in Table 5.1) at 145 F using the PR equation of state**



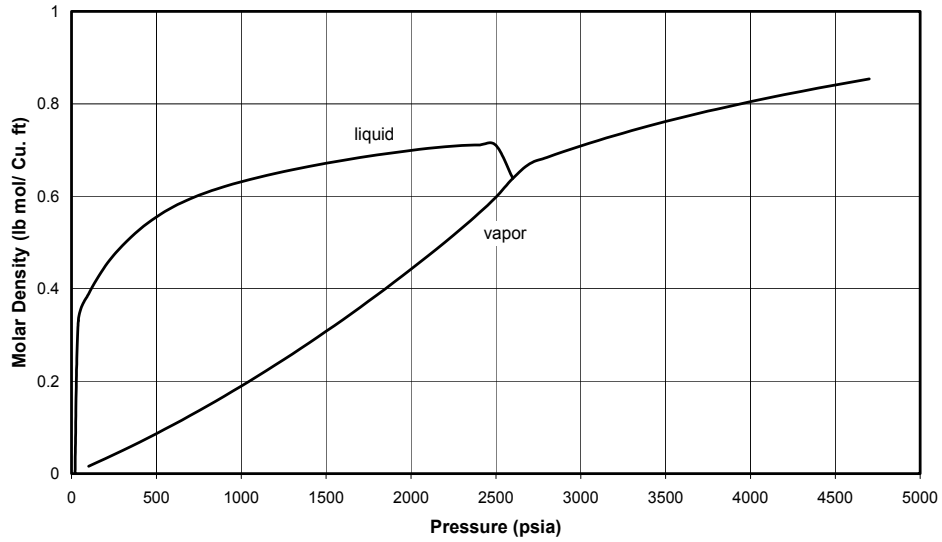


**Figure 5.13: Gas condensate molar density variation for a 10 mol % methanol and 90 mol % gas condensate mixture at 145 F using the PR equation of state**

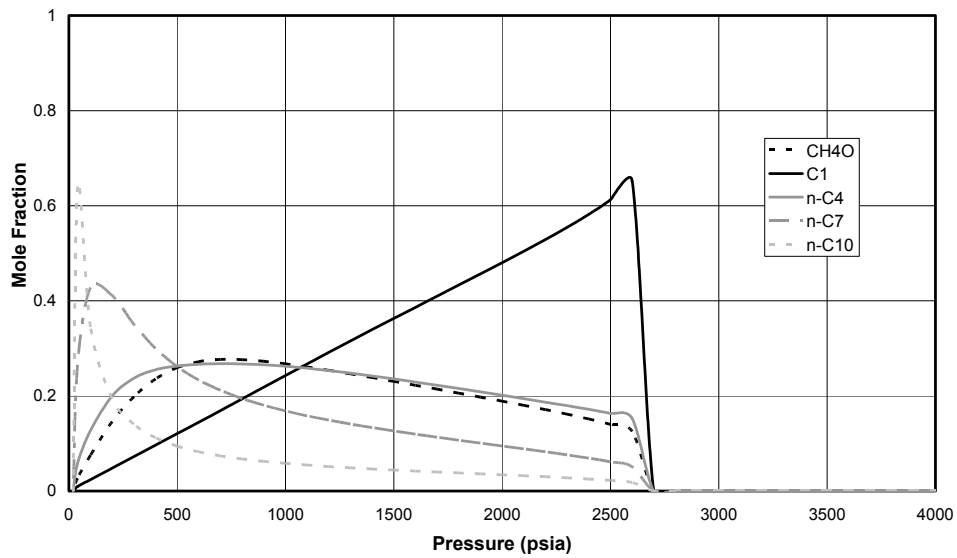


**Figure 5.14: Liquid phase compositions for a 10 mol % methanol and 90 mol % gas condensate mixture at 145 F using the PR equation of state**

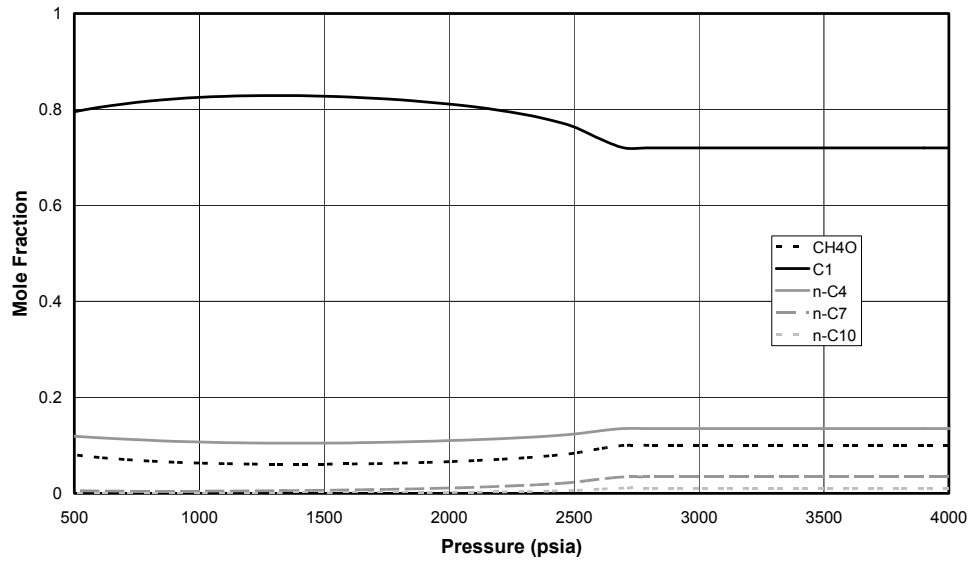


**Figure 5.15: Vapor phase compositions for a 10 mol % methanol and 90 mol % gas condensate mixture at 145 F using the PR equation of state**

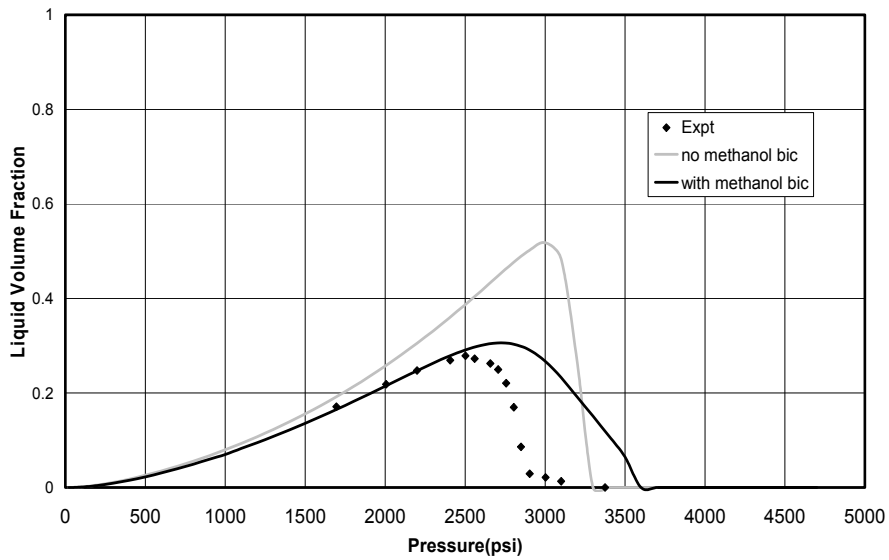


**Figure 5.16: Liquid volume fraction curves for a 10 mol % methanol and 90 mol % gas condensate mixture (Mixture 2 in Table 5.1) at 145 F using the SAFT equation**

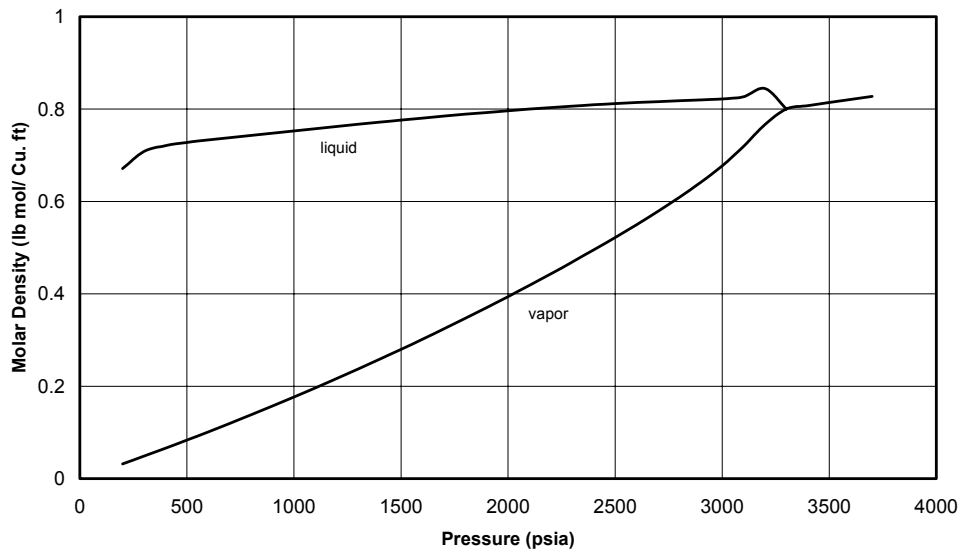


**Figure 5.17: Molar density curves for 10 mol % methanol and 90 mol % gas condensate fluids at 145 F using the SAFT equation without methanol binary interaction coefficients**

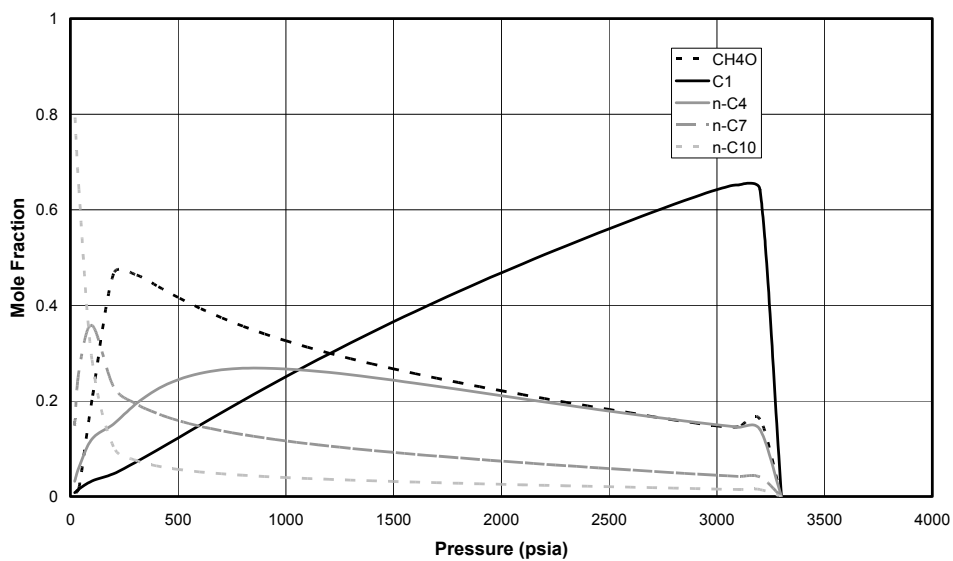


**Figure 5.18: Liquid phase compositions for 10 mol % methanol and 90 mol % gas condensate fluid at 145 F using SAFT without methanol binary interaction coefficients**

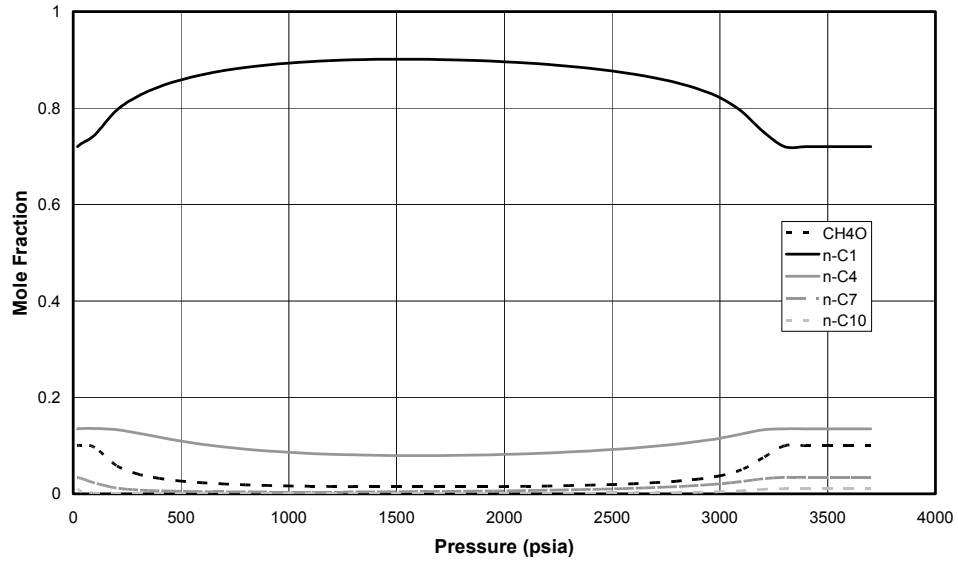


**Figure 5.19: Vapor phase compositions for 10 mol % methanol and 90 mol % gas-condensate fluid at 145 F using SAFT without methanol binary interaction coefficients**

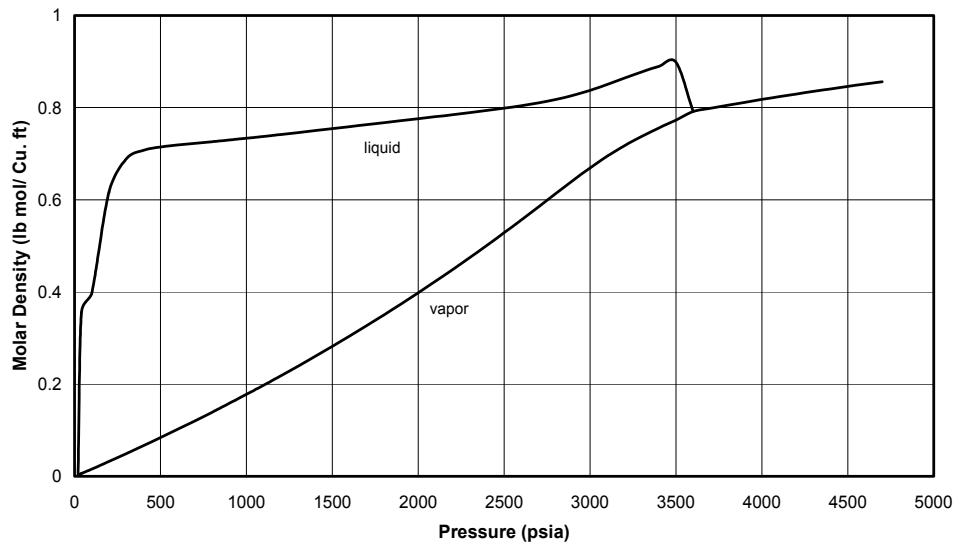


**Figure 5.20: Molar density curves for 10 mole % methanol and 90 mole % gas condensate fluids at 145 F using SAFT with methanol binary interaction coefficients**

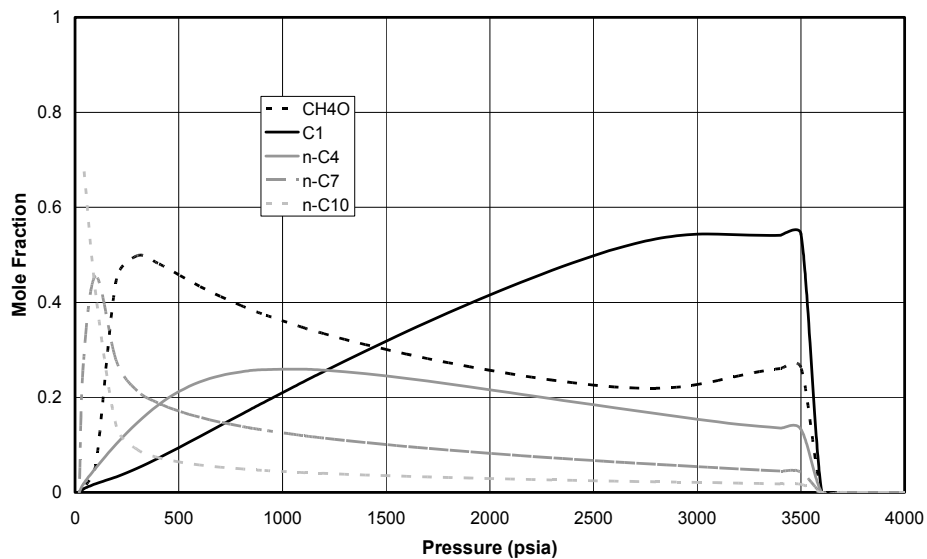


**Figure 5.21: Liquid phase compositions for 10 mol % methanol and 90 mol % gas-condensate fluid at 145 F using SAFT with methanol binary interaction coefficients**

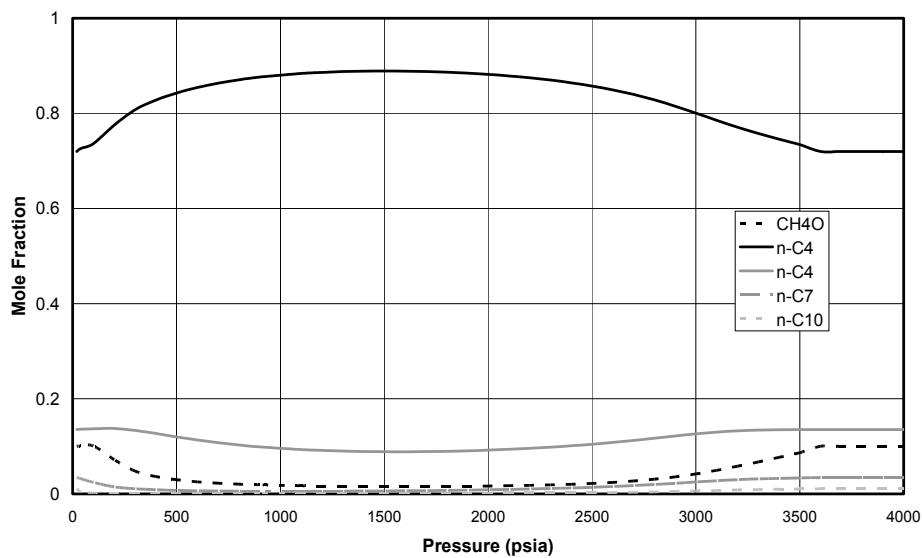


**Figure 5.22: Gas phase compositions for 10 mol % methanol and 90 mol % gas-condensate fluid at 145 F using SAFT with methanol binary interaction coefficients**

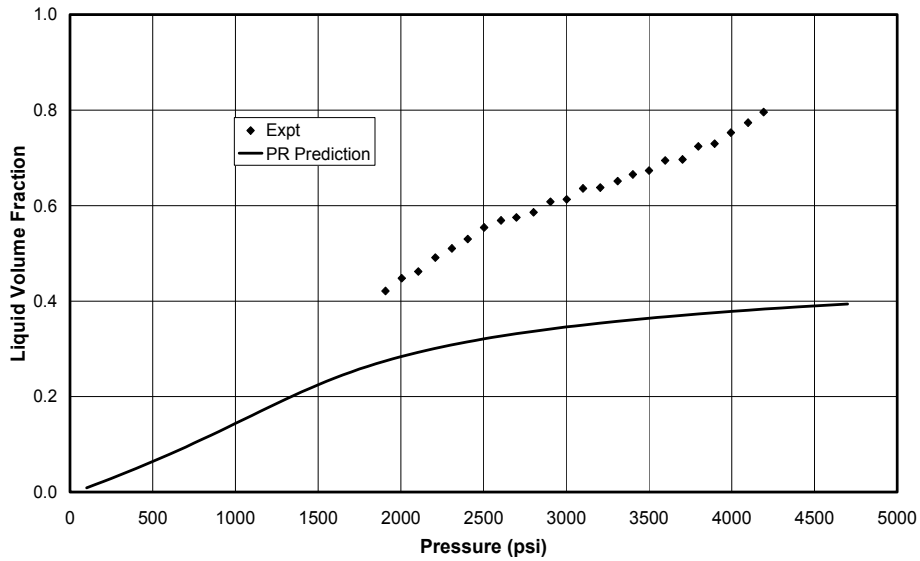


**Figure 5.23: Liquid volume fraction curves for a 50 mol % methanol and 50 mol % gas condensate mixture (Mixture 3 in Table 5.1) at 145 F using the PR equation**

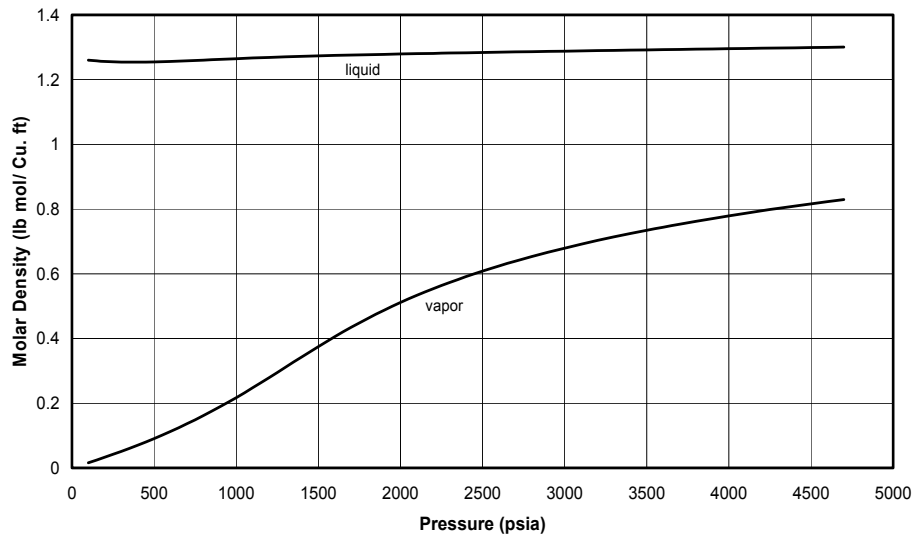


**Figure 5.24: Molar density curves for 50 mol % methanol and 50 mol % gas condensate fluids at 145 F using the PR equation**

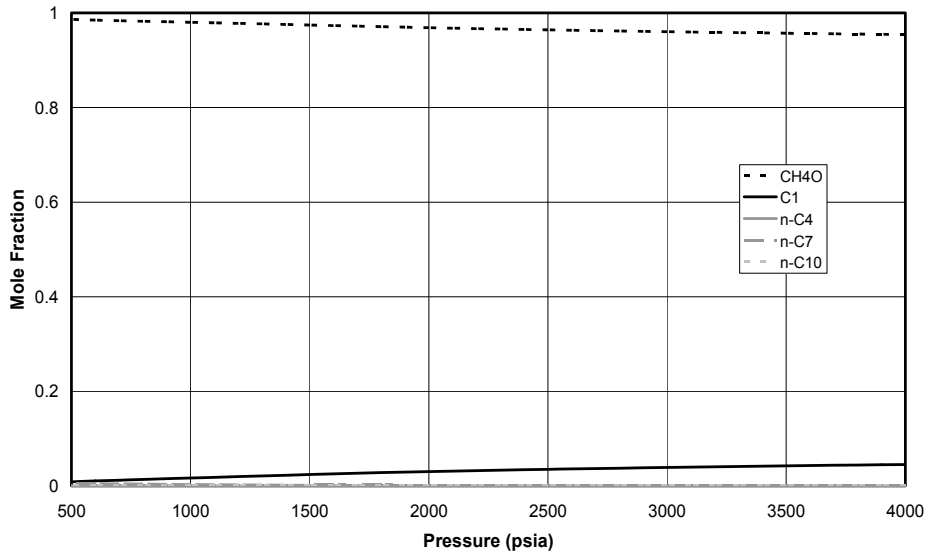


**Figure 5.25: Liquid phase compositions for 50 mol % methanol and 50 mol % gas-condensate fluid at 145 F using the PR equation**

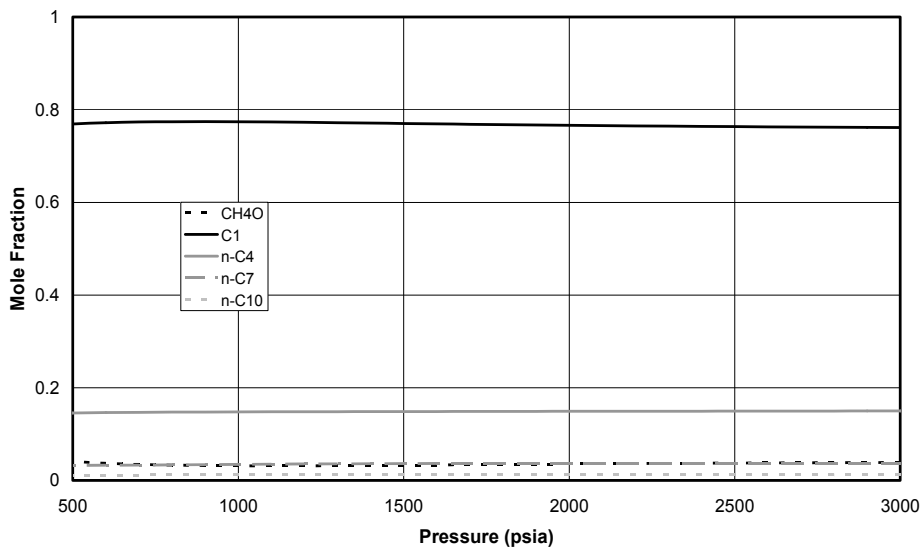


**Figure 5.26: Gas phase compositions for 50 mol % methanol and 50 mol % gas-condensate fluid at 145 F using the PR equation**

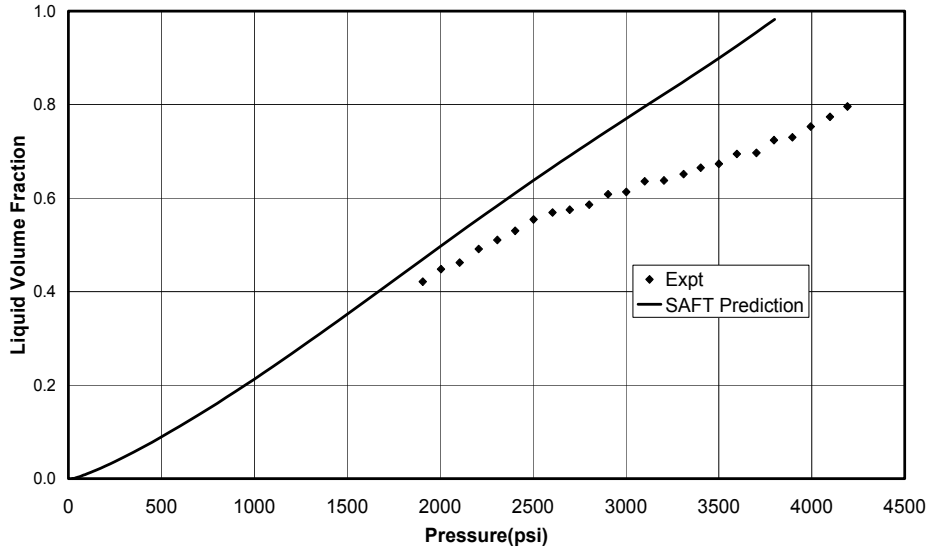


**Figure 5.27: Liquid volume fraction curves for a 50 mol % methanol and 50 mol % gas condensate mixture (Mixture 3 in Table 5.1) at 145 F using the SAFT equation**

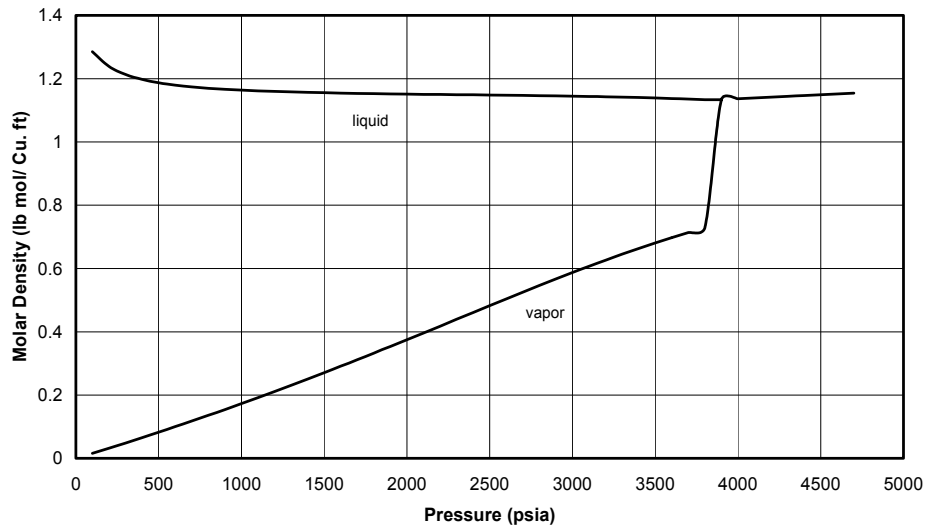


**Figure 5.28: Molar density curves for 50 mol % methanol and 50 mol % gas condensate fluids at 145 F using the SAFT equation**



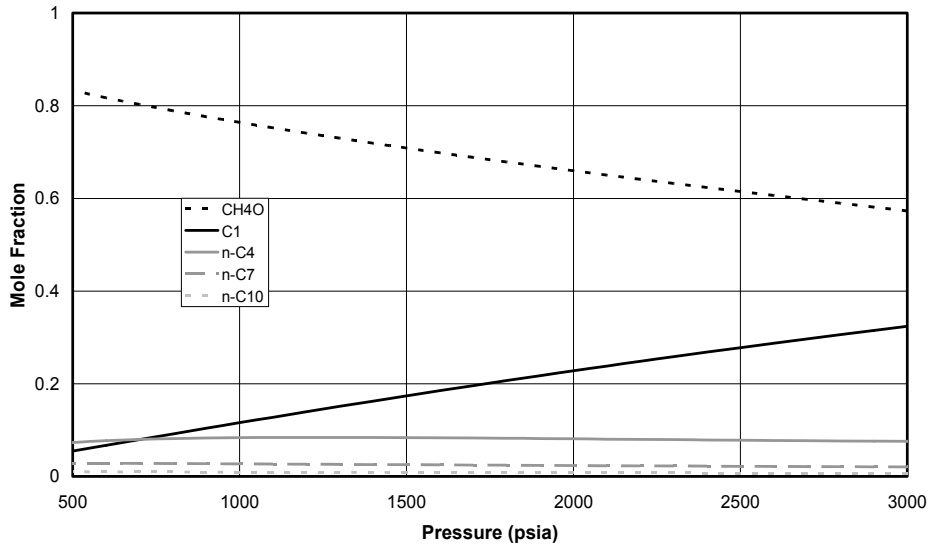


**Figure 5.29: Liquid phase compositions for 50 mol % methanol and 50 mol % gas-condensate fluid at 145 F using SAFT with binary interaction coefficients**

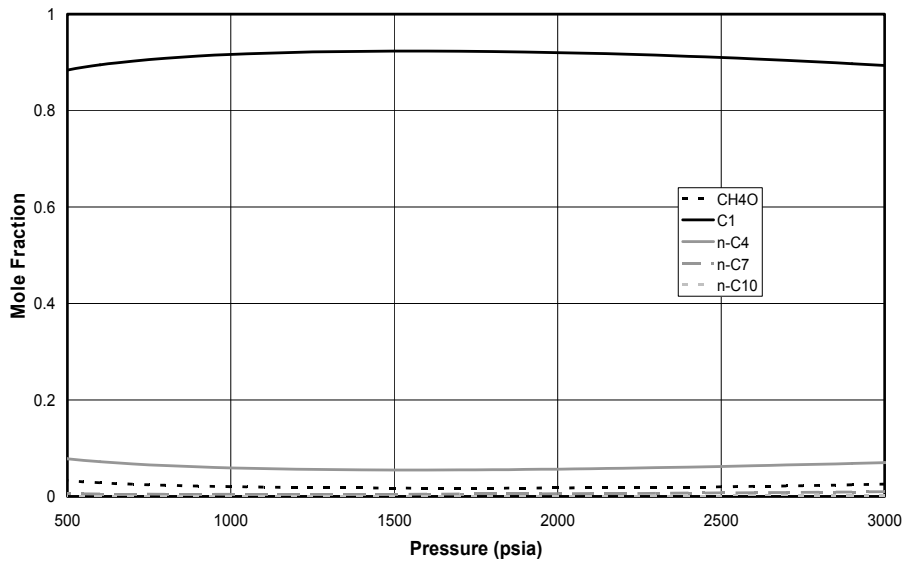


**Figure 5.30: Gas phase compositions for 50 mol % methanol and 50 mol % gas-condensate fluid at 145 F using SAFT with binary interaction coefficients**

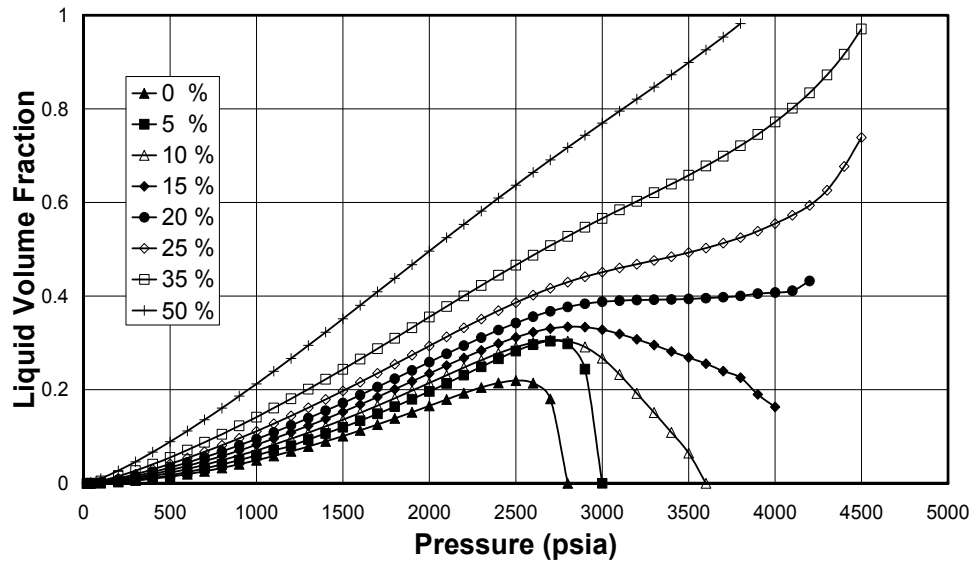


**Figure 5.31: Liquid volume fraction curves for gas condensate mixtures at 145 F with change in methanol concentration**

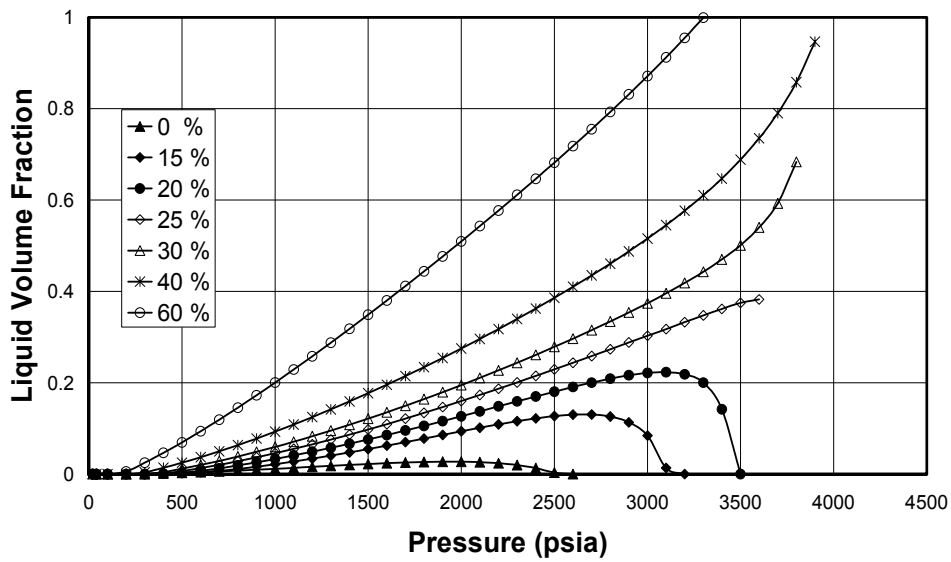


**Figure 5.32: Liquid volume fraction curves for gas condensate mixtures at 250 F with change in methanol concentration**

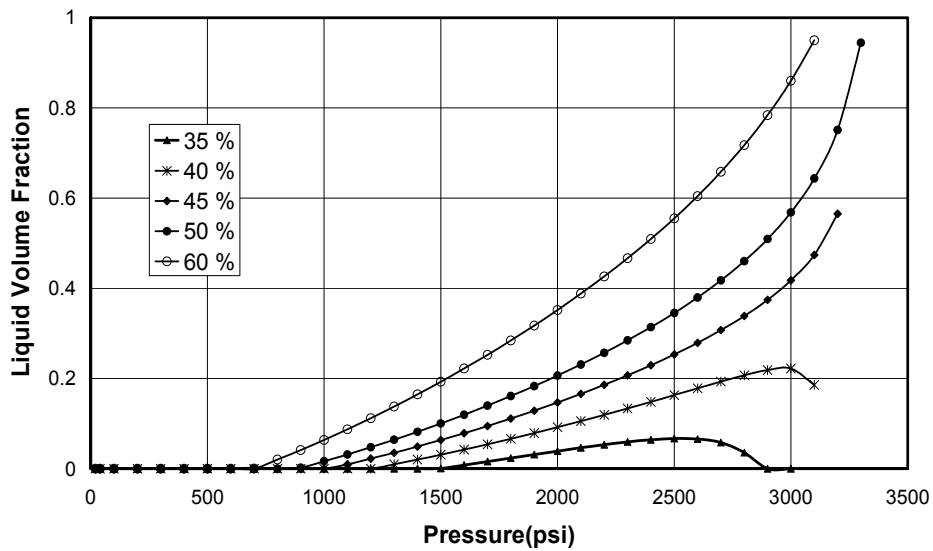


**Figure 5.33: Liquid volume fraction curves for gas condensate mixtures at 350 F with change in methanol concentration**

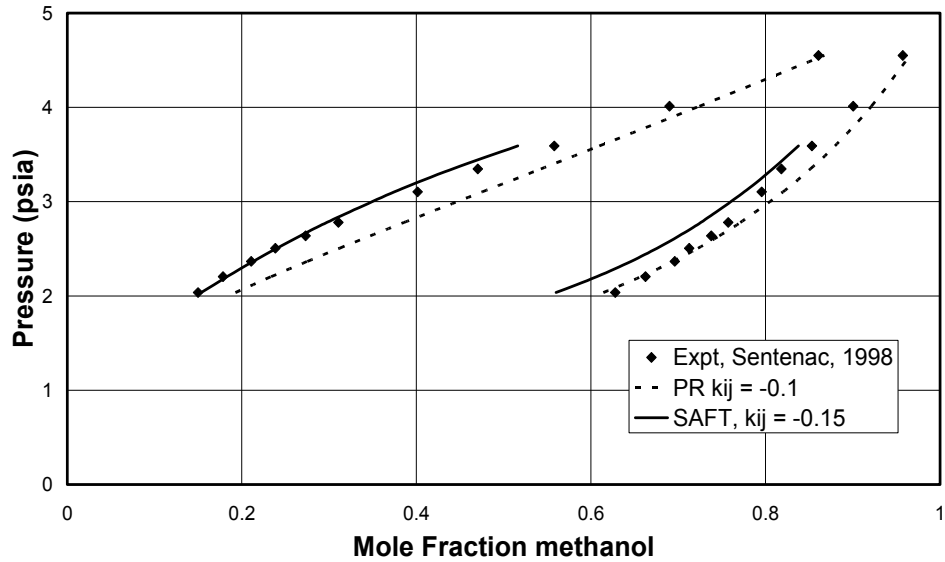


**Figure 5.34: Vapor liquid equilibrium of methanol-water at 39.9 C with the PR and SAFT equation**

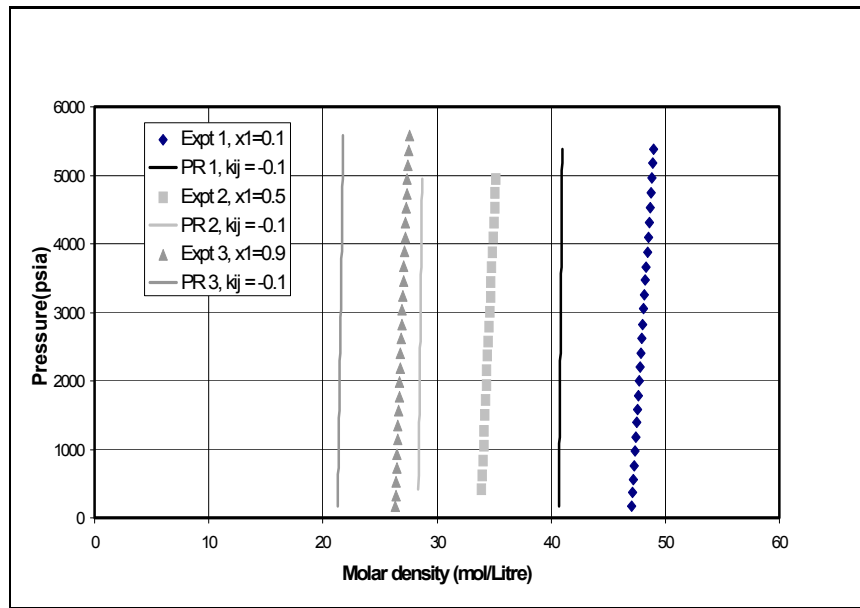


Figure 5.35: Density of methanol-water(2) mixtures at 140 F with the PR equation (Sentenac, 1998)

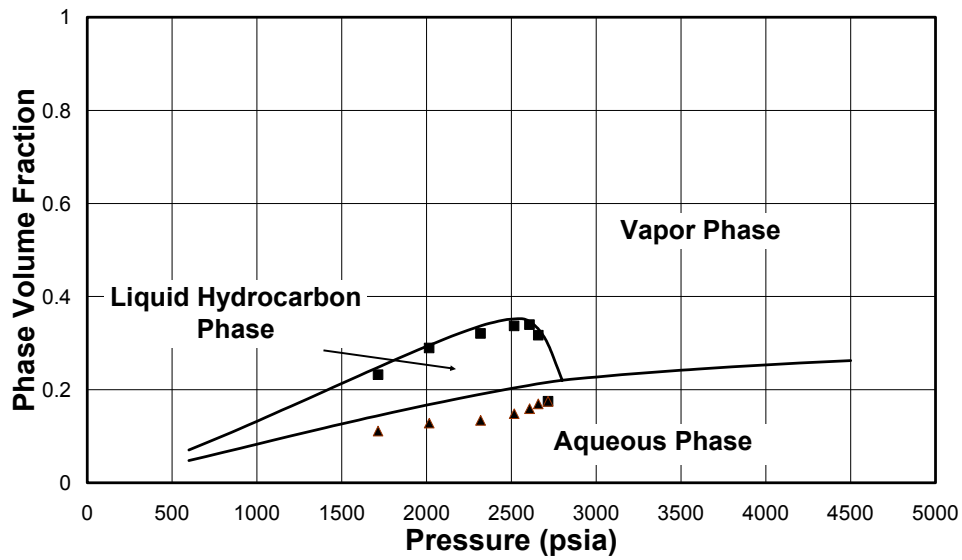
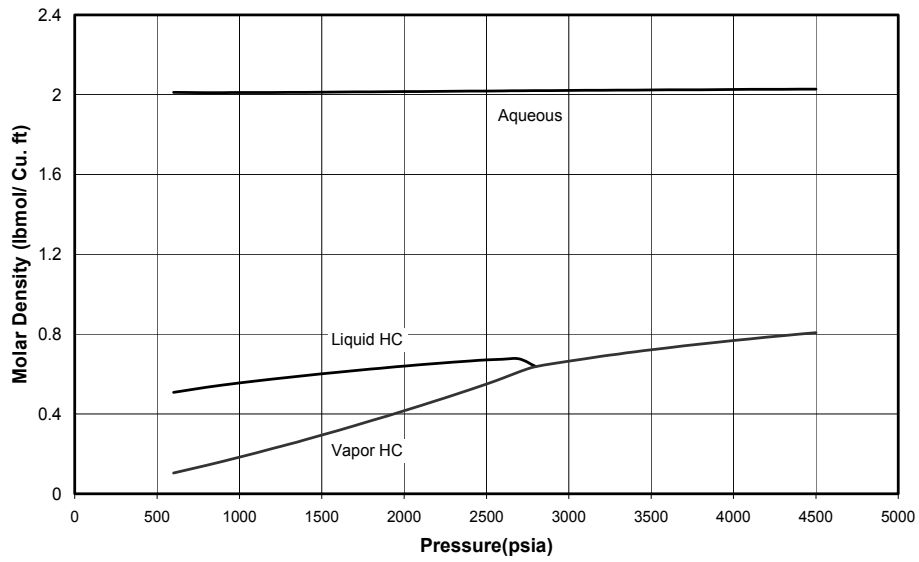
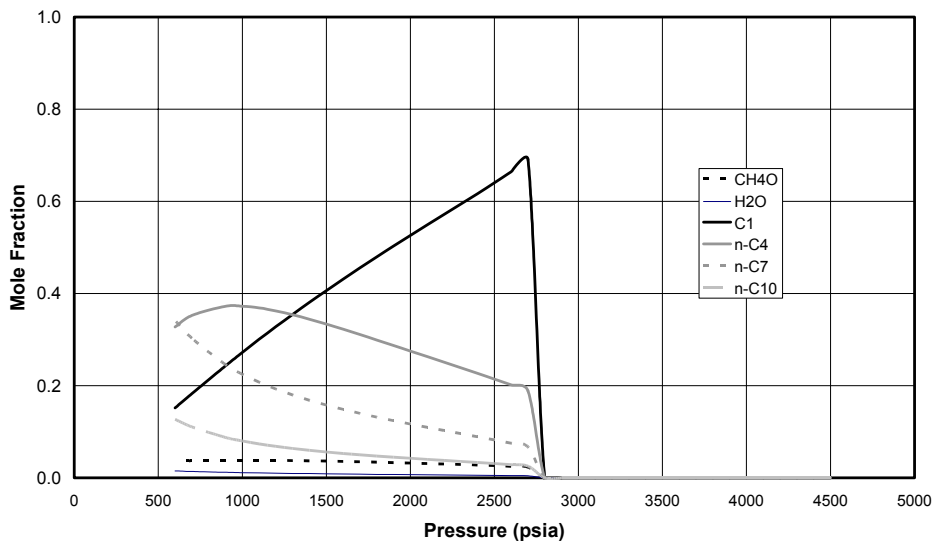


Figure 5.36: Volume fraction diagram for Mixture 4 in Table 5.1 with the PR equation at 145 F



**Figure 5.37: Molar density curves for for Mixture 4 in Table 5.1 with the PR equation at 145 F**



**Figure 5.38: Mole fraction of various components in liquid phase for Mixture 4 in Table 5.1 with PR equation**

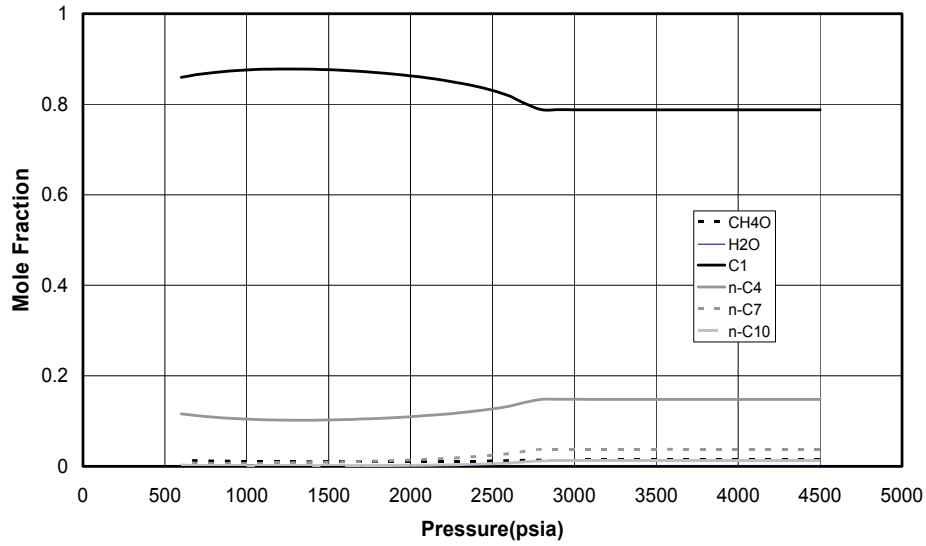


**Figure 5.39: Mole fraction of various components in vapor phase for Mixture 4 in Table 5.1 with PR equation**

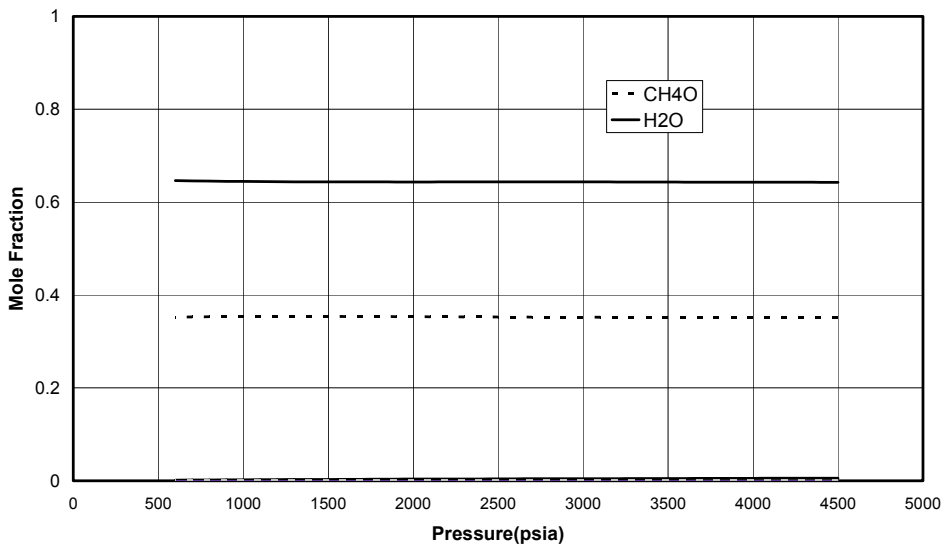


**Figure 5.40: Mole fraction of various components in aqueous phase for Mixture 4 in Table 5.1 with PR equation**

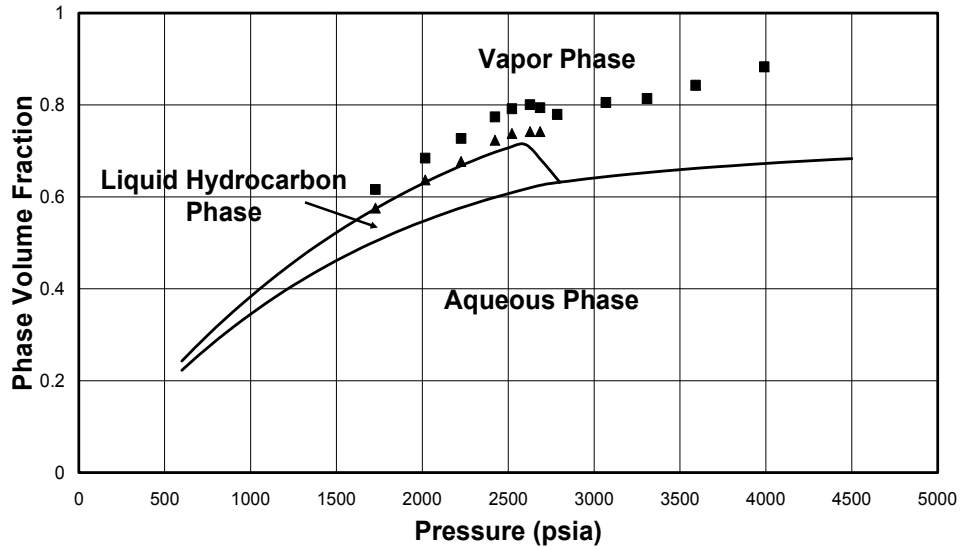


**Figure 5.41: Volume fraction diagram for Mixture 5 in Table 5.1 at 145 °F with PR equation**

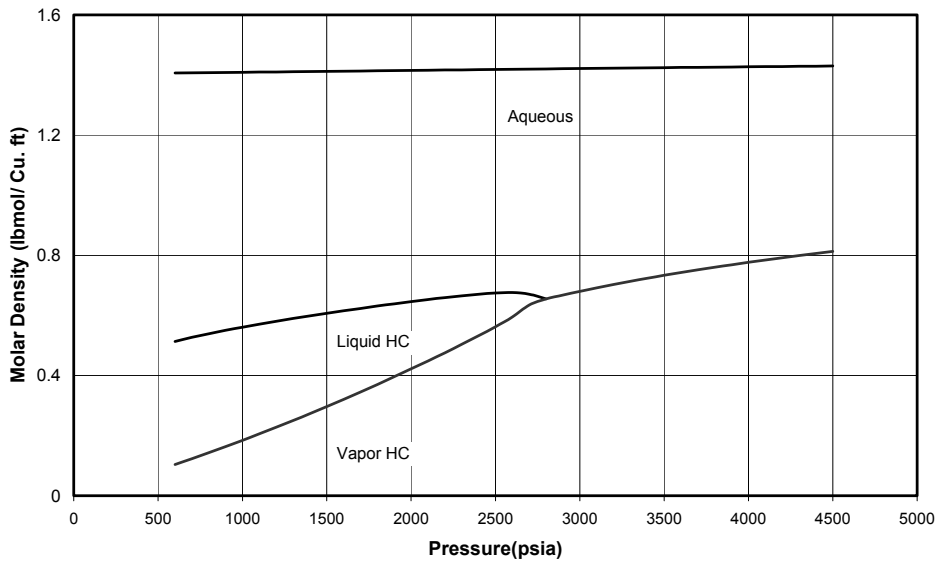


**Figure 5.42: Molar density curves for Mixture 5 in Table 5.1 with the PR equation at 145 F**

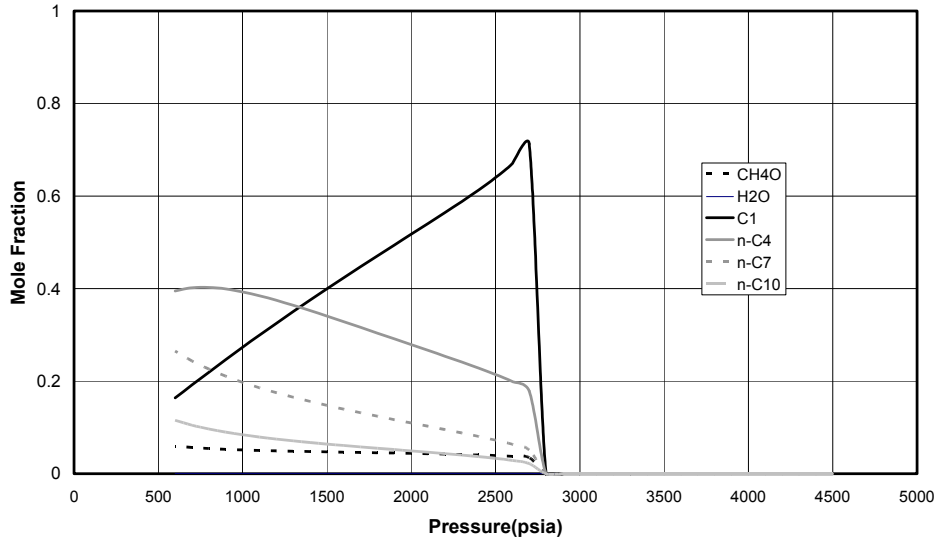


**Figure 5.43: Mole fraction of various components in liquid phase for Mixture 5 in Table 5.1 with PR equation**

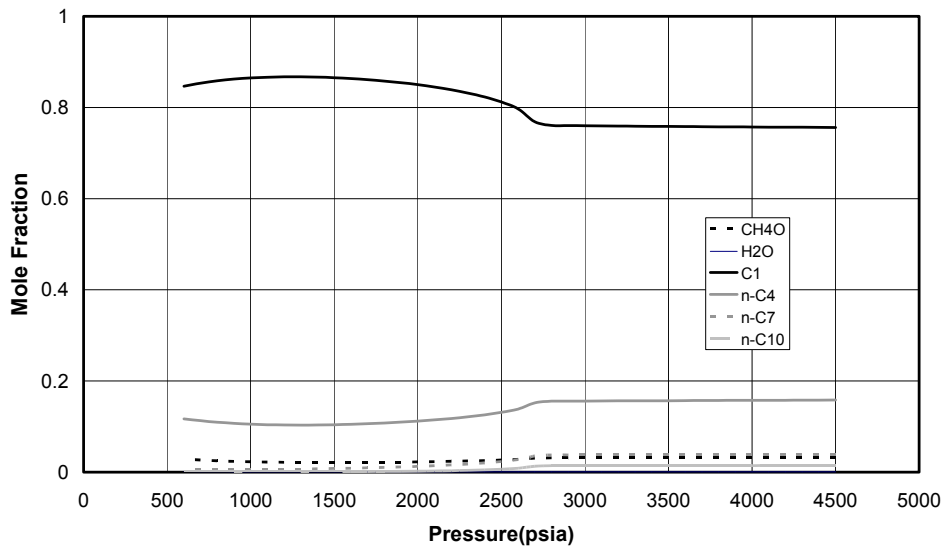


**Figure 5.44: Mole fraction of various components in vapor phase for Mixture 5 in Table 5.1 with PR equation**



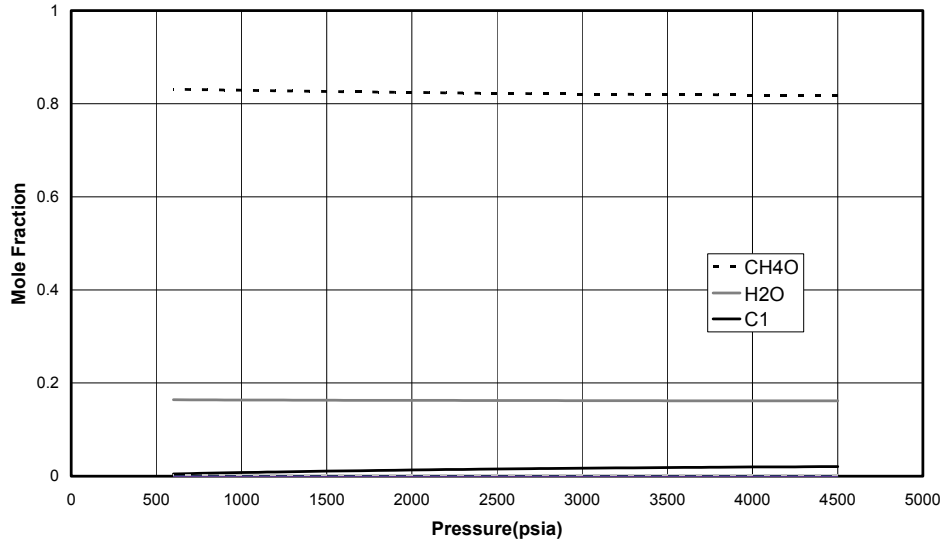


**Figure 5.45: Mole fraction of various components in aqueous phase for Mixture 5 in Table 5.1 with PR equation**

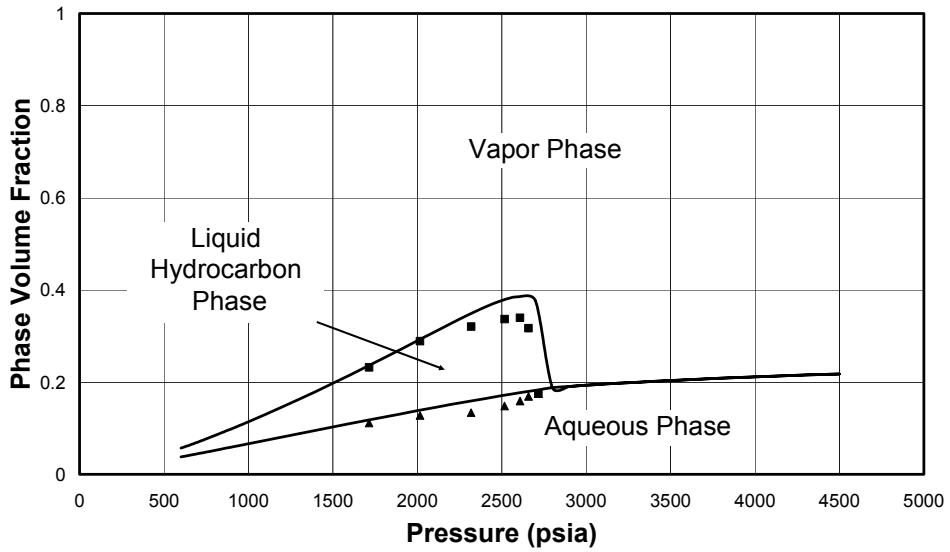


**Figure 5.46: Volume fraction diagram for Mixture 4 in Table 5.1 at 145 °F with SAFT Equation**

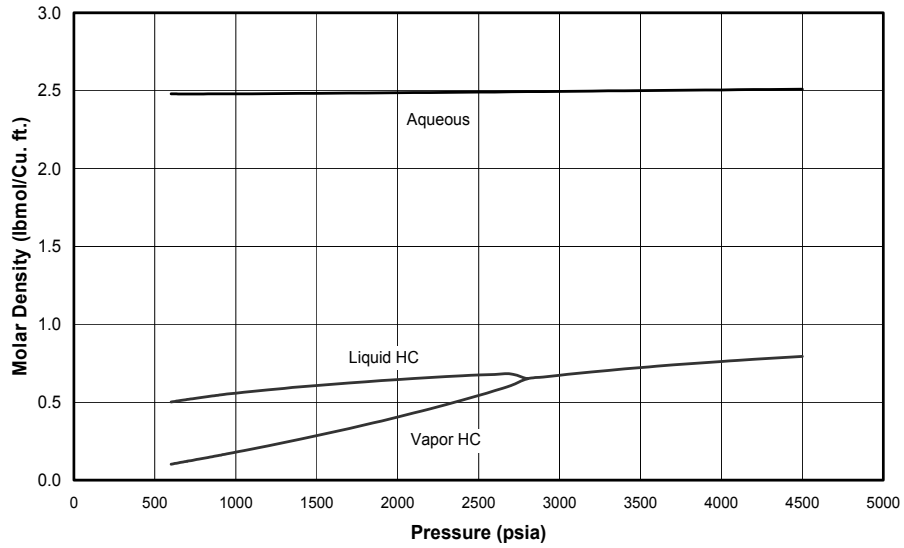


**Figure 5.47 Molar density curves for Mixture 4 in Table 5.1 with the SAFT equation at 145 F**

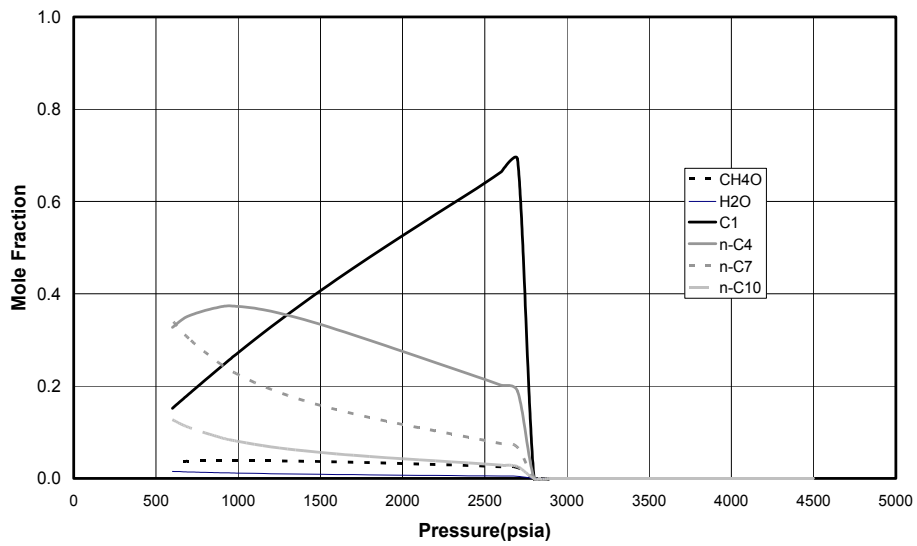


**Figure 5.48: Mole fraction of various components in liquid phase for Mixture 4 in Table 5.1 with SAFT equation**

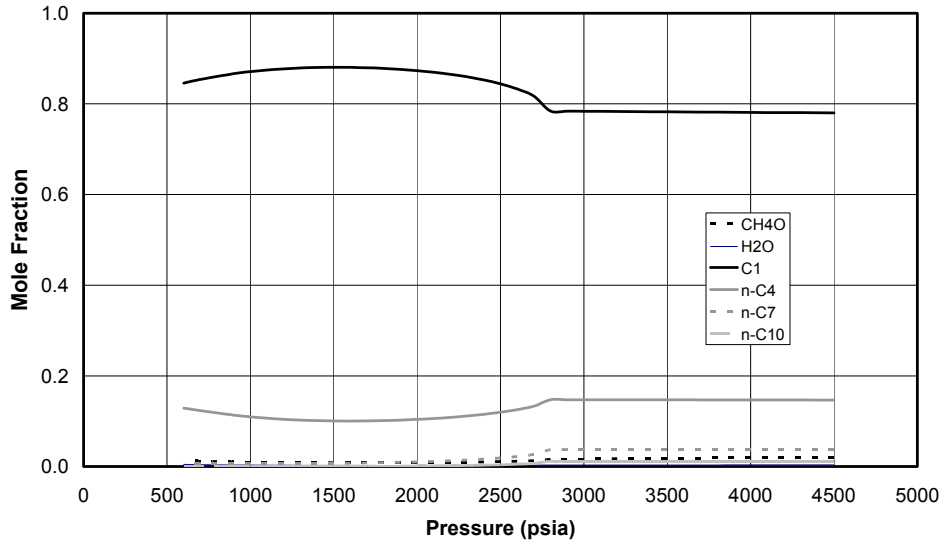


**Figure 5.49: Mole fraction of various components in vapor phase for Mixture 4 in Table 5.1 with SAFT equation**

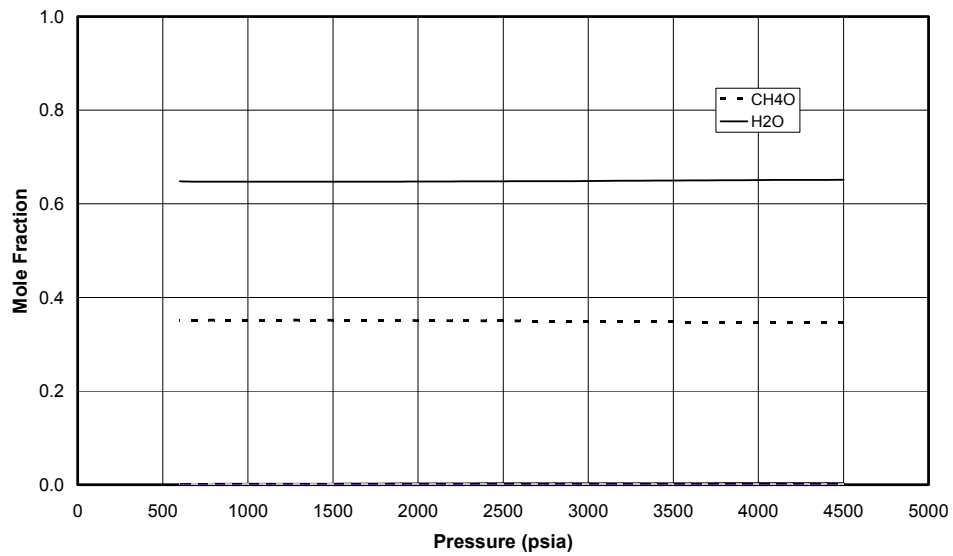


**Figure 5.50: Mole fraction of various components in aqueous phase for Mixture 4 in Table 5.1 with SAFT equation**

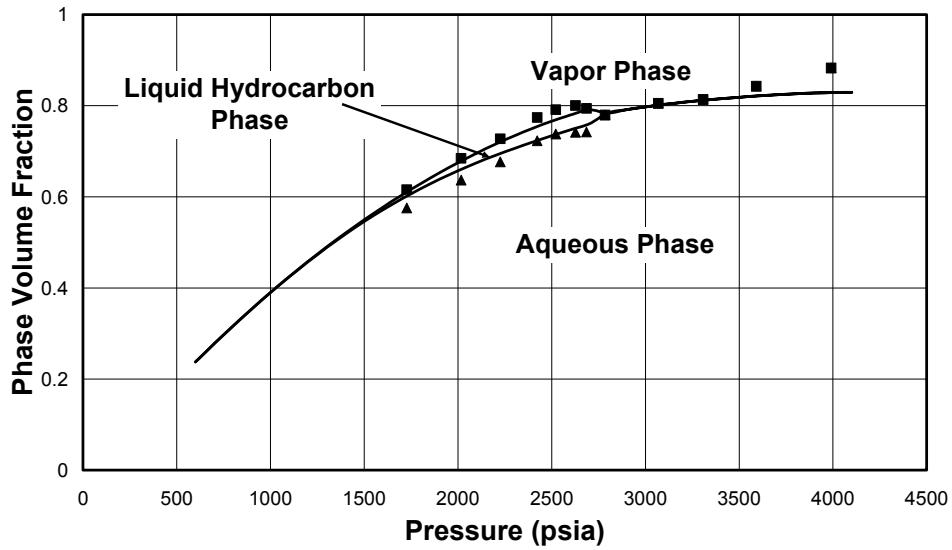


Figure 5.51: Volume fraction diagram for Mixture 5 in Table 5.1 at 145 °F with SAFT equation

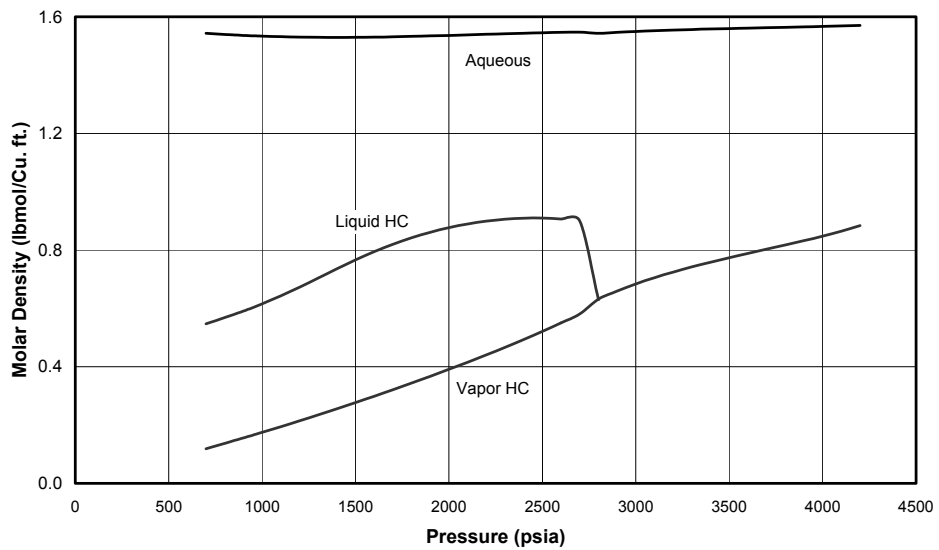
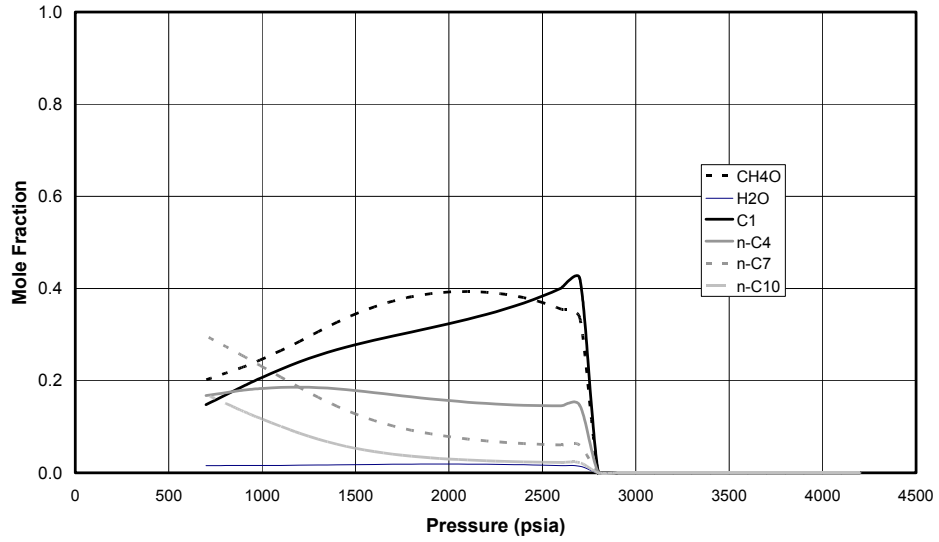
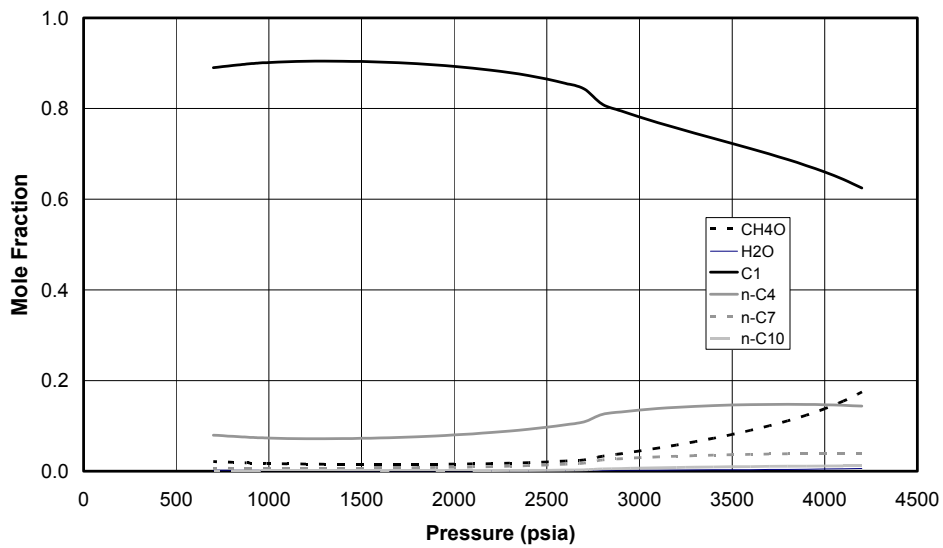


Figure 5.52: Molar density curves for Mixture 5 in Table 5.1 with the SAFT equation at 145 F



**Figure 5.53: Mole fraction of various components in liquid phase for Mixture 5 in Table 5.1 with SAFT equation**



**Figure 5.54: Mole fraction of various components in vapor phase for Mixture 5 in Table 5.1 with SAFT equation**

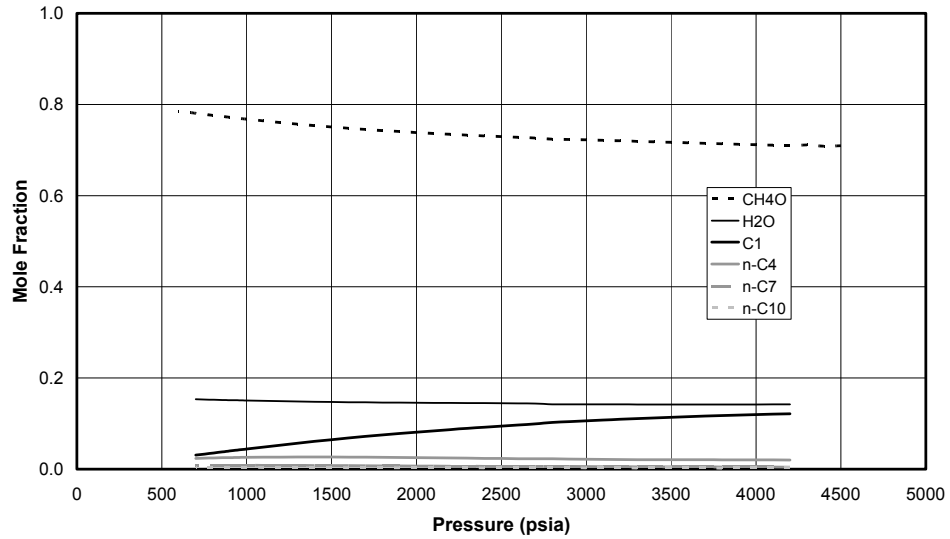


**Figure 5.55: Mole fraction of various components in aqueous phase for Mixture 5 in Table 5.1 with SAFT equation**

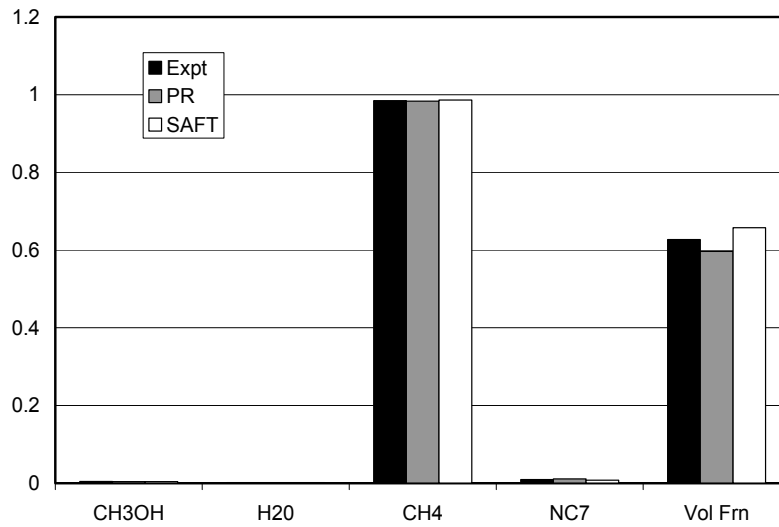


**Figure 5.56: Vapor hydrocarbon phase mole fractions at 122 F hydrocarbon-water-methanol (Mixture 1) in Table 5.5**

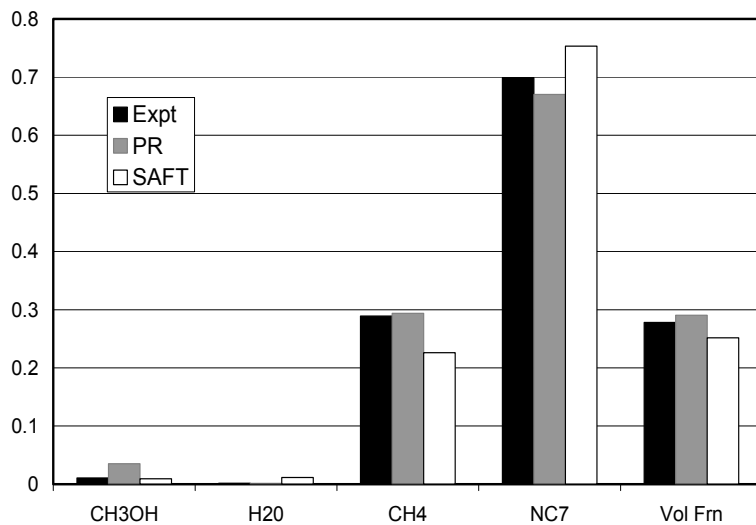


**Figure 5.57: Liquid hydrocarbon phase mole fractions at 122 F hydrocarbon-water-methanol (Mixture 1) in Table 5.5**

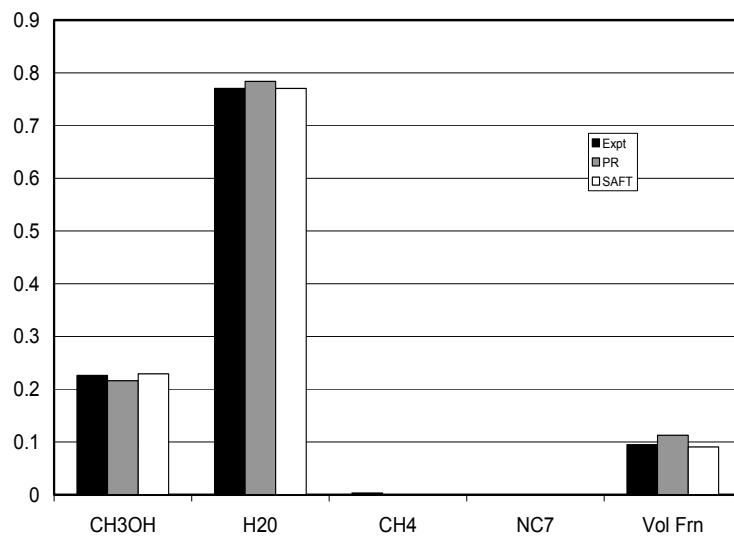


**Figure 5.58: Aqueous phase mole fractions at 122 F hydrocarbon-water-methanol (Mixture 1) in Table 5.5**

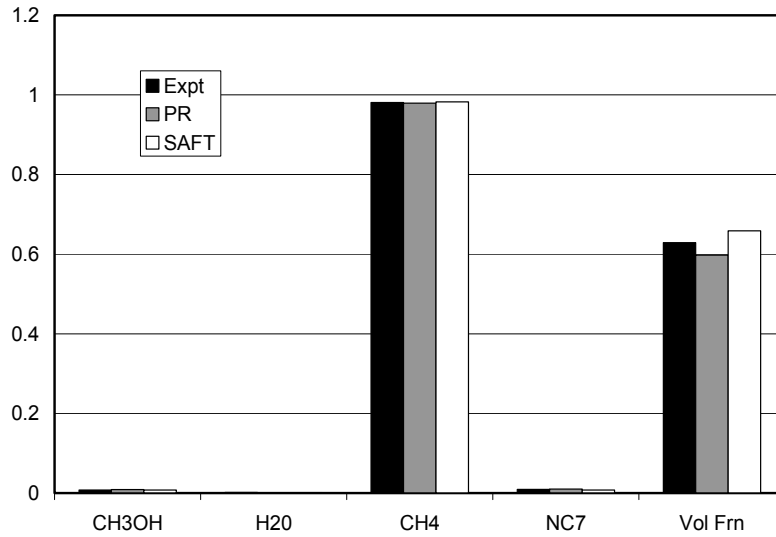


**Figure 5.59: Vapor phase mole fractions at 122 F hydrocarbon-water-methanol (Mixture 2) in Table 5.5**

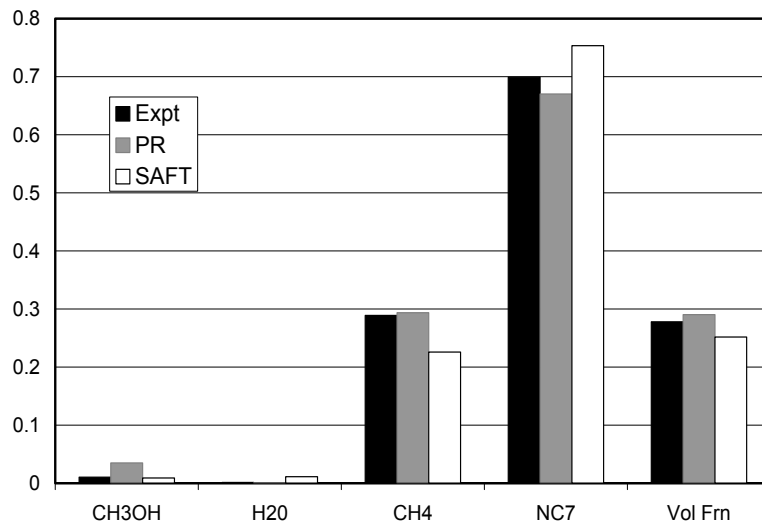


**Figure 5.60: Liquid hydrocarbon phase mole fractions at 122 F for hydrocarbon-water-methanol (Mixture 2) in Table 5.5**



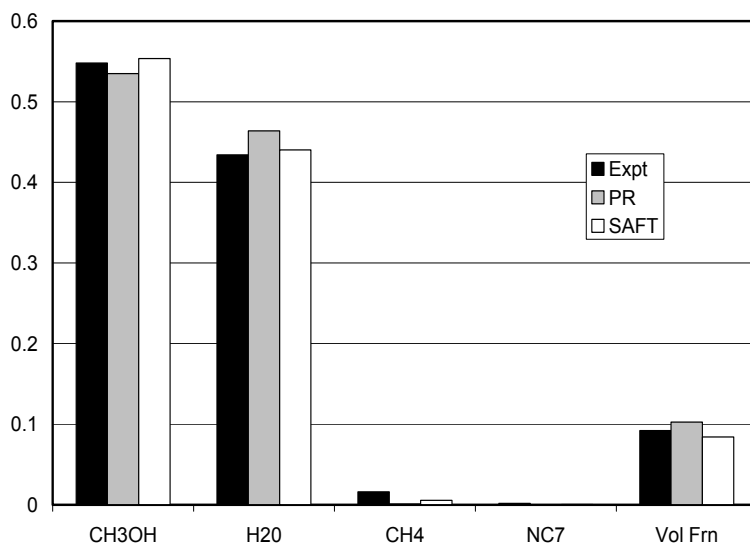


**Figure 5.61: Aqueous phase mole fractions at 122 F for hydrocarbon-water-methanol (Mixture 2) in Table 5.5**

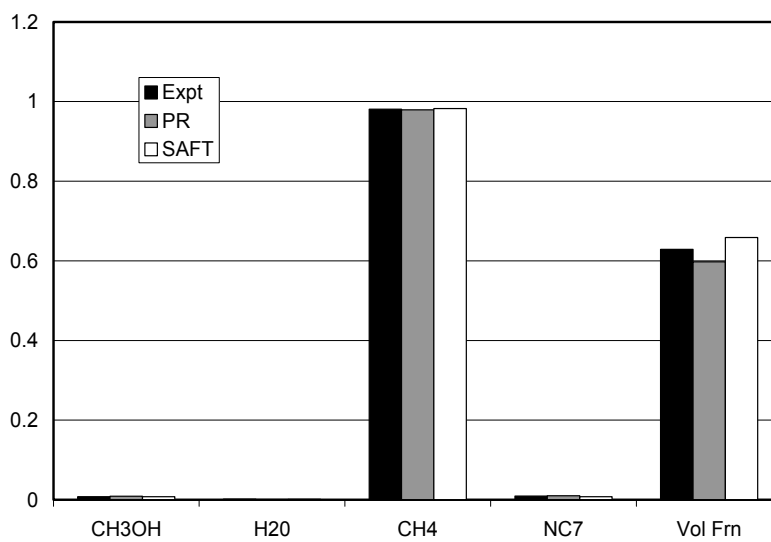


**Figure 5.62: Vapor phase mole fractions at 68 F hydrocarbons-water-methanol (Mixture 3) in Table 5.5**

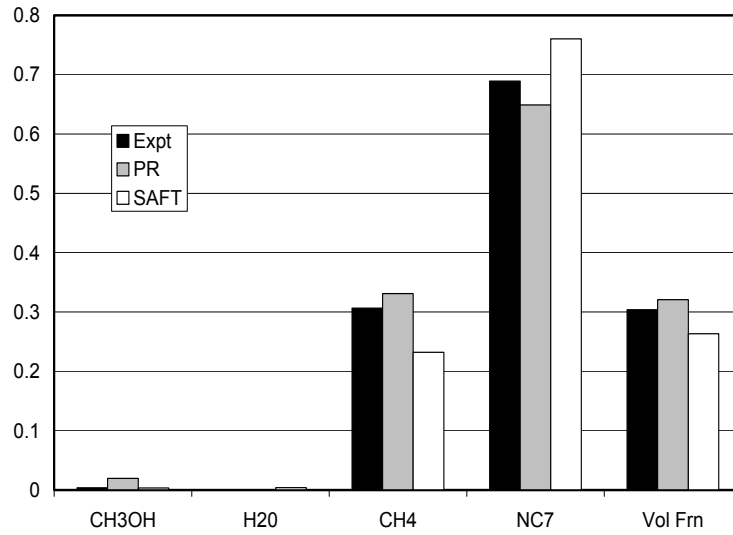


**Figure 5.63: Liquid hydrocarbon phase mole fractions at 68 F for hydrocarbon-water-methanol (Mixture 3) in Table 5.5**

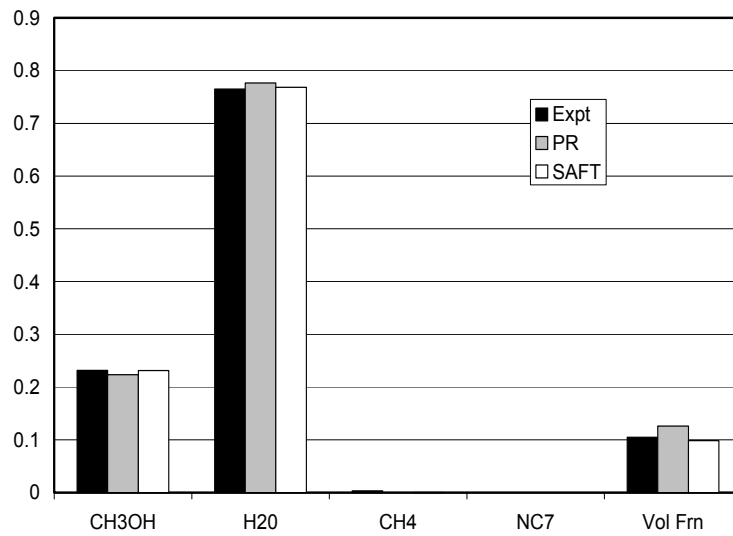


**Figure 5.64: Aqueous phase mole fractions at 68 F for hydrocarbon-water-methanol (Mixture 3) in Table 5.5**

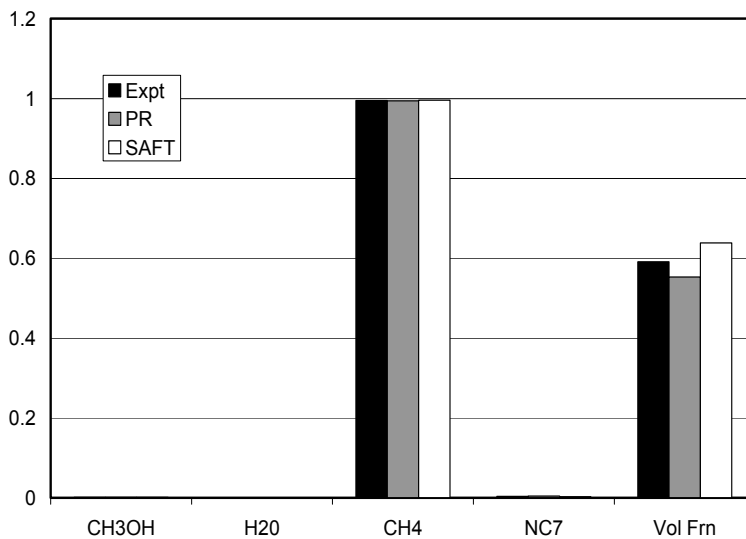


**Figure 5.65: Vapor phase mole fractions at 68 F for hydrocarbon-water-methanol (Mixture 4) in Table 5.5**

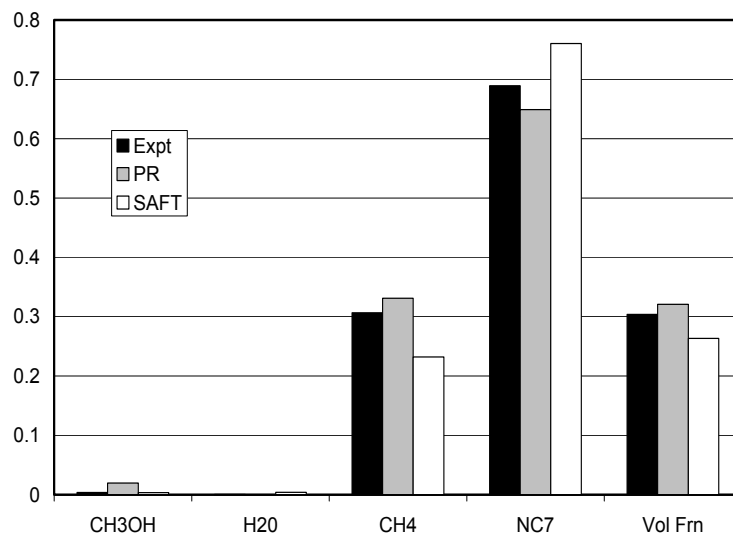


**Figure 5.66: Liquid hydrocarbon phase mole fractions at 68 F for hydrocarbon-water-methanol (Mixture 4) in Table 5.5**

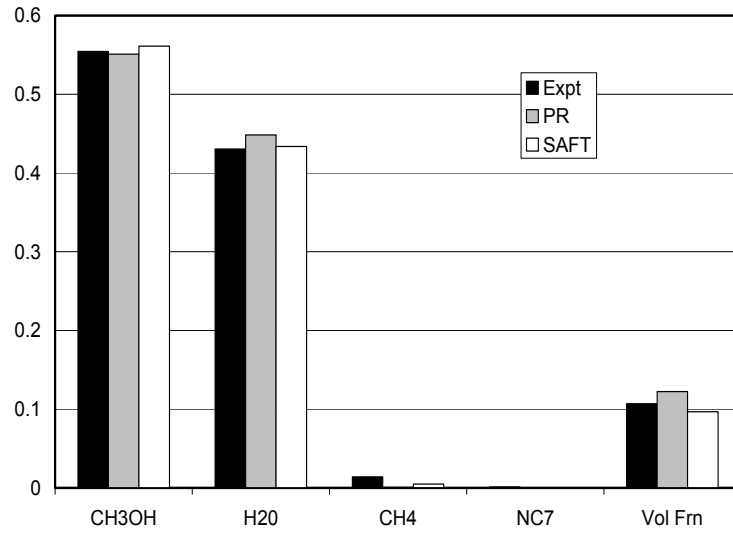


**Figure 5.67: Aqueous phase mole fractions at 68 F for hydrocarbon-water-methanol (Mixture 4) in Table 5.5**

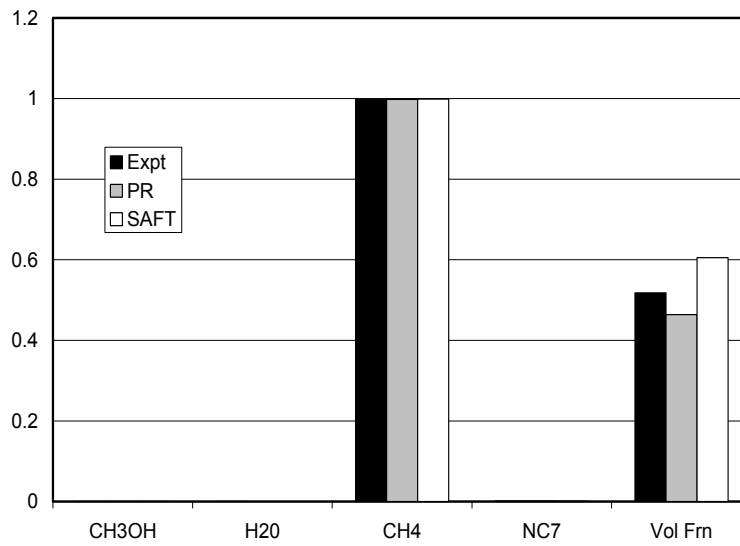


**Figure 5.68: Vapor phase mole fractions at 14 F for hydrocarbon-water-methanol (Mixture 5) in Table 5.5**

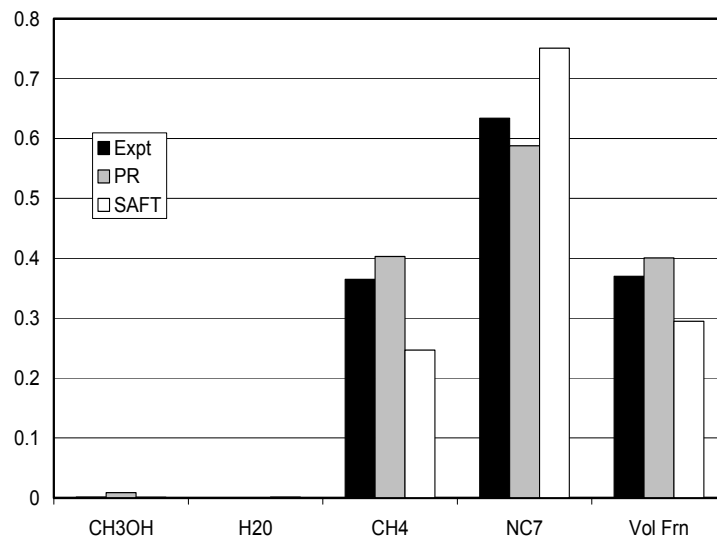


**Figure 5.69: Liquid hydrocarbon phase mole fractions at 14 F for hydrocarbon-water-methanol (Mixture 5) in Table 5.5**

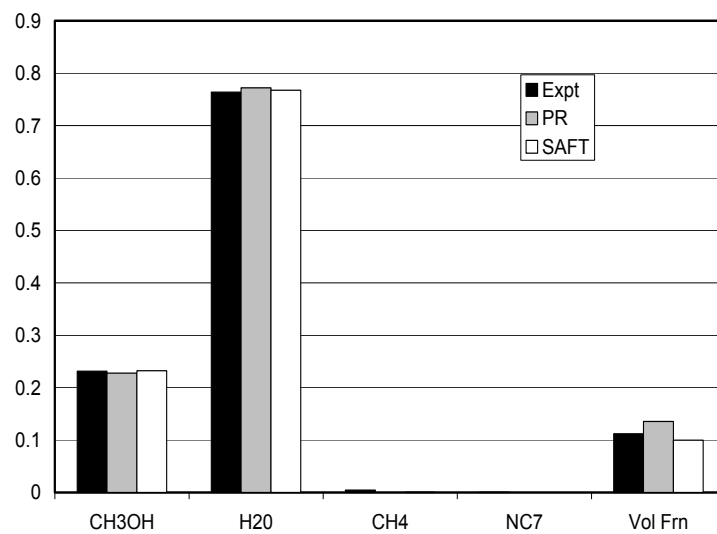


**Figure 5.70: Aqueous phase mole fractions at 14 F for hydrocarbon-water-methanol (Mixture 5) in Table 5.5**

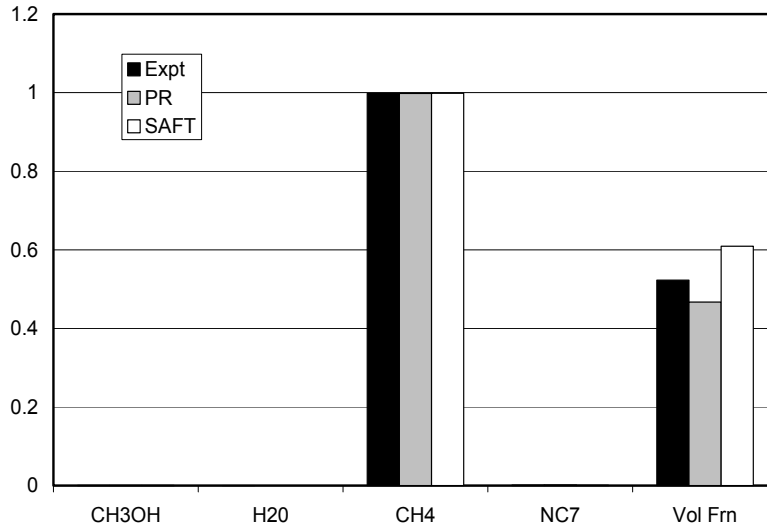


**Figure 5.71: Vapor phase mole fractions at 14 F for hydrocarbon-water-methanol (Mixture 6) in Table 5.5**

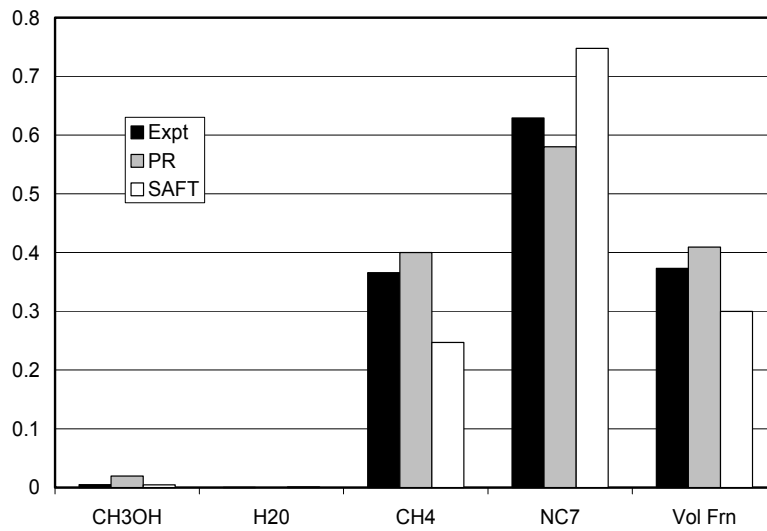


**Figure 5.72: Liquid hydrocarbon phase mole fractions at 14 F for hydrocarbon-water-methanol (Mixture 6) in Table 5.5**

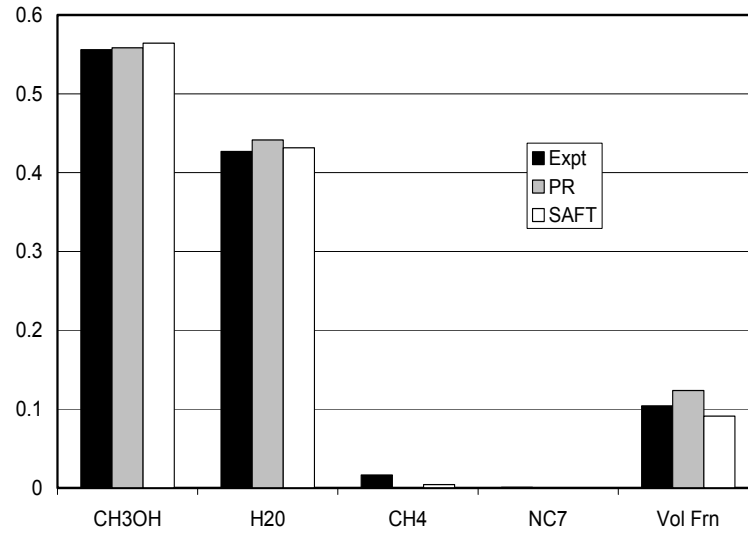


**Figure 5.73: Aqueous phase mole fractions at 14 F for hydrocarbon-water-methanol (Mixture 6) in Table 5.5**

## CHAPTER 6

### SAFT BASED INTERFACIAL TENSION MODEL

#### 6.1 BACKGROUND

The earliest theoretical models for describing the forces acting near a fluid interface were studied as far back as the early 19<sup>th</sup> century. Laplace [1] was the first to describe the intermolecular forces and their effect on capillary phenomena. He introduced a concept of internal pressure which is the force per unit area needed to separate an infinite body of liquid into two semi-infinite bodies bounded by their surfaces. The quantity that arises is the work per unit area that is done to separate the two surfaces which is equal to twice the interfacial tension because of the creation of two new surfaces.

Young [2] derived a relationship describing the interfacial tension at the solid-liquid-vapor three phase boundary by introducing the concept of contact angles.

$$\gamma_{sg} - \gamma_{ls} - \gamma_{lsg} \cos \theta \quad (6.1)$$

The three interfacial forces are in equilibrium at the three phase boundary. When the contact angle is zero the liquid completely wets the solid surface and is said to be completely spreading on the solid surface. If the contact angle is between 0 and 90 then the fluid is weakly wetting and the contact angles above represent the



degree of wetting. When the contact angle is equal to  $\pi$  then the fluid is known to be completely non-wetting.

## 6.2 SOLUBILITY PARAMETERS AND SURFACE TENSION

The earliest empirical model for prediction of interfacial energy is due to Macleod and Sugden using parachors [3,4,5]. The method developed by Macleod in 1923 and modified by Sugden in 1932 is given for pure fluids.

$$\gamma = [\Lambda (\Delta \rho)]^4 \quad (6.2)$$

where  $\Lambda$  is the parachor of the fluid and  $\Delta \rho$  is the density difference between vapor and liquid of pure species. The above correlation can be extended to mixtures as well [5].

$$\gamma = \sum_{i=1}^n [\Lambda_i (\rho_{ii} x_i - \rho_i y_i)]^4 \quad (6.3)$$

where  $n$  is the number of species  $i$ ,  $\Lambda_i$  is the parachor of species  $i$ ,  $\rho_{ii}$  is the density of denser phase and  $\rho_i$  is the density of the lighter phase.  $x_i$  and  $y_i$  are the compositions of the respective phases.

Fowkes [6] proposed splitting the interfacial energy term into non-associating and associating parts. Drago et al.[7,8], used the concept of splitting the enthalpy of adduct formation in acids and bases into weak and strong parts in a similar manner.

$$\gamma = \gamma^{\text{non-polar}} + \gamma^{\text{polar}} \quad (6.4)$$

The non-polar interaction in the surface tension also referred to in the literature as Lifshitz van der Waals interactions (LW) can be further split into their constituent forces.

$$\gamma^{LW} = \gamma^{\text{London}} + \gamma^{\text{Debye}} + \gamma^{\text{Keesom}} \quad (6.5)$$

$\gamma^{\text{London}}$  is the contribution to the interfacial tension due to dispersion forces. It arises due to the fluctuating atomic dipole caused by the instantaneous polarization of electrons rotating around a positive nucleus and thus is common to all molecules.  $\gamma^{\text{Debye}}$  is the interfacial tension contribution due to the permanent dipole- permanent dipole interactions and finally  $\gamma^{\text{Keesom}}$  is the permanent dipole – induced dipole interaction.

Fowkes also proposed simple mixing rules for the non-associating part of the interfacial tension. This approach has been found to be quite successful for many non-associating systems.

Van Oss [9] proposed a new set of mixing rules for the polar substrates. He introduced new parameters  $\gamma^+$  and  $\gamma^-$  in addition to the non-associating component  $\gamma^{LW}$  to account for the polar component of the interfacial tension also known as the Acid-Base contribution (AB).

$$\gamma^{AB} = 2 \sqrt{\gamma^+ \gamma^-} \quad (6.6)$$

Van Oss compiled a set of  $\gamma^{LW}$ ,  $\gamma^{AB}$ ,  $\gamma^+$  and  $\gamma^-$  values for several common non-polar and polar compounds. It has so far not been possible to extend the concepts of  $\gamma^+$  and  $\gamma^-$  to a system containing a mixture of several compounds.

Hansen [10] proposed a set of three-dimensional solubility parameters for bulk fluids similar to Fowkes approach. However, the solubility parameter of each molecule was split into a dispersion, polar and a hydrogen bonding part. The dispersion and the polar parts combined together form the non-associating component of Fowkes theory.

$$\delta = \delta^d + \delta^p + \delta^h \quad (6.7)$$

The solubility parameter above is defined as the cohesive energy density

$$\delta = \left[ \frac{\Delta H - RT}{V_m} \right]^{1/2} \quad (6.8)$$

Hansen had compiled the solubility parameters for several non-polar and polar compounds.

Hildebrand [11] proposed an empirical correlation to obtain surface tension from solubility parameters.

$$\delta = 16.8 \left( \frac{\gamma}{V^{1/3}} \right)^{1/3} \quad (6.9)$$

We made an attempt to correlate Hansen solubility parameters for several compounds with the solubility parameters calculated using Hildebrand correlation for the surface tension components proposed by van Oss. In Figure 6.1 it is seen that the LW components correlate reasonably well in both the theories. But there is a large discrepancy in the association part as seen in Figure 6.2. This can be attributed to the empirical nature of the above theories. In the next section we explore the development of the theories for prediction of interfacial tension based on statistical thermodynamics.

## 6.3 DENSITY FUNCTIONAL THEORY

### 6.3.1 Correlation Functions

In this section we present the basic concepts of the density functional theory involving inhomogeneous fluids. The grand canonical ensemble is used to develop a formalism for the square-gradient approximation of the free energy functionals. It must be noted that much of the theory discussed here is standard statistical thermodynamics and is available in the literature [12]

The Hamiltonian for a fluid of  $N$  atoms, each of mass  $m$ , is

$$H_N = \sum_{i=1}^N \frac{p_i^2}{2m} + \Phi(r_1, \dots, r_N) + \sum_{i=1}^N V(r_i) \quad (6.10)$$

where  $p_i$  is the momentum of atom  $i$  and  $\Phi$  is the total inter-atomic potential energy and  $V(r)$  is the total external potential. The statistical thermodynamic quantity, grand canonical potential ( $\Omega$ ) is a function of the inverse temperature  $\beta = (k_B T)^{-1}$ , the volume and the potential function  $u(r)$

$$u(r) = \mu - V(r) \quad (6.11)$$

A series of correlation functions are obtained by functional differentiation of  $\Omega$  with respect to  $u(r)$ . The first derivative, for example denotes the average one-body density

$$\rho(\mathbf{r}) \equiv \rho^{(1)}(\mathbf{r}) \equiv \langle \hat{\rho}(\mathbf{r}) \rangle = -\frac{\partial \Omega}{\partial u(\mathbf{r})} \quad (6.12)$$

where  $\langle \rangle$  denotes the ensemble average quantity.

A second derivative yields the density-density correlation function

$$G(\mathbf{r}_1, \mathbf{r}_2) = -\beta^{-1} \frac{\partial^2 \Omega}{\partial u(\mathbf{r}_2) \partial u(\mathbf{r}_1)} \quad (6.13)$$

The grand canonical potential  $\Omega$  is characterized by the grand canonical distribution function, which gives the probability  $P_N(\{\mathbf{r}^N, \mathbf{p}^N\})$  of finding the system with  $N$  particles with momenta and positions  $\{\mathbf{r}^N, \mathbf{p}^N\}$  in the phase space. This distribution function for the grand canonical ensemble with fixed chemical potential ( $\mu$ ), Temperature ( $T$ ) and the volume ( $V$ ) is given by the following equation[13]

$$f_N = \frac{\exp[-\beta (H_N - \mu N)]}{\Xi} \quad (6.14)$$

where  $\Xi$  is the grand canonical ensemble partition function.

We now define an intrinsic Helmholtz free energy functional which is a transformation on the grand canonical potential given by

$$F[\rho] = \Omega[\rho] - \int d\mathbf{r} u(\mathbf{r}) \rho(\mathbf{r}) \quad (6.15)$$

A second hierarchy of correlation functions, known as the direct correlation function can be generated by differentiating the excess Helmholtz free energy function  $F^{\text{Ex}}[\rho] = F[\rho] - F^{\text{ideal}}[\rho]$

$$c^{(1)}(\mathbf{r}) = - \frac{\partial(\beta F^{\text{Ex}}[\rho])}{\partial \rho(\mathbf{r})} \quad (6.16)$$

$$c^{(2)}(\mathbf{r}_1, \mathbf{r}_2) = - \frac{\partial^2(\beta F^{\text{Ex}}[\rho])}{\partial \rho(\mathbf{r}_2) \partial \rho(\mathbf{r}_1)} = \frac{\partial c^{(1)}(\mathbf{r}_1)}{\partial \rho(\mathbf{r}_2)} \quad (6.17)$$

and

$$c^{(n)}(\mathbf{r}_1, \mathbf{r}_2, \dots, \mathbf{r}_N) = \frac{\partial c^{(n-1)}(\mathbf{r}_1, \mathbf{r}_3, \dots, \mathbf{r}_{N-1})}{\partial \rho(\mathbf{r}_2)} \quad (6.18)$$

This discussion on distribution functions is completed with the introduction of the so called total correlation function and the Ornstein-Zernike equation. The total correlation function  $h(r_{12})$  is related to the radial distribution function  $g(r_{12})$  by

$$h(r_{12}) = g(r_{12}) - 1 \quad (6.19)$$

and is a measure of the total influence of molecule 1 on molecule 2 at a distance  $r_{12}$ . Ornstein and Zernike [14] had proposed the separation of the total correlation

function into two contributions: (1) a direct effect of 1 on 2 which is short ranged and is characterized by  $c(r_{12})$  and (2) an indirect effect, in which molecule 1 influences some other molecule  $c(r_{13})$  which in turn effects molecule 2. This indirect effect is the sum of all contributions from other molecules averaged over the volume of the system. So the Ornstein-Zernike equation relates the pairwise distribution functions and the direct correlation functions,

$$h(\mathbf{r}_1, \mathbf{r}_2) = c(\mathbf{r}_1, \mathbf{r}_2) + \int c(\mathbf{r}_1, \mathbf{r}_3) \rho(\mathbf{r}_3) h(\mathbf{r}_3, \mathbf{r}_2) d\mathbf{r}_3 \quad (6.20)$$

Note that the expression as written above is valid even for inhomogeneous systems.

### 6.3.2 Thermodynamic Functions

Once the correlation functions have been defined the appropriate thermodynamic functions can be evaluated by the functional integration over the density. Consider an initial fluid state with density  $\rho_i(\mathbf{r})$  and a final state with density  $\rho(\mathbf{r})$  at the same temperature  $T$ . Integration of the direct correlation equation (6.16) yields

$$\beta F^{\text{Ex}}[\rho] = \beta F^{\text{Ex}}[\rho_i] - \int_{\rho_i}^{\rho(\mathbf{r})} d\rho' \int d\mathbf{r} c^{(1)}([\rho_\alpha]; \mathbf{r}) \quad (6.21)$$



where  $c^{(1)}$  is shown as an explicit function of the density. Making a variable transformation

$$\alpha = \frac{\rho'(\mathbf{r}) - \rho_i(\mathbf{r})}{\rho(\mathbf{r}) - \rho_i(\mathbf{r})} \quad (6.22)$$

we have

$$\beta F^{\text{Ex}}[\rho] = \beta F^{\text{Ex}}[\rho_i] - \int_0^1 d\alpha \int d\mathbf{r} (\rho(\mathbf{r}) - \rho_i(\mathbf{r})) c^{(1)}([\rho_\alpha]; \mathbf{r}) \quad (6.23)$$

Similarly the integration of equation (6.17) yields [12]

$$c^{(1)}([\rho_\alpha]; \mathbf{r}_1) = c^{(1)}([\rho_i]; \mathbf{r}_1) + \int_0^\alpha d\alpha' \int d\mathbf{r}_2 (\rho(\mathbf{r}) - \rho_i(\mathbf{r})) c^{(2)}([\rho_\alpha]; \mathbf{r}_1, \mathbf{r}_2) \quad (6.24)$$

Combining Equations [6.23] and [6.24] we get

$$\begin{aligned} \beta F^{\text{Ex}}[\rho] &= \beta F^{\text{Ex}}[\rho_i] - \int d\mathbf{r} (\rho(\mathbf{r}) - \rho_i(\mathbf{r})) c^{(1)}([\rho_\alpha]; \mathbf{r}) \\ &\quad - \int_0^1 d\alpha \int d\mathbf{r}_1 (\rho(\mathbf{r}) - \rho_i(\mathbf{r})) \int_0^\alpha d\alpha' \int d\mathbf{r}_2 (\rho(\mathbf{r}_2) - \rho_i(\mathbf{r}_2)) c^{(2)}([\rho_\alpha]; \mathbf{r}_1, \mathbf{r}_2) \end{aligned} \quad (6.25)$$

This on further simplification results in

$$\begin{aligned} \beta F^{\text{Ex}} [\rho] = & \beta F^{\text{Ex}} [\rho_i] - \int d\mathbf{r} (\rho(\mathbf{r}) - \rho_i(\mathbf{r})) c^{(1)}([\rho_\alpha]; \mathbf{r}) \\ & - \int_0^1 d\alpha (\alpha - 1) \int d\mathbf{r}_1 \int d\mathbf{r}_2 (\rho(\mathbf{r}_1) - \rho_i(\mathbf{r}_1)) (\rho(\mathbf{r}_2) - \rho_i(\mathbf{r}_2)) c^{(2)}([\rho_\alpha]; \mathbf{r}_1, \mathbf{r}_2) \end{aligned} \quad (6.26)$$

If the integration path is taken from 0 density to the fluid density  $\rho$  and divided by the fluid volume we obtain the total Helmholtz free energy density

$$f(\rho) = f_{\text{id}}(\rho) + \beta^{-1} \rho^2 \int_0^1 d\alpha (\alpha - 1) \int d\mathbf{r} c^{(2)}(\alpha\rho; \mathbf{r}) \quad (6.27)$$

Note that the above formalism is exact and requires the evaluation of the second order direct correlation function as  $c^{(2)}$  as a function of density  $\rho(\mathbf{r})$  which is extremely difficult to obtain. Some approximations usually need to be made for this quantity.

Several theories have been put forward for the prediction of the interfacial tension of non-associating molecules in a lattice framework. Multi-layer adsorption theories [15-18] give an accurate picture of the interface. On the other hand the mono-layer theories of Defay et al., [19] and Prigogine-Marechal [20] are much simpler mathematically and reasonably accurate for the prediction of interfacial tension. In recent years there have been several attempts to combine a model for the association bonding interaction with the lattice theories to predict the behavior of mixtures of associating and non-associating molecules. Suresh et

al., [21] have used two theories the chemical theory and the Thermodynamic Perturbation Theory with the Prigogine-Marechal lattice model for various associating mixtures.

#### **6.4 SAFT BASED IFT MODEL WITH GRADIENT THEORY**

The associating lattice theory proposed by Suresh et al., [21] has several limitations. Although it gives very accurate predictions, it needs several empirical parameters in addition to the SAFT parameters. The radial distribution functions in the bulk and the surface are calculated by empirical correlations and are assumed to be constant. The number of neighbors in the same plane and in the adjacent planes may not be well determined for very complex spatial arrangement of molecules. It is often difficult to predict the non-associating part of interfacial tension independently from Fowkes theory or van-Oss theory (for e.g., the liquid may be completely spreading). Moreover, the theory is most useful when comparing the interfacial tension of mixtures with pure component interfacial tensions as the assumptions made about the spatial conformations of mixtures and pure components cancel out when the IFTs are compared with that of pure components. Since the Prigogine-Marechal theory is a close-packed lattice theory compressibility effects are not accounted for. The lattice theory of dispersion interaction is combined with a statistical mechanical model of association bonding, both of which are based on two entirely different physical frameworks.

In this section we propose to extend the SAFT formulation to evaluate the interfacial thermodynamic properties using a gradient theory approach. This allows us to model changes in the radial distribution function across the interface. Evans [12] has discussed the foundations of density functional theory. Davis et al.,[22] have presented the basic ideas in the use of gradient theory in the calculation of interfacial profiles and interfacial tension based on the Cahn-Hilliard approach. Most density functional methods are based on the idea that the free energy in the interfacial phase is a function of the density profile.

As discussed in Section 6.3, the Helmholtz's free energy can be divided into the ideal and the excess parts.

$$F[\rho(\mathbf{r})] = F^{\text{id}}[\rho(\mathbf{r})] + F^{\text{ex}}[\rho(\mathbf{r})] \quad (6.28)$$

The capital F denotes that we are referring to the total Helmholtz energy of the mixture. The ideal gas functional is known exactly.

$$F^{\text{id}}[\rho(\mathbf{r})] = \sum N_i(\mathbf{r}) kT [\ln \rho(\mathbf{r}) - 1] \quad (6.29)$$

$N_i$  is the total number of molecules of component  $i$  and  $\rho$  is the total mixture density at the point  $\mathbf{r}$  in space. The Helmholtz free energy across the interface is given by free energy gradient approximation obtained by assuming that the molar free energy  $f(\mathbf{r})$  is a function of the local density  $n(\mathbf{r})$  and all its

derivatives at  $r$  and expanding about the homogeneous state to obtain gradients in the Cahn-Hilliard form:

$$f(r : \{n\}) = f_0(n) + \sum_i \frac{1}{2} A_i \nabla^2 n_i + \sum_{i,j} \frac{1}{2} B_{i,j} \nabla n_i \nabla n_j \quad (6.30)$$

where  $A_i$  and  $B_{ij}$  are properties of homogeneous fluid. The total free energy of the entire inhomogeneous system can thus be expressed as

$$F = \int \left[ f(n) + \sum_{i,j} \frac{1}{2} c_{i,j} \nabla n_i \nabla n_j \right] d^3 r \quad (6.31)$$

The chemical potential of species  $i$  given by

$$\mu_i = \frac{\partial F}{\partial n_i} \quad (6.32)$$

The chemical potential of component  $i$  computed from the integral equation (6.31) with minor rearrangement can be written as

$$\sum_j \nabla \cdot (c_{ij} \nabla n_j) - \frac{1}{2} \sum_{k,j} \frac{\partial c_{kj}}{\partial n_i} \nabla n_k \nabla n_j = \frac{\partial \omega}{\partial n_i} \quad (6.33)$$

where  $\omega$  is a thermodynamic potential defined by

$$\omega(\mathbf{n}) \equiv f(\mathbf{n}) - \sum_i n_i \mu_i \quad (6.34)$$

Equation (6.33) above is a non-linear ordinary differential equation with appropriate boundary conditions which can be solved to obtain the interfacial profile of components. The microstructure of the interface, whether it is planar, spherical or a thin-film is determined by the total Helmholtz free energy function ( $\omega$ ).

For a planar system,  $n_i = n_i(x)$ , the partial differential equation (6.33) can be reduced to a one-dimensional form,

$$\sum_{i,j} \frac{1}{2} c_{ij} \frac{dn_i}{dx} \frac{dn_j}{dx} = \omega(\mathbf{n}) + K \quad (6.35)$$

where  $K$  is a constant of integration.

For a planar interface, the boundary conditions are  $n(x = -\infty) = n^{(1)}$  and  $n(x = \infty) = n^{(2)}$ , which are the bulk compositions of each phase. This implies

$$\left. \frac{\partial \omega}{\partial n_i} \right|_{(n^{(i)})} = 0 \quad (6.36)$$

and

$$\omega(n^{(i)}) + K = 0 \quad (6.37)$$

which on further simplification yields the bulk properties

$$\mu_i = \mu_i^0(n^{(P)}) \quad \text{for } P = 1, n_P \quad (6.38)$$

and

$$P_N = P_0(n^{(P)}) \quad \text{for } i = 1, n_P \quad (6.39)$$

These two boundary conditions can be now used in equation (6.35) to obtain the following expression

$$F = \sum_i N_i \mu_i^0 - P_0 V + A \int_{-\infty}^{\infty} \sum_{i,j} c_{ij} \frac{dn_i}{dx} \frac{dn_j}{dx} dx \quad (6.40)$$

from which the interfacial tension of the system is given by Davis et al [22]., as

$$\gamma = \sum_{i,j} \int_{-\infty}^{\infty} c_{ij} \frac{dn_i}{dx} \frac{dn_j}{dx} dx \quad (6.41)$$

Gradient theory is comparatively mathematically simple and presents the physics of interfaces very clearly. The homogeneous system free energy and the influence parameters for the inhomogeneous fluid are separated clearly.

If we consider a one component fluid for a planar interface, the boundary conditions are  $n(x) \rightarrow n^{(1)}$  as  $x \rightarrow -\infty$  and  $n(x) \rightarrow n^{(2)}$  as  $x \rightarrow +\infty$ , where  $n^{(i)}$  is the bulk composition of phase  $i$ . For a one-component system, the above boundary conditions simplify as follows,

$$dx = \sqrt{\frac{c}{2}} \frac{dn}{\sqrt{\Delta \omega(n)}} \quad (6.42)$$

where  $\Delta \omega(n) \cong \omega(n) - \omega_B$ .

With the above simplification the interfacial tension for a pure component is given by

$$\gamma = \sqrt{2} \int_{n_g}^{n_l} [c \Delta \omega(n)]^{1/2} dn \quad (6.43)$$

Geometrically  $\Delta \omega(n)$  can be represented as the vertical line between the curve of  $f_0(n)$  versus  $n$  and a straight line touching  $f_0$  at the vapor and liquid densities,  $n_g$  and  $n_l$ .

Another simplifying assumption to the above expression is that the cross interaction parameter also known as the influence parameter is taken to be independent of the density and hence can be taken outside of the integral.



The above equation defines the system for pure components. For multi-component systems the equation (6.33) can be rewritten as follows

$$\sum_{j=1}^n c_{ij} \frac{\partial^2 n_i}{\partial x^2} = \mu_i^0(n) - \mu_i(n) \quad i=1, n \quad (6.44)$$

with the boundary conditions

$$\begin{aligned} n &\rightarrow n^I && \text{from } x \rightarrow -\infty \\ n &\rightarrow n^{II} && \text{from } x \rightarrow \infty \end{aligned} \quad (6.45)$$

To remain consistent with the one-component system the influence parameter is taken to be independent of the density.

The above set of second order non-linear partial differential equations (Equation 6.44) can not be solved analytically in general. The above equations are usually solved numerically using different schemes.

One of the most elegant approaches which has been found to be extremely useful is the space transformation first suggested by Carey et al.,[23]

$$y = \tanh x \quad (6.46)$$

Using this transformation the governing equations above can be written as

$$\sum_{j=1}^n c_{ij} \left[ (1-y^2)^2 \frac{\partial^2 n_i}{\partial y^2} - 2y(1-y^2) \frac{\partial n_i}{\partial y} \right] = \mu_i^0(n) - \mu_i \quad i=1, n \quad (6.47)$$

The boundary conditions in the transformed conditions are

$$\begin{aligned} n &\rightarrow n^I && \text{from } y \rightarrow -1 \\ n &\rightarrow n^{II} && \text{from } y \rightarrow 1 \end{aligned} \quad (6.48)$$

It is to be noted that the boundary condition is now over a finite domain rather than over the infinite domain in the original formulation.

The cross interaction coefficient  $c_{ij}$  for mixtures is obtained from the pure component interaction coefficient by the following equation.

$$c_{ij} = (1 - m_{ij}) \sqrt{c_{ii} c_{jj}} \quad (6.49)$$

$m_{ij}$  is the mixing interaction coefficient defined for the interfaces. Usually, the binary interaction coefficient ( $k_{ij}$ ) for the bulk phases is taken as the mixing interaction coefficient ( $m_{ij}$ ) for most cases. In some cases, however, the mixing interaction coefficient had to be adjusted to get a good prediction of the experimental interfacial tension values.

Carey [23] noted that the original formulation allows for infinite solutions. If  $n(x)$  is a solution to the original set of differential equations any transformation  $n(x+k)$  will also satisfy the system of equations. This is true of the new  $\tanh x$  transformation as well. Nevertheless, this method in combination with a general finite difference scheme has been found to be very successful in this study.

Carey et al.[23], and Cornelisse et al.[24], have used the Peng-Robinson equation of state as the underlying model for free energy and the chemical potential calculation in the equations presented so far. Sanchez et al., [25] have used lattice fluid models with the gradient theory to predict interfacial tensions. In this study we have used the SAFT equation of state as the basis for the free energy model. Although, we still need to obtain the pure component influence parameter from the pure component experimental data, it is much simpler than the multi-parameter fit needed for the Associating Lattice Fluid model. Since we have used the gradient theory with the SAFT equation of state it is a more realistic representation of polar fluids as against the models based on the Peng-Robinson equation of state.

## Nomenclature

$\gamma$	surface tension/ interfacial tension (N/m)
$\Lambda_i$	parachor of species i
$\rho_{II}$	density of denser phase (mol/m <sup>3</sup> )
$\rho_I$	density of lighter phase (mol/m <sup>3</sup> )
$x_i$	mole fraction of species i in denser phase
$y_i$	mole fraction of species i in lighter phase
$\delta_i$	solubility parameter of compound i
$v_i$	specific volume of compound i (m <sup>3</sup> / mol)
$H_N$	Hamiltonian for a fluid of N atoms
$p_i$	momentum of atom i
$\Phi$	total interatomic potential energy
$V(\mathbf{r})$	total external potential function
$\Omega$	grand canonical potential function
$\rho(\mathbf{r})$	average one body density (mol/m <sup>3</sup> )
$G(r_1, r_2)$	two body density correlation function
$\mu$	chemical potential (J/mol)
$V$	volume (m <sup>3</sup> )
$T$	temperature (K)
$\Xi$	grand canonical ensemble partition function
$F(\rho)$	Helmholtz free energy functional
$c^{(n)}(r_1, r_2, \dots, r_N)$	nth order direct correlation function
$h(r_{12})$	total correlation function
$g(r_{12})$	radial distribution function
$N_i$	number of molecules of component i
$\mu_i^0$	chemical potential of component i in the bulk homogeneous phase

$P^0$	pressure in the bulk homogeneous phase
$A$	interfacial area
$x$	distance across the interface
$c_{ij}$	cross-interaction coefficient between species $i$ and $j$
$m_{ij}$	mixing interaction coefficient for interfaces between species $i$ and $j$

## References

- 1) Laplace, P.S. , *Traite de Mecanique Celeste; Supplement au dixieme livre, Sur l Action Capillaire*, 1806, Courcier, Paris,
- 2) Young, T., (1816), reprinted in *Miscellaneous Works of the late Thomas Young*, ed. G. Peacock, Vol. I, p. 454, Murraray, London, 1855.
- 3) Macleod, D.B., “On a relation between surface tension and density”, *Trans. Faraday Soc.*, **19**, 38 (1923)
- 4) Sugden, S., “The variation of surface tension with temperature and some related functions”, *J. Chem. Soc.*, **125**, 32 (1924).
- 5) Sugden, S.; “A relation between surface tension, density, and chemical composition”, *J. Chem. Soc.*, **125**, 1177 (1924)
- 6) Fowkes, F.M., “Ideal Two-dimensional solutions. II. A new isotherm for soluble and “gaseous” monolayers”, *J. Phys. Chem.*, **66**,3,385 (1962).
- 7) Drago R.S., Vogel G. C., and Needham T.E., “A four-parameter equation for predicting enthalpies of adduct formation”, *J. Am. Chem. Soc.*, **93**,23, 6014 (1971).
- 8) Drago R.S., Parr L.B.,Chamberlain C. S., “Solvent effects an their relationship to the E and C equation”, *J. Am. Chem.. Soc.*, **99**,10, 3203 (1977).
- 9) Van Oss, C. J., *Interfacial Forces in Aqueous Media*, Marcel Dekker, New York, 1985.
- 10)Hansen C. M., “The three dimensional solubility parameter – key to paint component affinities: I solvents, plasticizers, polymers and resins”, *Journal of Paint Technology*, **39**, 505 (1967).
- 11) Kaelble D.H., *Physical chemistry of adhesion*, Wiley-Interscience 1971.
- 12) Evans, R., in *Fundamentals of Inhomogeneous Fluids*, edited by D. Henderson, Marcel Dekker, New York, 1992.
- 13) Hill, T.L., *Statistical Mechanics*, 1956, McGraw-Hill, New York

- 14) Ornstein, L.S., and Zernike, F., "The kinetic theory of solid substrates. III. The equation of state of isotropic solid substrates", 1914, *Proc. Roy. Acad. Sci., Amsterdam*, **17**, 793
- 15) Roe, R.J., "Multilayer theory of adsorption from a polymer solution", *J. Chem. Phys.*, **60**, 4192 (1974).
- 16) Helfand, E., "Theory of inhomogeneous polymers: Lattice model for polymer-polymer interfaces", *J. Chem. Phys.*, **63**, 2192 (1974).
- 17) Scheutjens, J.M.H.M., and Fler, C.J., "Statistical theory of the adsorption of interacting chain molecules. 1. Partition function, segment density distribution, and adsorption isotherms", *J. Phys. Chem.*, **83**, 1619 (1979).
- 18) Scheutjens, J.M.H.M., and Fler, C.J., "Statistical theory of the adsorption of interacting chain molecules. 2. Train, loop and tail size distribution", *J. Phys. Chem.*, **84**, 178 (1980).
- 19) Defay, R., Prigogine, I., Bellemans, A., and Everett, D.H., *Surface tension and adsorption*, Wiley: New York, 1966.
- 20) Prigogine, I., Marechal, J., "The influence of differences in molecular size on the surface tension of solutions. IV", *J. Colloid Sci.*, **7**, 2,122 (1950).
- 21) Suresh S.J., and Naik V.M., "Predictive models for interfacial properties of associating systems. A statistical thermodynamic approach", *Langmuir*, **12**, 6151 (1996).
- 22) Davis, H.T., and Scriven L.E., "Stress and structure in fluid interfaces", Chapter in *Advances in Chemical Physics*, Vol XLIX, Wiley, New York, 1982.
- 23) Carey, B.S., *Molecular thermodynamics of multicomponent interfaces*, Ph.d Thesis, University of Minnesota, 1979
- 24) Cornelisse P.M.W., *The Square Gradient Theory Applied: Simultaneous modelling of interfacial tension and phase behavior*, Ph.D dissertation, Technische Universiteit Delft, Denmark
- 25) Poser C.I., and Sanchez I.C., "Interfacial tension theory of low and high molecular weight liquid mixtures", *Macromolecules.*, **14**, 361, 1981.

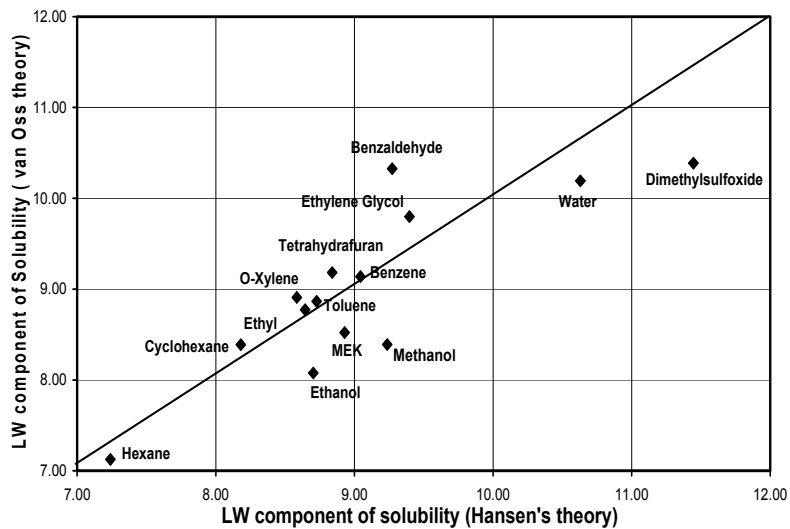


**Figure 6.1: Comparison of solubility factor calculations from van Oss parameters with the Hansen solubility parameter for the LW component**

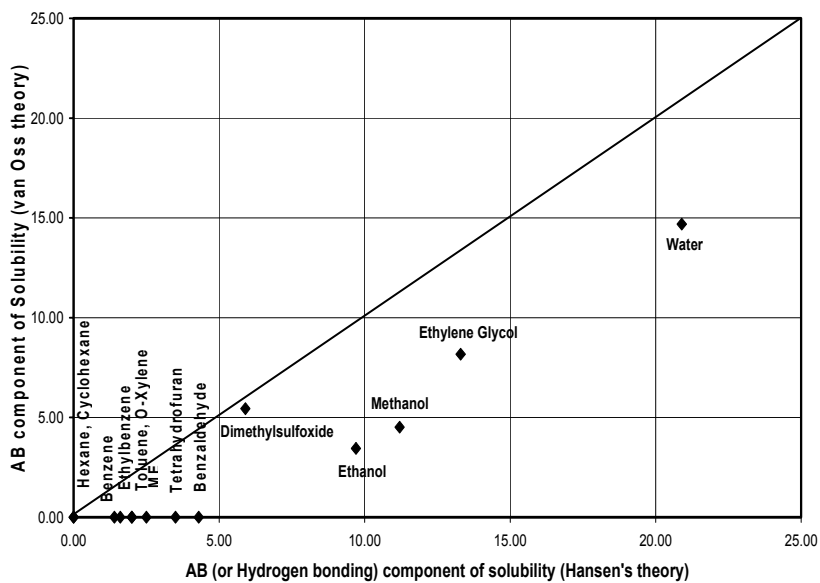


**Figure 6.2: Comparison of solubility factor calculations from van Oss parameters with the Hansen solubility parameter for the Acid-Base component**



## CHAPTER 7

### INTERFACIAL PROPERTIES OF PURE COMPONENTS AND MIXTURES

In this chapter we present results and discuss the effectiveness of using the gradient theory formulation presented in the last chapter together with the SAFT EOS for predicting the interfacial properties of two-phase multi-component mixtures.

#### 7.1 PURE COMPONENTS

Figure 7.1 shows the interfacial tension of pure CO<sub>2</sub>. We observe that SAFT is able to predict the interfacial tension using the gradient theory fairly accurately. It is to be noted that the interaction parameter ( $c_{ii}$ ) has been obtained by fitting the experimental interfacial tension value at 242 K. Figure 7.2 shows the interfacial tension predictions for nitrogen. Again the match with the SAFT equation of state is very good. The average absolute deviation between the predicted values and experiments is about 1.1 %. Figure 7.3 shows the interfacial tension predictions for heptane. The average absolute deviation in this case is found to be 6.9 %. Figure 7.4 shows the interfacial tensions for decane. The average interfacial tensions in this case were found to be 10 %.

Next we examine the effectiveness of the gradient theory combined with the SAFT equation of state for polar molecules. In Figure 7.5 we present the interfacial tension of methanol. The average absolute deviation in this case is 7.9 % . So we see that SAFT in combination with the gradient theory can effectively describe the interfacial behavior of polar molecules. Figure 7.6 shows the interfacial tension predictions for ethanol. We observe that SAFT does a very good job of predicting the interfacial tension. The average absolute deviation in this case is only 1.7 %. Figure 7.7 show the SAFT predictions for butanol and we find that the average absolute deviation in this case is 7.6 %. Figure 7.8 shows the SAFT predictions for water over a wide range of temperature and the average absolute deviation in this case is 10 %. The interfacial tension interaction parameters for these fluids are shown in Table 7.1.

## 7.2 BINARY MIXTURES

Now we present the SAFT-GT predictions of the interfacial tensions of mixtures. Figure 7.9 to Figure 7.12 show the interfacial profiles of CO<sub>2</sub> – decane mixtures. We observe that for all compositions of the equilibrium mixture the interfacial profile of decane is monotonically increasing. CO<sub>2</sub> on the other hand shows increased surface concentration at intermediate as well as high concentrations of CO<sub>2</sub>. Figure 7.9 show the interfacial profile for a CO<sub>2</sub> – decane mixture for 344 K and 6.04 M Pa. The interfacial tension for this mixture predicted is 8.29 mN/m which compares very well with the experimental values. The binary interaction coefficient ( $k_{ij}$ ) for this mixture is 0.14 which is also the

value of the mixing interaction coefficient ( $m_{ij}$ ) used for the interfaces. We see that the SAFT based IFT model does a fairly good job of predicting the interfacial tension of non-polar mixtures as shown in Figure 7.13. We also show the parachor calculations of interfacial tension for this mixture and we observe that the parachor predictions are off at very low  $\text{CO}_2$  concentrations in the liquid phase.

Figure 7.14 to Figure 7.22 show the interfacial profiles of an ethanol-heptane mixture. Note that this is essentially a three component mixture as nitrogen is added to the mixture to form a gas-liquid interface. At the system pressure of 0.101 MPa and temperature of 298.15 K ethanol and heptane form a single phase binary mixture over the entire heptane concentration range, so that we measure the interfacial tension over nitrogen. We observe that when there is significantly small amount of ethanol present in the liquid phase (Figure 7.14) the interfacial profiles of ethanol are monotonously increasing and heptane exhibits a slight interfacial activity. Similarly when the heptane concentration is high in the mixture then the interfacial profiles (Figures 7.20 to Figure 7.22) of heptane are monotonously increasing whereas ethanol exhibits slight interfacial activity. At intermediate ethanol concentrations it is interesting to note that; ethanol shows an increased interfacial activity whereas the heptane concentration is suppressed in the interfacial region. This is because ethanol is a polar molecule so that the polar sites tend to be localized near the interface. The binary interaction coefficient ( $k_{ij}$ ) is 0.03 which is also the value of the mixing interaction coefficient used for this

mixture. We observe that SAFT together with gradient theory provides very good predictions of interfacial tension of the ethanol-heptane mixture as shown in Figure 7.23. On the other hand, the parachor calculations significantly over predict the interfacial tension of this mixture.

Next we present the results for a methanol-water mixture at 263.15 K and 0.101 MPa. Here again we introduce nitrogen in the mixture so as to be able to calculate the tension of the vapor-liquid interface. In this case the cross-interaction parameter for the binary mixture had to be adjusted similar to the binary interaction coefficients used for predicting the bulk thermodynamic properties. It is interesting to note, however, that even for two very different values of mixing interaction coefficients ( $m_{ij} = 0$  and  $1$ ), we have been able to predict the interfacial tension of the mixture fairly accurately as shown in Figure 7.30. We observe that at high concentrations of methanol, Figure 7.24 and Figure 7.25, the interfacial profiles are monotonic. At low concentrations of methanol (Figure 7.27 to Figure 7.29), although the water profiles are monotonically increasing the methanol interfacial profiles show increased interfacial activity. The mixing interaction coefficient ( $m_{ij}$ ) used to generate the above interfacial profiles is zero. Figure 7.30 also shows the interfacial tension predictions of SAFT with gradient theory for methanol – water and also parachor predictions. The SAFT predictions are clearly much better than the parachor calculations.

Figures 7.31 to 7.35 show the interfacial tension profiles of ethanol-water mixtures. The temperature of the mixture is 288.15 K and the pressure is 0.101 MPa. Nitrogen is present as a third component to provide a vapor-liquid interface. The behavior observed in the interfacial profiles is similar to what we have seen earlier in the methanol water mixtures. As low concentrations of ethanol (Figure 7.31) the profiles are monotonic. As we increase the water concentration the water profile is monotonic whereas ethanol shows increased interfacial activity. Figure 7.36 show the interfacial tension predictions with both SAFT – Gradient Theory and also the corresponding parachor calculations. The mixing interaction coefficient ( $m_{ij}$ ) is set to zero. We observe that the interfacial tension predictions with the adjustment of mixing interaction coefficient are very good. The parachor predictions on the other hand are not very accurate.

Figure 7.37 to 7.40 show the interfacial profile of water-methane mixtures at 25 C at high pressures. The interfacial profile have been obtained by adjusting the mixing interaction coefficient ( $m_{ij}$ ) to 0.35. We observe that at pressures even as high as 1450 psia methane exhibits interfacial activity. The water interfacial profiles are monotonic over the entire pressure range. Figure 7.41 shows the SAFT predictions of the interfacial tension with experimental data and parachor predictions. SAFT predicts the interfacial tension very well at this temperature whereas the parachor predictions are not very good. Next we study the effect of temperature on the interfacial tension for this same mixture. Figure 7.42 to 7.44 show the interfacial profiles of methane-water mixtures at 106 C. The interfacial

tensions predictions with the mixing interaction coefficient of 0.35 are fairly accurate as seen in Figure 7.45. We observe similar behavior at still higher temperature of 176.6 F. Figure 7.46 to Figure 7.48 show the interfacial profiles at this temperature with the value of the mixing interaction coefficient given ( $m_{ij}$ ) given as 0.35. We are able to predict the variation of the interfacial tension with pressure at this temperature without further adjusting the mixing interaction coefficient as shown in Figure 7.49.

Figure 7.50 to Figure 7.52 show the interfacial tension profile for a water-CO<sub>2</sub> mixture at 25 C. The mixing interaction coefficient used is 0.15. Figure 7.53 shows the interfacial tension predictions for this mixture. We observe that the SAFT predictions are reasonably accurate. The parachor predictions as expected are not very accurate, especially at higher pressures.

### 7.3 CONCLUSIONS

We have used the SAFT equation of state with the gradient theory to predict the interfacial tension of pure components and mixtures. We have shown that this model predicts the interfacial tension of both non-polar and polar, pure components very accurately. We have introduced the pure component interaction parameters for the calculation of interfacial tension with the SAFT equation. We have also presented interfacial tension calculations for non-polar and polar mixtures. We have shown that SAFT with the gradient theory does a fairly good

job of predicting interfacial tension. The interfacial tensions of water-ethanol, water-methanol and a few other mixtures have been satisfactorily predicted .by the SAFT equation of state by introducing a mixing interaction coefficient. We have studied the effect of temperature and pressure on a methane-water mixture with this and have found that the theory holds well at different temperatures and pressures although we need to adjust the mixing interaction coefficients for interfaces ( $m_{ij}$ ) initially.

## References

- 1) Vargaftik, N.B., *Tables on the Thermophysical properties of Liquids and Gases*, John Wiley & Sons, New York, 1970
- 2) Hsu, J-C., Nagarajan, N., and Robinson Jr., R.L., , “Equilibrium Phase Compositions, Phase Densities, and Interfacial Tension for CO<sub>2</sub> +Hydrocarbon Systems. 2. CO<sub>2</sub> + n-Decane”, *J. Chem. Eng. Data.*, 30, 485 (1985).
- 3) Papaioannou, D., Panayiotou, C.G., “Surface Tensions and Relative Adsorptions in Hydrogen-Bonded Systems”, *J. Chem. Eng. Data*, 39(3), 457 (1994).
- 4) Teitelbaum, B. Ya., Gortalova, T.A., Ganelina S.G., “The surface layer of liquid systems. I. Surface tension of binary liquid systems in the instance of surface separation of layers”, *Kolloid. Zhur.*, 12, 294, (1950)
- 5) Bircumshaw, L.L., *J. Chem. Soc.*, 121, 887 (1922).
- 6) Sachs, W., and Meyn, V., “Pressure and temperature dependence of the surface tension in the system natural gas/water. Principles of investigation and the first precise experimental data for pure methane/water at 25 C up to 46.8 M Pa”, *Colloids and Surfaces, A: Physicochemical and engineering Aspects*, 94, 291, (1995).
- 7) Jennings, H.Y., and Newman, G.H., “Effect of temperature and pressure on the interfacial tension of water against methane- normal decane mixtures” *J. Soc. Pet. Eng.*,6, 171, (1971)
- 8) Massoudi, R., and King, A.D., “Effect of pressure on the surface tension of water. Adsorption of low molecular weight gases on water at 25 C”, *J.Phys. Chem.*, 78,22, 2262 (1974).



<b>Component</b>	<b>Interfacial Tension Parameter (<math>c_{ii}</math>), <math>\text{J/m}^5\text{mol}^2</math></b>	<b>% Average Absolute Deviation</b>	<b>Parachor</b>
Nitrogen	1.38e-20	1.0	35.00
CO <sub>2</sub>	2.33e-20	3.5	77.50
Methane	2.79e-20	5.0	72.60
Propane	2.33e-20	2.6	150.8
Butane	2.33e-20	4.4	190.3
Heptane	4.63e-19	6.9	311.36
Decane	7.52e-19	10.0	431.20
Methanol	2.77e-20	7.9	88.80
Ethanol	5.26e-20	1.8	126.80
Butanol	1.29e-19	7.6	203.4
Water	9.32e-21	1.7	52.60

**Table 7.1: Interfacial tension parameter for gradient theory with SAFT equation of state**

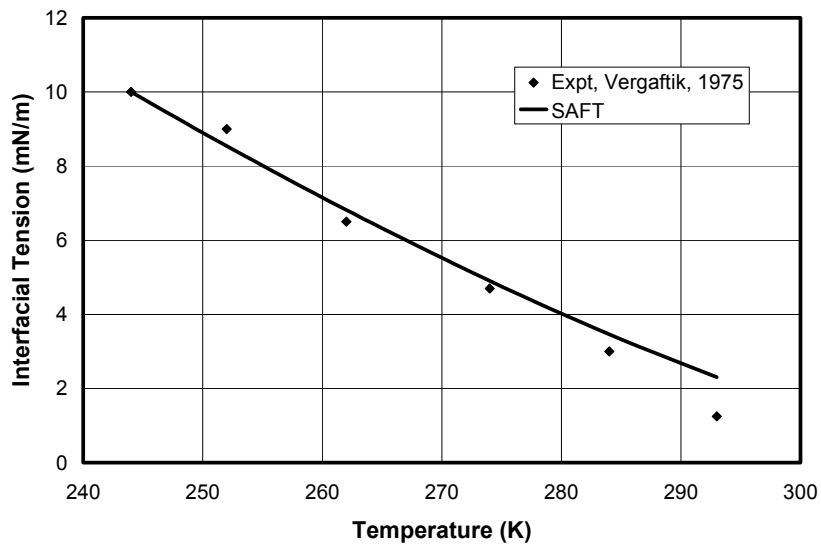


**Figure 7.1: Prediction of interfacial tension with SAFT equation for CO<sub>2</sub>**

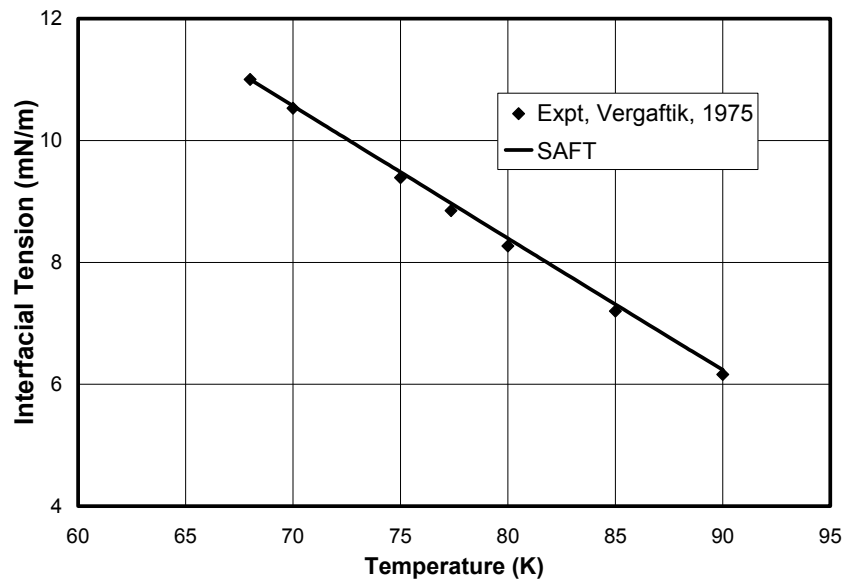


**Figure 7.2: Prediction of interfacial tension with SAFT equation for N<sub>2</sub>**

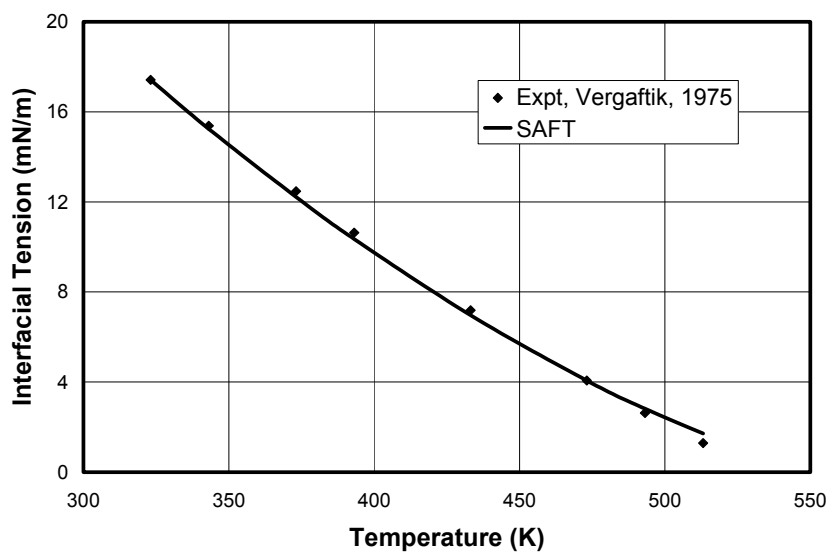


**Figure 7.3: Prediction of interfacial tension with SAFT equation for heptane**

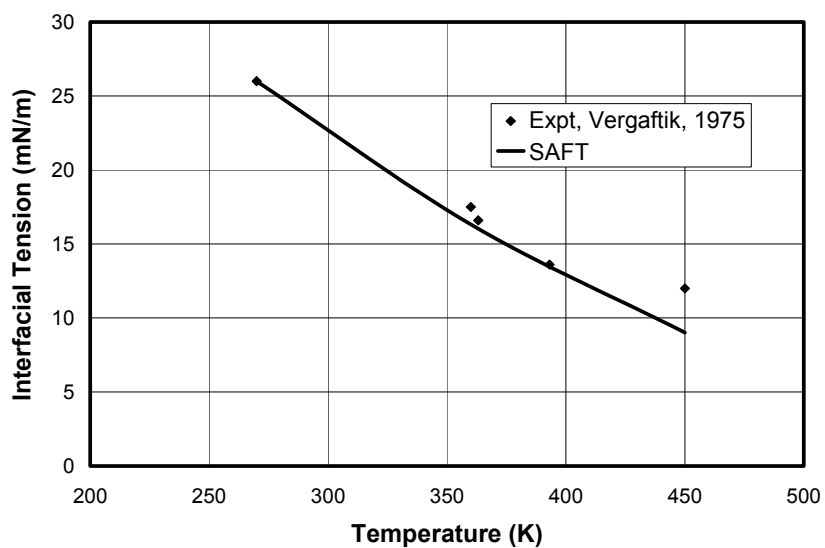


**Figure 7.4: Prediction of interfacial tension with SAFT equation for decane**

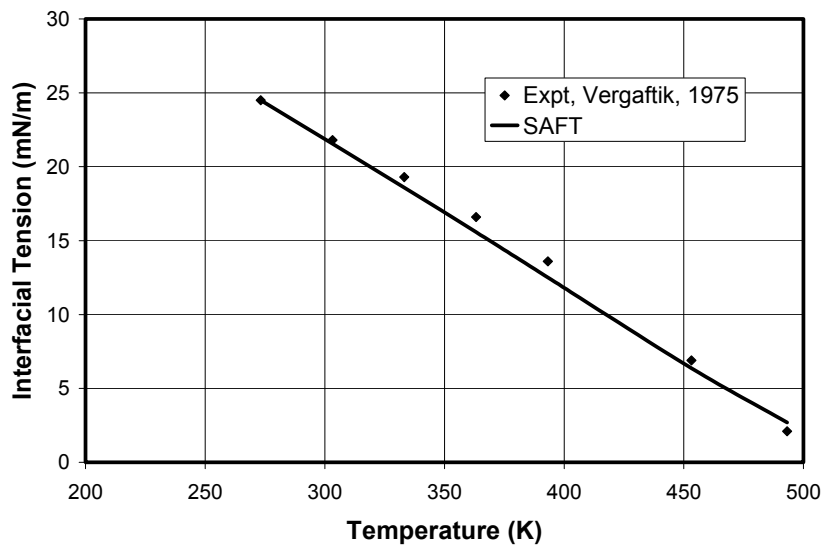


**Figure 7.5: Prediction of interfacial tension with SAFT equation for methanol**

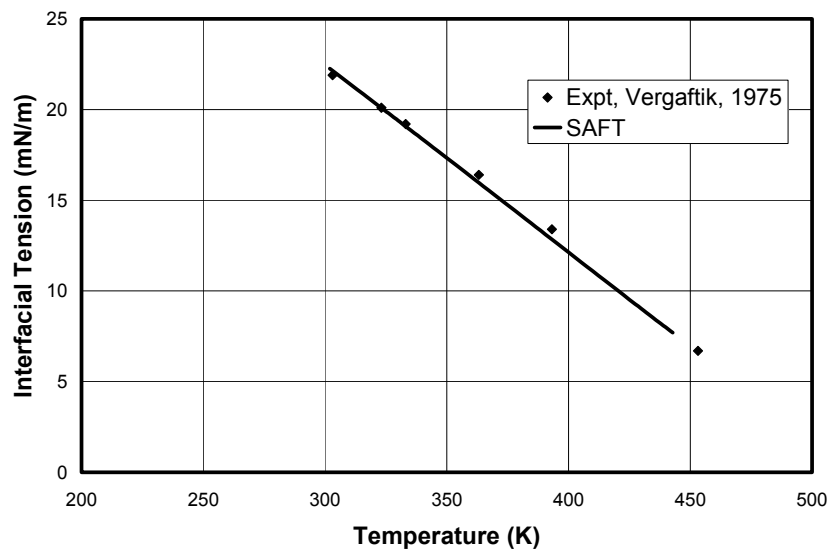


**Figure 7.6: Prediction of interfacial tension with SAFT equation for ethanol**

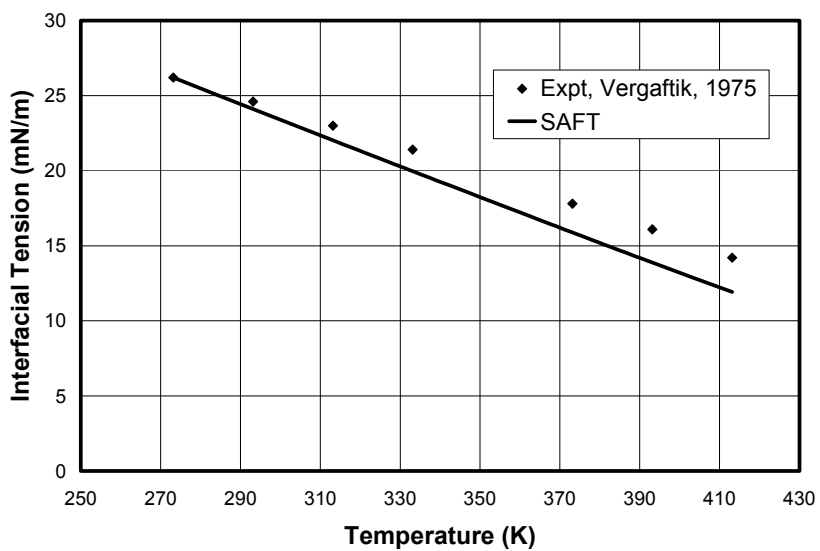


**Figure 7.7: Prediction of interfacial tension with SAFT equation for butanol**

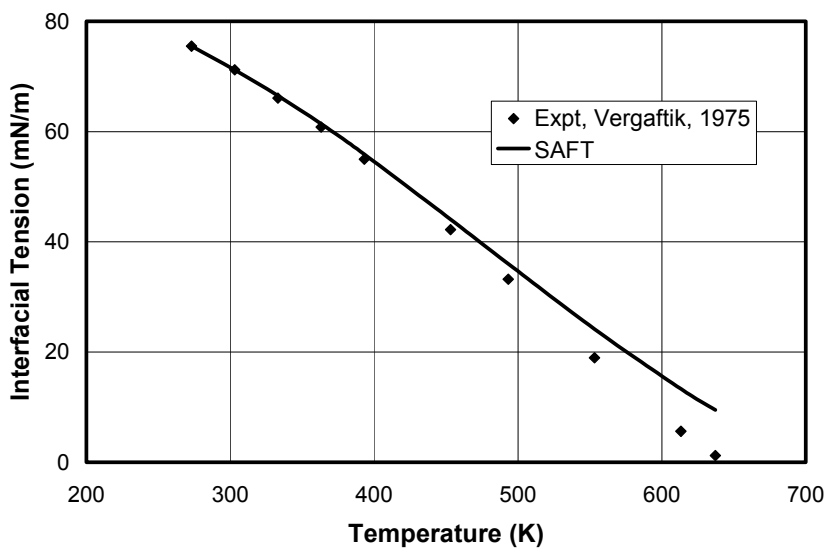


**Figure 7.8: Prediction of interfacial tension with SAFT equation for water**

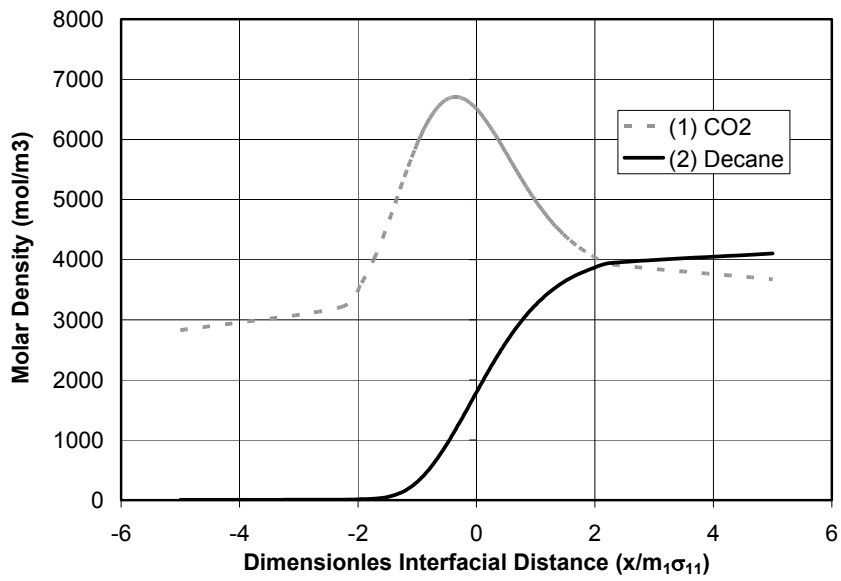


**Figure 7.9: Interfacial profile of CO<sub>2</sub> -Decane mixture at 344 K and 6.94 MPa**

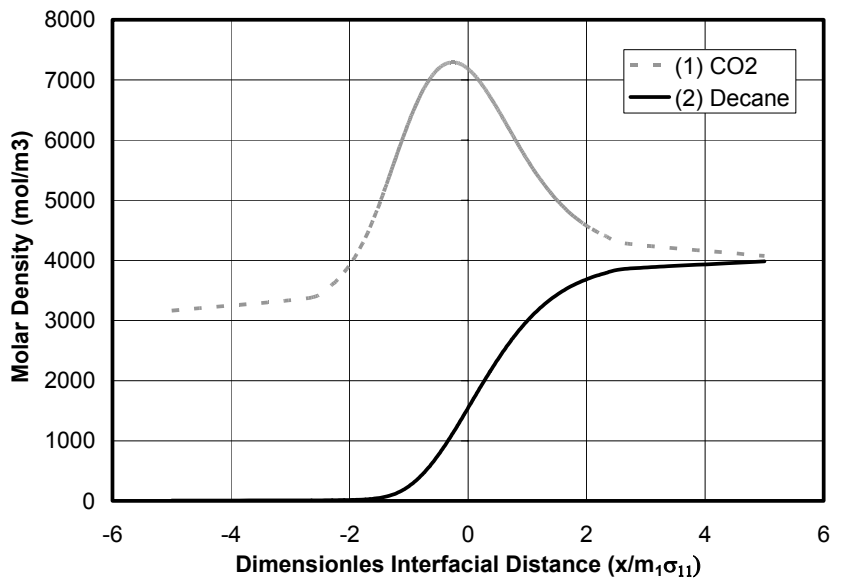


**Figure 7.10: Interfacial profile of CO<sub>2</sub> -Decane mixture at 344 K and .94 MPa**

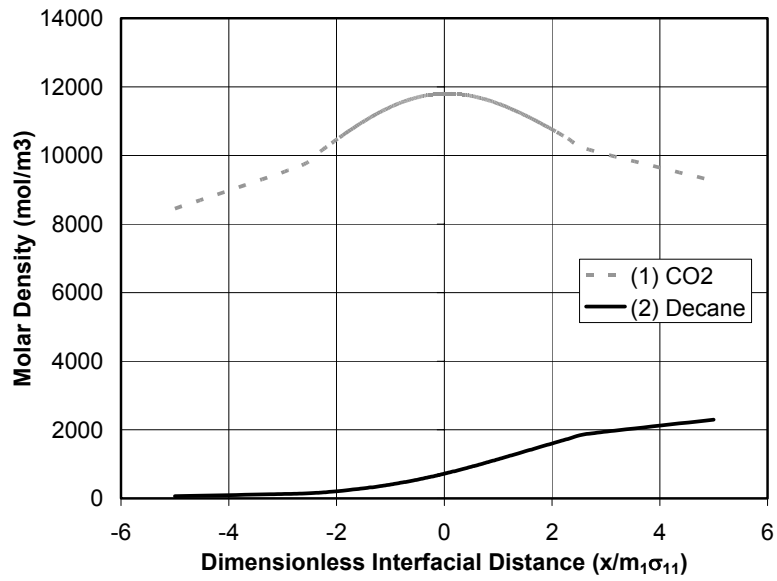


**Figure 7.11: Interfacial profile of CO<sub>2</sub>-Decane mixture at 344 K and 11.7 MPa**

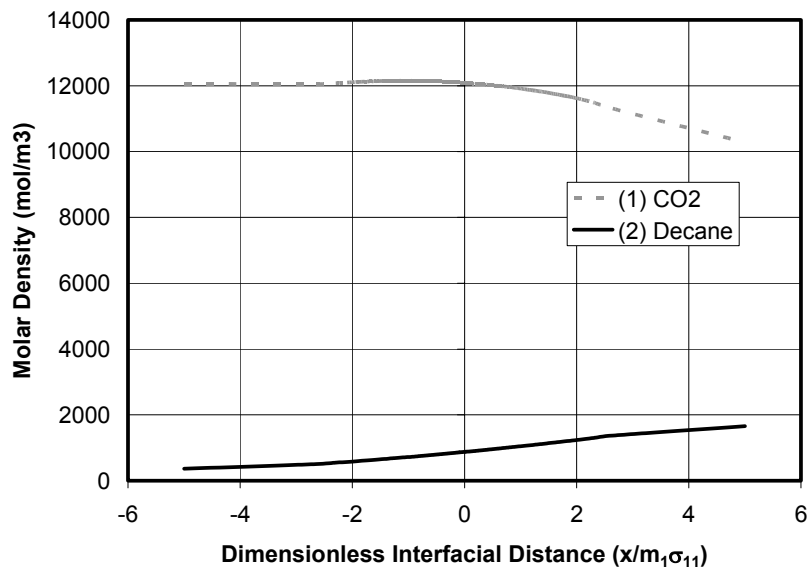


**Figure 7.12: Interfacial profile of CO<sub>2</sub>-Decane mixture at 344 K and 12.2 MPa**

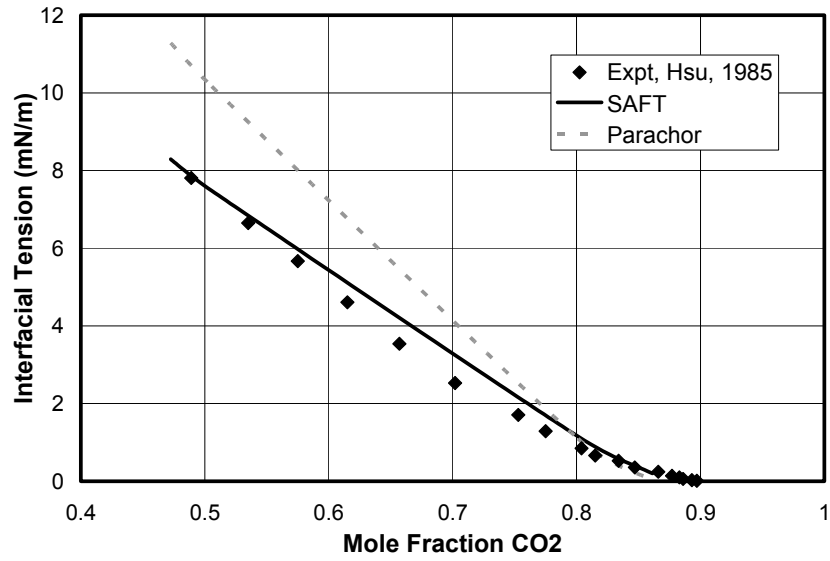


**Figure 7.13: Interfacial Tension of CO<sub>2</sub> – Decane mixture with equilibrium CO<sub>2</sub> composition**

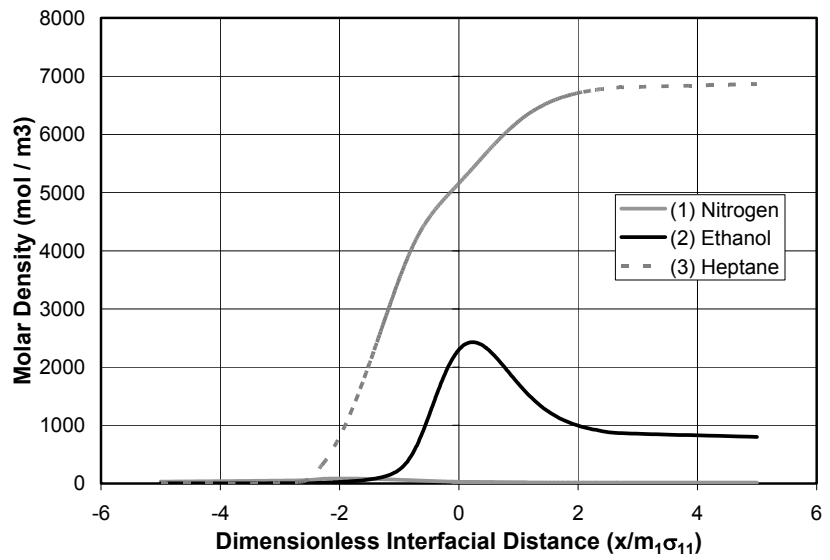


**Figure 7.14: Interfacial profile for 10.4 % ethanol - 90.3 % heptane mixture at 0.101 Mpa, 298.1 K**



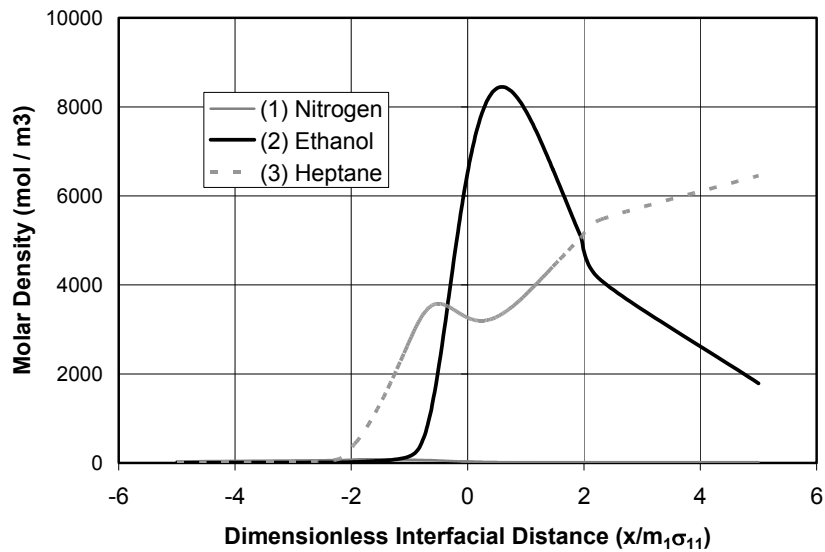


**Figure 7.15: Interfacial profile for 21.6 % ethanol – 78.1 % heptane mixture at 0.101 Mpa, 298.1 K**

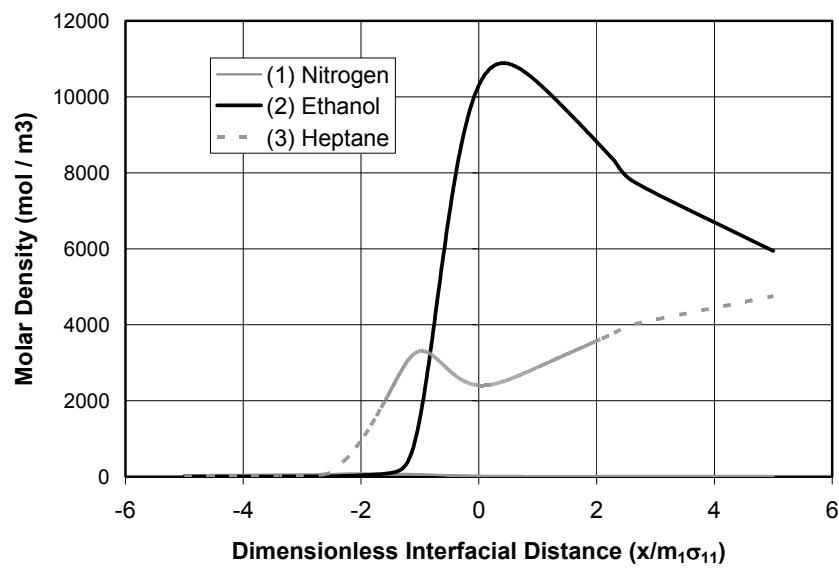


**Figure 7.16: Interfacial profile for 55.5 % ethanol – 44.3 % heptane mixture at 0.101 Mpa, 298.1 K**

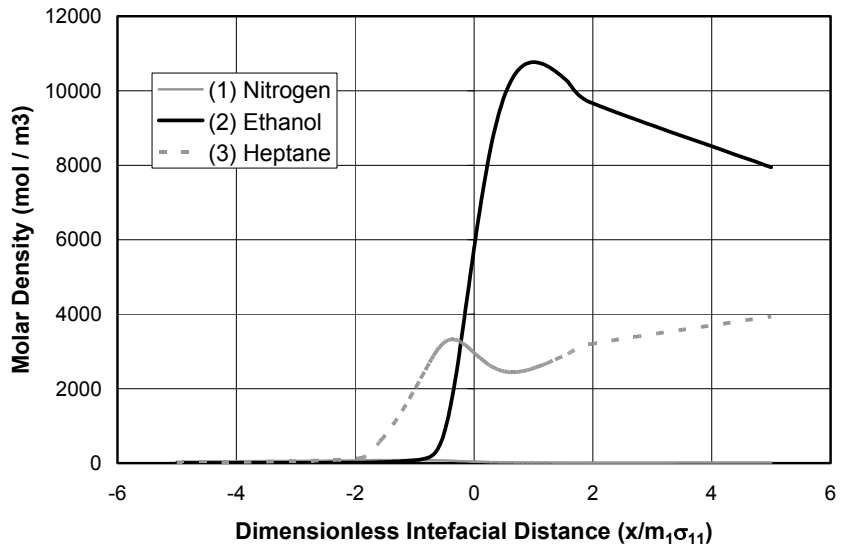


**Figure 7.17: Interfacial profile for 66.7 % ethanol – 33 % heptane mixture at 0.101 Mpa, 298.1 K**

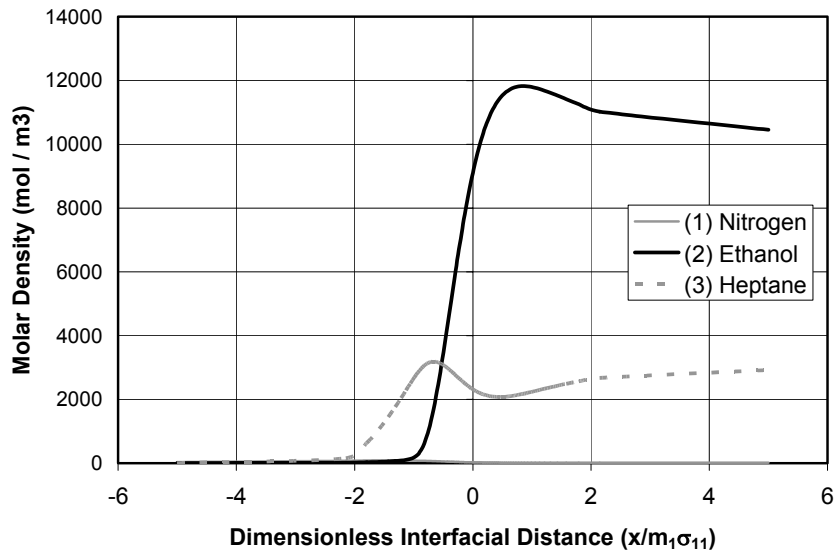


**Figure 7.18: Interfacial profile for 78 % ethanol – 21.8 % heptane mixture at 0.101 Mpa, 298.1 K**

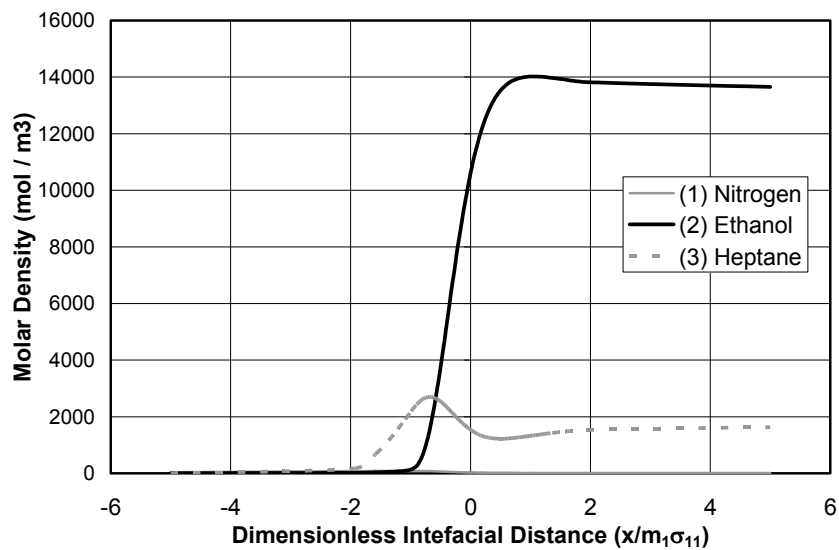


**Figure 7.19: Interfacial profile for 87.7 % ethanol – 7.47 % heptane mixture at 0.101 Mpa, 298.1 K**

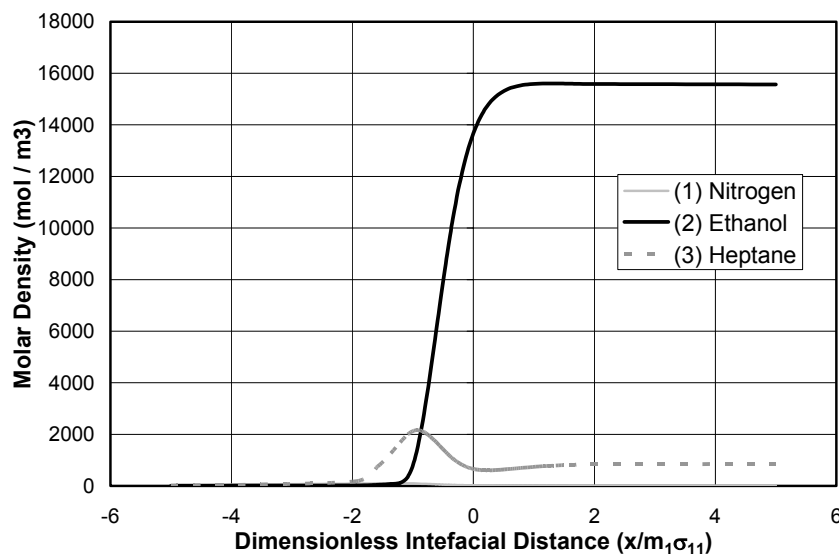


**Figure 7.20: Interfacial profile for 88.9 % ethanol – 7.7 % heptane mixture at 0.101 Mpa, 298.1 K**

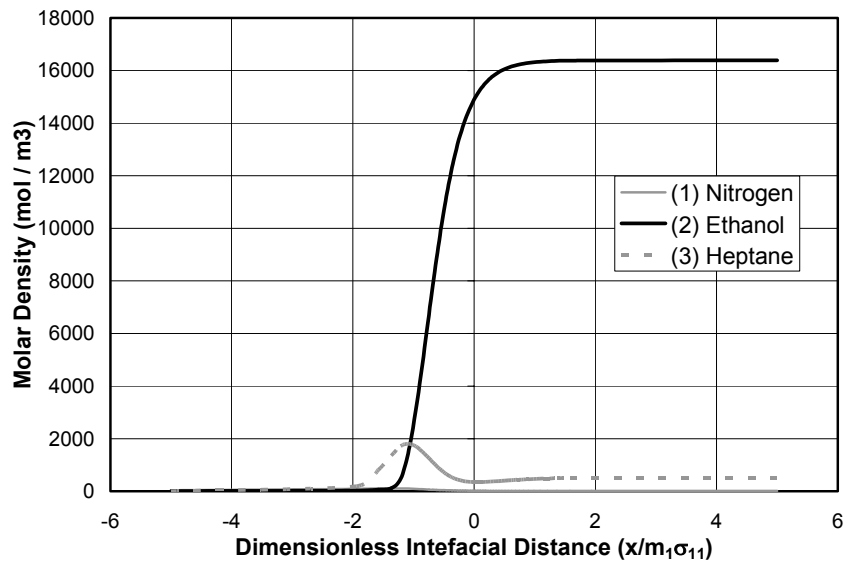


**Figure 7.21: Interfacial profile for 89.8 % ethanol – 7.8 % heptane mixture at 0.101 Mpa, 298.1 K**

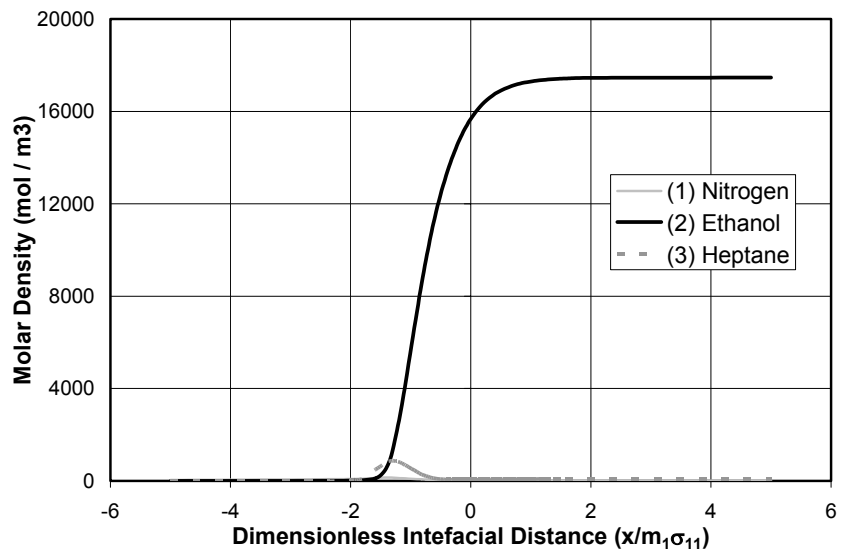


**Figure 7.22: Interfacial profile for 91.5 % ethanol – 8.5 % heptane mixture at 0.101 Mpa, 298.1 K**

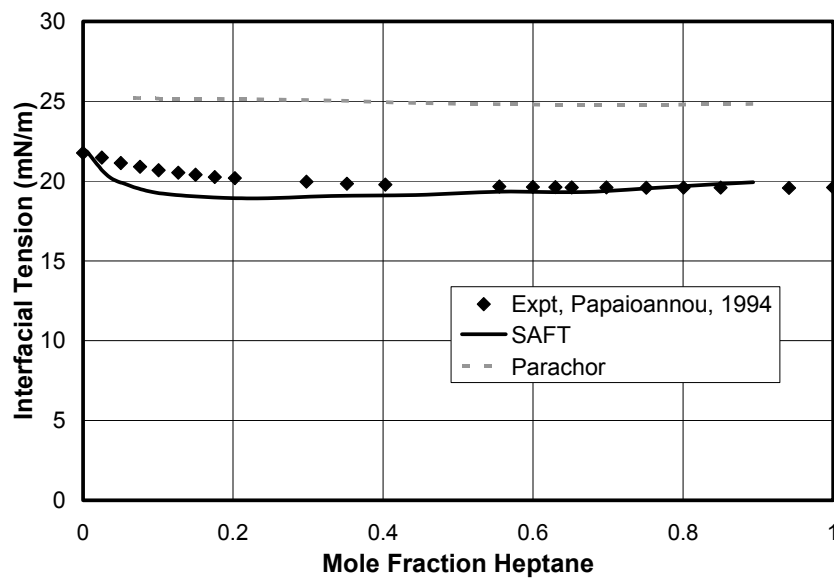


**Figure 7.23: Interfacial tension of ethanol-heptane mixture at 0.101 MPa and 298.15 K**

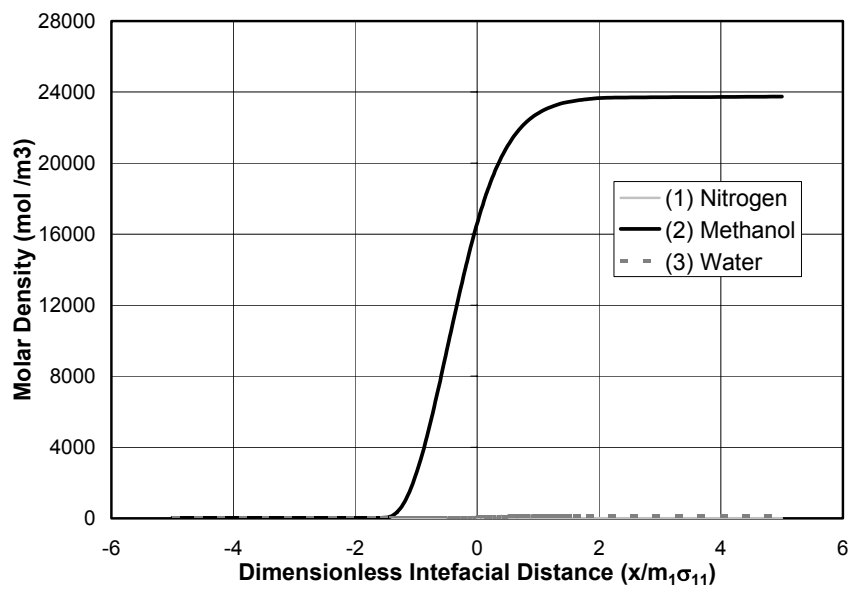


**Figure 7.24: Interfacial profile for 99.47 % methanol – 0.5 % water mixture at 0.101 Mpa, 263.15 K**

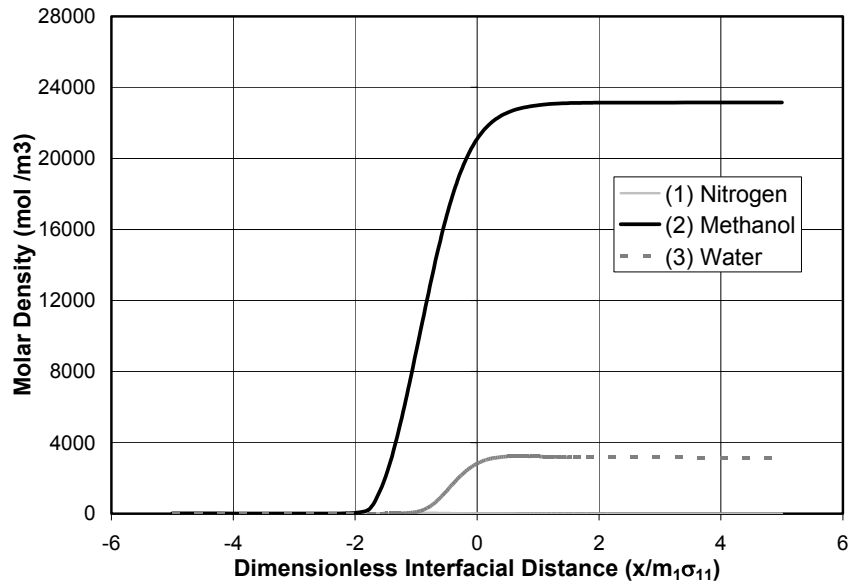


**Figure 7.25: Interfacial profile for 87.9 % methanol – 12 % water mixture at 0.101 Mpa, 263.15 K**

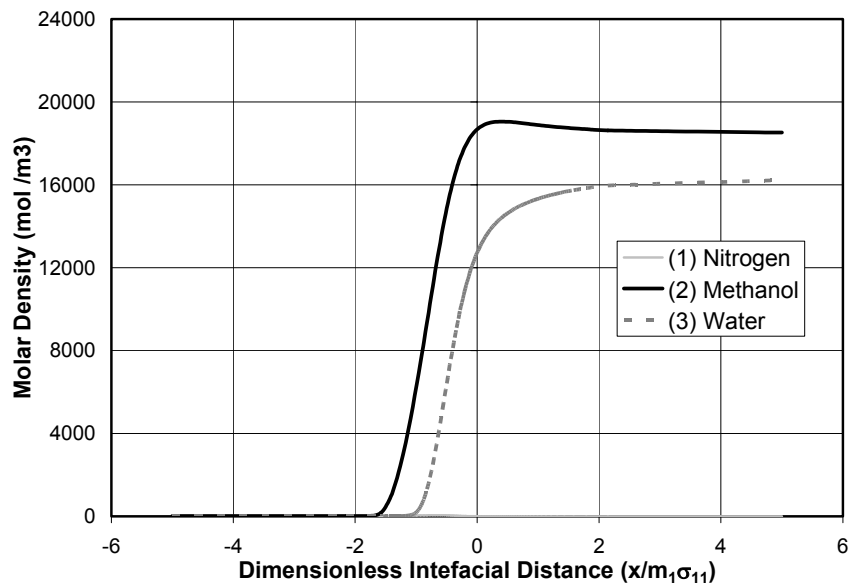


**Figure 7.26: Interfacial profile for 53.29 % methanol – 46.7 % water mixture at 0.101 Mpa, 263.15 K**

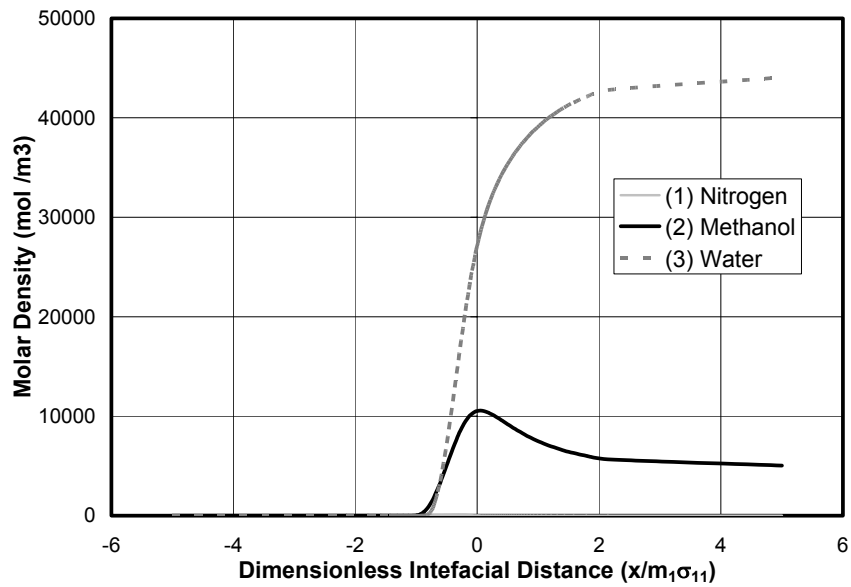


**Figure 7.27: Interfacial profile for 10.245 % methanol – 89.75 % water mixture at 0.101 Mpa, 263.15 K**

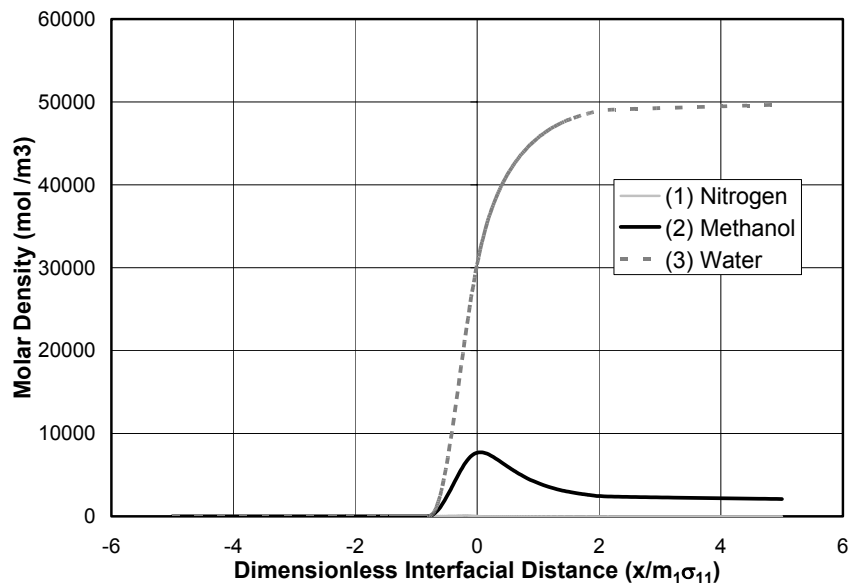


**Figure 7.28: Interfacial profile for 4 % methanol – 96 % water mixture at 0.101 Mpa, 263.15 K**

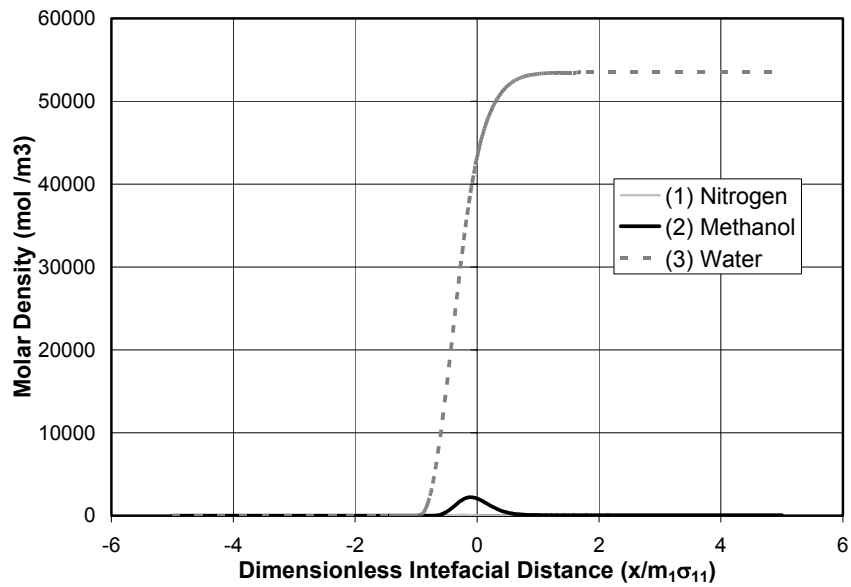


**Figure 7.29: Interfacial profile for 1 % methanol – 99 % water mixture at 0.101 Mpa, 263.15 K**

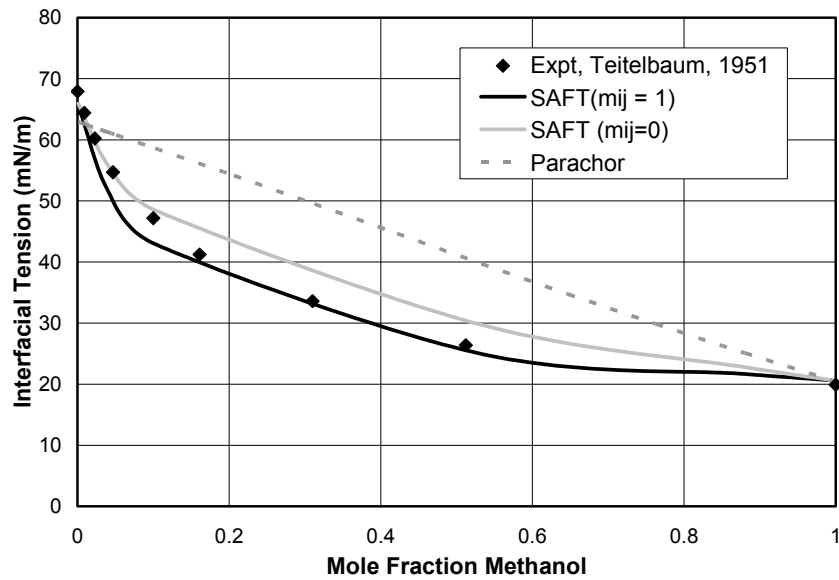


**Figure 7.30: Interfacial tension of methanol-water mixture at 0.101 MPa and 263.15 K**



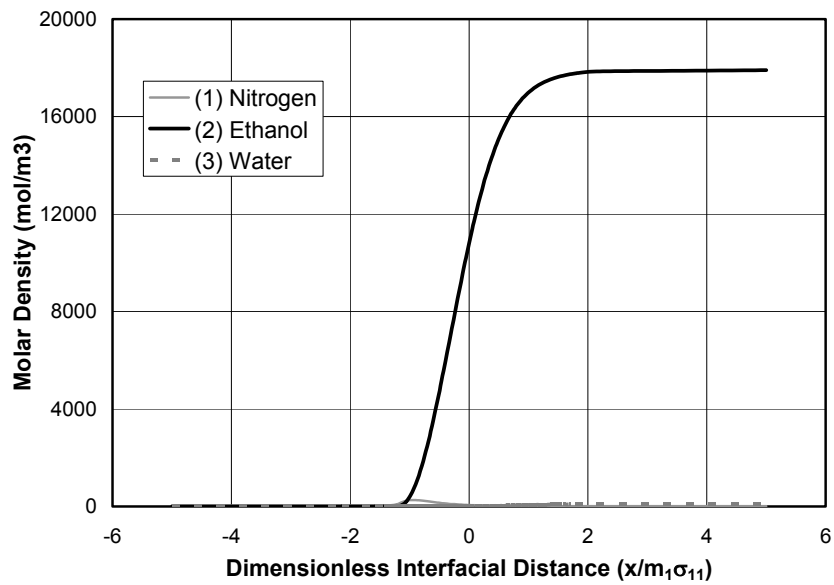


**Figure 7.31: Interfacial profile for 99.5 % ethanol – 0.5 % water mixture at 0.101 Mpa, 288.1 K**

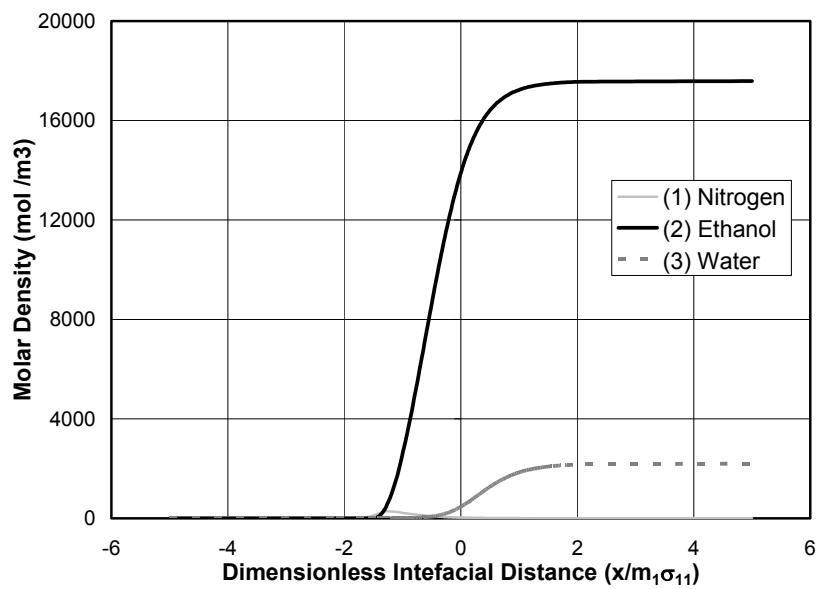


**Figure 7.32: Interfacial profile for 88.8 % ethanol – 11.2 % water mixture at 0.101 Mpa, 288.1 K**

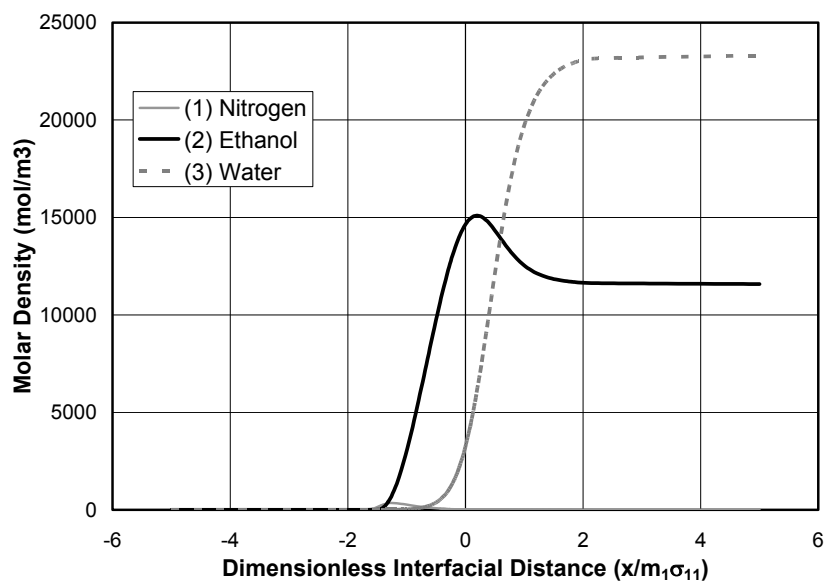


**Figure 7.33: Interfacial profile for 33.8 % ethanol – 66.2 % water mixture at 0.101 Mpa, 288.1 K**

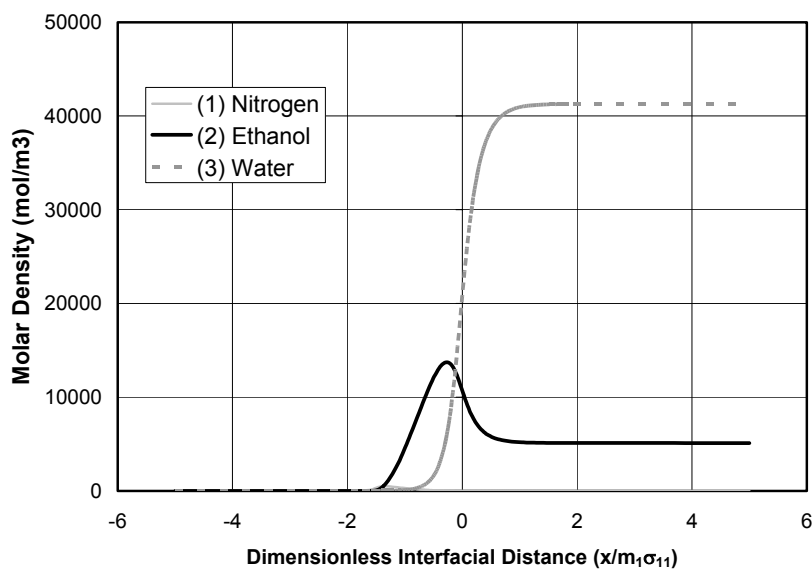


**Figure 7.34: Interfacial profile for 4 % ethanol – 96 % water mixture at 0.101 Mpa, 288.1 K**

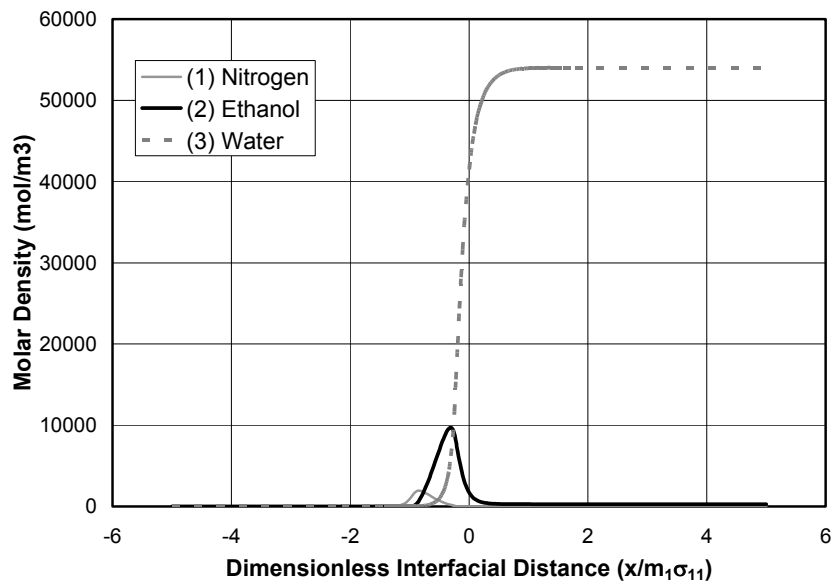


**Figure 7.35: Interfacial profile for 0.5 % ethanol – 99.5 % water mixture at 0.101 Mpa, 288.1 K**

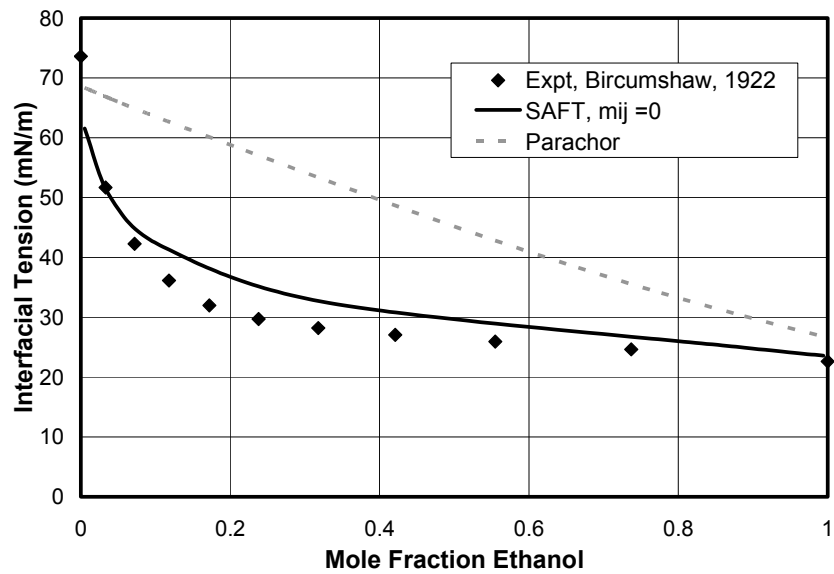


**Figure 7.36: Interfacial tension of ethanol-water mixture at 0.101 MPa and 288.1 K**

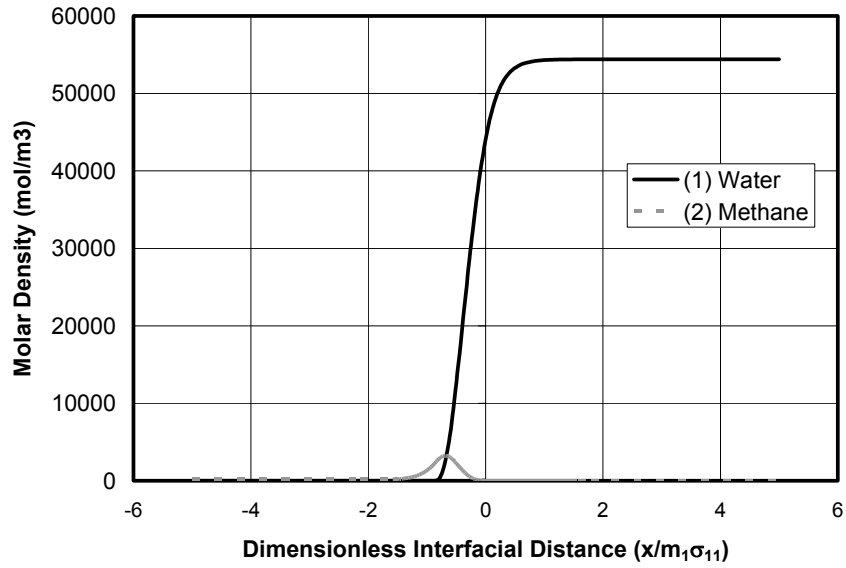


**Figure 7.37: Interfacial profile for methane-water mixture at 25 C and 63.38 psia**

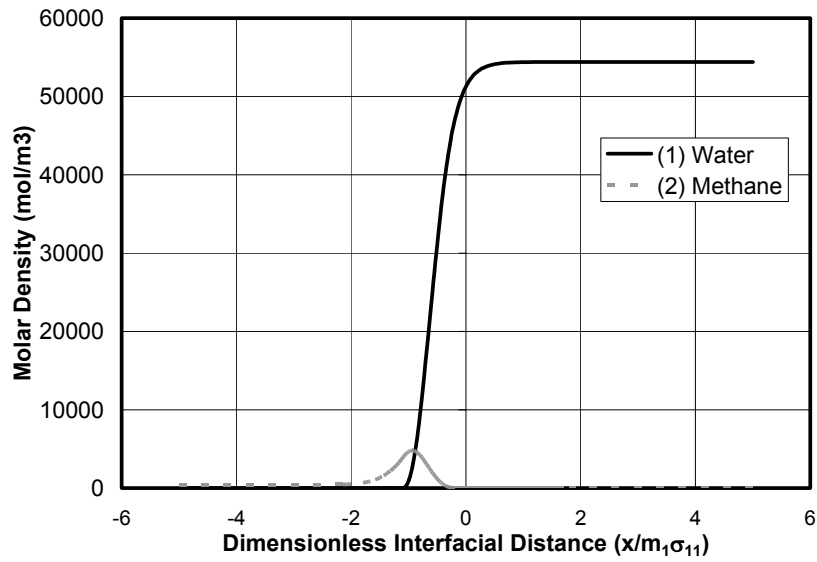


**Figure 7.38: Interfacial profile for methane-water mixture at 25 C and 145.03 psia**

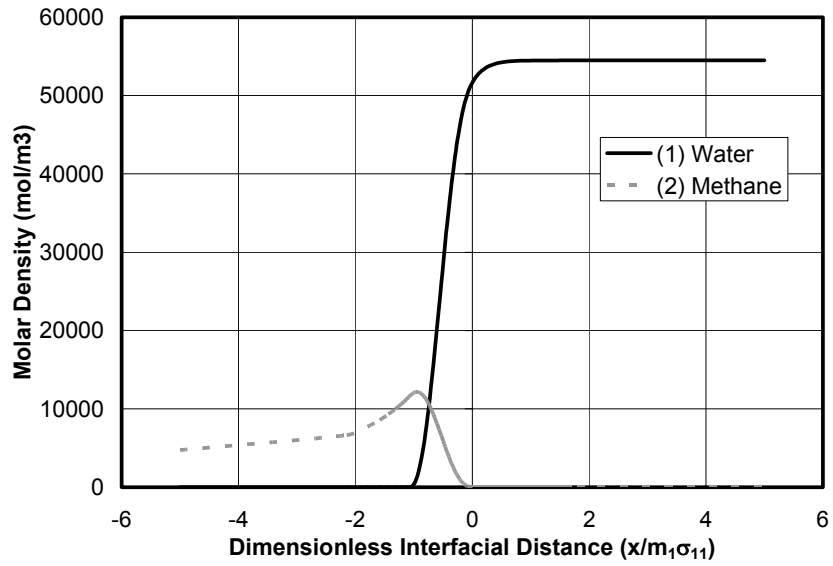


**Figure 7.39: Interfacial profile for methane-water mixture at 25 C and 1450.3 psia**

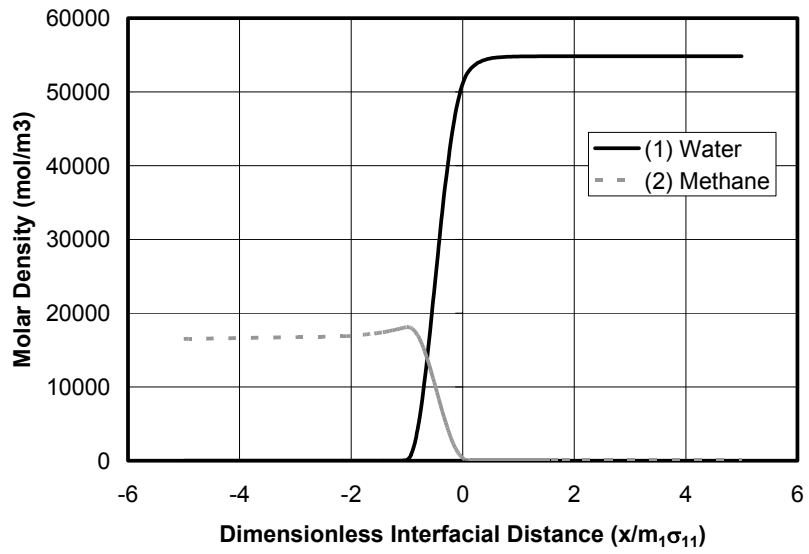


**Figure 7.40: Interfacial profile for methane-water mixture at 25 C and 6677.8 psia**

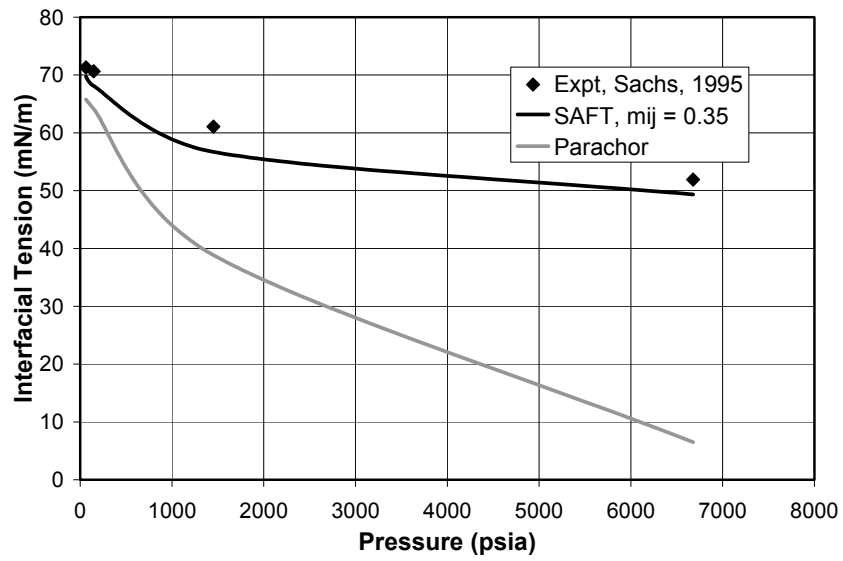


**Figure 7.41: Interfacial tension of Methane-Water mixture at 25 C**

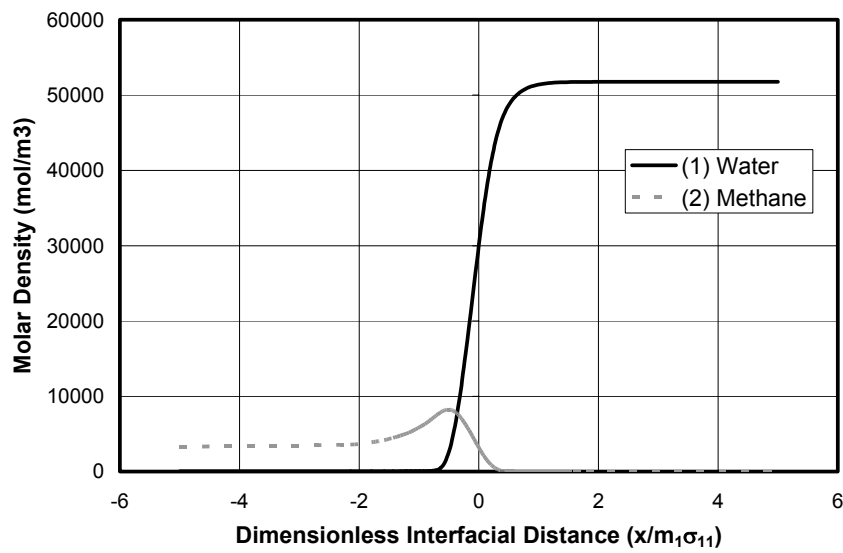


**Figure 7.42: Interfacial profile for methane-water mixture at 106 C and 10 MPa**

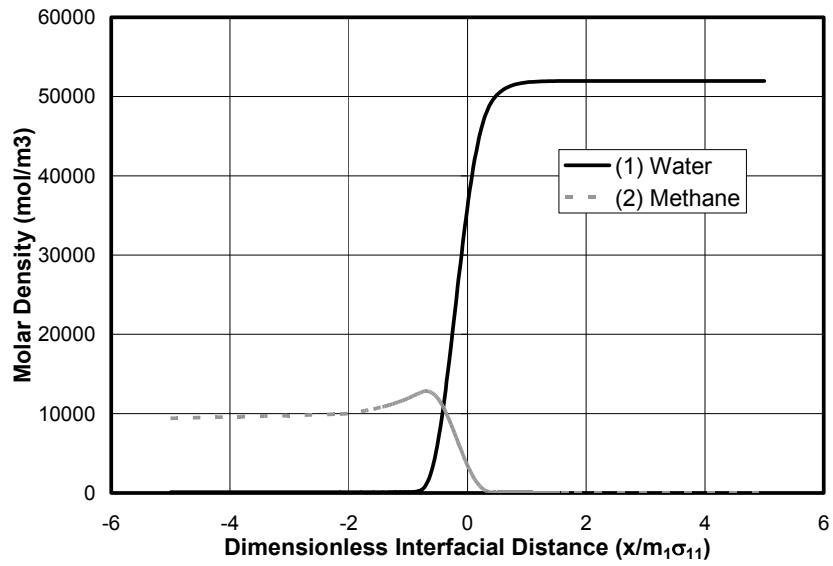


**Figure 7.43: Interfacial profile for methane-water mixture at 106 C and 30 MPa**

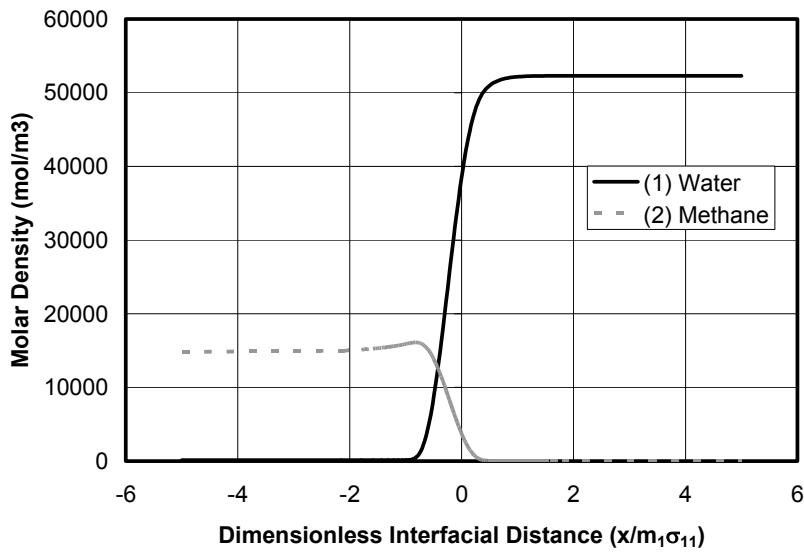


**Figure 7.44: Interfacial profile for methane-water mixture at 106 C and 60 MPa**

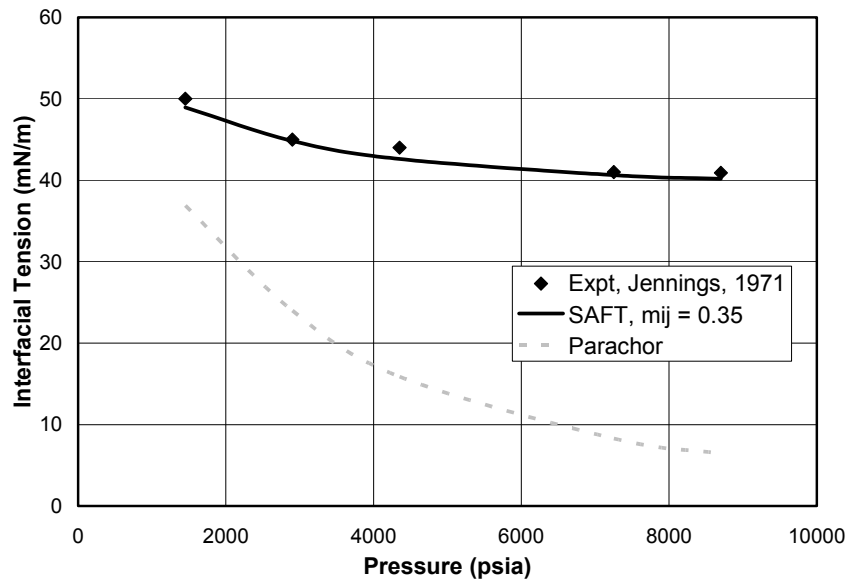


Figure 7.45: Interfacial tension of methane-water mixture at 106 C

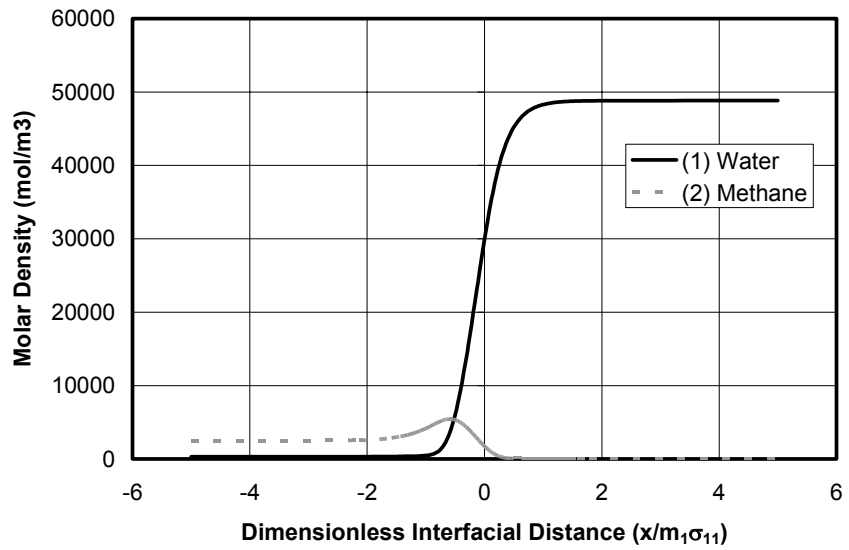
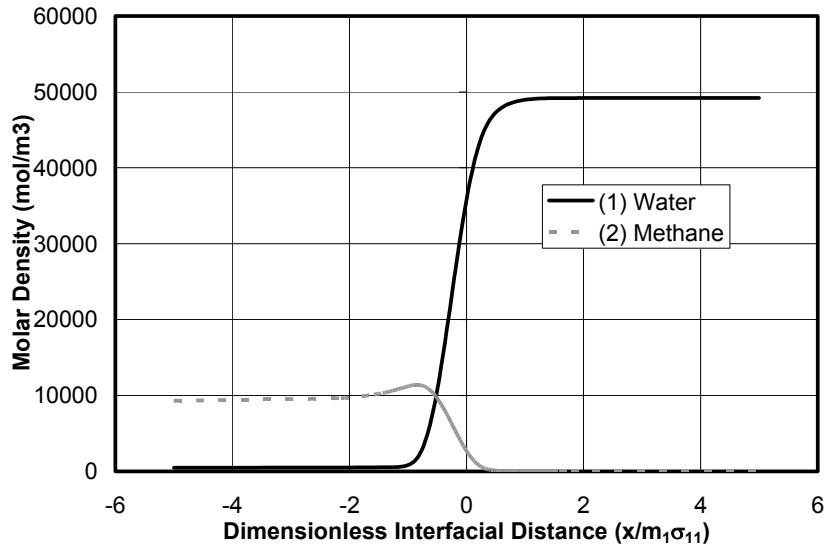
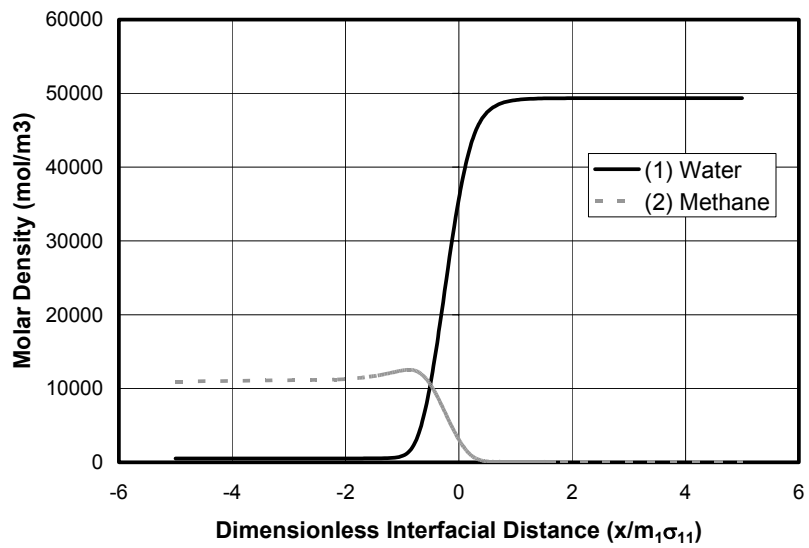


Figure 7.46: Interfacial profile for methane-water mixture at 176.7 C and 10 MPa





**Figure 7.47: Interfacial profile for methane-water mixture at 176.7 C and 40 Mpa**



**Figure 7.48: Interfacial profile for methane-water mixture at 176.7 C and 50 MPa**

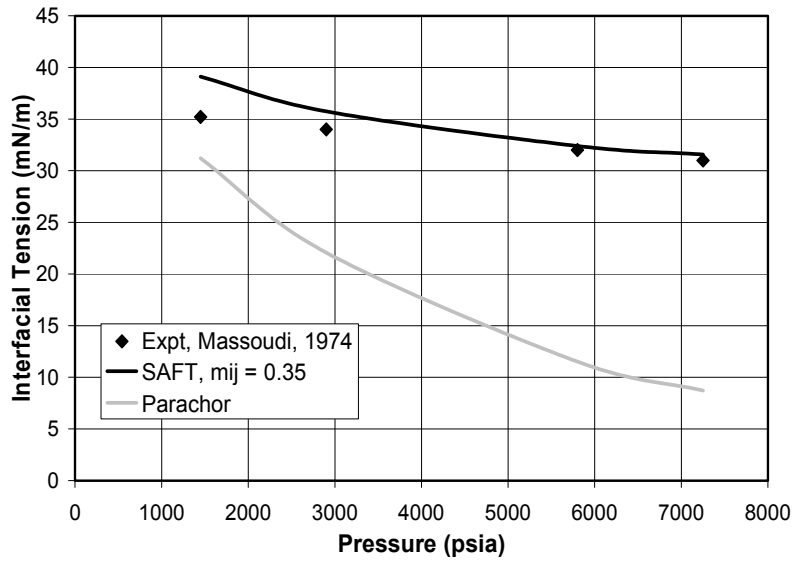


**Figure 7.49: Interfacial tension of methane-water mixture at 176.7 C**

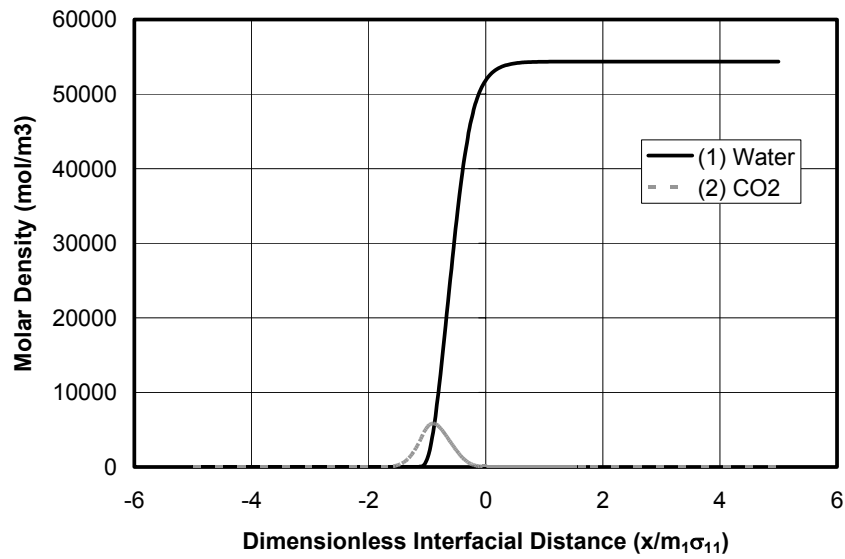


**Figure 7.50: Interfacial profile for water-CO<sub>2</sub> mixture at 25 C and 1 atm**

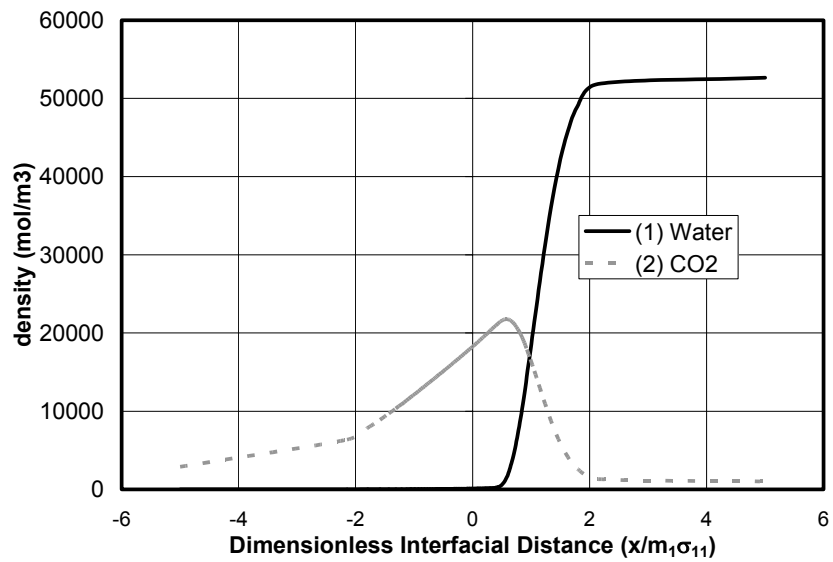


**Figure 7.51: Interfacial profile for water-CO<sub>2</sub> mixture at 25 C and 50 atm**

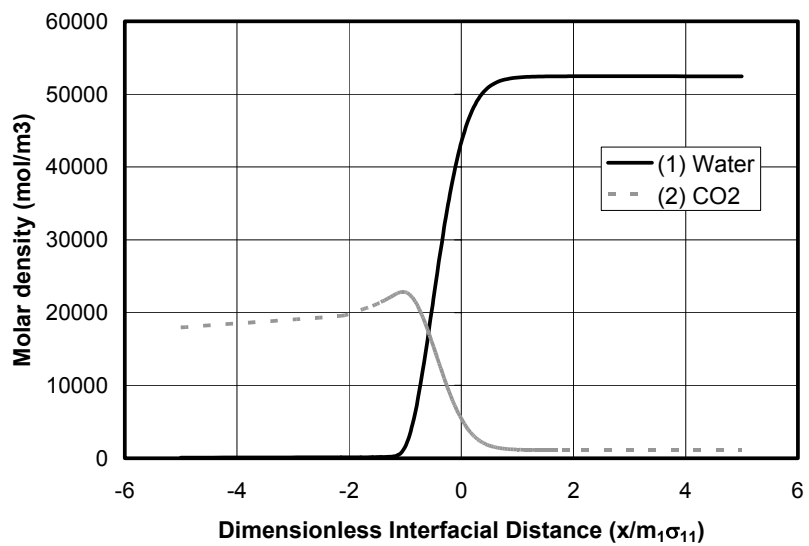


**Figure 7.52: Interfacial profile for water-CO<sub>2</sub> mixture at 25 C and 60 atm**

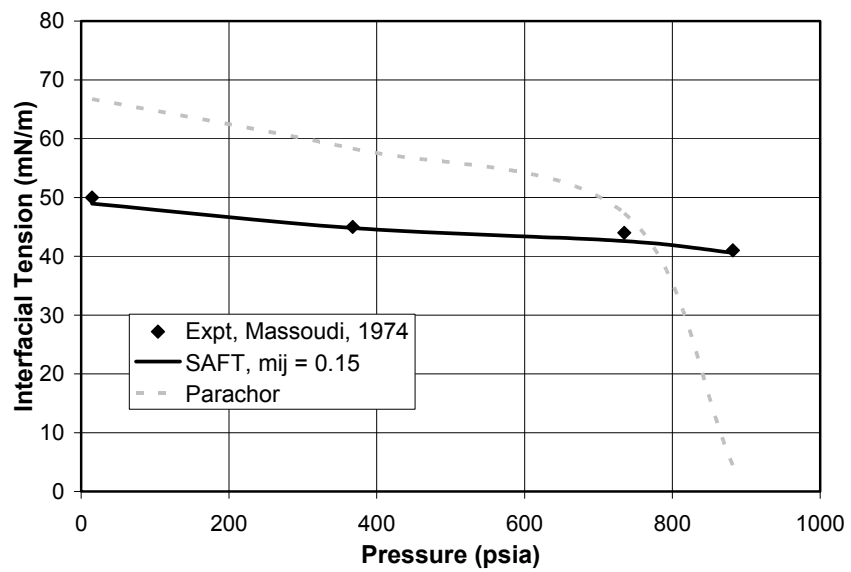


**Figure 7.53: Interfacial tension of water-CO<sub>2</sub> mixture at 25 C**

## CHAPTER 8

### SAFT BASED PHASE BEHAVIOR MODEL IN A RESERVOIR FLOW SIMULATOR

#### 8.1 INTRODUCTION

Reservoir flow simulators are very widely used in the petroleum industry and in the environmental engineering community to computationally study the flow behavior of oil, gas and water through porous media. Compositional models, which accurately describe the phase behavior of fluids, are very important when the fluid properties are dependent on the composition and on phase temperatures and pressure. Some examples of reservoir processes where compositional models play a key role are miscible flooding by enriched gas, carbon dioxide flooding and depletion of gas-condensate reservoirs.

There are several compositional simulators available in the literature. Chang et al.,[1] have developed a compositional reservoir simulator, UTCOMP, which is a three-dimensional, four-phase, equation of state based compositional simulator for miscible gas flooding. The equation of state used in this simulator is the Peng-Robinson equation which is very popular for hydrocarbon mixtures. As has been shown in the previous chapters, SAFT is based on theoretical considerations and does better predictions for methanol-water-hydrocarbon

mixtures. In this chapter we adapt the SAFT equation of state so that it can be used in a flow mode in a reservoir simulator instead of only being able to do batch flash calculations. In the next section we present the basic equations involved in a compositional reservoir simulator (UTCOMP) and the phase behavior properties that need to be evaluated from the equation of state so as to be applicable in a flow mode. In the following sections we outline how the SAFT model has been incorporated with the compositional flow simulator.

## **8.2 BASIC EQUATIONS**

The following assumptions have been made in developing the mathematical model for the reservoir simulator

- 1) Reservoir is isothermal
- 2) No-flow outer boundary conditions exist
- 3) There is no precipitation , chemical reaction or adsorption on the rock surfaces
- 4) Fluid flow is characterized by Darcy's law for multiphase flow
- 5) The porous media is slightly compressible

The model permits four phases to co-exist in the porous medium namely an aqueous phase, an oil phase, a gas phase and an additional nonaqueous liquid phase. The model assumes local thermodynamic equilibrium between

hydrocarbon phases, and negligible capillary pressure effects on hydrocarbon phase equilibrium. With these assumptions, the basic conservation equation for component i is given as

$$\frac{\partial W_i}{\partial t} + \vec{\nabla} \cdot \vec{F}_i - R_i = 0 \quad (8.1)$$

where  $W_i$ ,  $F_i$  and  $R_i$  are the accumulation, flux and source terms respectively. The accumulation term can be written in terms of the phase mole fraction, phase density and saturations as

$$W_i = \phi \sum_{j=1}^{n_p} \xi_j S_j x_{ij} \quad (8.2)$$

where  $\phi$  is the porosity,  $\xi_j$  is the molar density of phase j,  $S_j$  is defined as a fraction of the pore space occupied by phase j, and  $x_{ij}$  is the mole fraction of component i the phase j.

The second term in the conservation equation, flux  $F$ , consists of two terms, convective flux and dispersive flux, and can be written as

$$\vec{F}_i = \sum_{j=1}^{n_p} \xi_j x_{ij} \vec{u}_j - \phi \sum_{j=1}^{n_p} \xi_j S_j \vec{K}_{ij} x_{ij} \quad (8.3)$$

where  $\vec{u}_j$  represents the superficial fluid velocity of phase j and  $\vec{K}_{ij}$  is the dispersion tensor. The relationship between the pressure gradient across the porous media and the flux is governed by the multiphase Darcy's law.

$$\vec{u}_j = -\vec{k} \frac{k_{rj}}{\mu_j} (\nabla P_j - \gamma_j \nabla D) \quad (8.4)$$

where  $\vec{k}$  is the permeability tensor,  $k_{rj}$  is the relative permeability of phase j, (which is a function of saturation),  $\mu_j$  is the viscosity of phase j,  $\gamma_j$  is the specific gravity of phase j and D is the depth.

The source terms in Equation 8.1 above arise from the superposition of injection/production wells at several locations in the reservoir.

$$R_i = \frac{q_i}{V_b} \quad \text{for } i = 1, \dots, n_c, n_c + 1 \quad (8.5)$$

### 8.3 PRESSURE EQUATION

Apart from the mass conservation equation the other important equation in describing the flow in a reservoir is the pressure equation. The pressure equation is derived based on the assumption that the pore volume is completely filled by the fluid.



$$V_t(P, \vec{N}) = V_p(P) \quad (8.6)$$

The fluid volume is assumed to be a function of pressure and the total number of moles of each component whereas the pore volume is assumed to be a function of the pressure only. Differentiating both the volumes with respect to time and then applying the chain rule on the independent variables we obtain

$$\left( \frac{\partial V_t}{\partial P} \right)_{N_i} \left( \frac{\partial P}{\partial t} \right) + \sum_{i=1}^{n_c} \left( \frac{\partial V_t}{\partial N_i} \right)_{P, N_{k(k \neq i)}} \left( \frac{\partial N_i}{\partial t} \right) = \left( \frac{\partial V_p}{\partial P} \right) \left( \frac{\partial P}{\partial t} \right) \quad (8.7)$$

All the above equations are combined to form the basic equations in a reservoir simulator.

We observe in the above equation that we have to evaluate the volume derivatives with respect to the pressure and with respect to the component moles.

The partial derivative of the total fluid volume with respect to the component mole numbers is given by

$$\left( \frac{\partial V_t}{\partial N_i} \right)_{P, N_{r(r \neq i)}} = \frac{\partial}{\partial N_i} \left( \sum_{j=1}^{n_p} n_j v_j \right) \quad \text{for } i = 1, \dots, n_c \quad (8.8)$$

where  $v_j$  is the molar volume of phase  $j$ . which can be further written as

$$\left(\frac{\partial V_t}{\partial N_i}\right)_{P, N_r(r \neq i)} = \sum_{j=2}^{n_p} \sum_{k=1}^{n_c} \left[ v_j + n_j \frac{\partial v_j}{\partial n_{kj}} \right] \left(\frac{\partial n_{kj}}{\partial N_i}\right)_{P, N_r(r \neq i)} \quad \text{for } i = 1, \dots, n_c \quad (8.9)$$

The partial molar volume derivative can be analytically computed from the formula

$$\frac{\partial v_j}{\partial n_{kj}} = \frac{RT}{P} \left(\frac{\partial Z_j}{\partial n_{kj}}\right) \quad \text{for } j = 2, \dots, n_p \text{ and} \\ \text{for } k = 1, \dots, n_c \quad (8.10)$$

The remaining partial derivatives in Equation 8.9 above can be evaluated by solving the set of simultaneous equations [1].

$$\sum_{k=1}^{n_c} \left[ \left(\frac{\partial \ln f_{s2}}{\partial n_{k2}}\right) + \left(\frac{\partial \ln f_{s3}}{\partial n_{k3}}\right) \right] \left(\frac{\partial n_{k2}}{\partial N_i}\right) + \sum_{k=1}^{n_c} \left(\frac{\partial \ln f_{s3}}{\partial n_{k3}}\right) \left(\frac{\partial n_{k4}}{\partial N_i}\right) = \left(\frac{\partial \ln f_{s3}}{\partial n_{i3}}\right) \quad (8.10)$$

$$\sum_{k=1}^{n_c} \left(\frac{\partial \ln f_{s2}}{\partial n_{k2}}\right) \left(\frac{\partial n_{k2}}{\partial N_i}\right) + \sum_{k=1}^{n_c} \left(\frac{\partial \ln f_{s4}}{\partial n_{k4}}\right) \left(\frac{\partial n_{k4}}{\partial N_i}\right) = 0 \quad (8.11)$$

for  $s = 1, \dots, n_c$  and  $i = 1, \dots, n_c$

and

$$\frac{\partial n_{k3}}{\partial N_i} = \delta_{i,k} - \frac{\partial n_{k2}}{\partial N_i} - \frac{\partial n_{k4}}{\partial N_i} \quad (8.12)$$

The details of the above equations are given elsewhere (Chang et al., [1]). Similarly, for the evaluation of the total fluid volume derivative with respect to the pressure, we need to solve the following set of simultaneous equation

$$\sum_{k=1}^{n_c} \left[ \left( \frac{\partial \ln f_{s2}}{\partial n_{k2}} \right) + \left( \frac{\partial \ln f_{s3}}{\partial n_{k3}} \right) \right] \left( \frac{\partial n_{k2}}{\partial P} \right) + \sum_{k=1}^{n_c} \left( \frac{\partial \ln f_{s3}}{\partial n_{k3}} \right) \left( \frac{\partial n_{k4}}{\partial P} \right) = \left( \frac{\partial \ln f_{s3}}{\partial P} \right) - \left( \frac{\partial \ln f_{s2}}{\partial P} \right) \quad (8.13)$$

$$\sum_{k=1}^{n_c} \left( \frac{\partial \ln f_{s2}}{\partial n_{k2}} \right) \left( \frac{\partial n_{k2}}{\partial P} \right) + \sum_{k=1}^{n_c} \left( \frac{\partial \ln f_{s4}}{\partial n_{k4}} \right) \left( \frac{\partial n_{k4}}{\partial P} \right) = \left( \frac{\partial \ln f_{s4}}{\partial P} \right) - \left( \frac{\partial \ln f_{s2}}{\partial P} \right) \quad (8.14)$$

and

$$\frac{\partial n_{k3}}{\partial P} = - \frac{\partial n_{k2}}{\partial P} - \frac{\partial n_{k4}}{\partial P} \quad \text{for } k = 1, \dots, n_c \quad (8.15)$$

Now, that we have shown the significance of the volume and mole number derivatives of the fugacity coefficient and the compressibility factor in the flow equation, we present these derivatives for a SAFT equation of state.

## 8.4 CHEMICAL POTENTIAL AND COMPRESSIBILITY DERIVATIVES WITH SAFT EQUATION

### 8.4.1. Hard Sphere Terms

The hard-sphere chemical potential expressions are given in Chapter 3.

The chemical potential derivative with respect to the mole number is given as

$$\begin{aligned}
 \frac{\partial}{\partial N_k} \left( \frac{\mu_i^{\text{hs}}}{kT} \right) = & -\frac{1}{(1-\zeta_3)} \frac{\partial \zeta_3}{\partial N_k} + \frac{\Pi d_i^3}{6kT} \frac{\partial P_{\text{CS}}^{\text{hs}}}{\partial N_k} + \frac{3 d_i}{1-\zeta_3} \frac{\partial \zeta_2}{\partial N_k} + \frac{3 \zeta_2 d_i}{(1-\zeta_3)^2} \frac{\partial \zeta_3}{\partial N_k} \\
 & + \frac{3 \zeta_1 d_i^2}{(1-\zeta_3)^2} \frac{\partial \zeta_3}{\partial N_k} + \frac{9 \zeta_2 d_i^2}{(1-\zeta_3)^2} \frac{\partial \zeta_2}{\partial N_k} + \frac{9 \zeta_2^2 d_i^2}{(1-\zeta_3)^3} \frac{\partial \zeta_3}{\partial N_k} \\
 & + \left\{ \frac{6 \zeta_2 d_i^2}{\zeta_3^2} \frac{\partial \zeta_2}{\partial N_k} - \frac{6 \zeta_2^2 d_i^2}{\zeta_3^2} \frac{\partial \zeta_3}{\partial N_k} \right\} \left[ \ln(1-\zeta_3) + \frac{\zeta_3}{1-\zeta_3} + \frac{\zeta_3^2}{2(1-\zeta_3)^2} \right] \\
 & - 3 \left( \frac{\zeta_2 d_i}{\zeta_3} \right)^2 \left( \frac{\zeta_3^2}{(1-\zeta_3)^3} \right) \frac{\partial \zeta_3}{\partial N_k} \\
 & - \left\{ \frac{3 \zeta_2^2 d_i^3}{\zeta_3^2} \frac{\partial \zeta_2}{\partial N_k} - \frac{3 \zeta_2^3 d_i^3}{\zeta_3^2} \frac{\partial \zeta_3}{\partial N_k} \right\} \left[ 2 \ln(1-\zeta_3) + \frac{\zeta_3(2-\zeta_3)}{1-\zeta_3} \right] \\
 & - \left( \frac{\zeta_2 d_i}{\zeta_3} \right)^3 \left[ \frac{-2\zeta_3}{(1-\zeta_3)} + \frac{\zeta_3(2-\zeta_3)}{(1-\zeta_3)^2} \right] \left( \frac{\partial \zeta_3}{\partial N_k} \right)
 \end{aligned} \tag{8.16}$$

where

$$\frac{\partial P^{hs}}{\partial N_k} = \frac{6kT}{\Pi} \left[ \frac{1}{(1-\zeta_3)} \frac{\partial \zeta_0}{\partial N_k} + \frac{\zeta_0}{(1-\zeta_3)^2} \frac{\partial \zeta_3}{\partial N_k} + \frac{3\zeta_2}{(1-\zeta_3)^2} \frac{\partial \zeta_1}{\partial N_k} + \frac{3\zeta_1}{(1-\zeta_3)^2} \frac{\partial \zeta_2}{\partial N_k} \right. \\ \left. + \frac{6\zeta_1\zeta_2}{(1-\zeta_3)^3} \frac{\partial \zeta_3}{\partial N_k} + \frac{9\zeta_2^2}{(1-\zeta_3)^3} \frac{\partial \zeta_2}{\partial N_k} + \frac{9\zeta_2^3}{(1-\zeta_3)^4} \frac{\partial \zeta_3}{\partial N_k} \right. \\ \left. - \frac{3\zeta_3\zeta_2^2}{(1-\zeta_3)^3} \frac{\partial \zeta_2}{\partial N_k} - \frac{\zeta_2^3}{(1-\zeta_3)^3} \frac{\partial \zeta_3}{\partial N_k} - \frac{3\zeta_3\zeta_2^3}{(1-\zeta_3)^4} \frac{\partial \zeta_3}{\partial N_k} \right] \quad (8.17)$$

The derivatives of the reduced molar density  $\zeta_i$  with respect to the mole numbers is given as

$$\frac{\partial \zeta_i}{\partial N_k} = \frac{1}{V} \frac{\Pi}{6} m_k d_{kk}^i \quad (8.18)$$

$k = 1, \dots, n_c$

and  $i = 0, 1, 2, 3$

The compressibility factor derivative with the mole numbers is

$$\frac{\partial Z^{hs}}{\partial N_k} = \frac{1}{\rho kT} \frac{\partial P^{hs}}{\partial N_k} - \frac{P^{hs}}{\rho^2 kT} \left( \frac{1}{V} \right) - \left( \frac{m_i - m}{\rho} \right) \left( \frac{1}{V} \right) \quad (8.19)$$

In a similar fashion, the volume derivatives of the hard-sphere term are determined as

$$\begin{aligned}
\frac{\partial}{\partial V} \left( \frac{\mu_i^{\text{hs}}}{kT} \right) &= -\frac{1}{(1-\zeta_3)} \frac{\partial \zeta_3}{\partial V} + \frac{\Pi d_i^3}{6kT} \frac{\partial P_{\text{CS}}^{\text{hs}}}{\partial V} + \frac{3 d_i}{1-\zeta_3} \frac{\partial \zeta_2}{\partial V} + \frac{3 \zeta_2 d_i}{(1-\zeta_3)^2} \frac{\partial \zeta_3}{\partial V} \\
&+ \frac{3 \zeta_1 d_i^2}{(1-\zeta_3)^2} \frac{\partial \zeta_3}{\partial V} + \frac{9 \zeta_2 d_i^2}{(1-\zeta_3)^2} \frac{\partial \zeta_2}{\partial V} + \frac{9 \zeta_2^2 d_i^2}{(1-\zeta_3)^3} \frac{\partial \zeta_3}{\partial V} \\
&+ \left\{ \frac{6 \zeta_2 d_i^2}{\zeta_3^2} \frac{\partial \zeta_2}{\partial V} - \frac{6 \zeta_2^2 d_i^2}{\zeta_3^2} \frac{\partial \zeta_3}{\partial V} \right\} \left[ \ln(1-\zeta_3) + \frac{\zeta_3}{1-\zeta_3} + \frac{\zeta_3^2}{2(1-\zeta_3)^2} \right] \\
&- 3 \left( \frac{\zeta_2 d_i}{\zeta_3} \right)^2 \left( \frac{\zeta_3^2}{(1-\zeta_3)^3} \right) \frac{\partial \zeta_3}{\partial V} \\
&- \left\{ \frac{3 \zeta_2^2 d_i^3}{\zeta_3^2} \frac{\partial \zeta_2}{\partial V} - \frac{3 \zeta_2^3 d_i^3}{\zeta_3^2} \frac{\partial \zeta_3}{\partial V} \right\} \left[ 2 \ln(1-\zeta_3) + \frac{\zeta_3(2-\zeta_3)}{1-\zeta_3} \right] \\
&- \left( \frac{\zeta_2 d_i}{\zeta_3} \right)^3 \left[ \frac{-2\zeta_3}{(1-\zeta_3)} + \frac{\zeta_3(2-\zeta_3)}{(1-\zeta_3)^2} \right] \left( \frac{\partial \zeta_3}{\partial V} \right)
\end{aligned} \tag{8.20}$$

Along the same lines as shown above the other derivatives can also be written as

$$\begin{aligned}
\frac{\partial P^{\text{hs}}}{\partial V} &= \frac{6 kT}{\Pi} \left[ \frac{1}{(1-\zeta_3)} \frac{\partial \zeta_0}{\partial V} + \frac{\zeta_0}{(1-\zeta_3)^2} \frac{\partial \zeta_3}{\partial V} + \frac{3 \zeta_2}{(1-\zeta_3)^2} \frac{\partial \zeta_1}{\partial V} + \frac{3 \zeta_1}{(1-\zeta_3)^2} \frac{\partial \zeta_2}{\partial V} \right. \\
&+ \frac{6 \zeta_1 \zeta_2}{(1-\zeta_3)^3} \frac{\partial \zeta_3}{\partial V} + \frac{9 \zeta_2^2}{(1-\zeta_3)^3} \frac{\partial \zeta_2}{\partial V} + \frac{9 \zeta_2^3}{(1-\zeta_3)^4} \frac{\partial \zeta_3}{\partial V} \\
&\left. - \frac{3 \zeta_3 \zeta_2^2}{(1-\zeta_3)^3} \frac{\partial \zeta_2}{\partial V} - \frac{\zeta_2^3}{(1-\zeta_3)^3} \frac{\partial \zeta_3}{\partial V} - \frac{3 \zeta_3 \zeta_2^3}{(1-\zeta_3)^4} \frac{\partial \zeta_3}{\partial V} \right]
\end{aligned} \tag{8.21}$$

The  $\zeta_k$  derivatives with the volume are given as

$$\frac{\partial \zeta_i}{\partial V} = -\frac{1}{V} \sum_{k=1}^{N_c} \frac{\Pi}{6} m_k d_{kk}^i \rho \quad (8.22)$$

The hard sphere compressibility factor derivative with the volume is given as

$$\frac{\partial Z^{hs}}{\partial V} = \frac{1}{\rho kT} \frac{\partial P^{hs}}{\partial V} + \frac{P^{hs}}{\rho kT} \left( \frac{1}{V} \right) \quad (8.23)$$

#### 8.4.2. Mixture of Chains Term

The chemical potential derivatives arising from the chain terms is given by

$$\begin{aligned} \frac{\partial}{\partial N_k} \left( \frac{\mu_i^{chain}}{RT} \right) &= (1 - m_i) \left( \frac{1}{V} \right) \frac{1}{g_{ii}} \frac{\partial g_{ii}}{\partial \rho_i} + (1 - m_k) \left( \frac{1}{V} \right) \frac{1}{g_{kk}} \frac{\partial g_{kk}}{\partial \rho_k} \\ &+ \sum_j \left( \frac{1}{V} \right) x_j \rho (1 - m_j) \left\{ \frac{1}{g_{kk}} \frac{\partial^2 g_{jj}}{\partial \rho_k \partial \rho_i} - \frac{1}{g_{kk}^2} \frac{\partial g_{jj}}{\partial \rho_k} \frac{\partial g_{jj}}{\partial \rho_i} \right\} \end{aligned} \quad (8.24)$$

where  $g_{ij}$  is the short hand notation for  $g_{ij} (d_i, d_j)^{hs}$  defined in Chapter 3 The compressibility factor derivative is thus given as

$$\frac{\partial Z^{chain}}{\partial N_k} = -\frac{(1 - m_i)}{\rho g_{ii}} \frac{\partial g_{ii}}{\partial V} + \sum_i x_i (1 - m_i) \rho \left[ \begin{aligned} &\frac{-1}{\rho g_{ii}} \frac{\partial}{\partial \rho_k} \left( \frac{\partial g_{ii}}{\partial V} \right) + \frac{1}{\rho^2 g_{ii}} \left( \frac{\partial g_{ii}}{\partial V} \right) \\ &+ \frac{1}{\rho (g_{ii})^2} \left( \frac{\partial g_{ii}}{\partial \rho_k} \right) \left( \frac{\partial g_{ii}}{\partial V} \right) \end{aligned} \right] \quad (8.25)$$

Now we present the volume derivatives of the chemical potential and the compressibility factor

$$\frac{\partial}{\partial V} \left( \frac{\mu_i^{\text{chain}}}{RT} \right) = (1 - m_i) \frac{1}{g_{ij}} \frac{\partial g_{ij}}{\partial V} + \sum_j x_j \rho (1 - m_j) \left\{ \begin{array}{l} -\frac{1}{g_{ij}} \frac{\partial g_{ij}}{\partial \rho_i} + \\ \frac{1}{g_{ij}} \frac{\partial^2 g_{ij}}{\partial V \partial \rho_i} - \frac{1}{g_{ij}^2} \frac{\partial g_{ij}}{\partial V} \frac{\partial g_{ij}}{\partial \rho_i} \end{array} \right\} \quad (8.26)$$

The compressibility factor derivative with volume is

$$\frac{\partial Z^{\text{chain}}}{\partial V} = \sum_j x_j (1 - m_j) \left[ -\frac{1}{g_{ij}} \left( \frac{\partial g_{ij}}{\partial V} \right) - \frac{1}{g_{ij}} \frac{\partial}{\partial V} \left( \frac{\partial g_{ij}}{\partial V} \right) + \frac{1}{(g_{ij})^2} \left( \frac{\partial g_{ij}}{\partial V} \right) \left( \frac{\partial g_{ij}}{\partial V} \right) \right] \quad (8.27)$$

The mole number and the volume derivatives of the radial distribution function are given as

$$\begin{aligned} \frac{\partial g_{ij}}{\partial V} &= \frac{1}{(1 - \zeta_3)^2} \frac{\partial \zeta_3}{\partial V} + \frac{3d_i d_j}{d_i + d_j} \frac{1}{(1 - \zeta_3)^2} \frac{\partial \zeta_2}{\partial V} + \frac{6d_i d_j}{d_i + d_j} \frac{\zeta_2}{(1 - \zeta_3)^3} \frac{\partial \zeta_3}{\partial V} \\ &+ 4 \left[ \frac{d_i d_j}{d_i + d_j} \right]^2 \frac{\zeta_2}{(1 - \zeta_3)^3} \frac{\partial \zeta_2}{\partial V} + 6 \left[ \frac{d_i d_j}{d_i + d_j} \right]^2 \frac{\zeta_2^2}{(1 - \zeta_3)^4} \frac{\partial \zeta_3}{\partial V} \end{aligned} \quad (8.28)$$

Similarly



$$\begin{aligned}
\frac{\partial}{\partial V} \left( \frac{\partial \mathbf{g}_{ij}}{\partial V} \right) = & -\frac{1}{V} \frac{\partial \mathbf{g}_{ij}}{\partial V} - \left[ \frac{1}{(1-\zeta_3)^2} \frac{\partial \zeta_3}{\partial V} + \frac{2\zeta_3}{(1-\zeta_3)^3} \frac{\partial \zeta_3}{\partial V} + \frac{3d_i d_j}{d_i + d_j} \frac{1}{(1-\zeta_3)^2} \frac{\partial \zeta_2}{\partial V} \right. \\
& + \frac{12d_i d_j}{d_i + d_j} \frac{\zeta_2}{(1-\zeta_3)^3} \frac{\partial \zeta_3}{\partial V} + \frac{6d_i d_j}{d_i + d_j} \frac{\zeta_3}{(1-\zeta_3)^3} \frac{\partial \zeta_2}{\partial V} + \frac{18d_i d_j}{d_i + d_j} \frac{\zeta_2 \zeta_3}{(1-\zeta_3)^4} \frac{\partial \zeta_3}{\partial V} \\
& + 8 \left[ \frac{d_i d_j}{d_i + d_j} \right]^2 \frac{\zeta_2}{(1-\zeta_3)^3} \frac{\partial \zeta_2}{\partial V} + 18 \left[ \frac{d_i d_j}{d_i + d_j} \right]^2 \frac{\zeta_2^2}{(1-\zeta_3)^4} \frac{\partial \zeta_3}{\partial V} \\
& \left. + 12 \left[ \frac{d_i d_j}{d_i + d_j} \right]^2 \frac{\zeta_2 \zeta_3}{(1-\zeta_3)^4} \frac{\partial \zeta_2}{\partial V} + 24 \left[ \frac{d_i d_j}{d_i + d_j} \right]^2 \frac{\zeta_2^2 \zeta_3}{(1-\zeta_3)^5} \frac{\partial \zeta_2}{\partial V} \right]
\end{aligned}
\tag{8.29}$$

and

$$\begin{aligned}
& \frac{\partial}{\partial N_1} \frac{\partial \mathbf{g}_{jk}}{\partial \rho_i} \\
= & \frac{\Pi m_i}{6} \left[ \frac{2d_i^3}{(1-\zeta_3)^3} \frac{\partial \zeta_3}{\partial N_1} + \left( \frac{d_j d_k}{d_j + d_k} \right) \frac{6d_i^2}{(1-\zeta_3)^3} \frac{\partial \zeta_3}{\partial N_1} + \left( \frac{d_j d_k}{d_j + d_k} \right) \frac{6d_i^3}{(1-\zeta_3)^3} \frac{\partial \zeta_2}{\partial N_1} \right. \\
& + \left( \frac{d_j d_k}{d_j + d_k} \right) \frac{18d_i^3 \zeta_2}{(1-\zeta_3)^4} \frac{\partial \zeta_3}{\partial N_1} + \left( \frac{d_j d_k}{d_j + d_k} \right)^2 \frac{d_i^2}{(1-\zeta_3)^3} \frac{\partial \zeta_2}{\partial N_1} + \left( \frac{d_j d_k}{d_j + d_k} \right)^2 \frac{3d_i^2 \zeta_2}{(1-\zeta_3)^4} \frac{\partial \zeta_3}{\partial N_1} \\
& \left. + \left( \frac{d_j d_k}{d_j + d_k} \right)^2 \frac{3d_i^3 \zeta_2}{(1-\zeta_3)^4} \frac{\partial \zeta_2}{\partial N_1} + \left( \frac{d_j d_k}{d_j + d_k} \right)^2 \frac{6d_i^3 \zeta_2^2}{(1-\zeta_3)^5} \frac{\partial \zeta_3}{\partial N_1} \right]
\end{aligned}
\tag{8.30}$$

The term  $\frac{\partial}{\partial V} \frac{\partial \mathbf{g}_{jk}}{\partial \rho_i}$  is similar to the term shown, only the reduced densities are derived with respect to the volume  $V$  instead of the mole numbers  $N_i$

### 8.4.3 Mixture of Associating Spheres Term

$$\begin{aligned} \frac{\partial}{\partial N_k} \left( \frac{\mu_i^{\text{assoc}}}{RT} \right) &= \sum_{A_i} \left[ \frac{1}{Y^{A_i}} - \frac{1}{2} \right] \frac{\partial Y^{A_j}}{\partial \rho_k} \frac{1}{V} + \sum_{A_k} \left[ \frac{1}{Y^{A_k}} - \frac{1}{2} \right] \frac{\partial Y^{A_k}}{\partial \rho_i} \frac{1}{V} \\ &\quad + \frac{1}{V} \sum_j \rho_j \left[ \sum_{A_j} \frac{\partial}{\partial \rho_k} \left( \frac{\partial Y^{A_j}}{\partial \rho_i} \right) \left[ \frac{1}{Y^{A_j}} - \frac{1}{2} \right] + \sum_{A_j} \left( \frac{\partial Y^{A_j}}{\partial \rho_i} \right) \left( \frac{\partial Y^{A_j}}{\partial \rho_k} \right) \frac{-1}{(Y^{A_j})^2} \right] \end{aligned} \quad (8.31)$$

Now we have to evaluate the second derivative of  $Y^A_i$  with mole numbers

$$\begin{aligned} &\frac{\partial}{\partial \rho_i} \left( \frac{\partial Y^{A_j}}{\partial \rho_i} \right) \\ &= -2(Y^{A_j}) \left( \frac{\partial Y^{A_j}}{\partial \rho_i} \right) \left[ \sum_{B_i} Y^{B_i} \Delta^{A_j B_i} + \sum_k \sum_{B_k} \rho_k \left[ \Delta^{A_j B_k} \left( \frac{\partial Y^{B_k}}{\partial \rho_i} \right) + Y^{B_k} \left( \frac{\partial \Delta^{A_j B_k}}{\partial \rho_i} \right) \right] \right] \\ &\quad - (Y^{A_j})^2 \left[ \sum_{B_k} \left[ \Delta^{A_j B_k} \left( \frac{\partial Y^{B_k}}{\partial \rho_i} \right) + Y^{B_k} \left( \frac{\partial \Delta^{A_j B_k}}{\partial \rho_i} \right) \right] + \sum_{B_i} \left[ \Delta^{A_j B_i} \left( \frac{\partial Y^{B_i}}{\partial \rho_i} \right) + Y^{B_i} \left( \frac{\partial \Delta^{A_j B_i}}{\partial \rho_i} \right) \right] \right] \\ &\quad + \sum_k \sum_{B_k} \rho_k \left[ \left( \frac{\partial \Delta^{A_j B_k}}{\partial \rho_i} \right) \left( \frac{\partial Y^{B_k}}{\partial \rho_i} \right) + \Delta^{A_j B_k} \frac{\partial}{\partial \rho_i} \left( \frac{\partial Y^{B_k}}{\partial \rho_i} \right) + \left( \frac{\partial \Delta^{A_j B_k}}{\partial \rho_i} \right) \left( \frac{\partial Y^{B_k}}{\partial \rho_i} \right) \right] \\ &\quad + Y^{B_k} \frac{\partial}{\partial V} \left( \frac{\partial \Delta^{A_j B_k}}{\partial \rho_i} \right) \end{aligned} \quad (8.32)$$

Note that the above expression is a set of non-linear equations which need to be solved simultaneously. The compressibility factor derivative with respect to the mole numbers is

$$\frac{\partial Z^{\text{assoc}}}{\partial N_k} = \sum_i x_i \frac{\partial}{\partial N_k} \left( \frac{\mu_i^{\text{assoc}}}{RT} \right) + \frac{1}{V} \frac{(1-x_k)}{\rho} \left( \frac{\mu_i^{\text{assoc}}}{RT} \right) - \frac{\partial}{\partial N_k} \left( \frac{a^{\text{assoc}}}{RT} \right) \quad (8.33)$$

where the derivative of the free energy is given as

$$\begin{aligned} \frac{\partial}{\partial N_k} \left( \frac{a^{\text{assoc}}}{RT} \right) &= \sum_i x_i \left[ \sum_{A_i} \left[ \frac{1}{Y^{A_i}} - \frac{1}{2} \right] \left( \frac{\partial Y^{A_j}}{\partial \rho_i} \right) \left( \frac{1}{V} \right) \right] \\ &\quad + \frac{1-x_k}{\rho} \sum_{A_k} \left[ \ln Y^{A_k} - \frac{Y^{A_k}}{2} + \frac{1}{2} \right] \left( \frac{1}{V} \right) \end{aligned} \quad (8.34)$$

Similarly the chemical potential derivatives with respect to the volume are

$$\begin{aligned} \frac{\partial}{\partial V} \left( \frac{\mu_i^{\text{assoc}}}{RT} \right) &= \sum_{A_i} \left[ \frac{1}{Y^{A_i}} - \frac{1}{2} \right] \frac{\partial Y^{A_j}}{\partial V} - \sum_{A_k} \rho_j \left[ \frac{1}{Y^{A_k}} - \frac{1}{2} \right] \frac{\partial Y^{A_k}}{\partial \rho_i} \frac{1}{V} \\ &\quad + \sum_j \rho_j \left[ \sum_{A_j} \frac{\partial}{\partial V} \left( \frac{\partial Y^{A_j}}{\partial \rho_i} \right) \left[ \frac{1}{Y^{A_j}} - \frac{1}{2} \right] + \sum_{A_j} \left( \frac{\partial Y^{A_j}}{\partial \rho_i} \right) \left( \frac{\partial Y^{A_j}}{\partial V} \right) \frac{-1}{(Y^{A_j})^2} \right] \end{aligned} \quad (8.35)$$

The volume derivative of the free associating bond sites is

$$\left[ \frac{\partial Y^{A_j}}{\partial V} \right] = -(Y^{A_j})^2 \sum_k \sum_{B_k} \rho_k \left[ -Y^{B_k} \Delta^{A_j B_k} + \Delta^{A_j B_k} \left( \frac{\partial Y^{B_k}}{\partial V} \right) + Y^{B_k} \left( \frac{\partial \Delta^{A_j B_k}}{\partial V} \right) \right] \quad (8.36)$$

and

$$\begin{aligned} & \frac{\partial}{\partial V} \left( \frac{\partial Y^{A_j}}{\partial \rho_i} \right) \\ &= -2(Y^{A_j}) \left( \frac{\partial Y^{A_j}}{\partial V} \right) \left[ \sum_{B_i} Y^{B_i} \Delta^{A_j B_i} + \sum_k \sum_{B_k} \rho_k \left[ \Delta^{A_j B_k} \left( \frac{\partial Y^{B_k}}{\partial \rho_i} \right) + Y^{B_k} \left( \frac{\partial \Delta^{A_j B_k}}{\partial \rho_i} \right) \right] \right] \\ &- (Y^{A_j})^2 \left[ \sum_{B_i} \left[ \Delta^{A_j B_i} \left( \frac{\partial Y^{B_i}}{\partial V} \right) + Y^{B_i} \left( \frac{\partial \Delta^{A_j B_i}}{\partial V} \right) \right] - \sum_{B_k} \left[ \Delta^{A_j B_k} \left( \frac{\partial Y^{B_k}}{\partial \rho_i} \right) + Y^{B_k} \left( \frac{\partial \Delta^{A_j B_k}}{\partial \rho_i} \right) \right] \left( \frac{1}{V} \right) \right. \\ &\quad \left. + \sum_k \sum_{B_k} \rho_k \left[ \left( \frac{\partial \Delta^{A_j B_k}}{\partial V} \right) \left( \frac{\partial Y^{B_k}}{\partial \rho_i} \right) + \Delta^{A_j B_k} \frac{\partial}{\partial V} \left( \frac{\partial Y^{B_k}}{\partial \rho_i} \right) + \left( \frac{\partial \Delta^{A_j B_k}}{\partial \rho_i} \right) \left( \frac{\partial Y^{B_k}}{\partial V} \right) \right] \right. \\ &\quad \left. + Y^{B_k} \frac{\partial}{\partial V} \left( \frac{\partial \Delta^{A_j B_k}}{\partial \rho_i} \right) \right] \end{aligned} \quad (8.38)$$

The compressibility factor derivatives are given as similar to the derivation shown above

$$\frac{\partial Z^{\text{assoc}}}{\partial V} = \sum_i x_i \frac{\partial}{\partial V} \left( \frac{\mu_i^{\text{assoc}}}{RT} \right) - \frac{\partial}{\partial N_k} \left( \frac{\mathbf{a}^{\text{assoc}}}{RT} \right) \quad (8.39)$$

and the association free energy derivative with volume is

$$\frac{\partial}{\partial V} \left( \frac{\mathbf{a}^{\text{assoc}}}{RT} \right) = \sum_i x_i \rho \left[ \sum_{A_i} \left[ \frac{1}{Y^{A_i}} - \frac{1}{2} \right] \left( \frac{\partial Y^{A_j}}{\partial V} \right) \left( \frac{1}{V} \right) \right] \quad (8.40)$$

### 8.4.3 Dispersion Term

The dispersion chemical potential derivatives with mole numbers is

$$\begin{aligned}
\frac{\partial \mu_i^{\text{disp}}}{\partial N_1} &= m_i \sum_j \sum_k j D_{jk} \left[ \frac{u}{kT} \right]^{j-1} \left[ \frac{\zeta_3}{\tau} \right]^k \frac{\partial}{\partial n_1} \left( \frac{u}{kT} \right) \\
&+ m_i \sum_j \sum_k k D_{jk} \left[ \frac{u}{kT} \right]^j \left[ \frac{\zeta_3}{\tau} \right]^{k-1} \frac{1}{\tau} \frac{\Pi}{6} m_1 \rho d_i^3 \\
&+ m_1 \sum_j \sum_k j D_{jk} \left[ \frac{u}{kT} \right]^{j-1} \left[ \frac{\zeta_3}{\tau} \right]^k \frac{\partial}{\partial n_1} \left( \frac{u}{kT} \right) \\
&+ m \sum_j \sum_k j(j-1) D_{jk} \left[ \frac{u}{kT} \right]^{j-2} \frac{\partial}{\partial n_1} \left( \frac{u}{kT} \right) \frac{\partial}{\partial n_1} \left( \frac{u}{kT} \right) \left[ \frac{\zeta_3}{\tau} \right]^k \\
&+ m \sum_j \sum_k j D_{jk} \left[ \frac{u}{kT} \right]^{j-1} \frac{\partial}{\partial n_1} \left( \frac{\partial}{\partial n_1} \left( \frac{u}{kT} \right) \right) \left[ \frac{\zeta_3}{\tau} \right]^k \\
&+ m \sum_j \sum_k j k D_{jk} \left[ \frac{u}{kT} \right]^{j-1} \frac{\partial}{\partial n_1} \left( \frac{u}{kT} \right) \left[ \frac{\zeta_3}{\tau} \right]^{k-1} \left( \frac{1}{\tau} \frac{\Pi}{6} m_1 \rho d_i^3 \right) \\
&+ m \sum_j \sum_k j k D_{jk} \left[ \frac{u}{kT} \right]^{j-1} \frac{\partial}{\partial n_1} \left( \frac{u}{kT} \right) \left[ \frac{\zeta_3}{\tau} \right]^{k-1} \left( \frac{1}{\tau} \frac{\Pi}{6} m_1 \rho d_i^3 \right) \\
&+ m \sum_j \sum_k k(k-1) D_{jk} \left[ \frac{u}{kT} \right]^j \left[ \frac{\zeta_3}{\tau} \right]^{k-2} \left( \frac{1}{\tau} \frac{\Pi}{6} m_1 \rho d_i^3 \right) \left( \frac{1}{\tau} \frac{\Pi}{6} m_1 \rho d_i^3 \right) \\
&+ m \sum_j \sum_k k D_{jk} \left[ \frac{u}{kT} \right]^j \left[ \frac{\zeta_3}{\tau} \right]^{k-1} \frac{1}{\tau} \frac{\Pi}{6} m_1 \rho d_i^3
\end{aligned} \tag{8.41}$$

Similarly the compressibility factor derivatives with respect to the mole numbers is

$$\begin{aligned}
\frac{\partial Z^{\text{disp}}}{\partial N_1} &= m_1 \sum_j \sum_k k D_{jk} \left[ \frac{u}{kT} \right]^j \left[ \frac{\zeta_3}{\tau} \right]^k \\
&\quad + m \sum_j \sum_k j k D_{jk} \left[ \frac{u}{kT} \right]^{j-1} \left[ \frac{\zeta_3}{\tau} \right]^k \frac{\partial}{\partial n_1} \left( \frac{u}{kT} \right) \\
&\quad + m \sum_j \sum_k k^2 D_{jk} \left[ \frac{u}{kT} \right]^j \left[ \frac{\zeta_3}{\tau} \right]^{k-1} \frac{1}{\tau} \frac{\Pi}{6} m_1 \rho d_i^3
\end{aligned}
\tag{8.42}$$

The derivatives of the  $\frac{u}{kT}$  in the above equations are given by

$$\begin{aligned}
\frac{\partial}{\partial N_k} \left( \frac{u}{kT} \right) &= \frac{1}{\left( \sum_i \sum_j x_i x_j m_i m_j (v^o)_{ij} \right)^2} \left[ \left( \sum_i 2x_j m_k m_j \left[ \frac{u_{kj}}{kT} \right] (v^o)_{ij} \right) \right. \\
&\quad \left. \left( \sum_i \sum_j x_i x_j m_i m_j (v^o)_{ij} \right) - \left( \sum_i \sum_j 2x_j m_k m_j (v^o)_{kj} \right) \left( \sum_i \sum_i x_i x_j m_i m_j \left[ \frac{u_{ij}}{kT} \right] (v^o)_{ij} \right) \right]
\end{aligned}
\tag{8.43}$$

$$\begin{aligned}
\frac{\partial}{\partial N_l} \left( \frac{\partial}{\partial N_k} \left( \frac{\mathbf{u}}{kT} \right) \right) &= \frac{1}{\left( \sum_i \sum_j x_i x_j m_i m_j (v^\circ)_{ij} \right)^2} \\
&\quad \left[ \left( 2m_k m_l \left[ \frac{\mathbf{u}_{kl}}{kT} \right] (v^\circ)_{kl} \right) \left( \sum_i \sum_j x_i x_j m_i m_j (v^\circ)_{ij} \right) \right. \\
&\quad - \left( \sum_j 2x_j m_l m_j (v^\circ)_{lj} \right) \left( \sum_i 2x_j m_k m_j \left[ \frac{\mathbf{u}_{kj}}{kT} \right] (v^\circ)_{kj} \right) \\
&\quad - \left( 2m_k m_l (v^\circ)_{kl} \right) \left( \sum_i \sum_j x_i x_j m_i m_j \left[ \frac{\mathbf{u}_{ij}}{kT} \right] (v^\circ)_{ij} \right) \\
&\quad - \left. \left( \sum_j 2x_j m_l m_j (v^\circ)_{lj} \right) \left( \sum_i 2x_j m_k m_j \left[ \frac{\mathbf{u}_{kj}}{kT} \right] (v^\circ)_{kj} \right) \right] \\
&\quad - \frac{\left( \sum_i 4x_j m_k m_j \left[ \frac{\mathbf{u}_{kj}}{kT} \right] (v^\circ)_{ij} \right)}{\left( \sum_i \sum_j x_i x_j m_i m_j (v^\circ)_{ij} \right)^3} \\
&\quad \left[ \left( \sum_j 2x_j m_k m_j \left[ \frac{\mathbf{u}_{kj}}{kT} \right] (v^\circ)_{kj} \right) \left( \sum_i \sum_j x_i x_j m_i m_j (v^\circ)_{ij} \right) \right. \\
&\quad - \left. \left( \sum_i \sum_j 2x_j m_k m_j (v^\circ)_{kj} \right) \left( \sum_i \sum_j x_i x_j m_i m_j \left[ \frac{\mathbf{u}_{ij}}{kT} \right] (v^\circ)_{ij} \right) \right]
\end{aligned} \tag{8.44}$$

So the chemical potential derivatives with respect to volume are

$$\begin{aligned}
\frac{\partial \mu_i^{\text{disp}}}{\partial V} &= m_i \sum_j \sum_k D_{jk} \left[ \frac{u}{kT} \right]^j \left[ \frac{\zeta_3}{\tau} \right]^k \left( \frac{-1}{V} \right) \\
&+ m \sum_j \sum_k jk D_{jk} \left[ \frac{u}{kT} \right]^{j-1} \frac{\partial}{\partial n_i} \left( \frac{u}{kT} \right) \left[ \frac{\zeta_3}{\tau} \right]^k \left( \frac{-1}{V} \right) \\
&+ m \sum_j \sum_k k(k-1) D_{jk} \left[ \frac{u}{kT} \right]^j \left[ \frac{\zeta_3}{\tau} \right]^{k-1} \frac{1}{\tau} \frac{\Pi}{6} m_i \rho d_i^3 \left( \frac{-1}{V} \right) \\
&+ m \sum_j \sum_k k D_{jk} \left[ \frac{u}{kT} \right]^j \left[ \frac{\zeta_3}{\tau} \right]^{k-1} \frac{1}{\tau} \frac{\Pi}{6} m_i \rho d_i^3 \left( \frac{-1}{V} \right)
\end{aligned} \tag{8.45}$$

and

$$\frac{\partial z^{\text{disp}}}{\partial V} = m \sum_j \sum_k k D_{jk} \left[ \frac{u}{kT} \right]^j \left[ \frac{\zeta_3}{\tau} \right]^k \left( \frac{-1}{V} \right) \tag{8.46}$$

The above equations have been coded with the SAFT algorithm and have been linked with the corresponding flow variables in the UTCOMP reservoir flow simulator, so that they can be evaluated by the simulator at each time step.



## 8.5 SIMULATION OF CORE FLOOD EXPERIMENTS

We present the results for a few core flood simulations for a hydrocarbon mixture with the SAFT equation of state and compare the results with the experimental data as well as the simulation results from the PR equation of state. The simulation is for a one-dimensional flow in a laboratory core flow experiment. Synthetic gas condensate mixtures were prepared using methane (C1), n-butane (nC4), n-heptane (nC7) and n-decane (nC10) by Walker et al., [2] and Al Anazi et al., [3] to study the extent of condensate blocking in laboratory core flood experiments. The mixture has a measured dew-point of 2795 psia. A Corey type relative permeability model with trapping number effect proposed by Narayanaswamy et al., [4] and Pope et al., [5], have been used. The relative permeability parameters used in this study are given by Rai [6] who has extensively studied the simulation of core flood experiments with the PR equation of state and has proposed the relative permeability parameters for this system. In this work we study the effect of the SAFT equation of state for two different core flood experiments and determine the influence of the equation of state, if any, on these simulations. The two experiments selected are the Experiment 15 of Al. Anazi et al., [3] conducted at a low rate on a low permeability Texas cream limestone rock and Experiment 12 conducted at a high rate on a high permeability Berea sandstone rock. The coreflood summary of these two experiments is given in Table 8.1

Figure 8.1 shows the pressure profile for single phase gas flow with the PR and SAFT equation of state at different times for Experiment 15 of Al Anazi [3]. We observe that both the equations give the pressure profile accurately. At initial times till 5 pore volume, the pressure drop across the core is 12 psia, which is also the value predicted by both the equations. Figure 8.2 shows the pressure drop across the core during two phase injection. Here again we observe there is no significant advantage in using the SAFT equation of state over the PR equation of state in our simulations. Similarly Figure 8.3 shows the pressure drop during equilibrium gas injection phase for this mixture. Both the PR and SAFT equation are able to predict the steady state experimental pressure drop. We have not been able to obtain early time data with the SAFT equation as this data was not recorded in the output files. Figure 8.4 shows the same pressure drop during methanol injection. The steady state pressure drop predicted by the PR equation is 220 psi as against an experimental value of 160 psi whereas the SAFT prediction is 190 psi. In this case, the SAFT prediction are more in line with the experimental values, as expected, because SAFT is better suited for predicting properties of polar mixtures. The CPU runtime for the PR equation is 5090 sec whereas for the SAFT equation of state this time is 216330 sec on a Pentium III 1 G Hz processor with 256 MB memory in a Windows based environment. The very high CPU time for equation of state is because of large time the simulator takes in the flash algorithm.

Figure 8.5 shows the pressure profile for single phase gas injection with both the PR and SAFT equation of state at different times for Experiment 12 of Al Anazi [3]. We observe that both the equations give the pressure profile accurately. At initial times till 3 pore volumes, the pressure drop across the core is 1.6 psia, which is the value predicted by both the equations. Figure 8.6 shows the pressure drop across the core during two phase injection. Here again we observe there is no significant advantage in using the SAFT equation of state over the PR equation of state in our simulations. In fact the steady-state pressure drop of 22 psia predicted by the PR equation is closer to the experimental value of 25 psia than the steady state value of 20 psia predicted by the SAFT equation. Similarly Figure 8.7 shows the pressure drop during equilibrium gas phase injection for this mixture. Both the PR and SAFT equation are able to predict the steady state pressure drop as 2 psia whereas the experimental value is closer to 1 psia. We observe that there has been no data recorded in this case between 16 and 36 pore volumes of gas injection. Figure 8.8 shows the same pressure drop during methanol injection. The steady state pressure drop predicted by the SAFT equation is 6 psi which is closer to the experimental value of 5 psi whereas the PR prediction is 7 psia. Figure 8.9 shows the pressure drop during second condensate accumulation phase. We observe that both the PR and SAFT equation of state have not been able to capture early time experimental behavior. This may be because of non-equilibrium effects in the core during the condensate accumulation stage due to the high rate of injection through the core. Although there is a significant amount of scatter in the steady state data both the equations give a reasonably good agreement with the

experimentally measured pressure drop at late time. Finally, both the PR and SAFT equation of state give a steady state pressure drop of 2 psia as against an experimentally measured value of 1 psia during second equilibrium gas phase injection which is in reasonable agreement within the experimental limits. The CPU runtime on a Pentium III 1 G Hz processor with 256 MB memory in a Windows based environment for the PR equation is 168 sec whereas the CPU time for the SAFT equation of state in the same environment is 70222 sec.

## **8.6 CONCLUSIONS**

We have integrated the SAFT equation of state in a reservoir simulator so as to be able to do flow simulations for complex polar mixtures. We have been able to match the predictions of a SAFT equation with a conventional PR equation of state of pure hydrocarbon mixtures for a typical gas condensate problem. We observe that for the experimental core flood studies we have studied both the PR equation and SAFT equation give reasonable agreement with experimental data but, as expected, there is a slight advantage in using the SAFT equation of state during the methanol injection stage of the experiment. However, significantly larger computational time does not justify the use of the SAFT equation of state currently in such flow simulation problems.

## Nomenclature

$W_i$	accumulation of species $i$ (lb-moles/cu. ft.)
$F_i$	flux of species $i$ (lb-moles/sq. ft/day)
$R_i$	generation of species $i$ (lb-moles/cu. ft/day)
$\phi$	porosity
$\zeta_j$	molar density of phase $j$ (lb-moles/cu. ft/
$S_j$	saturation of phase $j$
$x_{ij}$	mole fraction of component $i$ in phase $j$
$\vec{u}_j$	superficial fluid velocity of phase $j$
$\vec{K}_{ij}$	dispersion tensor (sq. ft/day)
$\bar{k}$	permeability tensor (mD)
$k_{rj}$	relative permeability of phase $j$
$\mu_j$	viscosity of phase $j$ (cp)
$\gamma_j$	specific weight of phase $j$
$D$	depth (ft)
$P$	pressure (psi)
$V_T$	total fluid volume (cu ft)
$V_P$	pore volume (cu. ft.)
$t$	time (days)
$Z_j$	compressibility factor of phase $j$
$n_j$	number of moles of phase $j$
$n_p$	number of phases
$n_c$	number of components
$n_{ij}$	number of moles of component $i$ in phase $j$
$N_i$	number of molecules of component $i$

$f_{ij}$	fugacity coefficient of component i in phase j (psi)
$\zeta_3$	reduced density of the mixture
$m_i$	chain length of component i
$d_i$	temperature dependent segment diameter (A)
$\sigma_i$	temperature dependent segment diameter (A)
$u^o/k$	temperature independent energy parameter (K)
$P_{hs}^{CS}$	Carnahan-Starling Pressure contribution (Pa)
$\mu^{hs}$	hard sphere chemical potential (J/mol)
$Z^{hs}$	hard-sphere compressibility factor
$\mu^{chain}$	chain chemical potential (J/mol)
$Z^{chain}$	chain compressibility factor
$g_{ii}$	radial distribution function of component i
$Y_i^A$	mole fraction of molecules i not bonded at site A
$\Delta_{ij}^{A,B}$	association bonding strength between sites $A_i$ and $B_j$
$\varepsilon_{ij}^{A,B}$	association energy between sites $A_i$ and $B_j$ (
$\kappa_{ij}^{A,B}$	association entropy between sites $A_i$ and $B_j$
$\mu_i^{assoc}$	association chemical potential of component i
$Z^{assoc}$	association compressibility factor
$u_{ii}$	dispersion energy of component i
$D_{jk}$	Chen and Kreglewski constants for dispersion potential
$\tau$	closed packing density limit (0.74048)
$k_{ij}$	binary interaction coefficient between component i and j
$\mu^{disp}$	association chemical potential of component i
$Z^{disp}$	dispersion compressibility factor

## References

- 1) Chang, Y-B., “Development and application of an Equation of State Compositional Simulator”, Ph. D Dissertation, The University of Texas at Austin, August, (1990).
- 2) Walker, J.G., “Laboratory Evaluation of Alcohols and Surfactants to increase production from Gas-Condensate Reservoirs”, M.S. Thesis, The University of Texas at Austin, December, (2000).
- 3) Al-Anazi, H., Ph. D Dissertation, The University of Texas at Austin, (to be published).
- 4) Narayanaswamy, G., Pope, G.A., and Sharma, M.M., “Predicting Gas-Condensate Well Productivity using Capillary Number and Non-Darcy Effects”, *SPE 51910* presented at the SPE Reservoir Simulation Symposium, Houston, TX, (1999).
- 5) Pope G.A., Wu, W., Narayanaswamy, G., Delshad M., Sharma, M.M., and Wang P., “Modeling Relative Permeability effects in Gas-Condensate Reservoirs with a New Trapping Model”, *SPE Res. Eval. & Eng.*, 3(2), 171, (1986).
- 6) Rai R.R., M.S Thesis, The University of Texas at Austin (to be published).

	<b>Experiment 15</b>	<b>Experiment 12</b>
<b>Core Properties</b>		
Rock Type	Texas Cream Limestone	Berea Sandstone
Length (in)	8.01	8.01
Diameter (in)	0.972	0.972
Porosity (%)	20	20
Water Saturation (Sw)	0	0
Average Permeability (mD)	2.61	245.94
<b>Single Phase Gas Injection</b>	<b>@ 3000 psi</b>	
Injection Rate (lbmol/D)	2.68e-2	3.35e-1
Pressure Drop (psi)	10.95	1.56
<b>Condensate Accumulation</b>	<b>@ 1200 psi</b>	
Injection Rate (lbmol/D)	1.00e-2	3.35e-1
Pressure Drop (psi)	16.13	23.93
Gas Rel. Perm ( $K_g$ )	0.17	0.05
Oil Rel. Perm ( $K_o$ )	0.21	0.19
<b>Equilibrium Gas Flow</b>	<b>@ 1200 psi</b>	
Injection Rate (lbmol/D)	1.88e-2	1.14e-1
Pressure Drop (psi)	9.16	0.75
<b>Methanol Treatment</b>		
Injection Rate (lbmol/D)	1.88e-2	3.24e-1
Pressure Drop (psi)	164.07	5.23
<b>Condensate Accumulation</b>	<b>@ 1200 psi</b>	
Injection Rate (lbmol/D)		3.35e-1
Pressure Drop (psi)		23
Gas Rel. Perm ( $K_g$ )		0.05
Oil Rel. Perm ( $K_o$ )		0.2
<b>Equilibrium Gas Flow</b>	<b>@ 1200 psi</b>	
Injection Rate (lbmol/D)		1.14e-1
Pressure Drop (psi)		0.7
Gas Rel. Perm ( $K_g$ )		0.96

**Table 8.1: Coreflood experiment summary for Texas Cream limestone and Berea sandstone**



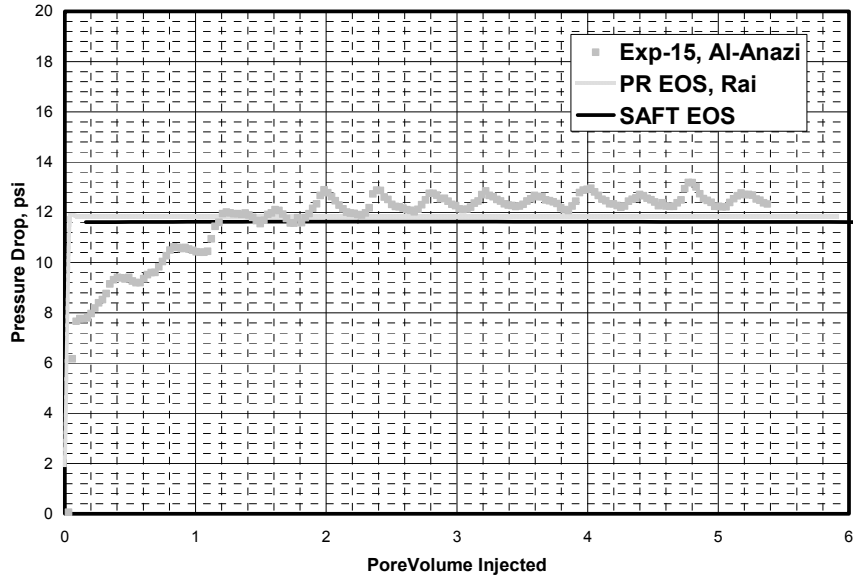


**Figure 8.1: Experiment 15 – Pressure drop across core during single phase gas mixture injection (  $T = 145$  F,  $P = 3000$  psi and  $Q = 48$  cc/hr)**

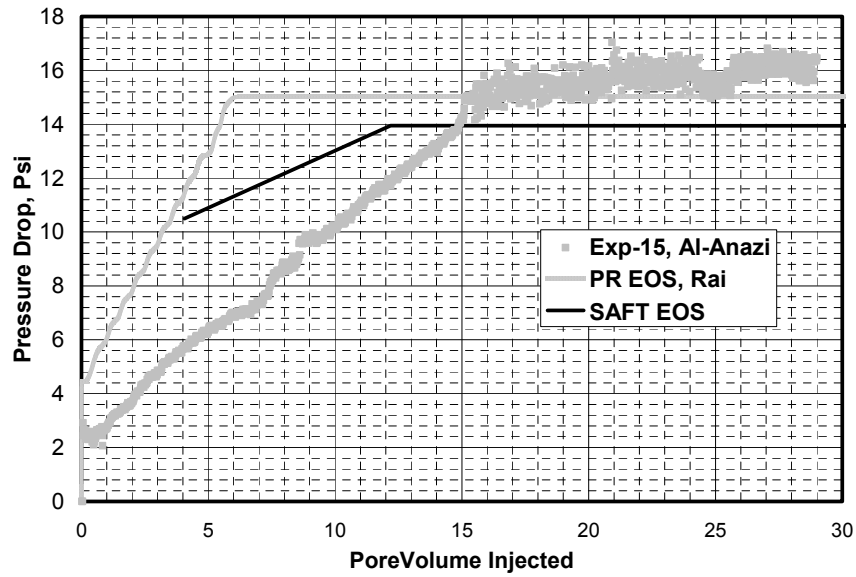


**Figure 8.2: Experiment 15 – Pressure drop across core during two phase mixture injection (  $T = 145$  F,  $P = 1200$  psi and  $Q = 18$  cc/hr)**

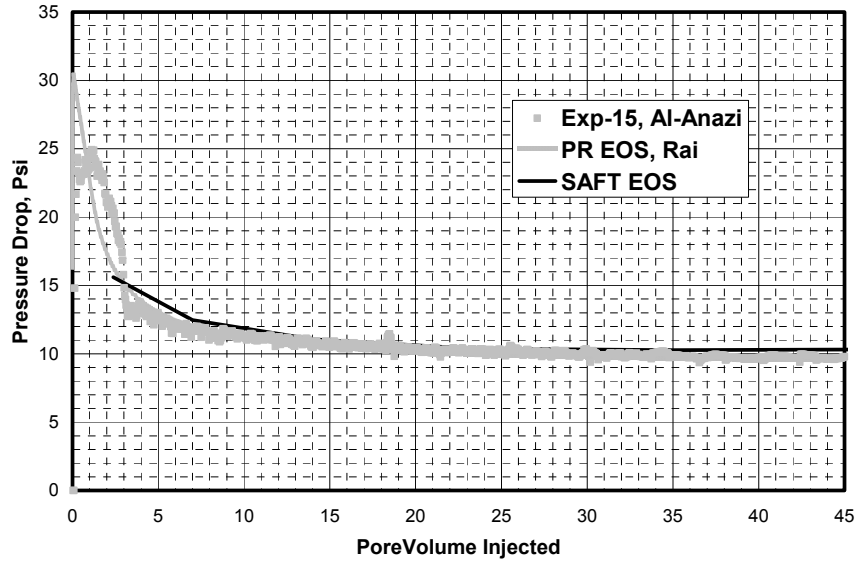


**Figure 8.3: Experiment 15 – Pressure drop across core during single phase equilibrium gas mixture injection (  $T = 145$  F,  $P = 1200$  psi and  $Q = 99$  cc/hr)**

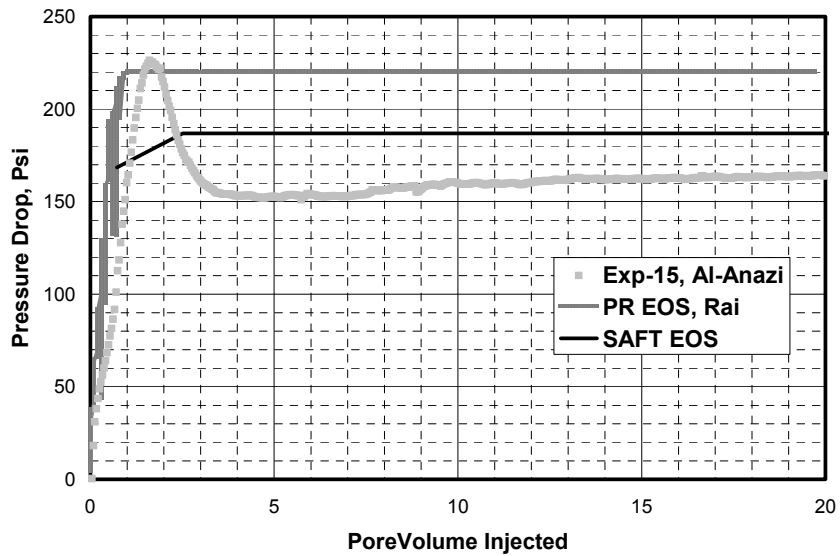


**Figure 8.4: Experiment 15 – Pressure drop across core during methanol treatment (  $T = 145$  F,  $P = 3000$  psi and  $Q = 99$  cc/hr)**

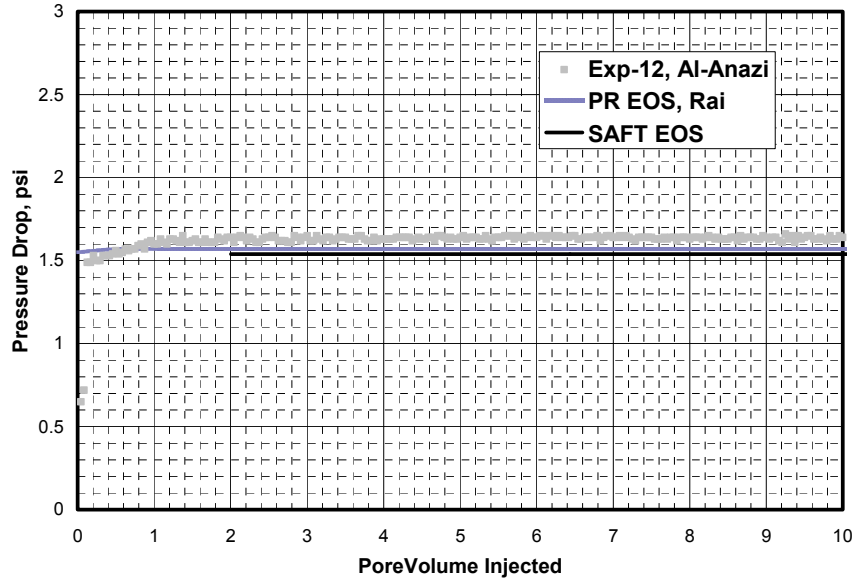


**Figure 8.5: Experiment 12 – Pressure drop across core during single phase gas mixture injection ( T = 145 F, P = 3000 psi and Q = 600 cc/hr)**

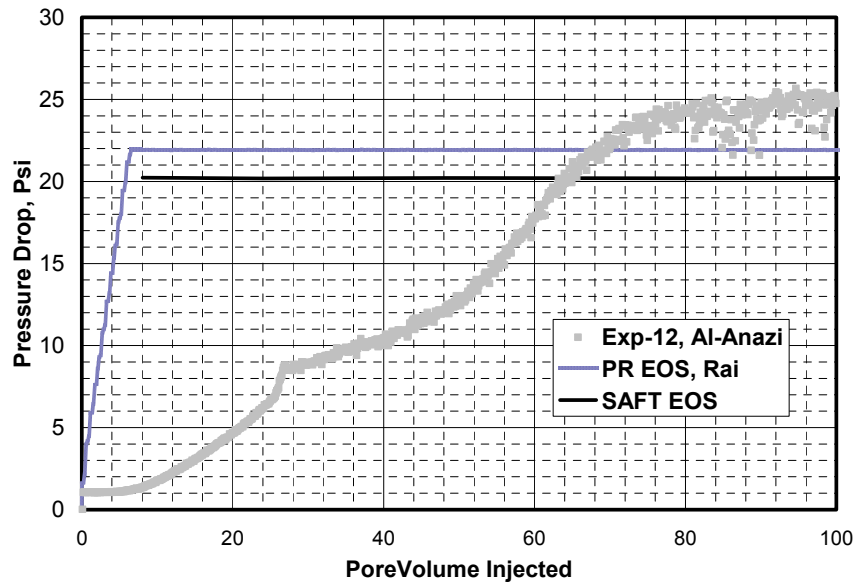


**Figure 8.6: Experiment 12 – Pressure drop across core during two phase mixture injection ( T = 145 F, P = 1200 psi and Q = 600 cc/hr)**

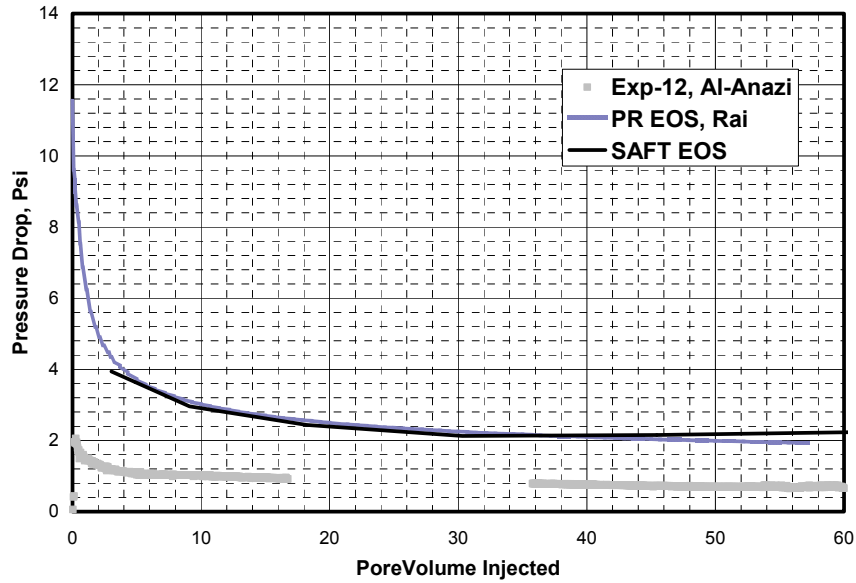


Figure 8.7: Experiment 12 – Pressure drop across core during single phase equilibrium gas mixture injection ( T = 145 F, P = 1200 psi and Q = 600 cc/hr)

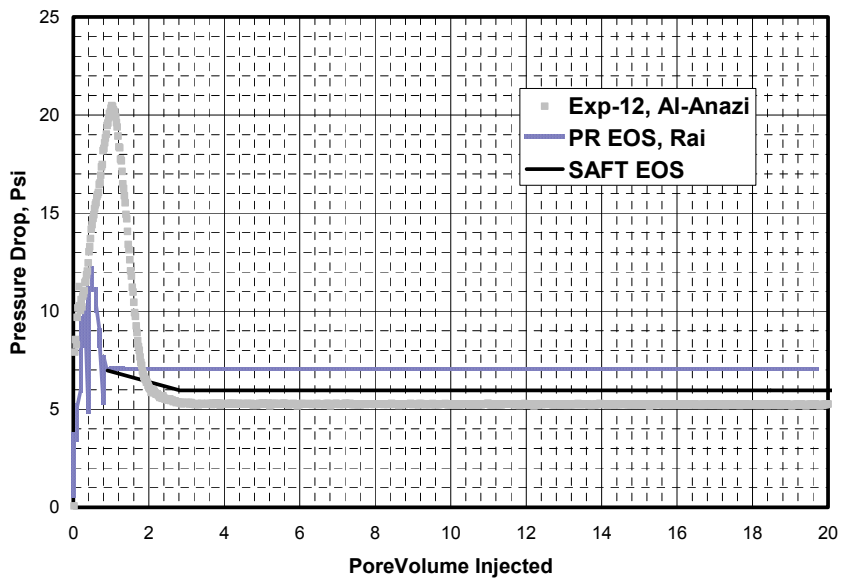
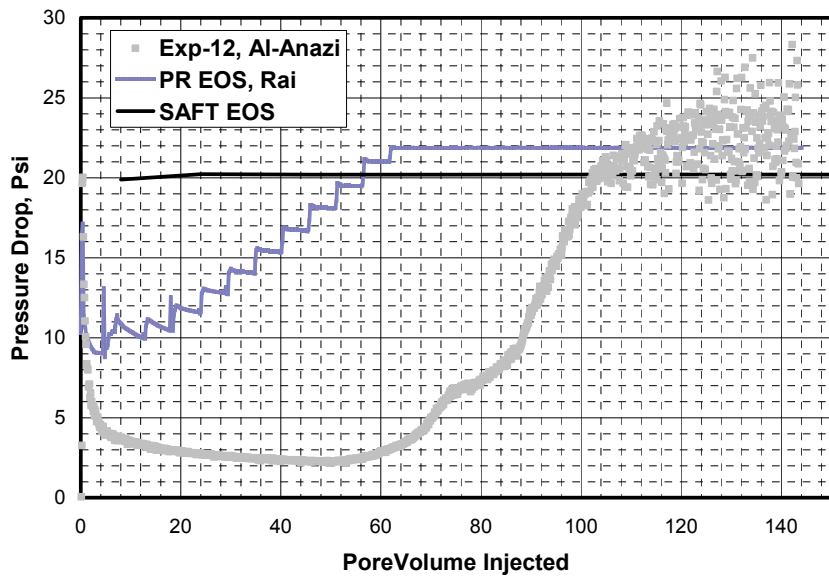
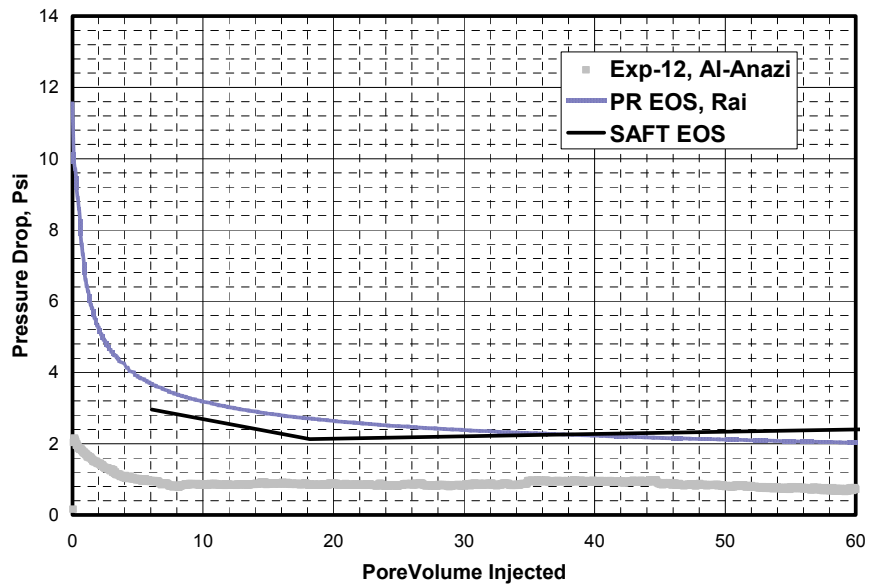


Figure 8.8: Experiment 12 – Pressure drop across core during methanol injection ( T = 145 F, P = 1200 psi and Q = 300 cc/hr)



**Figure 8.9: Experiment 12 – Pressure drop across core during second two phase gas mixture injection ( T = 145 F, P = 1200 psi and Q = 600 cc/hr)**



**Figure 8.10: Experiment 12 – Pressure drop across core during second equilibrium gas mixture injection ( T = 145 F, P = 1200 psi and Q = 600 cc/hr)**

## CHAPTER 9

### SUMMARY AND CONCLUSIONS

In this work a SAFT (Statistical Associating Fluid Theory) equation of state has been implemented with a stability algorithm and a flash algorithm to conduct the phase behavior calculations for complex polar mixtures. The stability algorithm utilized in this work is Michelsen's stationary point method and the flash algorithm used is the multi-phase version of the Rachford-Rice equation. The SAFT equation of state has been extensively tested with binary and ternary experimental vapor liquid equilibrium data for both non-polar as well as polar mixtures. The Peng-Robinson equation of state calculations has also been shown for comparison.

Our results show that the Peng-Robinson equation of state predicts the phase equilibrium of non-polar mixtures accurately without any adjustment of binary interaction coefficients. On the other hand, the SAFT equation of state seems to predict the vapor-liquid equilibrium of non polar – polar mixtures better than the Peng-Robinson equation of state without any adjustment of binary interaction coefficients. However there are still large discrepancies between the experimental liquid mole fractions and those predicted by SAFT. Hence the binary interaction coefficients still need to be adjusted for non polar – polar mixtures even with the SAFT equation of state. In the case of polar – polar

mixtures, both the binary interaction coefficient as well as the association interaction coefficient had to be adjusted to get a good fit to the binary vapor-liquid equilibrium data for certain cases. In the case of ethanol-water mixture two sets of binary and association interaction coefficients have been obtained which can describe the experimental data equally well.

The relationships suggested by Huang and Radosz for obtaining the SAFT parameters for any general component has been implemented in this work to study the phase behavior of pseudo components with the SAFT equation of state. However, SAFT predictions of dew point and gas phase compressibilities of two North Sea examples are very poor. This may be because the binary interaction coefficients have been taken to be zero, which is usually the case for hydrocarbons when using the Peng-Robinson equation. The Peng-Robinson equation usually predicts the phase equilibrium of mixtures containing pseudo components by adjusting the molecular weight of the heavy end which are often difficult to measure accurately from experiments.

The phase behavior of methanol-water-hydrocarbon mixtures is studied with the SAFT equation of state and the Peng-Robinson equation of state and comparisons are made with experimental liquid dropout data. The Peng-Robinson equation was able to predict the liquid dropout variation with pressure without any adjustment of the binary interaction coefficients whereas with SAFT the binary interaction coefficients amongst hydrocarbons had to be adjusted to get a

good fit to the experimental data. When methanol is present in the hydrocarbon mixture the methanol-hydrocarbon binary interaction coefficients had to be adjusted for both the Peng-Robinson as well as the SAFT equation of state. However, the SAFT equation of state predicts the liquid dropout behavior qualitatively at a different methanol concentration without further adjustment of the binary interaction coefficients. In the case of water-methanol-hydrocarbon mixtures the additional water-methanol and water-hydrocarbon binary interaction coefficient had to be adjusted for the two equations of state. As expected, the SAFT equation of state was able to predict quantitatively the liquid-liquid-vapor phase equilibrium accurately at a different mixture conditions without further adjustment of binary interaction coefficients. SAFT calculations also showed a transition from a dew-point behavior to a bubble point behavior with increasing methanol concentration and increasing temperature which confirm the earlier experimental findings.

Several empirical models available in the literature for the calculation of interfacial tension have been explored in this work. We have shown that the non-polar part of the solubility parameters proposed by Hansen for several compounds correlates reasonably well with the non-polar part of the surface tension proposed by van Oss by way of the Hildebrand expression connecting the solubility parameter and surface tension. However, the acid-base or the polar part of the interfacial tension does not correlate very well between the two theories. This is because of the empirical nature of both the models.



In this work we have coupled the SAFT equation of state with the Gradient Theory to calculate the interfacial tension of pure components as well as multi component mixtures. Pure component interfacial tension parameters are obtained for both non-polar as well as polar compounds and the average absolute deviation is less than 10 % in all cases. For a non-polar mixture of CO<sub>2</sub> and decane, SAFT with the Gradient Theory calculates the interfacial tension accurately whereas the parachor calculations deviate from the measured interfacial tensions at low CO<sub>2</sub> concentrations. For a non polar – polar mixture of ethanol and heptane, again SAFT with gradient theory is more accurate than the parachor calculations. In the case of polar – polar mixtures, for methanol-water and ethanol-water mixtures the mixing interaction coefficient had to be adjusted to get a good fit to the experimental interfacial tension data. In the case of methanol-water mixtures two values of mixing interaction coefficient ( 0 and 1) can describe the experimental data equally well. For a methane-water mixture the mixing interaction coefficient had to be adjusted to fit the experimental interfacial tension variation with pressure at 25 C. This mixing interaction coefficient was used to predict the interfacial tension at other temperatures also very accurately.

The SAFT equation of state has been integrated into the reservoir flow simulator (UTCOMP) so as to be able to conduct flow simulations of complex polar mixtures. The flow simulations with SAFT have also been compared with experimental core flood studies conducted on two different cores (Texas cream limestone and Berea sandstone) as well as the simulations with the PR equation of

state. In the initial stage of the core flood when there is single phase hydrocarbon gas flowing through the core both the Peng-Robinson and SAFT equation of state match accurately with the experimental data. Similarly during the condensate buildup stage and the equilibrium gas injection stage of the experiment both the Peng-Robinson equation and the SAFT equation give reasonably good agreement with the experimental data. During the methanol injection phase of the experiment the SAFT equation of state has been found to be slightly better than the Peng-Robinson equation. However, the simulations with SAFT equation of state are characteristically an order of magnitude slower than the corresponding simulations with the PR equation. Thus SAFT is currently not a viable tool for large scale field simulations.

## **9.1 Recommendations and Future Work**

The SAFT equation of state has been found to be slower than the Peng-Robinson equation of state for both phase behavior calculations as well as flow simulations. This is because PR equation is a three parameter equation of state in which the compressibility factor can be solved analytically for a give pressure, temperature and composition condition. On the other hand, with SAFT equation of state a complex non-linear equation needs to be solved for the density for every given pressure, temperature and composition. This is a computationally expensive step as a generalized non-linear equation solver which uses a modified Newton method has been used for most part of this work. This algorithm can be improved

so as to increase the overall speed of the SAFT equation in the phase behavior model. One way to do this is to do a binary search in the closed interval space of the reduced density  $\zeta_3$  as it is known that the reduced density can only vary from zero to the closed pack segment volume limit ( $\tau = 0.74048$ ). However, the algorithm will still need to account for the possibility of the presence of multiple roots in this interval.

It has been found in this work that the SAFT parameters suggested by Huang and Radosz based on fitting the vapor pressure and liquid density are not the best parameters when dealing with mixtures of hydrocarbons as binary interaction coefficients had to be introduced to fit the experimental data in these cases. An alternative approach to obtaining the pure component parameters is by matching the critical temperature and critical pressure data of the pure components. This is expected to give better predictions especially for hydrocarbon mixtures based on similar experiences with the Peng-Robinson equation.

Much of the work in the literature regarding calculating the interfacial profiles using the gradient theory focuses on planar interfaces. A fairly simple extension of the gradient theory can be the calculation of interfacial profiles across spherical surfaces such as a liquid drop. This can be easily accomplished by choosing the appropriate boundary conditions and the coordinates to solve the interfacial profile equations given in Chapter 6. The solution of these equations

and subsequent calculation of interfacial tension can improve the understanding of the interfacial forces across non-planar surfaces to a great extent.

## APPENDIX A

The SAFT equation of state is a volume explicit equation of state, so the chemical potential derivatives and the compressibility factor derivative with respect to the mole numbers are obtained with the volume held constant. On the other hand, the fugacity and the specific volume derivatives in the pressure equation (Equation 8.10) in Chapter 8 are evaluated with the pressure held constant. The following mathematical relations are useful in converting the constant volume derivatives of various thermodynamic properties to their corresponding constant pressure derivatives.

If  $u$ , as well as  $z$ , is a function of  $x$  and  $y$ , we may then express the total differential of  $z$  in terms of differential  $dx$  and  $dy$  given below

$$dz = \left( \frac{\partial z}{\partial x} \right)_y dx + \left( \frac{\partial z}{\partial y} \right)_x dy \quad (\text{A-1})$$

Since  $u$  is a function of  $x$  and  $y$  we may consider  $y$  as a function of  $u$  and  $x$ .

$$dy = \left( \frac{\partial y}{\partial x} \right)_u dx + \left( \frac{\partial y}{\partial u} \right)_x du \quad (\text{A-2})$$

Combining the two equations above we obtain

$$dz = \left( \frac{\partial z}{\partial x} \right)_y dx + \left( \frac{\partial z}{\partial y} \right)_x \left[ \left( \frac{\partial y}{\partial x} \right)_u dx + \left( \frac{\partial y}{\partial u} \right)_x du \right] \quad (\text{A-3})$$

Rearranging the terms in the above equation we obtain

$$dz = \left[ \left( \frac{\partial z}{\partial x} \right)_y + \left( \frac{\partial z}{\partial y} \right)_x \left( \frac{\partial y}{\partial x} \right)_u \right] dx + \left( \frac{\partial z}{\partial u} \right)_x du \quad (\text{A-4})$$

Comparing the first term on the right hand side of Equation A-4 with the corresponding expression in Equation A-1 we obtain the required relationship.

$$\left( \frac{\partial z}{\partial x} \right)_u = \left( \frac{\partial z}{\partial x} \right)_y + \left( \frac{\partial z}{\partial y} \right)_x \left( \frac{\partial y}{\partial x} \right)_u \quad (\text{A-5})$$

## APPENDIX B

UTCAMP is an isothermal, three-dimensional compositional reservoir simulator developed at the University of Texas at Austin. The phase behavior aspect of the reservoir simulator is incorporated in the subroutine FLASH. The algorithm for the working of FLASH is given in Figure (3.2) in Chapter 3. UTCAMP uses the Peng-Robinson equation of state and Redlich-Kwong equation of state. In this work we have incorporated the SAFT equation of state into the existing formulation. The SAFT formulation is used to compute the chemical potential of each of the components in each phase and also the compressibility factor. It is trivial to compute the fugacity coefficients from the chemical potential

$$\mu_i - \mu_i^{\text{ideal}} = -RT \ln \phi_i \quad (\text{B-1})$$

The subroutine “plfc” computes the fugacity coefficients at each step of the phase equilibrium calculation. Due to incorporation of SAFT, now “plfc” calls the appropriate subroutine “saft\_eos” to calculate the SAFT based fugacity coefficients. The input to SAFT is the pressure, P, temperature, T and the feed mole fractions, at each step of the algorithm. SAFT needs to compute the compressibility factor and the chemical potential and return these parameters to UTCAMP. The algorithm for implementing SAFT is

- 1) Solve  $P = f(T, \rho, x_i \ i = 1, \dots, n_c)$  for the phase density  $\rho$ , given the pressure  $P$ , temperature  $T$  and mole fractions  $x_i, i = 1, \dots, n_c$
- 2) Using the density computed in step 1 above calculate the compressibility factor,  $Z$  from the equation

$$Z = P / (\rho RT) \quad (B-2)$$

- 3) and also the chemical potential from the equation

$$\mu = f(T, \rho, x_i \ i = 1, \dots, n_c) \quad (B-3)$$

The solution to step (1) above usually has multiple roots for density. The problem is now to pick the correct root out of the different densities. Traditionally the root that minimizes the overall free energy of the phase is selected. The phase free energy is given by

$$G = \sum_{i=1}^{n_c} x_i \mu_i \quad (B-4)$$

The input parameters needed by “saft\_eos” at each step to compute the fugacity coefficients are the temperature, pressure and the feed mole fractions. These are the input variables that UTCOMP needs to supply to SAFT. The subroutine “saft\_eos” gets access to the above mentioned input parameters from



UTCOMP. These parameters are read into the corresponding SAFT parameters using the subroutine "input\_values". Similarly, the return parameters of the subroutine SAFT are the compressibility factor and the fugacity coefficients and these are again exchanged by using the COMMON statement for UTCOMP and module "saft\_declare" for SAFT. The subroutine SAFT\_EOS is the bridge between the UTCOMP and SAFT.

The module named "declare" in the file "saft\_declare\_deriv.f90" contains all the public variable declarations used in the actual SAFT formulation. The module "stat\_thermo" in the file "saft\_module\_deriv.f90" contains the SAFT formulation. It evaluates the contribution to the Helmholtz free energy, compressibility factor, chemical potential and their volume and mole number derivatives of the various terms involved in the SAFT equation of state. The subroutine "saft\_input\_values" in the file "saft\_input\_values.f90" reads the basic Huang and Radosz parameters needed to do the SAFT calculations. If there are any pseudocomponents involved the type of the pseudocomponent (for e.g., alkane or aromatic) is specified in the SAFT input file "SAFT\_input.dat" and the corresponding Huang and Radosz parameters are evaluated automatically.

## BIBLIOGRAPHY

- Abrams, D., and Prausnitz, J.M.,: “Statistical Thermodynamics of Liquid Mixtures: A New Expression for the Excess Gibbs Energy of Partly or Completely Miscible Systems”, *AIChE J.*, **21**, 116 (1975).
- Afidick, D., Kaczorowski N. J., and Bette., “Production Performance of a Retrograde Gas: A Case Study of the Arun Field”, paper *SPE 28749* presented at the 1994 Asia Pacific Oil & Gas Conference, Melbourne, Australia, Nov. 7-10
- Al-Anazi, H., Ph. D Dissertation, The University of Texas at Austin, (to be published).
- Alder, B.J., Young, D.A., and Mark, M.A., “Studies in Molecular Dynamics. X. Corrections to the Augmented van der Waals theory for the Square Well Fluid”, *J. Chem. Phys.*, **56**,3013 (1972).
- Andersen, H.C.,: “Cluster Expansions for Hydrogen Bonded Fluids. I. Molecular Association in Dilute Gases”, *J. Chem. Phys.*, **59**, 4714 (1973).
- Andersen, H.C.,: “Cluster Expansions for Hydrogen Bonded Fluids. II. Dense Liquids”, *J. Chem. Phys.*, **61**, 4985 (1974).
- Barker, J.A., and Fock, W., *Discuss. Faraday Soc.*, **15**, 188 (1953).
- Barker, J.A., and Henderson, D.,: “Perturbation Theory and Equation of State for Fluids. II. A Successful Theory of Liquids”, *J. Chem. Phys.*, **21**,1123 (1967).
- Benedict, M., Webb, G.B., and Rubin, L.C., “An Empirical Equation for Thermodynamic Properties of Light Hydrocarbons and their Mixtures. I. Methane, Ethane, Propane and n-Butane”, “An Empirical Equation for Thermodynamic Properties of Light Hydrocarbons and their Mixtures. I. Mixtures of Methane, Ethane, Propane and n-Butane”,*J. Chem. Physics.*, **8**, 334 (1940); **10**, 747 (1942).
- Benedict, M., Webb, G.B., and Rubin, L.C., “An Empirical Equation for Thermodynamic Properties of Light Hydrocarbons and their Mixtures. Constants for twelve Hydrocarbons”, *Chem. Eng. Progress*, **47(8)**, 419 (1951); “Thermodynamic Properties of Light Hydrocarbons – Fugacities and Liquid-Vapor Equilibria”, **47(9)**, 449 (1951).
- Beret, S., and Prausnitz, J.M., “Perturbed Hard-Chain Theory: An Equation of State for Fluids containing Small or Large Molecules”, *AIChE J.* **21**,1123 (1975).

- Bircumshaw, L.L., *J. Chem. Soc.*, 121, 887 (1922).
- Carey, B.S., *Molecular thermodynamics of multicomponent interfaces*, Ph.d Thesis, University of Minnesota, (1979).
- Carnahan, N. F., and Starling, K. E.,: “Equation of State for Nonattracting Rigid Spheres”, *J. Chem. Phys.*, **51**, 635 (1969).
- Chang, Y-B., “Development and Application of an Equation of State Compositional Simulator”, Ph. D Dissertation, The University of Texas at Austin, August, (1990).
- Chao, K.C., and Seader, J.D., “A General Correlation of Vapor-Liquid Equilibria in Hydrocarbon Mixtures”, *AIChE Journal*, **7**, 598 (1961).
- Chapman, W.G., Gubbins, K.E., Jackson, G., and Radosz, M.,: “New Reference Equation of State for Associating Liquids”, *Ind. Eng. Chem. Res.*, **29**, 1709 (1990).
- Chapman, W.G., Gubbins, K.E., Jackson, G., and Radosz, M.,: “SAFT Equation of State Solution Model for Associating Fluids”, *Fluid Phase Equilibrium.*, **52**, 31(1989).
- Chapman, W.G., Jackson G., and Gubbins K.E., : “Phase equilibria of associating fluids: Chain molecules with multiple bonding sites”, *Molecular Physics*, **65**, 5,1057 (1988).
- Chen, S.S., and Kreglewski, A.,: “Application of the Augmented van der Waals Theory of Fluids. I. Pure Fluids”, *Ber. Bunsen-Ges. Phys. Chem.*, **81**,1048 (1977).
- Cornelisse P.M.W., *The Square Gradient Theory Applied: Simultaneous modelling of interfacial tension and phase behavior*, Ph.D dissertation, Technische Universiteit Delft, Denmark (1991).
- Cummins, P.T., and Blum, L.,: “Analytical Solution of the Molecular Ornstein-Zernike Equation for Nonspherical Molecules. Spheres with Anisotropic Surface Adhesion”, *J. Chem. Phys.*, **84**, 1833 (1986).
- Cummins, P.T., and Stell, G. S.,: “Statistical Mechanical Models of Chemical Reactions: Analytic Solution of Models of  $A+B = AB$  in the Percus-Yevick Approximation”, *Molec. Phys.*, **51**, 253 (1984).
- Davis, H.T., and Scriven L.E., “Stress and structure in fluid interfaces”, Chapter in *Advances in Chemical Physics*, Vol XLIX, Wiley, New York, 1982.
- Defay, R., Prigogine, I., Bellemans, A., and Everett, D.H., *Surface tension and adsorption*, Wiley: New York, 1966.
- Dolezalek, F. Z., : “Theorie der Binaren Gemische und Konzentrierten Loungen”, *Z. Phys. Chem.*, **64**, 727(1908).

- Drago R.S., Parr L.B., Chamberlain C. S., "Solvent effects and their relationship to the E and C equation", *J. Am. Chem. Soc.*, **99,10**, 3203 (1977).
- Drago R.S., Vogel G. C., and Needham T.E., "A four-parameter equation for predicting enthalpies of adduct formation", *J. Am. Chem. Soc.*, **93,23**, 6014 (1971).
- Du, Liangui, Walker, J.G., Pope, G. A., Sharma, M. M., Wang, P., "Use of Solvents to Improve the Productivity of Gas Condensate Wells", Paper *SPE 62935* presented at the SPE Annual Technical Conference and Exhibition, Dallas, TX (October 1-4, 2000).
- Evans, R., in *Fundamentals of Inhomogeneous Fluids*, edited by D. Henderson, Marcel Dekker, New York, 1992.
- Fowkes, F.M., "Ideal Two-dimensional solutions. II. A new isotherm for soluble and "gaseous" monolayers", *J. Phys. Chem.*, **66,3**,385 (1962).
- Fredenslund, A.M., Gmehling J., Michlsen, M.L., Ramussen P., and Prausnitz., "Computerized Design of Multicomponent Distillation Columns using the UNIFAC Group Contribution Method for calculation of Activity Coefficients", *Ind. Eng. Chem. Process Des. Dev.*, **16**, 450 (1977).
- Guggenheim, E.A., *Applications of Statistical Mechanics*, Oxford University Press, Oxford, U.K., (1955).
- Gurkul S.M.K.A., Raju, B.N., "Isobaric Vapor-Liquid Equilibria of the 1-Propanol-n-Heptane System", *J. Chem. Eng. Data*, **11**, 501 (1966).
- Hansen C. M., "The three dimensional solubility parameter – key to paint component affinities: I solvents, plasticizers, polymers and resins", *Journal of Paint Technology*, **39**, 505 (1967).
- Helfand, E., "Theory of inhomogeneous polymers: Lattice model for polymer-polymer interfaces", *J. Chem. Phys.*, **63**, 2192 (1974).
- Hill, T.L., *Statistical Mechanics*, McGraw-Hill, New York (1956).
- Hoepfner, A., Kreiblich, U.T., and Schaefer, K., "Einfluß der Molekülform auf die thermodynamischen Eigenschaften binärer Organischer Nichteletrolytsysteme unpolarer Flüssigkeiten", *Ber. Bunsen-Ges. Phys. Chem.*, **74**, 1016 (1970).
- Hoye, J.S., and Olaussen, K., *Physica A.*, **104**, 435 (1980).
- Hsu, J-C., Nagarajan, N., and Robinson Jr., R.L., "Equilibrium Phase Compositions, Phase Densities, and Interfacial Tension for CO<sub>2</sub> +Hydrocarbon Systems. 2. CO<sub>2</sub> + n-Decane", *J. Chem. Eng. Data.*, **30**, 485 (1985).

- Huang, H.H., and Radosz, M.,:“Equation of State for Small, Large, Polydisperse, and Associating Molecules”, *Ind. Eng. Chem. Res.*, **29**, 2284 (1990).
- Huang, H.H., and Radosz, M., :“Equation of State for Small, Large, Polydisperse, and Associating Molecules: Extension to Fluid Mixtures”, *Ind. Eng. Chem. Res.*, **30**, 1994 (1991).
- Jackson G., Chapman, W.G., and Gubbins K.E.,: “Phase equilibria of associating fluids: Spherical molecules with multiple bonding sites”, *Molecular Physics*, **65**, 1,1 (1988).
- Jennings, H.Y., and Newman, G.H., “Effect of temperature and pressure on the interfacial tension of water against methane- normal decane mixtures” *J. Soc. Pet. Eng.*,**6**, 171, (1971)
- Kaelble D.H., *Physical chemistry of adhesion*, Wiley-Interscience (1971).
- Kokal, S., Al-Dokhi, M., and Sayegh, S., “Phase Behavior of Gas Condensate/Water System”, paper *SPE 62931* presented at the 200 SPE Annual Technical Conference and Exhibition held in Dallas, Texas, October 2000.
- Kreglewski, A., *Equilibrium Properties of Fluids and Fluid Mixtures.*, The Texas Engineering Experiment Station (TEES) Monograph Series; Texas A&M University Press: College Station., 1984.
- Laplace, P.S. , *Traite de Mecanique Celeste; Supplement au dixieme livre, Sur l Action Capillaire*, 1806, Courcier, Paris,
- Lee, B.I., and Kesler M.G., “A Generalized Thermodynamic Correlation based on three-parameter Corresponding States”, *AIChE Journal*, **21**, 510 (1975).
- Lee, L.L., *Molecular Thermodynamics of Non Ideal Fluids*, Butterworth Publishers,1988.
- Lin, H.M., Sebastian, H.M., Chao, K.C., “Gas-Liquid Equilibrium in Hydrogen + n-Hexadecane and Methane+n-Hexadecane at Elevated Temperatures and Pressures”, *J. Chem. Eng. Data*, **25**, 252 (1980).
- Macleod, D.B., “On a relation between surface tension and density”, *Trans. Faraday Soc.*, **19**, 38 (1923)
- Mansoori, G.A., Carnahan, N.F., Starling, K.E., and Leland,T.W.,: “Equilibrium Thermodynamic Properties of the Mixture of Hard Spheres”, *J. Chem. Phys.* **54**,1523 (1971).
- Massoudi, R., and King, A.D., “Effect of pressure on the surface tension of water. Adsorption of low molecular weight gases on water at 25 C”, *J.Phys. Chem.*, **78**,**22**, 2262 (1974).

- Mehra, R.K., Heidemann, R.A., and Aziz, K.,: “An Accelerated Successive Substitution Algorithm”, *Can. J. of Chem. Eng.*, **61**,590, (1983).
- Michelsen,M.L.,: “The Isothermal Flash Problem. Part I. Stability”, “The Isothermal Flash Problem. Part II Phase Split Calculation”, *Fluid Phase Equilibria*, **9**, 1,(1982).
- Narayanaswamy, G., Pope, G.A., and Sharma, M.M., “Predicting Gas-Condensate Well Productivity using Capillary Number and Non-Darcy Effects”, *SPE 51910* presented at the SPE Reservoir Simulation Symposium, Houston, TX, (1999).
- Ng, H.J., Robinson, D.B., “The Influence of Water and Carbon Dioxide on the Phase behavior and Properties of a Condensate Fluid”, paper *SPE 15401* prepared for presentation at 61<sup>st</sup> Annual Technical Conference and Exhibition of the Society of Petroleum Engineers held in New Orleans, Louisiana, October 5-8, 1986.
- Ng, H.J., Robinson, D.B.,: “The solubility of methanol or glycol in water-hydrocarbon systems”, *Gas Proc. Assn. RR 117*, March, 1988.
- Ohgaki, K., Katayama, T., “Isothermal Vapor-Liquid Equilibrium Data for Binary Systems Containing Carbon dioxide at High Pressures: Methanol-Carbon Dioxide, n-Hexane-Carbon Dioxide, and Benzene-Carbon Dioxide Systems”, *J. Chem. Eng. Data*, **21**, 53 (1979).
- Ornstein,L.S., and Zernike,F., “The kinetic theory of solid substrates. III. The equation of state of isotropic solid substrates”, 1914, *Proc. Roy. Acad. Sci.*, Amsterdam, **17**, 793
- Papaioannou, D., Panayiotou, C.G., “Surface Tensions and Relative Adsorptions in Hydrogen-Bonded Systems”, *J. Chem. Eng. Data*, **39**(3), 457 (1994).
- Pedersen, K.S., Fredenslund, Aa., Thomassen, P., *Properties of Oils and Natural Gases*, Gulf Publishing, 1989.
- Peng, D.Y., and Robinson, D.B.,: “A New Two Constant Equation of State”, *Ind. Eng. Chem. Fundamen.*, **15**, 59 (1976).
- Peng, D.Y., and Robinson, D.B.,: “The Characterization of Heptanes and Heavier Fractions for the GPA Peng-Robinson Programs”, *Ind. Eng. Chem. Fundamen.*, **15**, 59 (1976).
- Perschke, D.R.,: “Equation of State Phase Equilibria Calculations”, M.S. Thesis, University of Texas at Austin, 1984.
- Phutela, R.C., Kooner, Z.S. and Fenby, D.V., “Vapor Pressure study of Deuterium exchange Reactions in Water-Ethanol system: Equilibrium Constant Determination”, *Aust. J. Chem.*, **32**, 2353 (1979).

- Pope G.A., Wu, W., Narayanaswamy, G., Delshad M., Sharma, M.M., and Wang P., "Modeling Relative Permeability effects in Gas-Condensate Reservoirs with a New Trapping Model", *SPE Res. Eval. & Eng.*, 3(2), 171, (1986).
- Poser C.I., and Sanchez I.C., "Interfacial tension theory of low and high molecular weight liquid mixtures", *Macromolecules.*, 14, 361, (1981).
- Prausnitz, J.M., Lichtenthaler, R.N., De Azevedo, E.G., *Molecular Thermodynamics of Fluid Phase Equilibria*, Prentice-Hall:Englewood Cliffs, NJ, (1986).
- Prigogine, I., Marechal, J., "The influence of differences in molecular size on the surface tension of solutions. IV", *J. Colloid Sci.*, 7, 2,122 (1950).
- Raal, J.D., Code, R. K., Best, D. A., "Examination of Ethanol-n-Heptane, Methanol-n-Hexane Systems Using New Vapor-Liquid Equilibrium Still", *J. Chem. Eng. Data*, 17, 211 (1972).
- Rai R.R., M.S Thesis, The University of Texas at Austin (to be published).
- Redlich, O., and Kwong, J.N.S., "On the Thermodynamics of Solutions. V. An Equation of State. Fugacities of Gaseous Solutions", *Chem. Review.*, 44, 233 (1949).
- Reed, T.J., and Gubbins, K.E., *Applied Statistical Thermodynamics*, Mc. Graw-Hill, (1973).
- Renon, H., and Prausnitz, J.M.,: "Local Compositions in Thermodynamic Excess Functions for Liquid Mixtures", *AIChE J.*, 14, 135 (1968).
- Roe, R.J., "Multilayer theory of adsorption from a polymer solution", *J. Chem. Phys.*, 60, 4192 (1974).
- Sachs, W., and Meyn, V., "Pressure and temperature dependence of the surface tension in the system natural gas/water. Principles of investigation and the first precise experimental data for pure methane/water at 25 C up to 46.8 M Pa", *Colloids and Surfaces, A: Physicochemical and engineering Aspects*, 94, 291, (1995).
- Sarkar, R., Danesh A.S., and Todd A.C., "Phase Behavior Modeling of Gas-Condensate Fluids Using an Equation of State", paper *SPE 22714* presented at the 66<sup>th</sup> Annual Technical Conference and Exhibition of the Society of Petroleum Engineers, Dallas, Texas, October 6-9, (1991).
- Scheutjens, J.M.H.M., and Fleer, C.J., "Statistical theory of the adsorption of interacting chain molecules. 1. Partition function, segment density distribution, and adsorption isotherms", *J. Phys. Chem.*, 83, 1619 (1979).

- Scheutjens, J.M.H.M., and Fler, C.J., “Statistical theory of the adsorption of interacting chain molecules. 2. Train, loop and tail size distribution”, *J. Phys. Chem.*, **84**, 178 (1980).
- Sentenac, P., Bur, Y., Rauzy, E., and Berro, C., “Density of Methanol+Water between 250 K and 440 K and up to 40 Mpa and Vapor-Liquid Equilibria from 363 K to 440 K”, *J. Chem. Eng. Data.*, **43**, 592-600 (1998).
- Simnick, J.J., Lin, H.M., and Chao, K.C., *Adv. Chem. Ser.*, **182**, 209 (1979).
- Sugden, S., “The variation of surface tension with temperature and some related functions”, *J. Chem. Soc.*, **125**, 32 (1924).
- Sugden, S.; “A relation between surface tension, density, and chemical composition”, *J. Chem. Soc.*, **125**, 1177 (1924)
- Suresh S.J., and Naik V.M., “Predictive models for interfacial properties of associating systems. A statistical thermodynamic approach”, *Langmuir*, **12**, 6151 (1996).
- Suzuki, K., Sue, H., Ito, M., Smith, R.L, Inomata, H., Arai, K., Saito, S., “Isothermal vapor-liquid equilibrium data for binary systems at high pressures: carbon dioxide-methanol, carbon dioxide-ethanol, carbon dioxide – 1-propanol, methane-ethanol, methane-1-propanol, ethane-ethanol, and ethane-1-propanol systems”, *J. Chem. Eng. Data*, **35**, 63 (1990).
- Teitelbaum, B. Ya., Gortalova, T.A., Ganelina S.G., “The surface layer of liquid systems. I. Surface tension of binary liquid systems in the instance of surface separation of layers”, *Kolloid. Zhur.*, **12**, 294, (1950)
- Topliss, R. J., *Techniques to facilitate the use of equations of state for complex fluid-phase equilibria*. Ph.D. Dissertation, Univ. of California, Berkley, (1985).
- Trangenstein, J.A.: “Customized Minimization Techniques for Phase Equilibrium Computations in Reservoir Simulation”, *Chem. Eng. Sci.*, **42**, 2847, (1987).
- van der Waals, J.H, *Continuity of the Gaseous and Liquid State of Matter*, (1873).
- Van Oss, C. J., *Interfacial Forces in Aqueous Media*, Marcel Dekker, New York, 1985.
- Vargaftik, N.B., *Tables on the Thermophysical properties of Liquids and Gases*, John Wiley & Sons, New York, 1970
- Walker, J.G., “Laboratory Evaluation of Alcohols and Surfactants to increase production from Gas-Condensate Reservoirs”, M.S. Thesis, The University of Texas at Austin, December, (2000).



- Wang, P, Pope, G.A., Sepehrnoori, K., "Development of Equations of State for Gas condensate for Compositional Petroleum Reservoir Simulation", *In Situ*, **24** 2&3 (2000).
- Wertheim, M.S.: "Fluids with Highly Directional Attractive Forces. I. Statistical Thermodynamics", *Journal of Statistical Physics*, **35**,1,19 (1984).
- Wertheim, M.S.: "Fluids with Highly Directional Attractive Forces. II. Thermodynamic Perturbation Theory and Integral Equations", *Journal of Statistical Physics*, **35**,1,35 (1984).
- Wertheim, M.S.: "Fluids with Highly Directional Attractive Forces. III. Multiple Attraction Sites", *Journal of Statistical Physics*, **42**, 3, 459(1986).
- Wertheim, M.S.: "Fluids with Highly Directional Attractive Forces. III. Equilibrium Polymerization", *Journal of Statistical Physics*, **42**,3, 477(1986).
- Wichterle, I., and Kobayashi, R., "Vapor-Liquid Equilibrium of Methane-Ethane-Propane system at Low Temperatures and High Pressures", *J. Chem. Eng. Data*, **17**, 13 (1972).
- Wilson, G.M.: "A Modified Redlich-Kwong Equation of State – Application to General Physical Data Calculations", 65<sup>th</sup> National AIChE Meeting, Cleveland, OH, May 4-7, (1969).
- Wilson, G.M.: "Vapor-Liquid Equilibrium. XI. A New Expression for the Excess Free Energy of Mixing", *J. Am. Chem. Soc.*, **86**, 127 (1964).
- Young, T., (1816), reprinted in *Miscellaneous Works of the late Thomas Young*, ed. G. Peacock, Vol. I, p. 454, Murray, London, 1855.
- Zwanzig R. W., "High temperature Equation of State by a Perturbation Method. I. Nonpolar Gases", *J. Chem. Phys.*, **22**, 1420 (1954).

## **Vita**

Padmakar Ayyalasomayajula was born in Amalapuram, of the state of Andhra Pradesh in India on September 25th, 1974, the son of A. Sita and A.V.R.K.Paramahamsa. He received his degree of Bachelor of Technology in Chemical Engineering from the Indian Institute of Technology at Kharagpur in May 1995. He worked as a Graduate Engineer Trainee in Reliance Industries (India) Limited till August, 1996. He then joined the graduate school of Indian Institute of Tehcnology at Kanpur and earned a degree in Master of Tehcnology in Chemical Engineering in May 1998. In August 1998 he joined the doctoral program in the department of Chemical Engineering at the University of Texas at Austin. During his graduate study he worked as a Graduate Research Assistant.

Permanent address: 1-10-150/A , Temple Alwal  
Secunderabad, 500 010,  
Andhra Pradesh, INDIA

This dissertation was typed by the author.